Catalytic hydro-deoxygenation of bio-oil from biomass pyrolysis : comprehension of reaction pathways

Jundong Wang

Normandie Université

THESE

Pour obtenir le diplôme de doctorat

Spécialité (Génie des Procédés)

Préparée au sein de « l'Institut National des Sciences Appliquées de Rouen Normandie »

Catalytic hydro-deoxygenation of bio-oil from biomass pyrolysis: comprehension of reaction pathways

Présentée et soutenue par
Jundong WANG

Thèse soutenue publiquement le 26 Mai 2021 devant le jury composé de		
M. Edmond ABI AAD	Professeur, Université du Littoral Côte D'opale, France	Rapporteur
Mme. Claire COURSON	MCF HDR, Université de Strasbourg, France	Rapportrice
M. Pascal CARDINAEL	Professeur, Université de Rouen, France	Président
M. Vicente MONTES	Assistant Professor, Universidad de Extremadura, Spain	Examinateur
M. Lokmane ABDELOUAHED	MCF, INSA Rouen Normandie, France	Co-Encadrant de thèse
M. Bechara TAOUK	Professeur, INSA Rouen Normandie, France	Directeur de thèse

Thèse dirigée par Bechara TAOUK et co-encadrée par Lokmane ABDELOUAHED, Laboratoire de Sécurité des Procédés Chimiques-LSPC

Logo Etablissement

INSA ROUEN

Logo Ecole Doctorale

ED PSIME

Logo laboratoire

LSPC Laboratoire de sécurité des procédés chimiques

Catalytic hydro-deoxygenation of model molecules and bio-oil from biomass pyrolysis: comprehension of reaction pathways

2021.04.12

Rouen, France

Acknowledgment

This research from the years of 2017-2021 is supported by the joint program of China Scholarship Council (CSC) and UT-INSA. First of all, a great amount of gratitude must be given to the CSC organization for offering me the scholarship and INSA de Rouen in particular, Laboratoire de Sécurité des Procédés Chimiques (LSPC), for providing the experimental configuration.

Then, I would like to give the most sincere to my supervisor Prof. Bechara TAOUK (also the director of LSPC) for his professional and patient guidance. His scientific ability in research and detailed supervision manner let me lay a solid foundation for this research project. Your regular inspiration and humane help me overcome all the problems that occured during the last forty-two months. You always attentively corrected all the expressions of the experiments' results in my article draft. Again, I appreciate you deeply!

And, I would like to show my thanks and respect to my co-supervisor Dr. Lokmane ABDELOUAHED for his abundant research knowledge and the strong sense of responsibility. His excellent ideas and executive forces make me perform my study facilitate and high-efficiency. He always guides me to rigorously design all my experiments and analyze the results with simple but clear explanations. Here, I would like to express the great thanks to you once more!

In particular, my thanks link to all of the judges of my doctoral thesis defense: Prof. Edmond ABI AAD, Dr. Claire COURSON, Prof. Pascal CARDINAEL, and Dr. Vicente MONTES JIMÉNEZ. An overflowing thanks to you all for your golden time and suggestions.

Also, I would like to thank all the regular and temporary staffs and faculties in INSA Rouen or University of Rouen (France): Stéphane MARCOTTE, Laurent BALLAND Bruno DARONAT, Christine DEVOUGE, Lionel ESTEL, Alain LEDOUX, Maria Pereira De Araujo, Mélanie MIGNOT, Sylvie POUBELLE, Fabien BOUST, Jeremy DESHAIS, Isabelle DELAROCHE, Rachel MAEGHT, Soumaya MEZGHICH, Jean-pierre HEBERT, Raphaël DELAMARE, Giovanna DELAMARE, Axelle TRUFFERT,

Fatima MATTIUZ, etc. Thank you all so much for support me experimental platformand daily help!

Besides, I am willing to thank all my colleagues and friends in Rouen, Xiaoshuang CAI, Chetna MOHABEER, Yanjun WANG, Luis REYES ALONZO, Marie DÉCULTOT, Elizabeth GARCÍA HERNANDEZ, Xiaojia LU, Jie XU, Michael JABBOUR, Xuelian LIU, Yuzhen LOU, Yehya JAAFAR, Balkydia CAMPUSANO MERCEDES, Leonela MARTES HERNANDEZ, Duran MARTINEZ LAURA ELIZABETH, etc. All of you are an impartible part of my life in France. With your nice help and encouragement, my study and life here are much better.

Next, I also want to express my thanks to the smart renewable hydrogen project of generating energy secure communities (GENCOMM) and the laboratory of Chimie organique et bioorganique-réactivité et analyse (COBRA) for giving the help to me.

I would like to thank my supervisors during my master's study, Prof. Chunling LIU, and Prof. Wensheng DONG. Thanks for supporting me apply for the CSC/UT-INSA program so that I have the opportunity to experience the diverse living environments. Thanks are also given to my master's colleagues and friends: Yanqing MA, Haitao YUAN, Zhiling LI, Xiaoyang YUE, Bowen ZHAO, etc. Thanks a lot for your great help during the period of the doctoral application.

Finally, my best thanks are dedicated to my family members, my parents, my sisters, and other relatives. There is no doubt that it is your long-time support, encouragement, and selfless contribution to make my Ph.D. career come true. Special thanks to my girlfriend, Jingfeng WU, endless thanks to you for your ten-year companionship.

Contents

General introduction

Nowadays，the dramatic consumption of conventional fossil sources and the environmental issues of global warming have attracted a great deal of attention to the utilization of renewable biomass sources. Experts from different sectors reported that the petroleum-based economy would be transited to a more carbohydrate-based economy with predicted plant biomass usage of 20-25% by 2030.[1] Biomass can be transformed into crude bio-oil by various techniques, but the direct use of bio-oil is restricted by its high oxygen content. Thus, the main aim of the present study was to provide a detailed characterization of the catalytic hydro-deoxygenation (HDO) of bio-oil from biomass to give high-valued chemicals and/or biofuels and comprehension of the primary reaction pathways.

Figure I illustrates the entire diagram of this thesis including four parts. The first part involved the literature review and the subsequent preparation and characterization of catalysts. The second part was focused on the reaction parameters' evaluation of experimental runs for the single model molecule of bio-oil to understand the common operation conditions and basic reaction routes. The third part was aimed at investigating the more complicated reaction types that existed in the HDO of model molecules mixture. The last part was the preliminary exploration of HDO of crude bio-oil from biomass pyrolysis to produce high-quality biofuel and to comprehend the entire reaction pathways as well.

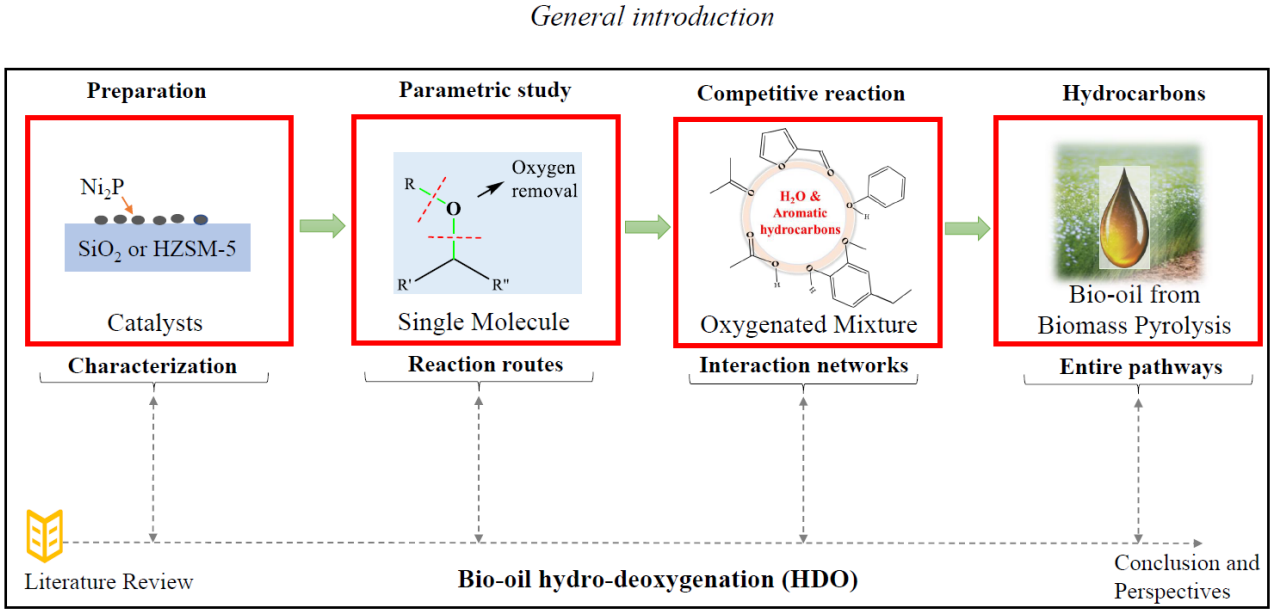

Figure I Diagram of thesis development

The implementation of this thesis was divided into five chapters. The specific explanation of these chapters was given below.

In Chapter 1, a broad literature review involving the state-of-the-art transformation technologies of biomass, the upgrading methods of bio-oil, and the types of set-up for bio-oil upgrading were first presented. Then, the application of different catalysts and their causes of deactivation were summarized. And a comparison of the advantages and disadvantages of the bio-oil upgrading methods and catalysts was made. Finally, the typical hydro-deoxygenation (HDO) of single, mixed model molecules and crude bio-oil were concluded to evaluate the development of bio-oil HDO. Among these catalysts, nickel phosphide catalysts are likely to possess both high-efficiency and low-cost properties during the bio-oil HDO process.

In Chapter 2, four home-made nickel phosphide catalysts were prepared by the incipient wetness impregnation method. These fresh catalysts and their supports were then characterized through various methods involving the N_2 adsorption/desorption (BET specific surface area and pore size calculation), ICP-OES elemental analysis, X-ray Powder Diffraction (XRD), pyridine adsorption by FT-IR, and H_2-TPR using differential scanning calorimetry (DSC). Besides, the special properties of these catalysts and supports were investigated based on the results obtained from these

technologies. It was proved that the acid sites of HZSM-5 and SiO_2 are partially displaced by the acid sites of Ni_2P active phase. A high acidity of supports and low initial content of Ni and P can help to form a stable $Ni_xP_yO_z$ species.

In Chapter 3, the catalytic hydro-deoxygenation of acetone as a model molecule of bio-oil using the HZSM-5 and the prepared catalysts was performed to optimize the reaction conditions of bio-oil HDO. The acetone HDO was focused on parametric study referred to the nature of the catalysts, the amount of supported phase, contact time, temperature, total pressure, and H_2 partial pressure. Probable HDO routes for acetone conversion were also proposed in this Chapter. Results show that the catalysts with zeolite exhibit a higher activity than catalysts with SiO_2. A multiple steps aldol condensation of acetone leads to the formation of methyl isobutyl ketone and the subsequent aromatic hydrocarbons.

In Chapter 4, the catalytic hydro-deoxygenation of other model compounds: acetic acid, 4-ethylguaiacol, and furfural, was examined based on different temperatures and pressures over the Ni_2P/HZSM-5 catalysts selected to comprehensively understand the detailed reaction routes in the bio-oil HDO. Then, the basic routes for these reactions of acetic acid, 4-ethylguaiacol, and furfural HDO were proposed based on the detailed analyses of gas and liquid products. It was found that the main reactions during HDO of acetic acid are self-ketonization to produce acetone and further condensation of acetone to form aromatic hydrcarbons. Phenol and aromatic hydrocarbons during 4-ethylguaiacol HDO can be produced from intermediates (alkyl-substituted phenols) by dealkylation, dihydroxylation, and isomerization. The principal reaction for furfural HDO is the direct decarbonylation to form furan and CO.

In Chapter 5, the HDO of two blends of model molecules (involving acetone, acetic acid, phenol, 4-ethylguaiacol, furfural, and water) was investigated with the HZSM-5 and prepared Ni_2P/HZSM-5 catalysts in order to comprehend the competitive and cross-reactions among different types of chemicals in bio-oil. Also, the bio-oil hydro-deoxygenation was explored based on the optimization of the total pressure and the bio-oil concentration in the feed. Finally, the entire reaction pathways were proposed to reveal the common reactions presented in the hydrotreatment process of bio-oil using Ni_2P/HZSM-5 catalysts. Results suggested that the temperature had a significant effect on the competition between acetic acid and phenol based on the different absorption

properties during mixture HDO. A percentage of hydrocarbons of 81.92% was obtained for the upgraded bio-oil.

To be concluded, decarboxylation, condensation, isomerization, and transalkylation were the main reactions. The simulation of bio-oil HDO using single model molecules and their mixture was proved to be an efficient method.

Résumé

Dans le contexte actuel de la consommation excessive des sources fossiles conventionnelles et des problèmes environnementaux liés au réchauffement climatique, l'attention de plusieurs pays s'est orientée vers l'utilisation de la biomasse comme source renouvelable. Des experts de différents secteurs ont rapporté que l'économie basée sur les énergies fossiles et plus particulièrement le pétrole devrait être remplacée par une économie basée sur des énergies renouvelables, avec une utilisation de la biomasse lignocellulosique de 20-25% d'ici 2030. La biomasse peut être transformée en bio-huile brute par différentes techniques, mais l'utilisation directe de la bio-huile reste limiter à cause de sa forte teneur en oxygène. Ainsi, le principal objectif de la présente étude est de fournir une caractérisation détaillée de l'hydro-désoxygénation catalytique (HDO) de la bio-huile issue de la pyrolyse de la biomasse. Le but est d'obtenir des biocarburants ou des produits chimiques à valeur ajoutée et également de mieux comprendre les voies et mécanismes des réactions mises en jeu lors de l'hydrodeoxygenation de la bio-huile.

La figure II illustre le déroulement de cette thèse incluant quatre parties. La première partie concerne la revue bibliographique, puis la préparation et la caractérisation des catalyseurs. La deuxième partie s'est concentrée sur l'évaluation des paramètres expérimentaux des réactions d'HDO de quelques molécules modèles afin de mieux comprendre les mécanismes réactionnels. La troisième partie visait à étudier l'effet de mélange et l'interaction de plusieurs molécules modèles entre elles et avec le catalyseur lors de la réaction. La dernière partie portait sur l'exploration préliminaire de l'HDO d'une bio-huile brute issue de la pyrolyse de la biomasse afin de produire un biocarburant de meilleure qualité et de comprendre également l'ensemble des mécanismes réactionnels d'HDO.

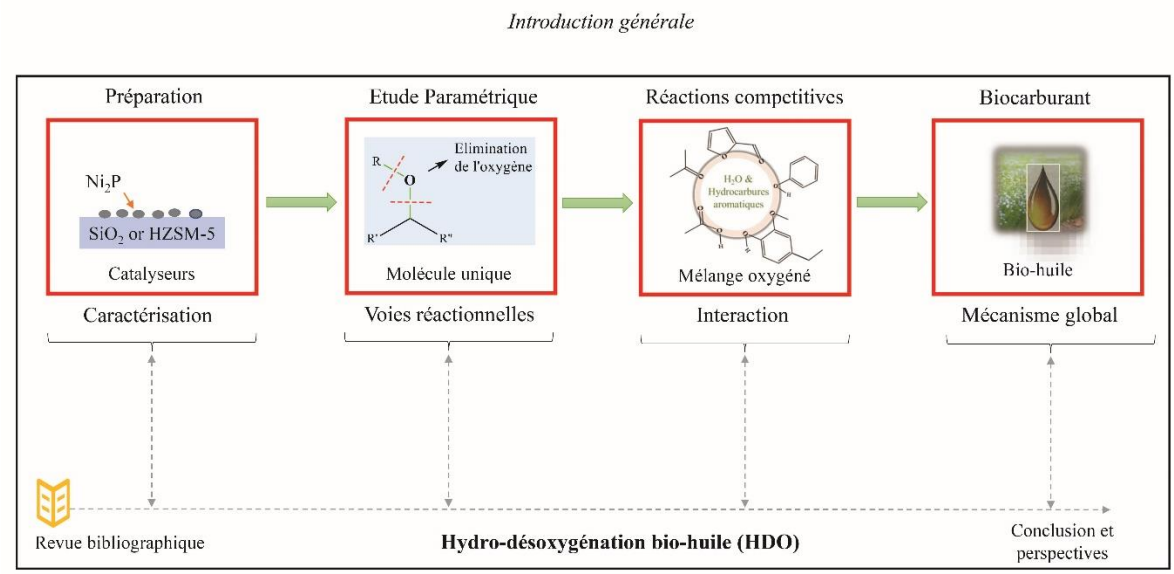

Figure II Déroulement de la thèse

Cette thèse comporte cinq chapitres. La description détaillée de ces chapitres est donnée ci-dessous.

Le chapitre 1 présente tout d'abord une revue de la littérature sur les techniques de transformation de la biomasse, les méthodes de valorisation de la biohuile et les différents types d'installations pour la valorisation de la biohuile. Ensuite, l'utilisation de différents catalyseurs et les causes de leur désactivation ont été résumées. Enfin, une comparaison des avantages et des inconvénients des méthodes de valorisation de la biohuile et des catalyseurs a été effectuée. Enfin, un point sur l'hydrodésoxygénation de molécules modèles pures, des mélanges de molécules modèles et de la bio-huile brute a été abordé. Cette étude bibliographique a montré que les catalyseurs à base de phosphure de nickel possèdent des propriétés catalytiques intéressantes pour l'HDO de la bio-huile avec des coûts raisonnables et compétitifs.

Dans le chapitre 2, quatre catalyseurs de phosphure de nickel ont été synthétisés par la méthode d'imprégnation par voie humide. Ces catalyseurs et leurs supports ont ensuite été caractérisés par diverses méthodes, comprenant l'adsorption/désorption de N_2 (calcul de la surface spécifique BET et de la taille des pores), l'analyse élémentaire par

ICP-OES, la diffraction des rayons X (DRX), l'IR-TF pour l'adsorption de pyridine, et le H_2-TPR (Réduction à Température Programmée) par calorimétrie différentielle à balayage (DSC). Il a été démontré que les sites acides de HZSM-5 et SiO_2 ont été partiellement remplacés par les sites acides de la phase active de Ni_2P. Également, il a été observé qu'une acidité élevée du support et une faible teneur initiale en Ni et P contribuent à la formation de la phase NixPyOz stable.

Dans le chapitre 3, l'hydrodésoxygénation catalytique de l'acétone comme molécule modèle de la famille des cétones sur les différents catalyseurs préparés a été réalisée dans le but d'optimiser les conditions opératoires de la réaction d'HDO. L'HDO de l'acétone a fait l'objet d'une étude paramétrique portant sur la nature des catalyseurs, la quantité de la phase supportée, le temps de contact, la température, la pression totale et la pression partielle de H_2. Des voies probables d'HDO pour la conversion de l'acétone ont également été proposées dans ce chapitre. Les résultats montrent que les catalyseurs supportés sur zéolite présentent une activité supérieure à celle des catalyseurs supportés sur SiO_2. Une condensation aldolique en plusieurs étapes de l'acétone conduit à la formation de méthyl-isobutyl-cétone et de plusieurs hydrocarbures aromatiques.

Dans le chapitre 4, l'hydrodésoxygénation catalytique d'autres molécules modèles, l'acide acétique, le 4-éthylguaiacol et le furfural, a été examinée à différentes températures et pressions sur le catalyseur Ni2P/HZSM-5. Ce dernier a été sélectionné pour ses bonnes performances et étudié pour mieux comprendre les voies complexes des réactions d'HDO de la bio-huile. Ensuite, des mécanismes des réactions d'HDO de ces trois molécules modèles ont été proposés sur la base des analyses détaillées des produits gazeux et liquides. Il a été constaté que les principales réactions au cours de l'HDO de l'acide acétique sont l'auto-cétonisation pour produire de l'acétone et la condensation de ce dernier pour former des hydrocarbures aromatiques. Le phénol et les hydrocarbures aromatiques pendant l'HDO du 4-éthylguaiacol peuvent être produits à partir d'intermédiaires (de type phénols alkyl-substitués) par désalkylation,

dihydroxylation et isomérisation. La principale réaction pour l'HDO du furfural est la décarbonylation directe pour former du furane et du CO.

Dans le chapitre 5, l'HDO de deux mélanges de molécules modèles (comprenant l'acétone, l'acide acétique, le phénol, le 4-éthylguaiacol, le furfural et l'eau) a été étudiée avec les catalyseurs HZSM-5 et Ni2P/HZSM-5 afin de comprendre l'interaction des produits lors de l'HDO sur ces catalyseurs. L'hydrodésoxygénation de la biohuile a également été étudiée en fonction de la pression totale du système et de la concentration de bio-huile dans l'alimentation. Egalement, les mécanismes de la réaction d'HDO des mélanges ont été proposés pour identifier les mécanismes communs entre les différentes molécules modèles. Les résultats montrent que la compétition entre l'acide acétique et le phénol est très influencée par la température de la réaction. Un pourcentage d'hydrocarbures de 81,92% a été obtenu lors de l'HDO des mélanges éxaminés, ce qui représente une bonne amélioration des propriétés des bio-huiles.

En conclusion, la décarboxylation, la condensation, l'isomérisation et la transalkylation sont les principales réactions ayant lieu lors de l'HDO. La simulation de la bio-huile en utilisant des molécules modèles séparées et de leur mélange s'est avérée une méthode d'étude intéressante et fiable afin de mieux comprendre les mécanismes et l'origine des produits finaux de la réaction d'HDO de la bio-huile.

Chapter 1

Literature review

1.1 Introduction

Energy as a fundamental production is essential for economic growth and social development worldwide. However, the main components of energy, traditional fossil resources, are not only undergoing a rapid depletion but are also a primary factor in the man-made emission of greenhouse gases.[2] The dramatic consumption and exhaustion of conventional fossil energy sources have attracted a great deal of attention to the utilization of renewable energy sources.[3] Globally, 14% of fuel consumption was attributed to renewable energy sources in 2016 (*Figure 1.1*).[4] Biomass comprised the largest proportion of 10%, which is about 70% of the total renewable energy sources and followed by an attribution of 2.5% for hydropower and 1.5% for other renewables (wind, solar, and geothermal) (*Figure 1.1*).[4] Generally, biomass is primarily made up of three main components (cellulose, hemicellulose, and lignin) and four minor components (proteins, sugars, aliphatic acids, and fats).[3]

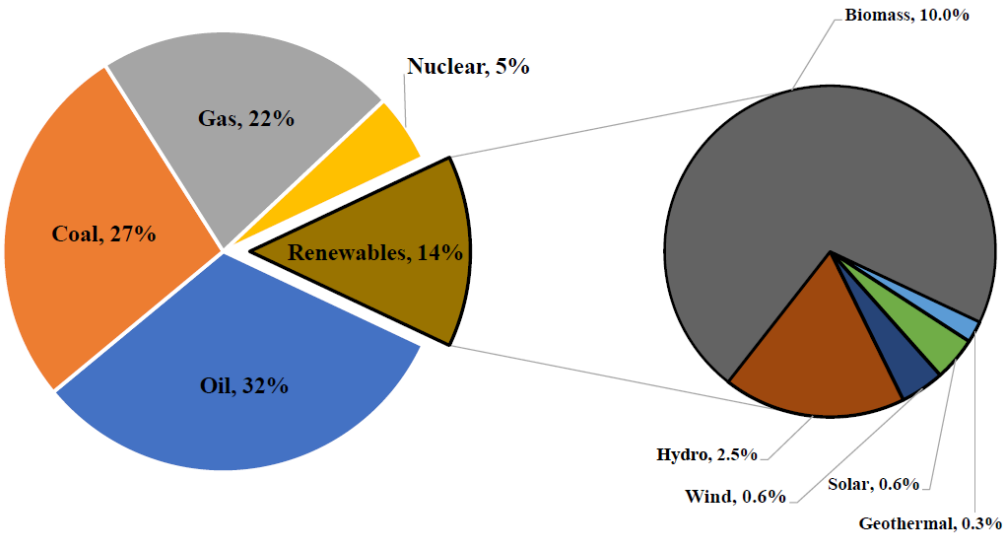

Figure 1.1 Global gross final energy consumption by fuel in 2016 (Adapted from Balázs et al.,[4] and redrawn by the author)

The utilization technologies of biomass mainly involve combustion,[5] thermochemical (torrefaction, pyrolysis, hydrothermal liquefaction, and gasification),[6,7] and biochemical (anaerobic digestion and fermentation)[8] treatments corresponding to the

production of energy, biofuels, and biochemicals, respectively. Among these technologies, pyrolysis and hydropyrolysis are considered to be the most promising and realistic routes with several prominent advantages such as a high yield of liquid bio-oil of up to70%, low cost of operation, and narrow distribution of products.[9] In particular, fast pyrolysis of biomass is highly effective in the decomposition of macromolecular structures, resulting in smaller organic compounds, the mixture of which has a similar appearance to liquid crude bio-oil. Furthermore, fast pyrolysis is one of the most promising large-scale routes among these techniques. A simplified scheme of the pyrolysis process of biomass was reported by Torres et al. and can be seen in ***Figure 1.2***.[10]

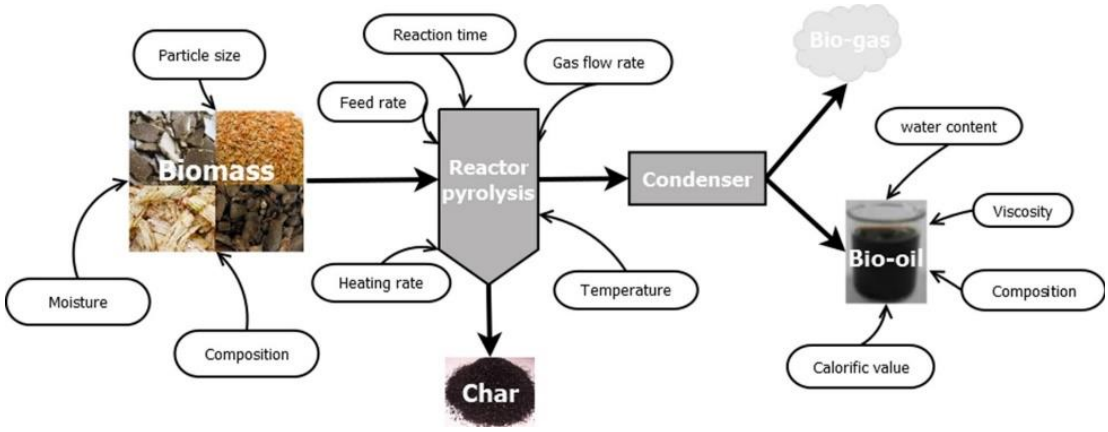

Figure 1.2 Scheme of the biomass pyrolysis process (Adapted from Torres et al.)[10]

1.2 Composition and properties of pyrolytic bio-oil

The pyrolytic bio-oil contains a significant amount of oxygenated compounds of different chemical families (ketones, aldehydes, organic acids, furans, phenolic derivatives, and lignin-derived oligomers),[11] which result in some undesirable characteristics, such as low calorific value, high acidity, high viscosity, and complexity.[12] All these undesirable properties in the use of bio-oil are attributed to the bio-oil's high oxygen content. As an example, the specific distribution of chemical families in pyrolytic oil from biomass, beech wood and flax shives, can be seen in ***Figure 1.3***.[13] It is clear that carboxylic acids are the primary chemical family in the pyrolytic bio-oil followed by phenols and ketones/Esters.

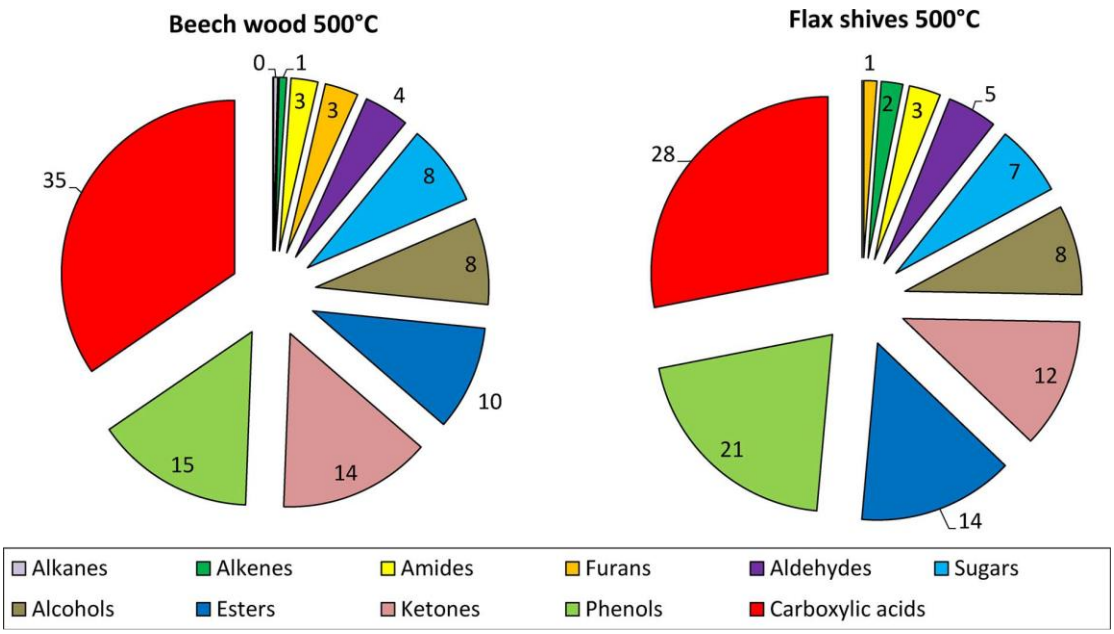

Figure 1.3 Chemical families in pyrolytic bio-oils of beech wood and flax shives at 500 °C (Adapted from Mohabeer et al.)[13]

1.3 Upgrading methods of bio-oil

Generally, the bio-oil from biomass is of inferior quality due to the high complexity of its oxygenated compounds and oxygen content compared to fossil-based fuels. Therefore, to meet the standard of conventional fossil-based fuels, bio-oil needs to be upgraded to some extent so that it can be used directly as a combustion fuel in transportation or boilers. In this regard, several main upgrading methods of bio-oil have been developed to produce more stable fuels, such as emulsification, esterification, steam reforming, supercritical fluids, and catalytic cracking.[14] An entire comparison of these current upgrading techniques of bio-oil associated with their advantages and disadvantages is presented in ***Table 1.1***.[15] A fuller introduction to these upgrading techniques will be discussed in the sections below.

Table 1.1 Comparison of various upgrading methods of bio-oil (Adapted from Lian et al.)[15]

Upgrading methods	**Process description**	**Advantages**	**Disadvantages**
Emulsification	Combines with diesel directly. Bio-oil is miscible with diesel fuels with the aid of surfactants	Simple, less corrosive	Requires high energy for production
Esterification	Organic acids (from acid, acetic acid, propionic acid, etc.) in bio-oil can be converted to their corresponding esters	The most practical approach (simplicity, the low cost of some solvents, and their beneficial effects on the oil properties)	Low oil production and poor performance
Catalytic Steam reforming	Catalytic steam reforming + water-gas shift	Produces H_2 as a clean energy resource	Complicated, requires steady, dependable, fully developed reactors
Subcritical/supercritical fluid	Promotes the reaction by its unique transport properties: gas-like diffusivity and liquid-like density, thus dissolved materials not soluble in either liquid or gaseous phase of solvents	Higher oil yield, better fuel quality (Lower oxygen content, lower viscosity)	Solvents are expensive
Catalytic crackings	Hydrogenation with simultaneous	Makes large quantities of light products	Need complicated equipment, excess cost, catalyst deactivation, reactor clogging
Catalytic hydrogenation	Hydrogenation without simultaneous cracking (eliminating N, O, and S as NH_3, H_2O, and H_2S)	A cheaper route, commercialized partially	High coking (8-25%) and poor quality of fuels obtained

1.3.1 Emulsification

Considering the low solubility of bio-oil in other hydrocarbon fuels, emulsification has been regarded as an efficient method to solve this problem by adding some surfactants into other fuel sources such as diesel or bio diesel.[14] The upgrading of bio-oil through emulsification with the usage of diesel oil can reduce the viscosity, and at the same time enhance both the calorific value and cetane number. Some of the following prerequisites must be satisfied before a stable and valid emulsion system is prepared:

1. Low compatibility of the two liquids
2. A completely dispersed state of the blend of the two liquids can be achieved by stirring
3. An appropriate emulsifier or mixing improver[16]

According to Liang et al.,[17] micro-emulsification technology has great potential for the utilization of emulsified fuels as engine fuels and for energy conversion and emissions abatement. In this study, the mixed surfactant, Span 80/Tween 80, with a ratio of 7/3 in 2% n-hexanol, was proved to be the optimal micro-emulsified formula. Jiang and Ellis[18] used octanol as an emulsifier to investigate the emulsification of bio-oil with biodiesel oil. A stable emulsion can be reached by using a surfactant amount of 4 vol% with an initial proportion of 4:6 for bio-oil/bio-diesel, a stirring rate of 1200 rpm, a mixing time of 15 min, and an emulsifying temperature of 30 °C.[18] In particular, Xu et al.[19] researched the tribological performances of an emulsified blend of bio-oil and diesel oil using a high-frequency reciprocating test rig (HFRR) and stated that the emulsified blend showed a superior lubrication ability when compared to traditional diesel fuels. In some cases, the organic solvents were regarded as a helpful reagent to produce bio-oil during hydrothermal liquefaction (HTL).[20] It is therefore that a study was performed to probe the effect of solvents used in HTL for upgrading bio-oil by the emulsification technique.[20] The results illustrated that the bio-oil obtained with methanol as a solvent in HTL was easier to upgrade by the water/diesel microemulsion compared to the use of acetone or ethanol solvent[20].

1.3.2 Esterification

Catalytic esterification is also a widely studied technique for bio-oil upgrading. In various studies, catalytic esterification can be presented in the case of catalyzing bio-oil with alcohols, such as ethanol or methanol.[21] As shown in ***Figure 1.4***, acetalization

and esterification are the chemical reactions occurring between bio-oil and ethanol or methanol.[14] The common organic acids (formic acid, acetic acid, propionic acid, etc.) in bio-oil underwent catalytic esterification and then formed their corresponding neutral esters, and this greatly improved the bio-oil's quality.[22]

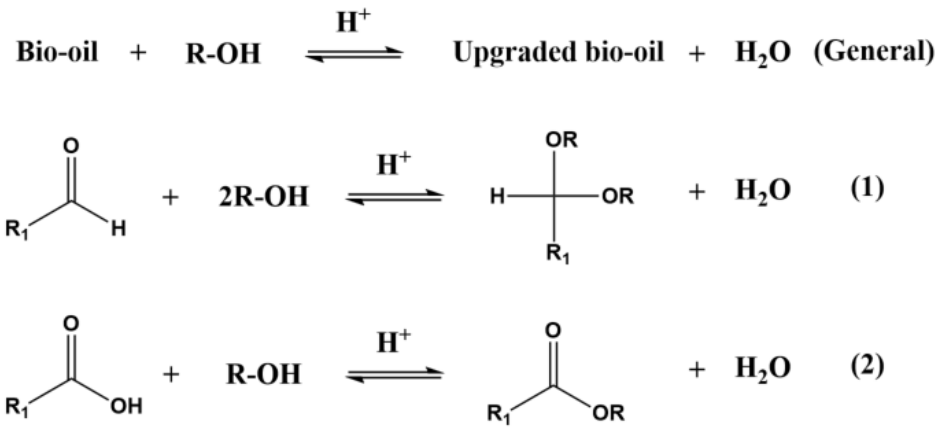

Figure 1.4 Reactions involved in bio-oil alcoholysis: (1) acetalization; (2) esterification (Adapted from Baloch et al.)[14]

To compare the composition of crude bio-oil and esterified bio-oil, Yao et al.[23] and Zhou et al.[24] characterized the specific components of upgraded bio-oil by esterification using gas chromatography/mass spectroscopy (GC/MS) and Fourier transform infrared spectroscopy (FT-IR). The former detected that the most abundant species in the residue were phenols, ketones, and hydrocarbons in sequence.[23] The latter demonstrated that significant improvement of the dispersity of bio-oil organic droplets and complete removal of the char particles of bio-oil were achieved. However, heavy species were still detected as the most abundant components in the upgraded bio-oil.[24] In other works, Wang et al.[25] studied the catalytic esterification process of bio-oil upgrading over two ion exchange resins catalysts, Amberlite IR-120 and Amberlyst 15. The results showed that a large number of organic acids were transformed to neutral esters associated with a remarkable reduction (88.54% and 85.95%, respectively) of the bio-oil's acid number. In addition, it was observed that the calorific value of the bio-oil increased by 32.26% and 31.64%, respectively, while, the water contents were decreased by 27.74% and 30.87%, respectively. The densities fell by 21.77% and the viscosities dropped by around 97%.

1.3.3 Steam reforming

Steam reforming as an efficient method for bio-oil and model compounds could be simultaneously applied to produce renewable and clean gaseous hydrogen.[26,27] Medrano et al.[28] studied the steam reforming of the aqueous fraction of bio-oil using a series of Ni-Al catalysts modified with Ca or Mg in a fluidized bed reactor. The results showed that the coke formation of bio-oil steam reforming was affected significantly by the catalyst composition. Calcium favored syngas products with lower H_2/CO ratios due to the formation of carbonaceous products, while magnesium was conducive to the water-gas shift reaction. In a similar catalytic steam reforming study, Remón et al.[29] carried out experiments using an aqueous fraction (steam to carbon ratio, S/C = 7.6) of pine sawdust bio-oil as feedstock over the Co- or Cu modifying Ni/Al-Mg-O solid catalysts in a fixed-bed and a fluidized-bed reactor. They found that the type of set-up plays an important role in the catalyst deactivation of the reforming process. They revealed that the fixed-bed reactor was more likely to lead to catalyst deactivation, although the initial H_2 and CO_2 yields were higher. In contrast, the catalysts had better resistance to deactivation in the fluidized-bed reactor.

Furthermore, Wang et al.[30] explored the feasibility of commercially available Ni-based catalysts on the pyrolysis of lignocellulosic biomass and on reforming of the pyroligneous oils to obtain hydrogen product and proved its efficiency in their screening tests. The results demonstrated that temperature was the most important parameter during steam reforming reactions.

In another work, Trane-Restrup et al.[31] investigated the steam reforming of several model molecules, including ethanol, acetic acid, acetone, 1-propanol, and propanal, using Ni/$MgAl_2O_4$ catalyst at temperatures ranging from 400 °C to 700 °C and at an S/C of 6. Experiments' results indicated that the increasing temperature promoted the conversion of feed and the release of H_2, while decreasing the yield of by-products. In addition, steam reforming and oxidative steam reforming (OSR) of furfural, 2-methylfuran, and guaiacol were also investigated by Trane-Restrup et al. [32] at an S/C ratio of 5 and temperatures from 400 °C to 800 °C over Ni/CeO_2-K/$MgAl_2O_4$ catalyst. The feed conversion, H_2 and CO yields enhanced with the increase of temperature. However, the CO_2 and byproducts yields for all the model compounds fell when the temperatures decreased. At present, a larger number of steam reforming studies for producing hydrogen are about the use of bio-oil model compounds, not real bio-oil, and

catalysts with a low coke rate, good stability, and low cost still need to be further researched.

1.3.4 Supercritical fluids (SCFs)

Recently, the utilization of supercritical fluids (SCFs) for upgrading the bio-oil from the fast pyrolysis of biomass has attracted great attention worldwide. SCFs can not only support reactions leading to the production of bio-oil, but are also superior mediums in bio-oil upgrading, and have shown great feasibility for producing high-level bio-oil with higher calorific values and much lower viscosity.[21] In order to obtain high yields and qualities of the bio-oil, some organic solvents,[33] such as ethanol,[34,35] methanol,[36–38] water[39] and CO_2,[40] were advocated in many related researches. For instance, Li et al.[37] investigated the upgrading reactions of the high-boiling fraction of bio-oil under a supercritical methanol condition and reported that the supercritical condition of methanol facilitated significantly the esterification during this upgrading process. Similarly, it was proved that the esterification of carboxylic acids, as well as real bio-oil with ethanol, was promoted under a supercritical CO_2 condition when compared to the atmospheric pressure.[40] Under the optimal conditions (80 °C and 28.0 MPa for 3 h), a total acid conversion of 86.78% was achieved, while an increase of the pH value from 3.78 to 5.11 was observed. Dang et al.[41] carried out experiments of the catalytic upgrading of pyrolysis bio-oil in supercritical ethanol and reported that the formation of coke can be effectively suppressed by higher initial hydrogen pressure (2.0 MPa). Enhancing the proportion (3:1, 5:1) of ethanol to bio-oil favored the formation of desired products and improvement of the heating value, and inhibited the formation of coke. More recently, Lee et al.[42] investigated the efficacy of pyrolysis bio-oil upgrading in supercritical ethanol using Ni-based catalysts. Their results showed that a higher quality of upgraded bio-oil with a total acid number (TAN) value of 6.2 mg KOH/g and a higher heating value (HHV) of 33.4 MJ/kg was produced, which were an obvious improvement compared to the original bio-oil (TAN, 48.0 mg KOH/g and HHV, 19.5 MJ/kg).

1.3.5 Catalytic cracking/deoxygenation

Some typical reaction pathways of catalytic upgrading are shown in ***Figure 1.5***.[12] Considering the complexity of the compounds in bio-oil, the most common studies of bio-oil upgrading refer to the catalytic cracking and deoxygenation,[43] in particular,

zeolite cracking and hydro-deoxygenation. These catalytic processes can take place in both a tubular fixed-bed reactor[44] and a micro fixed bed reactor.[45]

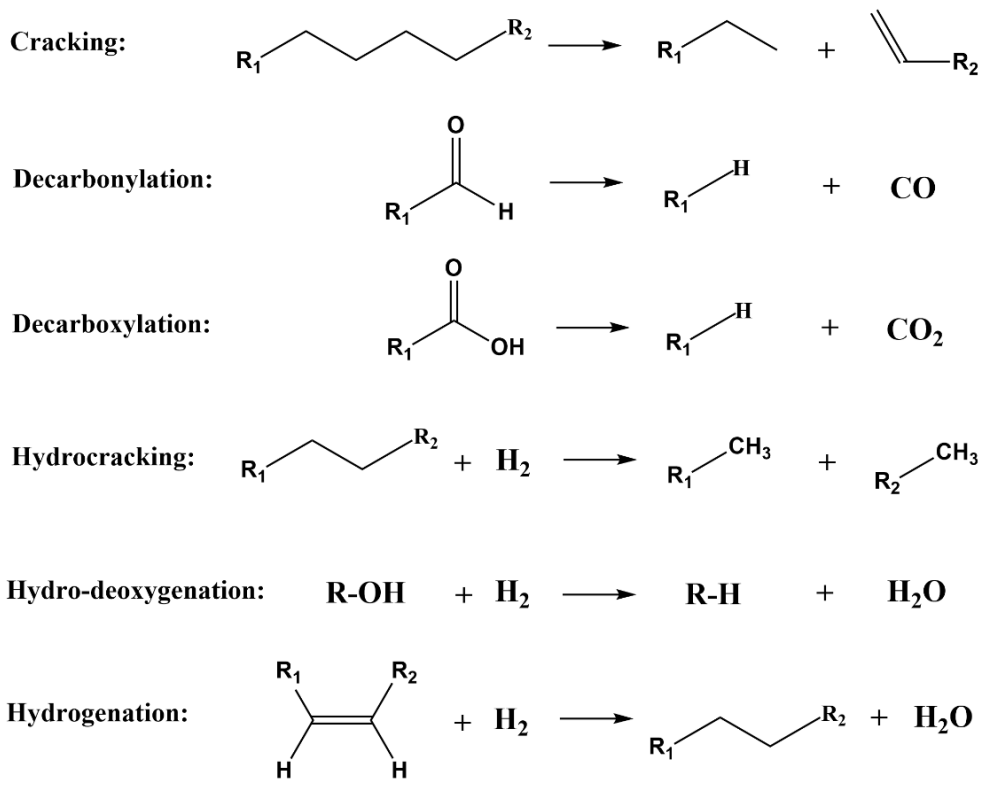

Figure 1.5 Reactions associated with catalytic upgrading of bio-oil[12] (Redrawn by the author)

1.3.5.1 Catalytic cracking

Catalytic cracking of bio-oil is a thermal transformation technique in the presence of catalysts such as zeolites when temperatures generally exceed 350 °C.[44] Notably, zeolite cracking of bio-oil had a close interrelation with the fluid catalytic cracking (FCC).[46] In general, all the reactions in ***Figure 1.5*** could be included in zeolite cracking and occur in theory, while the primary reactions are molecules cracking. Typically, general cracking can produce hydrocarbons, which are further converted into small fragments. The elimination of oxygen is mainly attributed to the dehydration route, which is followed by decarboxylation and decarbonylation.[47] Twaiq et al. [48] discussed the zeolite cracking of palm oil to gasoline using a composite of microporous HZSM-5 covered by a siliceous mesoporous crystalline substance MCM-41 and obtained a yield of 47% for gasoline. Judit et al.[49] investigated the in situ catalytic conversion of fast pyrolysis vapors from spruce wood. The quantity of hydrocarbon in the organic phase showed an increasing tendency while the carbonyl and acids decreased.

1.3.5.2 Deoxygenation

Referring to deoxygenation, a great of attention refers to hydro-deoxygenation (HDO), and it is a reformative method of catalytic upgrading applied in oxygen removal using various catalysts and hydrogen with high pressures. In the literature, Zhang et al.[50] focused on the upgrading of low-quality fuels and concluded that zeolite cracking reaction is not a competitive route compared with HDO. The oxygen, from different types of oxygenated chemical families in bio-oil such as aldehydes, acids, phenols, esters, and ketones,[51] was mainly removed in the form of CO_2 and H_2O in the HDO process, and an increasing temperature was contributed to give an upgraded bio-oil with lower oxygen content.[52] In a previous study, Hong et al.[53] recommended an appropriate bi-functional catalyst, Pt/HY, for the HDO of phenol and more complex phenolic mixtures. Hydrocarbons and elevated molecular weight were observed via hydrogenation-hydrogenolysis ring-coupling reactions of phenolic oxygenated compounds. In a similar study, Cheng et al.[54] carried out experiments of bio-oil HDO with a bimetallic catalyst Fe-Co/SiO_2 and found that the hydrocarbon content in the upgraded bio-oil was increased when compared to the raw bio-oil and reached the highest value of 22.44%. Zhang et al.[55] investigated the upgrading of bio-oil using tetralin as a hydrogen donor solvent in the presence of Co-Mo-P/Al_2O_3 catalyst at 360 °C and 2 MPa. It was observed that the oxygen content in the bio-oil showed a sharp drop from 41.8% to 3%.

As a conclusion of ***Section 1.3***, hydro-deoxygenation as a cheaper and promising route of bio-oil upgrading is considered to be a probably commercialized upgrading technique in the field of biomass energy. Considering the complicated reaction presented in the bio-oil upgrading, it is thus necessary to elucidate some basic reaction concepts and their interrelation. Generally, hydrotreatment of bio-oil is mainly associated with the process of hydrocracking and hydro-deoxygenation, but minor hydrodesulfurization and hydrodenitrification. Especially, hydrocracking is focused on the C-C bond breakage followed by hydrogenation to produce small hydrocarbons molecules. Hydro-deoxygenation is normally involved direct dehydration to give water, decarboxylation to form CO_2, and decarbonylation to release CO. However, hydro-deoxygenation of bio-oil can contain a few reaction types of hydrocracking. And, other types of reactions can also take place. In this thesis, although some of reactions

presented are generally not considered as a type of hydro-deoxygenation (for example, hydrocracking, aldol condensation, isomerization, etc.), but hydro-deoxygenation is globally the most popular reaction during the hydrotreatment of bio-oil.

1.4 Set-up of bio-oil hydro-deoxygenation

The HDO of bio-oil is primarily conducted in two typical types of reactor configurations, batch and continuous flow, the schematic drawings of which can be seen in ***Figure 1.6***. For the reaction parameters in both the batch and continuous set-up, the temperature was generally proved to be a key factor in governing the final oxygen content of the upgraded bio-oil.[56,57] Elliot et al.[18] investigated the effect of parameters on the oxygen removal of bio-oil via a two-step hydroprocessing (first step, low-temperature hydrotreating and second step, high-temperature hydrocracking). They found that a profound cracking of large oligomeric molecules needed high temperatures above 648 K in the second step.[18] However, high temperatures are generally associated with high hydrogen consumption as a result of ring saturation of liquid aromatics and gaseous hydrocarbon.[18,58,59]

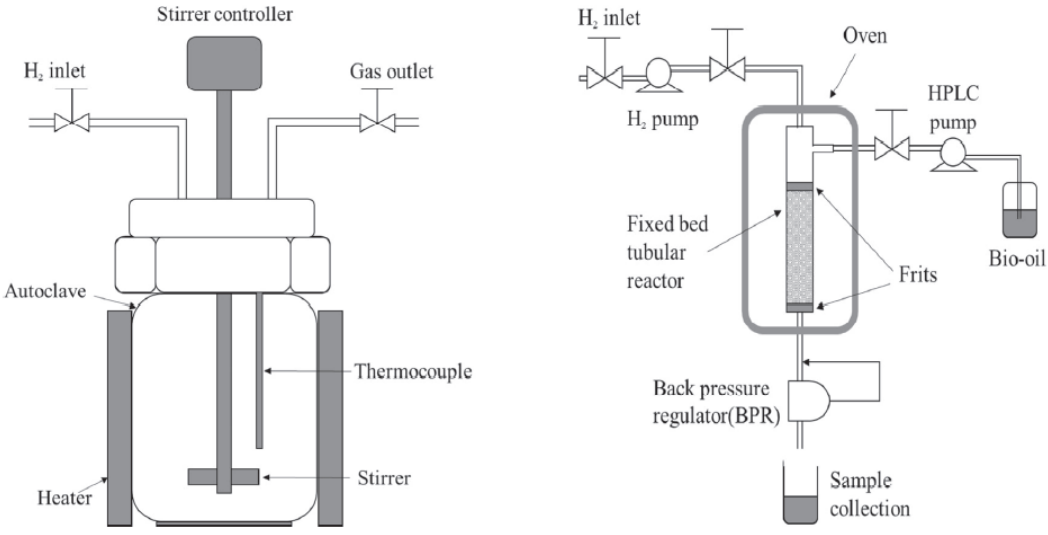

Figure 1.6 Scheme of the most common reactors used in the hydrotreatment of model compounds: (a) batch reactor, (b) continuous flow reactor (Redrawn by Han et al.)[60]

1.4.1 Batch reactors

In early research, batch reactors were typically adopted for the bio-oil HDO experiments, which normally occurred in the temperature range from 423 to 623 K (lower temperatures typically corresponding to stabilization), the pressure range from 29 to 290 bar, and hydrotreatment times between 0.5 and 4 h.[52,60–62] The final production yielded 17-92 wt% upgraded oil, which possessed an oxygen content of 1 to 16 wt%.[52,60–62] The typical consumption of hydrogen is between 100 and 300 NL/kg of bio-oil, and the formation of coke is between 4 and 30 wt%.[52,60–62]

In a systematic HDO study by Elkasabi et al.,[61] fast-pyrolysis bio-oil from various feedstocks underwent batch reactions at 320 °C under a high-pressure H_2 atmosphere. The results showed that some increasing temperatures were necessary for the significant deoxygenation of the post-pyrolysis bio-oil, and platinum catalysts were generally more efficient than ruthenium in deoxygenation, except in the case of manure bio-oil. Hogendoorn et al.[52] carried out a series of HDO experiments of pyrolysis oil in a standard refinery unit (5 L autoclave) at the highest temperatures of 230 and 340 °C. After HDO, a dry product yield of 47% to 50% for the organic phase was achieved. The hydrogen consumption increased from 232 to 326 NL/kg of feed oil with the increasing temperature. Guo et al.[62] explored the HDO of a wood-derived pyrolysis oil using a 100 ml bench-scale reactor at 300 °C and an initial hydrogen pressure of 50 bar for 3 h, based on phosphorus content effects of several inexpensive catalysts. The results illustrated that the H_2 consumption, oil yield, and the degree of deoxygenation (DOD) can be significantly elevated by improving the phosphorus content to a certain value (up to M/P = 3/2) on both Ni and Co catalysts. Further enhancing the content of P to a higher value was linked to a detrimental performance of these catalysts result in an increasing coke formation and deteriorating HDO activity. A yield of around 58-65% of the oil phase and a value of 4-4.8 mol/kg of hydrogen consumption were obtained, respectively.

1.4.2 Continuous reactors

In the case of down-flow operation in a packed-bed reactor, clogging can occur due to a low level of around 1-3 wt% for coke formation. These reactors are typically operated at temperatures ranging from 473 to 673 K, pressures ranging from 50 to 200 bar, and liquid hourly space velocity (LHSV) values from 0.05 to 2 h^{-1}.[63–65] The yield of upgraded oil is typically a minimum value of 30 wt% and a maximum value of 68 wt%

associated with oxygen content around 0.3-0.6 wt%.[63,65] The consumption of hydrogen consumption is approximately 600 NL/kg of bio-oil, and the formation of coke is lower than 13 wt%.[63–65]

In order to improve the commercial feasibility of the bio-oil hydrotreatment, the LHSV is likely to be the most key parameter and must be high enough to ensure an optimal design of such a hydrotreatment reactor. Thus, in the literature, the LHSV in a continuous reactor has been extensively investigated.[66–68] In early studies, Elliot et al.[67] minimized the negative aspects of crude bio-oil (fast pyrolysis oil from wood) by varying the LHSV between 0.1 and 0.5 h^{-1}, and an increasing trend of oxygen content from nearly zero to 30 wt% was observed. Baldauf et al.[68] conducted HDO tests of flash pyrolysis oil at temperatures between 350 °C and 370 °C by varying the weight hourly space velocity (WHSV) from 0.15 to 0.80 $(kg(kg \cdot h)^{-1})$ and also observed an increase of oxygen content for upgraded bio-oil from 0.02 to 3.06 wt%. In the results of the bench-scale experiments, high degree of deoxygenation (DOD) rates up to 88-99.9% were achieved. Low liquid (only 30-35%) and high water yields (above 50%) were obtained.

More recently, Gholizadeh et al.[66] investigated the effect of LHSV on mallee wood pyrolysis oil under mild conditions (375 °C, 70-80 bar) with a pre-sulfided $NiMo/Al_2O_3$ catalyst in a U-shape continuous pack-bed catalytic reactor. They found that higher LHSV led to the formation of heavy species and coke production. The initial contact between the heavy bio-oil and $NiMo/Al_2O_3$ catalyst under hydrogen atmosphere resulted in very obvious exothermic peaks but did not create a thermal runaway situation, probably due to the rapid deactivation of active sites of catalysts.[66] Their results also suggested that the lighter feed bio-oil underwent a short contact time with catalysts active sites, but longer contact time for the heavier bio-oil phase. It is also noted by Chaiwat et al. that different organic species may experience a wide range of residence times in the continuous reactor,[69] which is due to the difference of molecular size for heavy and light molecules and their functional groups. This phenomenon is likely to be associated with somewhat “chromatographic” functions in a packed bed of porous catalysts. Very light species in the bio-oil could exist as vapor and pass through a packed catalyst bed rapidly, whereas heavy polar molecules needed a long time before they are released. Although several studies of bio-oil HDO have been performed in continuous down-flow reactors, only a few of them were carried out in rapidly steady-state conditions due to the heavy species’ slow turn over frequencies.

To be compared with the use of batch reactor, the HDO of bio-oil in the continuous reactors showed a relatively higher reaction temperature and consumption of H_2, whereas a higher DOD rate (mainly due to H_2O formation) and lower coke formation were achieved. Thus, it is likely that a superior upgraded bio-oil and durable catalysts activity can be obtained in the case of a continuous reactor.

1.5 Catalysts of bio-oil hydro-deoxygenation

A variety of catalysts have been used for the hydrotreatment of bio-oil to improve the biofuel properties and reduce the formation of coke. The use of catalysts can effectively emit oxygen from the bio-oil through efficient HDO reactions. At the initial research stage, the HDO reaction of bio-oil was generally carried out using conventional sulfide CoMo and NiMo catalysts. Sulfided catalysts demonstrated excellent resistance to the sulfur-containing compounds in bio-oil and are thus considered to be a promising catalyst for the HDO reaction.[70–72] Generally, supports such as γ-Al_2O_3, SiO_2, activated carbon, TiO_2, ZrO_2, and zeolite are usually chosen as the carrying materials for sulfided catalysts.[70]

Some studies serve as examples, Yang et al.[70] used sulfided CoMo and CoMoP supported on MgO catalysts to hydrotreat phenol and obtained high yields of hydrocarbons, mainly including benzene and cyclohexyl aromatics, but their results also indicated a low catalytic behavior. In another study, Centeno et al.[73] added potassium and platinum to modify the sulfided CoMo and CoMoP catalysts and applied them to guaiacol and 4-methylactophenone HDO. For the guaiacol conversion, the potassium-modified CoMo/Al-K produced less activity when compared to the fresh CoMo/Al and platinum-modified CoMo/Al-Pt catalyst. The results also showed that the K- and Pt- modified catalysts were higher active in 4-methylacetophenone conversion than lab-made non-modified catalysts.[73] Although the HDO study has adopted an intensive range of sulfided catalysts, problems can be easily caused by their use, such as sulfur penetration in the production and the rapid deactivation of catalysts. Another potential problem of sulfided catalysts deactivation involves the contamination of the water used to eliminate the sulfur. Therefore, the further development of alternative catalysts is also being investigated.

1.5.1 Classification of catalysts

1.5.1.1 Noble metal catalysts

Recent attention to using noble metal catalysts for the HDO reaction is increasing among researchers. Noble metal catalysts such as Pd, Pt, Rh, and Ru are normally reduced at moderate temperatures 400 to 500 °C under hydrogen surroundings in order to offer enough activity to yield high-quality oil via the HDO reaction.[74] The high cost of noble metal catalysts is the main disadvantage of their use. Zhao et al.[75] explored the HDO of phenol using Pd/C catalyst, and Newman et al.[76] studied the HDO of phenol using Ru supported on carbon, silica, alumina, and titania catalysts. The former observed comparable formation rates of cyclohexanol via phenol hydrogenation and consumption rates via phenol alkylation with a combination of Pd/C and H-BEA.[75] The latter found that high dispersion of the ruthenium of catalysts catalyzed predominantly phenol by typical hydrogenation (HYD) on noble metal catalysts, which was linked to the high selectivity of direct deoxygenation and high activity.[76]

In the refining and petrochemical processes, zeolites are intensively used because of their strong acidity and suitable pore size.[77] Recently, the carrying materials of noble metal catalysts have been associated frequently with zeolites, such as HY, SBA-15, ZSM-5, mesoporous Y, mesoporous MFI, and mesoporous beta.[51]

1.5.1.2 Bi-functional catalysts

In addition, other effective catalysts could be bi-functional catalysts (Pt/HZSM-5. Pd/HZSM-5, Pt/SO_4^{2-}/ZrO_2/SBA-15, Pd/SO_4^{2-}/ZrO_2/SBA-15, Ru/HZSM-5, etc.).[78] This type of catalyst favors not only hydrogenation and hydrogenolysis reactions, but also dehydration, alkylation, isomerization, and condensation reactions due to the presence of active metals (reducible sites) and an acidic center (support or metal-support interface).[79] Therefore, these catalysts are becoming popular for bio-oil HDO because of the co-existence of both carbonyl (activated by metal) and hydroxyl groups (activated by acidic support) in the bio-oil.[80,81] As mentioned in ***Section 1.3.5***, Hong et al.[53] obtained a high yield of oil production with a high composition of hydrocarbons using a Pt/HY zeolite catalyst via the aqueous phenolics HDO reaction.

1.5.1.3 Nickel-based catalysts

Considering the cost of application, a nickel catalyst is considered to be an efficient and promising catalyst for the steam reforming and water gasification of bio-oil, and was

also used to examine the HDO reaction.[82–84] Nickel, as a cheaper element, can typically be used to prepare more economical catalysts than traditional noble metals, and showed advantages similar to those of non-sulfided catalysts. Mertensen et al.[12] compared 23 types of catalysts containing Ni active phase, such as Ni/Al_2O_3, Ni/CeO_2-ZrO_2, noble metal supported on carbon, NiO-MoO_3/Al_2O_3, $Cu/ZnO/Al_2O_3$, etc. Then the efficiency of phenol HDO was examined in a batch-type reactor at 275 °C and 100 bar. The order of catalytic HDO activity was listed as: Ni/ZrO_2 > Ni-V_2O_5/ZrO_2 > Ni-V_2O_5/SiO_2 > Ru/C > Ni/Al_2O_3 > Ni/SiO_2 >> Pd/C > Pt/C.[12]

1.5.1.4 Phosphide based catalysts

According to numerous recent reviews, the activity of single transition metal catalysts can be improved by forming phosphides.[85–87] Phosphides have been applied to the reactions of oxygen removal, which are mainly linked to both their surface acidic sites and H_2-activating sites. The acidity of phosphides is normally suggested to be due to Brønsted acid from PO-H sites. The second type of active site comes from activating hydrogen and can be associated with either an anion vacancy of MoP or a metallic site of Ni_2P.[88,89] The latter, Ni_2P, has attracted most research interest due to its superior performance in comparison with other phosphides. The activity of Ni_2P catalyst was investigated by Oyama et al. in a series of experiments for guaiacol HDO compared to a wide variety of other metal phosphides including Co_2P, Fe_2P, WP, and MoP.[90] An order of turnover frequency of active sites, Ni_2P > Co_2P > Fe_2P, WP, and MoP, was observed by CO titrating chemisorption.

To be concluded from ***Section 1.5.1***, it can be said that nickel phosphide catalysts are likely to possess both high-efficiency and low-cost properties when compared to all the types of catalysts mentioned above.

1.5.2 Causes of catalyst deactivation

Catalyst deactivation in HDO processes is normally caused by carbonaceous deposition, sintering and loss of surface area due to catalytic components like metals, and the poisoning of catalytic sites by compounds containing nitrogen, sulfur and phosphorus from biomass. For oxide-containing catalysts, both the initial water in bio-oil and water produced in HDO are also responsible for the instability of these catalysts at high temperatures.

Furthermore, the cause of deactivation of HDO catalysts was evidently considered to be due to the deposits of coke or similar materials, which not only cover catalytic sites but also block the pores of the catalysts, especially for small-pored materials such as zeolites. Generally, coke formation occurs through polymerization and polycondensation reactions and showed a strong relation of the rates associated with the nature of the catalysts, the bio-oil compositions, and the reaction conditions.

For instance, Li et al.[77] indicated the effects of the pore and acidity properties of the catalysts, the experimental conditions, and the nature of reactants during the n-butyl alcohol HDO, and showed that these factors probably led to catalyst deactivation. The TEM images of the spent catalysts were compared to reveal the differences of the coke morphology, which was shown in ***Figure 1.7***. At 250 °C, the spent catalyst showed a gray color that was extremely similar to the fresh catalyst, and at 280 °C, it turned a slightly darker gray. When the temperature continued to 330 °C, it turned black. They also stated that the formation of soft and hard coke was typically produced via the alkylation, aromatization followed by further hydrogen transfer, and the dehydrogenation reaction of organic compounds on active sites. In another study, Chen et al.[78] obtained a low yield of desired products (acids, alcohol/ethers, esters, and ketones) during crude bio-oil upgrading under supercritical ethanol due to a long time-on-stream of the catalyst. This was attributed to the coke deposition and the sintering of metal particles linked to BET and TEM analysis of fresh and spent catalysts.

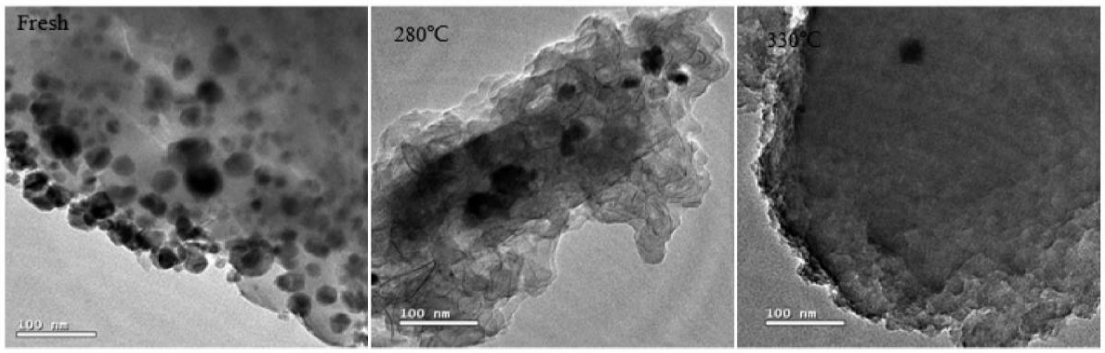

Figure 1.7 TEM photographs of the spent catalysts at different reaction temperatures (Adapted from Li et al.)[77]

In addition, the catalysts poisons may show an intense competition with the reactants in catalytic sites in HDO, which are due to aforementioned components, such as nitrogen-containing and even oxygen-containing compounds (e.g., water, CO). The adsorption of poisons on Lewis and Brønsted acidic sites depends normally on the

operating conditions. As real examples, water and other oxygen-containing compounds were proved to be an inhibiting force for conventional metal sulfide (MoS_2 and CoMoS catalysts)[91] and metal phosphide catalysts (silica-supported Ni_2P, MoP, and NiMoP catalysts).[92] In a wider range, water also led to the oxidation of phosphide catalysts, causing the formation of metal oxides and metal phosphates.[92] Odebunmi and Ollis[93] observed a reduction of activity during the HDO of m-cresol caused by water, and they successfully regenerated the catalyst by rebuilding. Jahromi et al.[94] evaluated the deactivating mechanism of Ni/RM (red mud) catalyst based on the HDO results of a queous-phase pinyon-juniper pyrolytic oil. The results suggested that the main controlling factors of oxidation and coke formation were the deactivation of the Ni and red mud, respectively.

1.6 Hydro-deoxygenation of single model molecule, mixture of model molecules and bio-oil

The high complexity of the composition of bio-oil and its intertwining interactions give rise to difficulties in understanding the reaction routes of bio-oil upgrading. Thus, studies have been focused mainly on the use of different single model molecules, followed by the application of mixed model molecules and real bio-oil.

1.6.1 Hydro-deoxygenation of single model molecules

To mimic the corresponding chemical families in bio-oil by means of catalytic HDO, numerous prior HDO studies of bio-oil were concentrated on model compounds of phenols (guaiacol,[95–97] phenol,[98] cresol,[99,100]), aldehydes (furfural),[101] ethers (anisole),[102,103] furans (2-methylfuran)[104], carboxylic acids (acetic acid)[105], etc. For instance, Le et al.[106] investigated the HDO of 2-furyl methyl ketone (2-FMK) in a fixed-bed reactor using a CoP/γ-Al_2O_3 catalyst. The results showed that complete HDO of 2-FMK into methyl cyclopentane and methane was achievable at 400 °C.

Recently, nickel phosphide supported on acid solids (Al_2O_3, HZSM-5, etc.) catalysts for HDO has attracted researchers' attention since acid supports can promote synergic interactions between the metal active phase and their intrinsic acid sites.[107,108] Furthermore, the use of acid supports also favored sequential hydrogenation-dehydration-hydrogenation reactions in the HDO of molecules.[109,110]

Notably, HDO studies of the chemical families (ketones, carboxylic acids, phenols, guaiacols, and aldehydes) were mainly focused on nickel catalysts with acid solids, but fewer works use nickel phosphide catalysts with acidic supports. Specific examples involving these HDO studies were presented in ***Sections 1.6.1.1*** to ***1.6.1.5*** below.

1.6.1.1 Hydro-deoxygenation of ketones

Li et al. investigated the HDO of ketones as bio-oil model compounds for hydrocarbon fuel via a series of Ni/HZSM-5-γ-Al_2O_3 catalysts modified by metal oxides (Al, La, and Ga),[111] and proposed the reaction pathways of hydroxyacetone HDO ***Table 1.2.*** Witsuthammakul and Sooknoi discussed the HDO of various ketones (acetone, methyl ethyl ketone, and cyclohexanone) to olefins via hydrogenation (HYD)–dehydration in a fixed-bed reactor at 373–573 K under H_2.[112] The results revealed that an alcohol intermediate could be produced by HYD of ketone and subsequently dehydrated to an olefin. Acetone was hydrogenated to IP on metal/SiO_2 catalysts (Fe, Cu, Co, Ni, Cr, and Pd). The order of reactivity of these ketones was acetone > cyclohexanone > methyl ethyl ketone, and this depended on both the adsorption onto the metal surface and the steric hindrance.

Table 1.2 The proposed pathways for intermediates in the HDO of hydroxyacetone, (1), dehydration; (2) self-condensation; (3) demethylation; (4) aldol condensation (Adapted from Li et al.)[111]

Entry	Main reaction pathways	
1		(1)
2	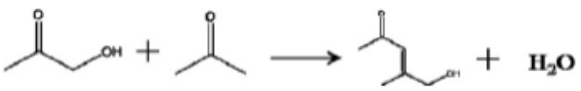	(2)
3	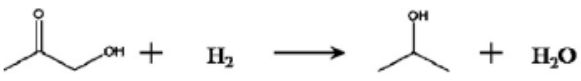	(3)
	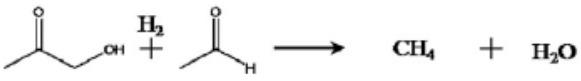	(3)
4	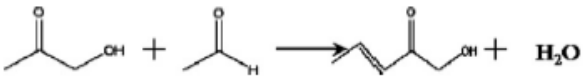	(4)

1.6.1.2 Hydro-deoxygenation of carboxylic acids

In their study of acetic acid HDO using reduced sulfided NiMo/Al_2O_3 catalysts, Joshi and Lawal explored the effects of various parameters (temperature, pressure, flow velocity, particle size, reactor diameter, etc.).[113] They reported that HDO of acetic acid could take place below 300 °C at atmospheric pressure and showed a reducing trend of conversion as the internal reactor diameter increased. The results also depicted that external and internal mass transfer resistance respectively were inappreciable at an overall flow velocity of 2.54 m/s and an average particle size of 113 μm. Eventually, a probable reaction pathway of acetic acid HDO was proposed, as shown in ***Figure 1.8***.

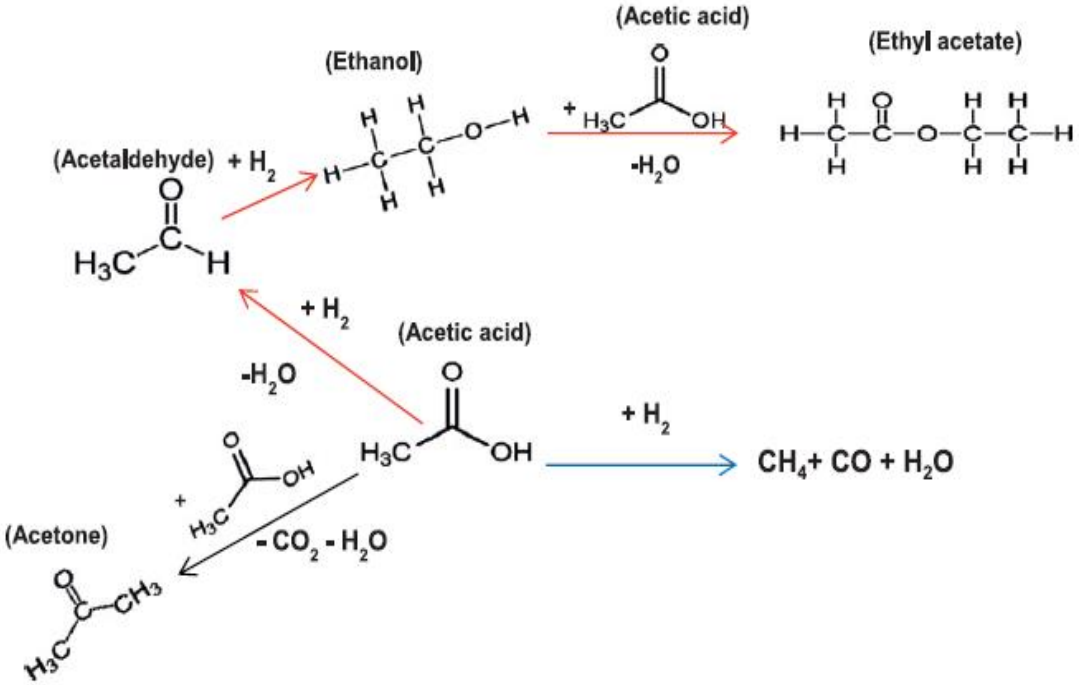

Figure 1.8 Reaction pathways of acetic acid HDO (Adapted from Joshi and Lawal)[113]

Falconer et al.[114] studied the HDO of formic acid via temperature-programmed reaction (TPR) using a Ni/Al_2O_3 catalyst and found a total conversion of formic acid. Their results showed that CO was the main product, followed by CO_2 and a small amount of CH_4. Similarly, Lercher et al.[115] explored the HDO conversion of palmitic acid with a Ni/ZrO_2 catalyst. The deoxygenation mechanism in ***Figure 1.9*** indicated that hexadecanal and 1-hexadecanol were the initial products, and then underwent decarbonylation to produce n-pentadecane and CO.

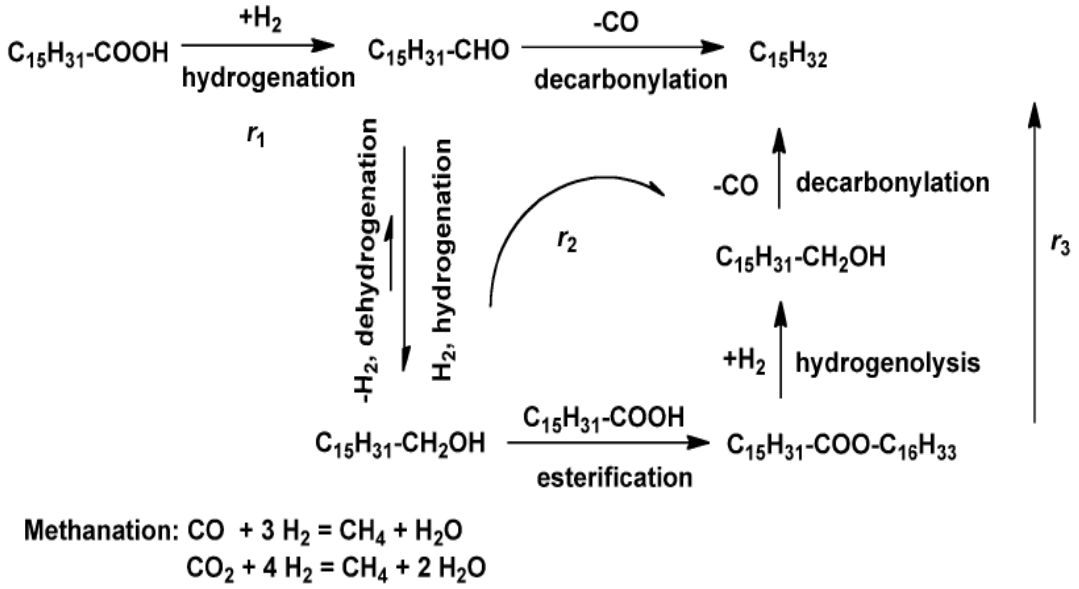

Figure 1.9 Mreaction pathways for palmitic acid HDO over a Ni/ZrO_2 catalyst (Adapted from Lercher et al.)[115]

1.6.1.3 Hydro-deoxygenation of phenols

For HDO of phenols, Berenguer et al.[116] carried out m-cresol HDO tests and found that Ni_2P/h-ZSM-5 showed a higher selectivity of methylcyclohexane product (above 97%) than Ni_2P/SiO_2 catalyst and a strong effect on turnover frequencies of m-cresol HDO depending on the Ni_2P particle size. They reported the reaction pathways of m-cresol, which were shown in ***Figure 1.10***. In addition, Tu et al.[117] investigated the HDO of bio-derived anisole using three different catalysts (nickel supported on γ-Al_2O_3, ZSM-5-m, and IM-5), and the anisole was converted with the highest value of 0.5%, 34.2%, and 98.7%, respectively.

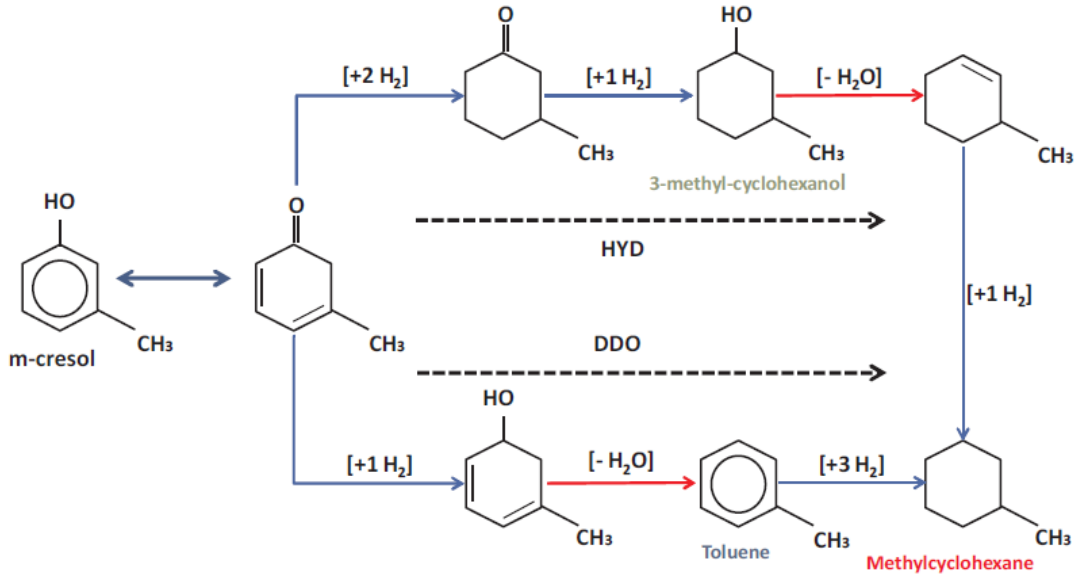

Figure 1.10 Proposed reaction pathways in m-cresol HDO (Adapted from Berenguer et al.)[116]

1.6.1.4 Hydro-deoxygenation of guaiacols

In other works, the HDO of another important family of bio-oil products, the guaiacols, has also been studied. Ardizzone et al.[118] performed experiments on guaiacol HDO using Ni/alumina-silica catalysts with varying amounts of Ni and silica. High conversions of guaiacol were achieved (up to 84%) in a very short time scale (1 h) and, generally, methylguaiacol and phenol were the primary products at 300 °C under H_2 (50 bar). Song et al.[119] studied the catalytic HDO of guaiacol using a series of high-loading nickel phosphide catalysts supported on SiO_2-TiO_2. Cyclohexane, cyclohexanol, and 2-methoxycyclohexanol were the main products over all these catalysts from 200 to 260 °C. A reaction network of guaiacol proposed by Song et al. can be seen in ***Figure 1.11***.

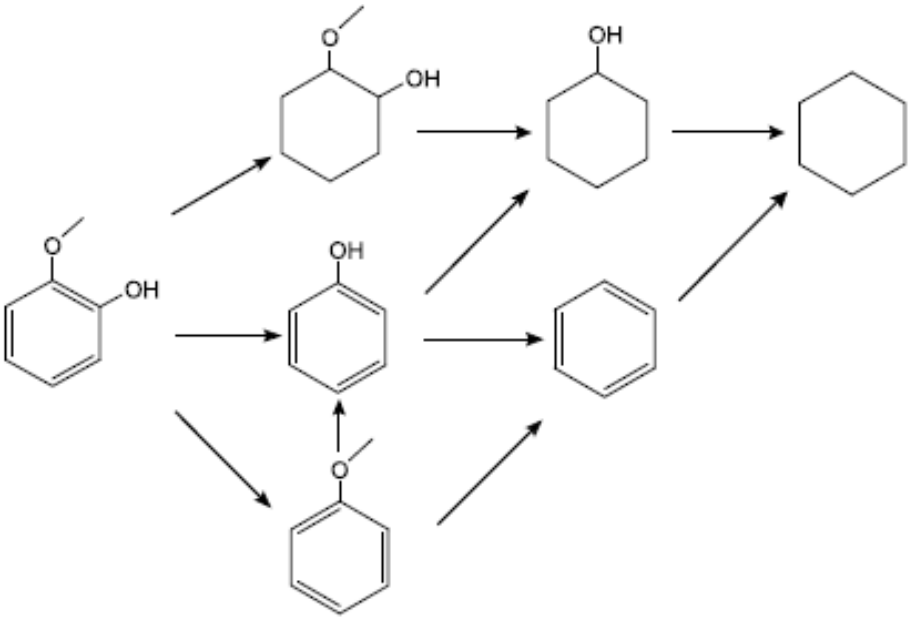

Figure 1.11 Hydrodeoxygenation reaction network of guaiacol proposed for nickel phosphide catalysts supported on SiO_2-TiO_2 (Adapted from Song et al.)[119]

In addition, Oyama et al.[120] investigated the guaiacol HDO using Ni_2P/ASA, Ni_2P/FCC, and Ni_2P/ZSM-5 catalysts. As a whole, the dominant products were cresol and phenol. In particular, the effect of the contact time indicated that the main pathway on Ni_2P/ASA was the conversion of guaiacol to catechol as a primary intermediate, followed by dehydroxylation to phenol. At the same time, it has been observed that guaiacols lead to effortless coke formation,[71] which results in obstacles in bio-oil upgrading.

1.6.1.5 Hydro-deoxygenation of aldehydes

Apart from ketones, carboxylic acids, phenols, and guaiacols, aldehydes (like furfural) are also one of the numerous families of pyrolysis oil components. Zhang et al.[121] investigated a one-pot hydrogenation/dehydration conversion of furfural using Ni/SiO_2–Al_2O_3 bifunctional catalysts in a batch reactor and found a highly selective conversion pathway to pentane (***Figure 1.12***) and a conversion of 62.99% of furfural.

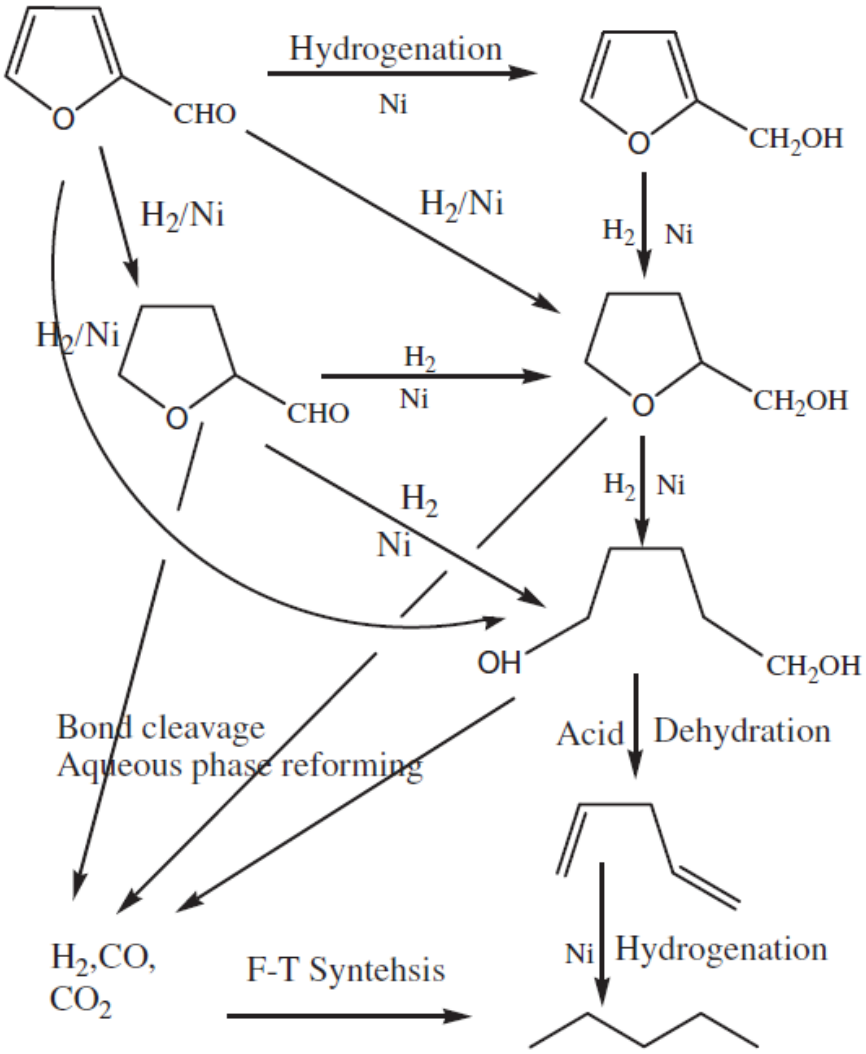

Figure 1.12 Reaction pathways for the production of pentane from furfural (Adapted from Zhang et al.)[121]

In their study of HDO of n-hexane-extracted pyrolysis oil, Zhao et al.[122] found that furfural underwent HDO/hydrolysis to form n-pentane (64%) and tetrahydropyran (36%) over a Ni/HZSM-5 catalyst at 250 °C under 5 MPa H_2 for 2 h. In addition, Wang et al.[123] studied the in-situ hydrodeoxygenation of furfural in an aqueous solution over Ni/Al_2O_3 catalysts under 1 MPa N_2. The results showed that the high temperature and amount of Ni loading facilitated the conversion of furfural, and a total yield above 85% for furan and 2-methylfuran was achieved at 260 °C and at the methanol-to-water ratio of 2:1.

1.6.2 Hydro-deoxygenation of mixed model molecules

Some other authors also explored the HDO of mixed model compounds to further understand the bio-oil HDO routes, which are mainly related to noble metal catalysts,[124–129] but relatively less to zeolite[124,130] and non-noble metal catalysts (Ni-based).[131–133] The specific examples were concluded in the following ***Sections 1.6.2.1*** and ***1.6.2.2***.

1.6.2.1 Hydro-deoxygenation of mixtures over noble metal catalysts

Zeng et al.[125] investigated the HDO of phenol with formic acid over Pd, Pt, and Ru catalysts using MCM-41 as support. The highest conversion rate of 73.9% for phenol and a deoxygenation degree of 72.2% were achieved over Ru/MCM-41. An appropriate increase of the ratio of formic acid to phenol could enhance the HDO degree of phenol.

In another similar study, Subramaniam et al.[126] explored the aqueous phase HDO of a mixed feed of acetic acid and p-cresol using Ru/C catalyst. They found that p-cresol HDO was favored as a result of the high selectivity of methylcyclohexane, but the degree of acetic acid HDO was suppressed.

For the typical phenols, Funkenbusch et al.[127] performed HDO experiments of two blends (anisole/m-cresol and anisole/phenol) over Pt/Al_2O_3 and Pd/C catalysts. Competition adsorption for catalyst active sites was reflected in the magnitude, but only a weak interaction between model compounds was observed.

In terms of more complex blends, Fisk et al.[129] studied the HDO of synthetic bio-oil containing various model molecules using Pt/Al_2O_3 catalyst. After upgrading, the major components of the products were alkyl-substituted benzenes, alkyl-substituted cyclohexanes and CO_2, and the model oil showed a sharply decreasing oxygen content from 41.4 wt% to 2.8 wt%.

1.6.2.2 Hydro-deoxygenation of mixtures over zeolites and non-noble metal catalysts

When it comes to low-cost catalysts, Gayubo et al.[130] carried out the catalytic transformation of mixtures involving some oxygenated compounds of bio-oil over the HZSM-5 catalyst. A synergy among these compounds was observed and the effortless formation of carbonaceous residue led to the deactivation of the catalyst and a low reactivity of 2-methoxyphenol and furfural in the mixture.

Especially for Ni-based catalysts, Boateng et al.[131] investigated the catalytic transfer hydrogenation of p-cresol and furfural mixtures over Ni-Cu catalysts using isopropanol as hydrogen donor solvent. At low temperature, a greater than 95% yield of products with a high selectivity for 4-methylcyclohexanol was achieved and furfuryl alcohol from furfural was in a similarly high yield. The reaction pathways in ***Figure 1.13A*** and ***B*** reveal separately the reaction routes of p-cresol and isopropanol, furfural, and isopropanol.

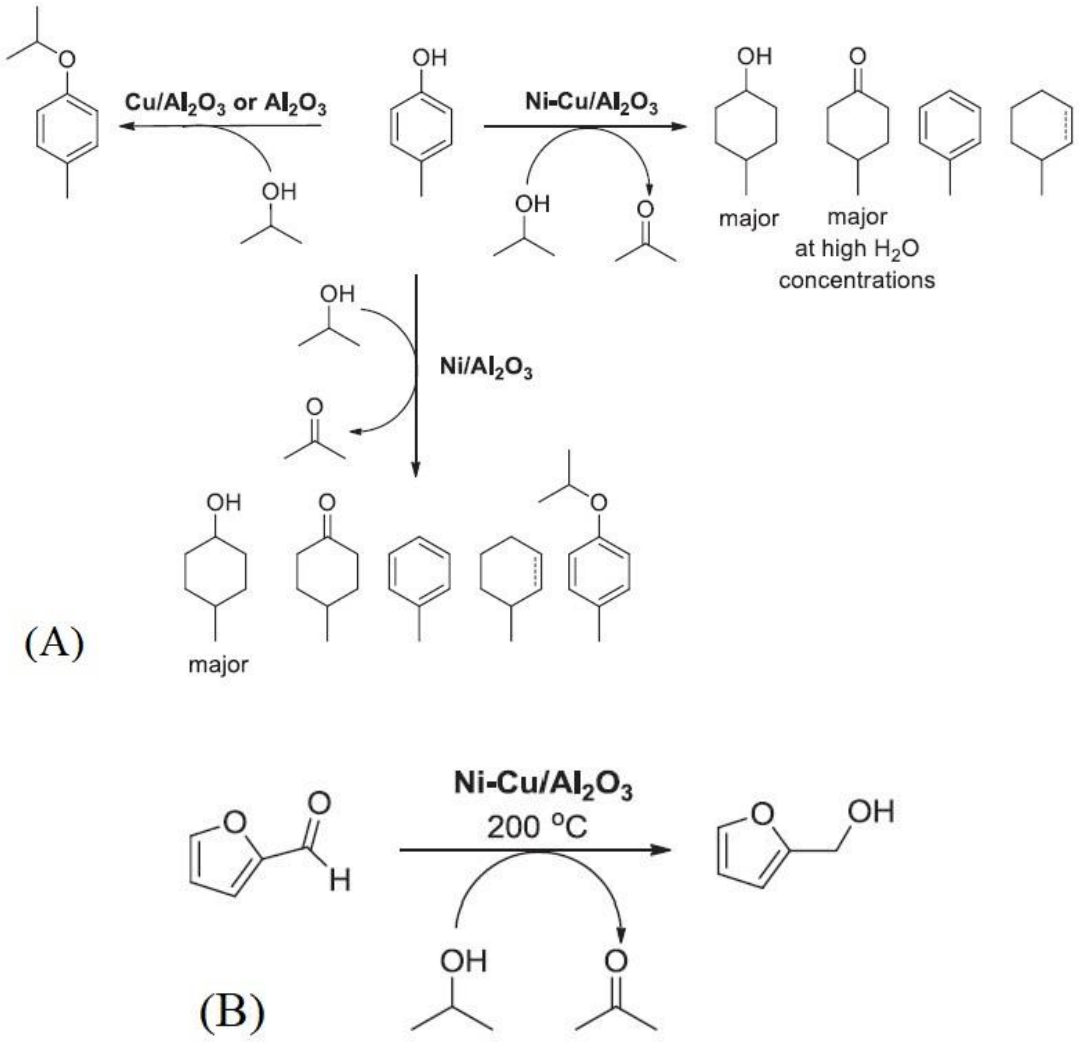

Figure 1.13 A), Transfer hydrogenation of p-cresol and isopropanol; B), transfer hydrogenation of furfural and isopropanol (Adapted from Boateng et al)[131]

Coronado et al.[133] studied the HDO of guaiacol and acetic acid blends over Ni_2P/ZSM-5. Their results illustrated that partial inhibition of guaiacol HDO occurred because of the competence of acetic acid for the active sites of the catalyst. Also, Sankaranarayanan et al.[132] reported an almost 100% HDO value and significant esterification activity

during the HDO of blends of guaiacol and propionic acid over Ni/H-ZSM-5 catalysts. As can be seen in ***Figure 1.14***, they concluded an across-activity pathway of guaiacol and propionic acid mixture HDO.

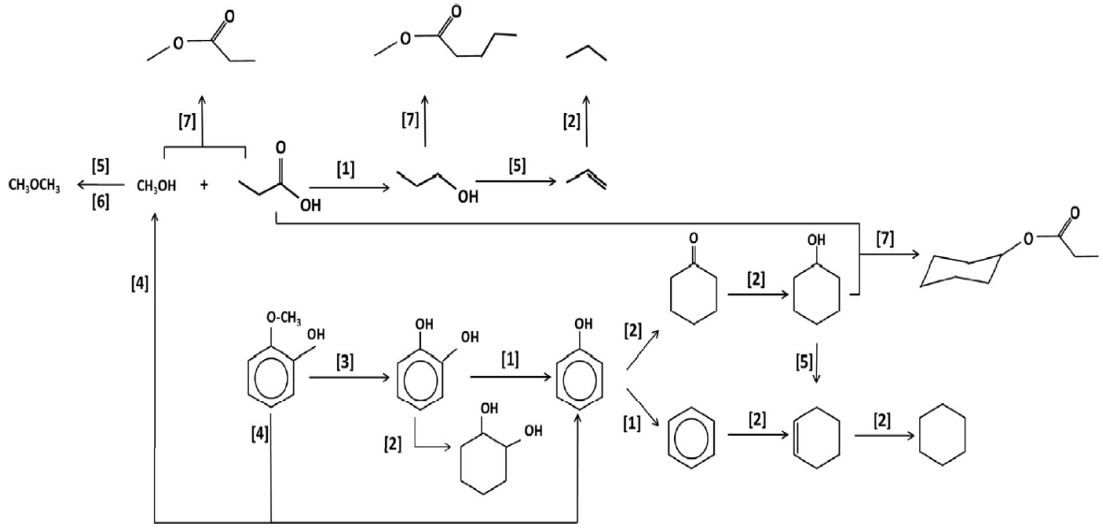

Figure 1.14 Major pathways of guaiacol and propionic acid transformations in HDO conditions: (1), hydrogenolysis; (2) hydrogenation; (3), demethylation; (4), demethoxylation; (5), dehydration; (6). Etherification; (7), esterification (Adapted from Sankaranarayanan et al.)[132]

1.6.3 Hydro-deoxygenation of real bio-oil

The HDO of bio-oil involves two main classifications: vegetable oil and pyrolysis oil, as exampled in the subsequent ***Sections 1.6.3.1*** and ***1.6.3.2***.

1.6.3.1 Hydro-deoxygenation of vegetable oil

Liu et al.[134] explored the influence of additive (SiO_2) during the preparation of Ni_2PPd/α-Al_2O_3 catalyst on HDO of triglyceride using soybean oil as the model feed. The results showed that the addition of SiO_2 made a conversion rate of above 99% and suppressed the reaction between H_2O and Ni_2P, which is the main reason for P loss and consequent deactivation, as the subsequent formation of metallic nickel promotes carbon formation.

Zarchin et al.[135] conducted a set of HDO experiments of soybean oil over 25 wt% Ni_2P/silica and Ni_2P/HY catalysts in a trickle-bed reactor. High HDO activity of both the catalysts was observed. It produced straight paraffins with a relatively narrow distribution with the Ni_2P/silica catalyst, and 47% of oxygen was removed from the

feed as CO_2 and CO thus reducing the organic liquid yield compared with the yield obtained with Pt/Al_2O_3-SAPO-11.[135]

In another work, bio-aviation fuel was firstly synthesized by hydroprocessing castor oil based on the nickel-based bifunctional catalysts in a continuous-flow fixed-bed microreactor.[136] The highest aviation range alkane yield (91.6 wt%) was achieved with a high isomer/n-alkane ratio of 4.4-7.2, and the entire hydroprocessing network was summarized in ***Figure 1.15***.

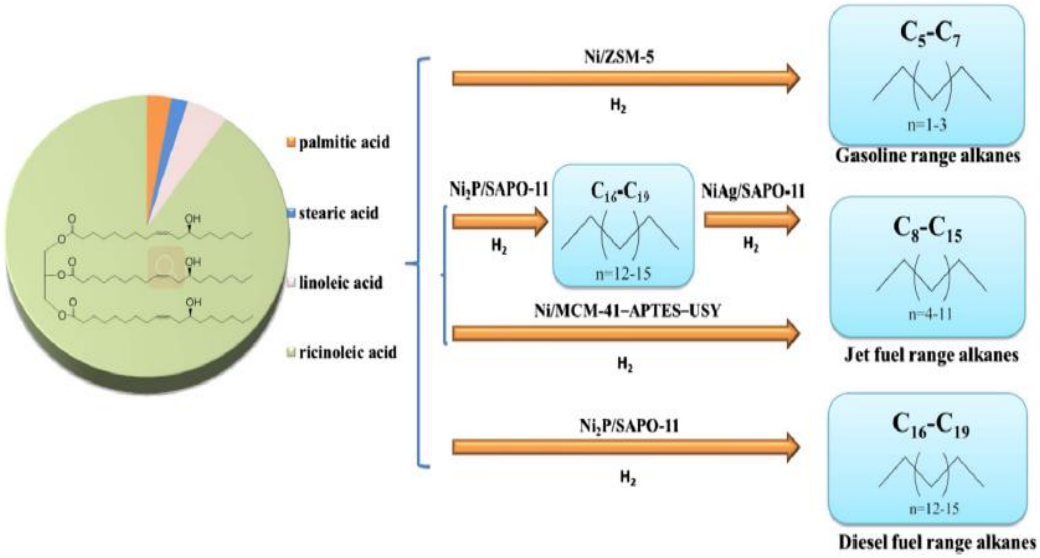

Figure 1.15 Hydroprocessing castor oil by Ni-based bifunctional catalysts with variable acidity (Adapted from Liu et al.)[136]

1.6.3.2 Hydro-deoxygenation of pyrolysis oil

In addition to the HDO of bio-oil from vegetable oil, biomass-derived pyrolysis oils HDO has recently been more attractive for researchers. In this regard, a study for the HDO of a real feed such as wood-derived pyrolysis oil was investigated using a series of NixP/AC catalysts by Guo et al.[62] They found that the properties of the upgraded bio-oil were substantially altered by the phosphorus content, and a yield of 66% for the oil phase was obtained with a Ni/P ratio of 3/2.

Jahromi and Agblevor explored the upgrading of pinyon-juniper catalytic pyrolysis oil via HDO over Ni/SiO_2-Al_2O_3 catalyst in a batch reactor.[56] The maximum HDO of bio-oil was achieved at 450 °C when the initial hydrogen pressure was 7 MPa and the reaction time was 30 min. The obtained product had an HHV of 45.58 MJ/kg compared

to 27.64 MJ/kg, a water content of 0.05 wt% compared to 1.63 wt%, and viscosity of 1.26 cP compared to 119 cP for the original bio-oil.

In more studies, Pham et al.[137] made experiments of Napier grass pyrolysis vapor using a Ni_2P/C catalyst. The catalyst Ni_2P/C with the Ni:P ratio 1.5 and 5.37 mmol of Ni showed the best performance for the pyrolysis oil upgrading. They proposed a deoxygenation pathway of Napier grass based on the production analysis, which can be seen in ***Figure 1.16***. The upgraded bio-oil was rich in furan and phenolic compounds which is great for gasoline additives production.

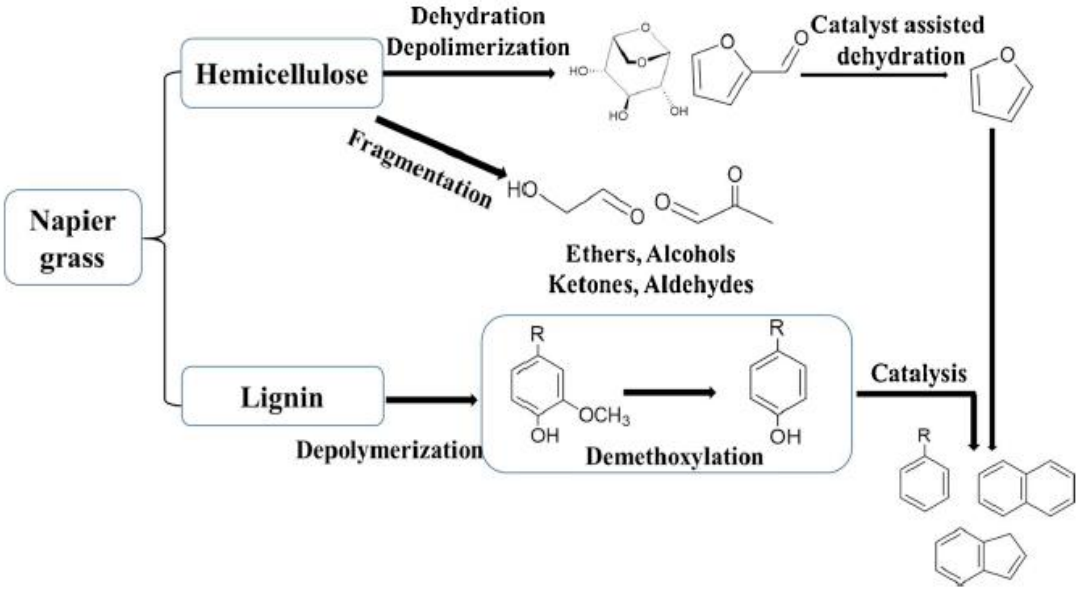

Figure 1.16 Proposed deoxygenation pathways of Napier grass with the Ni_2P/C catalyst (Ni: P ratio of 1:5 and a 5.37 mmol Ni loading level) in the integrated pyrolysis and upgrading reactor system (Adapted from Pham et al.)[137]

Besides, Shafaghat et al.[138] studied the HDO of crude bio-oil in supercritical fluid (ethanol, methanol, and 2-propanol) using a batch high-pressure reactor and an HBeta-supported nickel catalyst (10 wt%). The heating value of the crude bio-oil was improved from 12.61 MJ/kg to 24.17 MJ/kg through over 10Ni/HBeta using supercritical methanol as a solvent. The maximum deoxygenation degree (46.37%) and HHV (26.04 MJ/kg) of the bio-oil were obtained at a hydrogen pressure of 20 bar and a reaction time of 4 h.

1.7 Conclusion

This literature review has provided an overall comprehension of the state-of-the-art techniques of biomass conversion and knowledge in the catalytic upgrading fields of biomass-derived bio-oil. The methods applied in bio-oil upgrading (mainly emulsification, esterification, steam reforming, supercritical fluids, and catalytic cracking) have been intensively explored in the studies presented. A wide variety of catalysts including noble metal-based, bi-functional, and transition metal-based catalysts has also been examined for the bio-oil upgrading via catalytic hydro-deoxygenation, involving various operation conditions (generally, reactor types, nature of the catalyst, temperature, vapor contact time, and pressure). Among these catalysts, nickel phosphide catalysts are likely to possess both high-efficiency and low-cost properties during the bio-oil upgrading process. For this reason, we have selected this active phase to prepare our catalysts supported on HZSM-5 and SiO_2 for the realization of this thesis work.

However, firstly, there is still lacking of investigations on the efficiency of transition metal phosphide catalysts concerning the catalytic hydro-deoxygenation of the feeds such as single model molecules, mixed model molecules, and crude bio-oil under the optimal conditions. Secondly, the distribution of chemicals in the upgraded bio-oil and their reaction pathways during the course of hydro-deoxygenation also need in-depth exploration. Finally, although many hydro-deoxygenation investigations of bio-oil, mainly single model molecules, have indeed been examined in previous studies, the data associated with the detailed study of the components in the upgraded production and of the interaction routes in the catalytic hydro-deoxygenation of more complex model molecules mixtures and real bio-oil and the efficiency of catalysts for real bio-oil hydro-deoxygenation is still missing. This present work is devoted to overcoming these barriers remaining in the literature.

Chapter 2

Preparation and characterization of catalysts

2.1 Introduction

Four home-made nickel phosphide catalysts, 5% and 10% Ni_2P/HZSM-5, 5% and 10% Ni_2P/SiO_2 were prepared by the incipient wetness impregnation method. These fresh catalysts and their supports (HZSM-5 and SiO_2) were then characterized through various methods involving the N_2 adsorption/desorption (BET specific surface area and pore size calculation), ICP-OES elemental analysis, X-ray Powder Diffraction (XRD), pyridine adsorption by FT-IR, and H_2-TPR using differential scanning calorimetry (DSC). A detailed analysis was conducted based on the results obtained from these technologies to investigate these catalysts and supports.

2.2 Materials and methods

2.2.1 Materials

$(NH_4)_2HPO_4$ (AR, ≥99.0%) was bought from VWR Chemicals. $Ni(NO_3)_2{\cdot}6H_2O$ (AR, 99.9985%) was purchased from Alfa Aesar. HNO_3 (PrimarPlus, trace analysis grade, 70%) was supplied by Fisher Scientific. HZSM-5 (Φ=3 mm, L=30 mm, Si/Al ratio 38) was provided by ACS Material LLC. SiO_2 (powder, 0.007 μm) was acquired from Sigma-Aldrich.

2.2.2 Preparation of the catalysts

5% Ni_2P/HZSM-5 was prepared by the incipient wetness impregnation method as a first step and temperature-programmed reduction (TPR) as the second step. A weight of 3.06 g (0.0231 mol) of $(NH_4)_2HPO_4$ was dissolved in 10 ml of distilled water, and 3.37 g (0.0116 mol) of $Ni(NO_3)_2.6H_2O$ was added. Here, the initial phosphorus molar fraction was twice that of nickel, as phosphorus is partially volatilized and lost during the preparation process. A precipitate may be formed in the aqueous solution, and in order to dissolve this, several drops of concentrated HNO_3 (70%) were added to the aqueous solution with moderate magnetic stirring. A weight of 10 g for HZSM-5 pre-treated by drying at 120 °C for 12 h and calcining at 500 °C for 4 h was then added.

The aqueous solution was used with equivalent-pore volume to impregnate the support with a maturation time of 24 h. After impregnation, water was eliminated by vaporization using a Miniwatt hot plate. The resulting product was then dried for 12 h at 120 °C and calcined at 500 °C for 4 h.

The second step consisted of reducing the catalyst in a tubular reactor. The temperature was increased with a heating rate of 3 °C/min up to 600 °C and kept at this temperature for 2 h under a flow rate of 0.15 L/min of H_2 diluted in N_2 (33 vol% H_2/N_2). The resulting sample was cooled to room temperature using 0.1 L/min of nitrogen, and then passivated for 3 h in a flow of 100 mL/min of 0.5 vol% O_2/N_2. The other three catalysts, 10% Ni_2P/HZSM-5, 5% Ni_2P/SiO_2, and 10% Ni_2P/SiO_2, were synthesized using the same process with $(NH_4)_2HPO_4$, using 0.0464 mol (6.12 g), 0.0231 mol (3.06 g), 0.0464 mol (6.12 g), and with $Ni(NO_3)_2.6H_2O$, using 0.0232 mol (6.74 g), 0.0116 mol (3.37 g) and 0.0232 mol (6.74 g).

Furthermore, elemental analyses were carried out by inductively coupled plasma-optical emission spectrometry (ICP-OES) from Thermo-Fisher Scientific to measure the Ni and P content in the Ni-based catalysts (***Table 2.1***). ICP-OES analysis showed the close weight percentage of nickel and phosphorus on the catalysts.

Table 2.1 Nickel and phosphorus contents of the prepared catalysts

Element content (wt%)	5% Ni_2P/HZSM-5	10% Ni_2P/HZSM-5	5% Ni_2P/SiO_2	10% Ni_2P/SiO_2
Nickel	4.33	7.08	4.17	6.83
Phosphorus	4.44	8.34	3.26	5.73

2.3 Characterization of catalysts prepared and supports

2.3.1 N_2 adsorption/desorption characterization

The BET surface area and pore volume of the catalysts were determined based on their N_2 adsorption/desorption behavior at 77 K using a Micromeritics 2020 volumetric adsorption analyzer at Laboratoire de Catalyse et Spectrochime (LCS). Prior to using the N_2 adsorption/desorption, the catalyst samples were degassed at 200 °C for 1 h. The textural properties of the catalysts and their supports are summarized in ***Table 2.2***. The Ni_2P catalysts showed globally a lower BET surface area and pore volume than those

of their supports HZSM-5 and SiO_2, however, the average pore diameter was the opposite.

Table 2.2 Textural properties of different catalysts and supports

Catalysts	BET surface area (m^2/g^{-1})	Pore volume (cm^3/g^{-1})	Average pore diameter [a] (nm)
HZSM-5	328	0.28	6.0
5% Ni_2P/HZSM-5	267	0.22	6.4
10% Ni_2P/HZSM-5	236	0.18	6.8
SiO_2	315	1.3	20.1
5% Ni_2P/SiO_2	166	0.99	26.3
10% Ni_2P/SiO_2	132	0.72	27.0

[a] From BJH (Barrett-Joyner-Halenda) analysis.

The nitrogen gas adsorption-desorption isotherms for the catalysts samples and their supports as mentioned above, are illustrated in ***Figure 2.1***. It can be seen from ***Figure 2.1A***, ***B,*** and ***C*** that HZSM-5, 5% Ni_2P/HZSM-5 and 10% Ni_2P/ HZSM-5 basically show a combination of IUPAC types I and IV isotherms with a typical type H4 of hysteresis loop.[139] Hence, it can be said that these samples exhibited the co-existence of microporous and mesoporous structures: the extensive adsorption observed below relative pressures ($P/P0 < 0.2$) is characteristic of microporous structures, while intermediate relative pressures are attributed to mesoporous structures. Type H4 hysteresis is generally associated with narrow slit pores.[140] Furthermore, it is clear in ***Figure 2.2*** that HZSM-5 and Ni_2P/HZSM-5 catalyst possess a majority of mesoporous distribution from 3 nm to 18 nm and a pinch of the microporous distribution below 2 nm.

On the other hand, the curves of SiO_2, 5% Ni_2P/SiO_2, and 5% Ni_2P/SiO_2 in ***Figure 2.1D***, ***E,*** and ***F*** were typically attributed to the IUPAC type IV isotherms with a type H2(b) hysteresis loop, which are often disordered where the distribution of pore size and shape is not well defined and also indicative of bottleneck constrictions.[139] As shown in ***Figure 2.2***, SiO_2 support and Ni_2P/SiO_2 catalysts had an abundant distribution of mesoporous

from 22.5 nm to 35 nm and a little bit of the microporous. To be concluded from ***Table 2.2***, ***Figure 2.1***, and ***Figure 2.2***, the pore structures of supports were thus partially filled by the additional Ni_2P active phase.

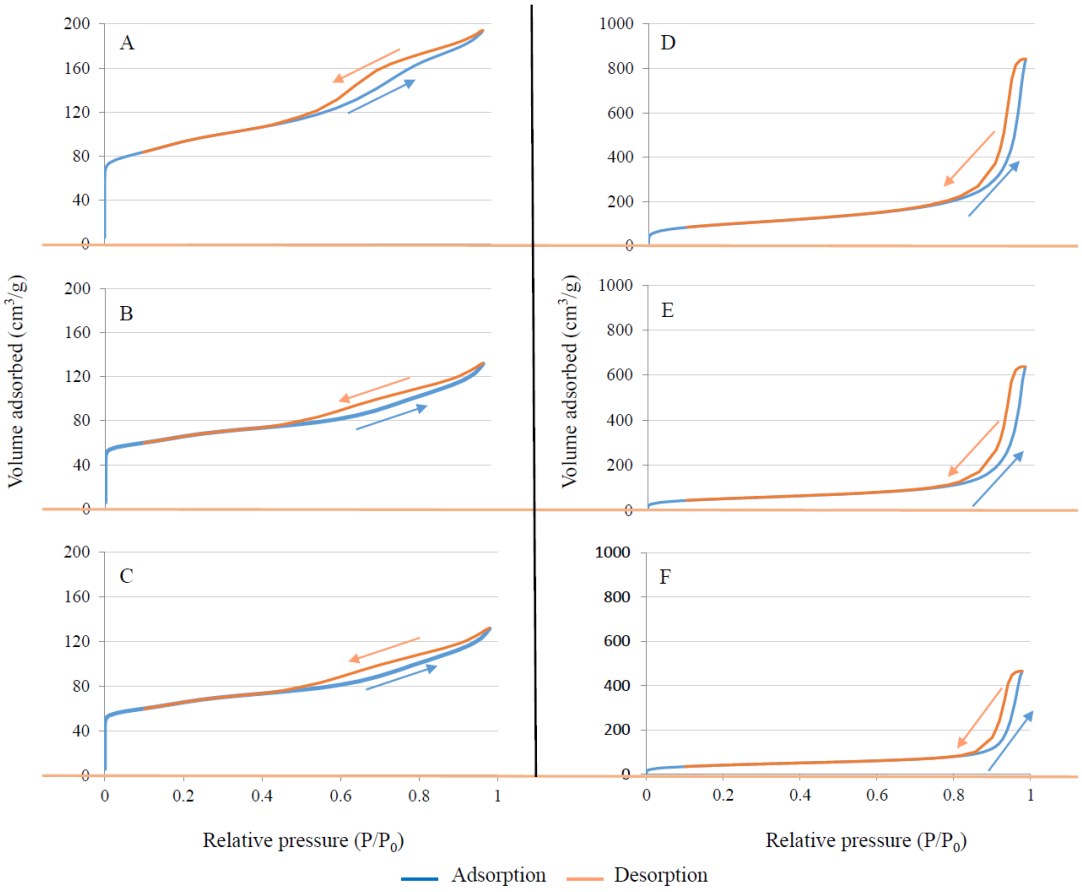

Figure 2.1 N_2 adsorption/desorption isotherms of supports and catalysts: A) HZSM-5; B) 5% Ni_2P/HZSM-5; C) 10% Ni_2P/HZSM-5; D) SiO_2; E) 5% Ni_2P/SiO_2; F) 10% Ni_2P/SiO_2

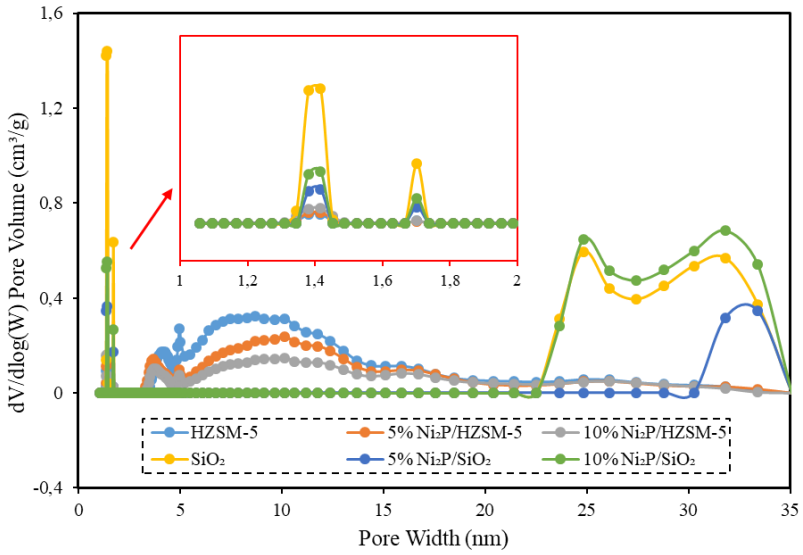

Figure 2.2 Pore size distributions of the fresh catalysts and supports

2.3.2 X-ray Powder Diffraction (XRD) characterization

XRD analysis was carried out on a D5000 diffractometer at 40 kV and 40 mA with Cu Kα (λ=0.15406 nm) radiation in the range of 2θ from 10 to 80 °C. ***Figure 2.3*** shows XRD patterns for the raw SiO_2, 5% Ni_2P/SiO_2, 10% Ni_2P/SiO_2, HZSM-5, 5% Ni_2P/HZSM-5, and 10% Ni_2P/HZSM-5 samples. All of the XRD curves for the SiO_2-supported catalysts contain a broad diffraction line at 2θ = 20–30°, which is typical of amorphous SiO_2. The 5% Ni_2P/SiO_2 pattern shows 3 weak characteristic peaks of Ni_2P phase, i.e. 2θ(111)=40.6°, 2θ(201)=44.5°, and 2θ(201)=47.9°. The 10% Ni_2P/SiO_2 pattern also shows characteristic peaks of Ni_2P phase, i.e. 2θ(201)=47.9° and 2θ(002)=54.3°, as does the 5% Ni_2P/HZSM-5 pattern, i.e. 2θ(201)=44.5°. The 10% Ni_2P/HZSM-5 catalyst sample shows characteristic peaks of the Ni_2P phase at 2θ(201)=47.9°. Similar peak positions of Ni_2P phase over Ni_2P/hierarchical ZSM-5 catalysts were also found by Berenguer et al.[99] The Ni_2P phase is not obviously shown by the 10% Ni_2P/SiO_2 and 5% Ni_2P/HZSM-5 samples, which can be attributed to the formation of small particles that are not detectable by XRD because of the low acidity of SiO_2 support and the low content nickel and phosphorus, respectively. The Ni_2P phase has no effect on the HZSM-5 crystal structure based on the comparison of the characteristic peaks of HZSM-5 and Ni_2P/HZSM-5.

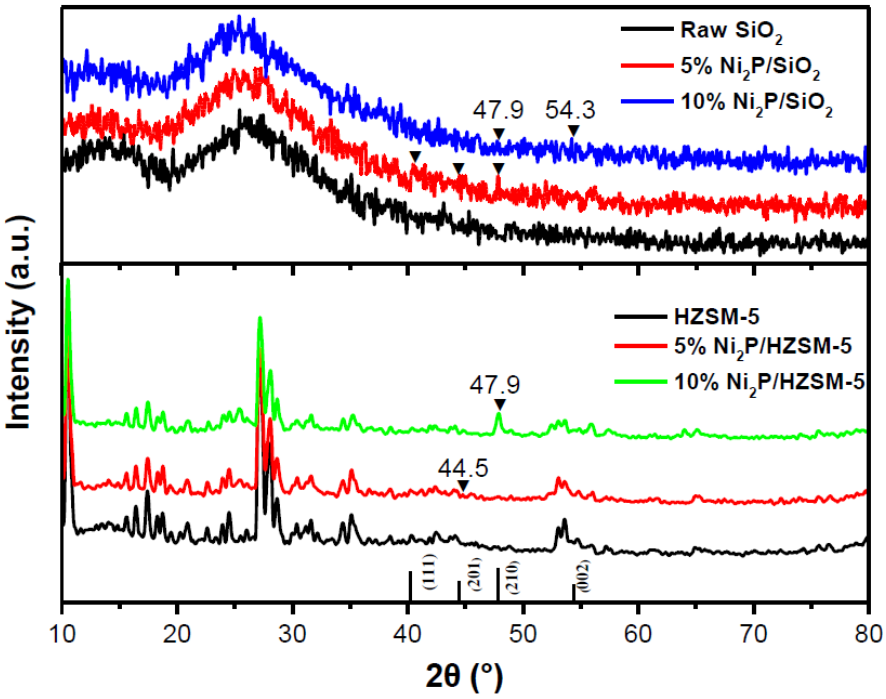

Figure 2.3 XRD patterns of catalysts

2.3.3 Pyridine Fourier Transform Infrared Spectroscopy (FT-IR) characterization

The acidity of the catalysts was characterized by Fourier Transform Infrared Spectroscopy (FT-IR, Spectrum BX, Perkin-Elmer) of adsorbed pyridine, which can be used to investigate the nature of acid sites and the bonding of ions on the surface of catalysts. In the literature, pyridine is frequently chosen as a probe molecule to examine the acidity of zeolites and zeolites-like catalysts used in bio-oil upgrading.[141,142] Here, FT-IR profiles were obtained in a range of 600-4000 cm^{-1}. The catalysts samples were saturated with a small amount of pyridine vapor and conducted stepwise desorption at 100, 150, 275, and 400 ºC. Prior to the pyridine adsorption, all the samples were dried at 200 ºC for 2 h. The FT-IR spectra were obtained after the pyridine treatment by subtracting from those of the untreated catalysts to obtain the peaks associated only with pyridine-acid sites interactions.[143]

Figure 2.4 represented the IR spectra of the catalysts and their corresponding supports with pyridine desorption at 100 ºC. The SiO_2 and HZSM-5 supports were calcined at 500 ºC for 4 h. The spectra at 150 ºC in *Appendix A* (*Figure A.1*) showed the same tendency. Catalysts generally possess two kinds of acid sites, Brønsted acid and Lewis acid. Brønsted acid sites are normally linked to the H-form (hydroxyl groups associated

with Si and Al atoms). Then, Lewis acid sites usually show a relationship with extra-framework Al and O species. For Ni_2P-based catalysts, the Brønsted acid sites could be attributed to the surface PO-H groups, and Lewis acid sites are the Ni species with a partial positive charge ($Ni^{\delta+}$).[144]

Concerning the spectra in ***Figure 2.4*** and our previous work,[145] the bands that appeared at 1440, 1445, and 1588 cm^{-1} were assigned to pyridine adsorbed on the Brønsted acid sites, whereas the presence of bands at 1488 and 1597 cm-1 was attributed to pyridine adsorbed on the Lewis acid sites. For the Ni_2P/HZSM-5 catalysts in ***Figure 2.4***, the principal effect of the nickel phosphide modification on the HZSM-5 support was an increase of Lewis acidity at 1488 cm^{-1}, but a decrease of Brønsted acidity at 1440 cm^{-1}. However, the nickel phosphide modification for the SiO_2 support affected apparently both the Brønsted (1445 cm^{-1}) and Lewis acidity (1597 cm^{-1}). These results, therefore, provided pieces of evidence that the acid sites, in particular Brønsted, were displaced by the Ni_2P active phase.

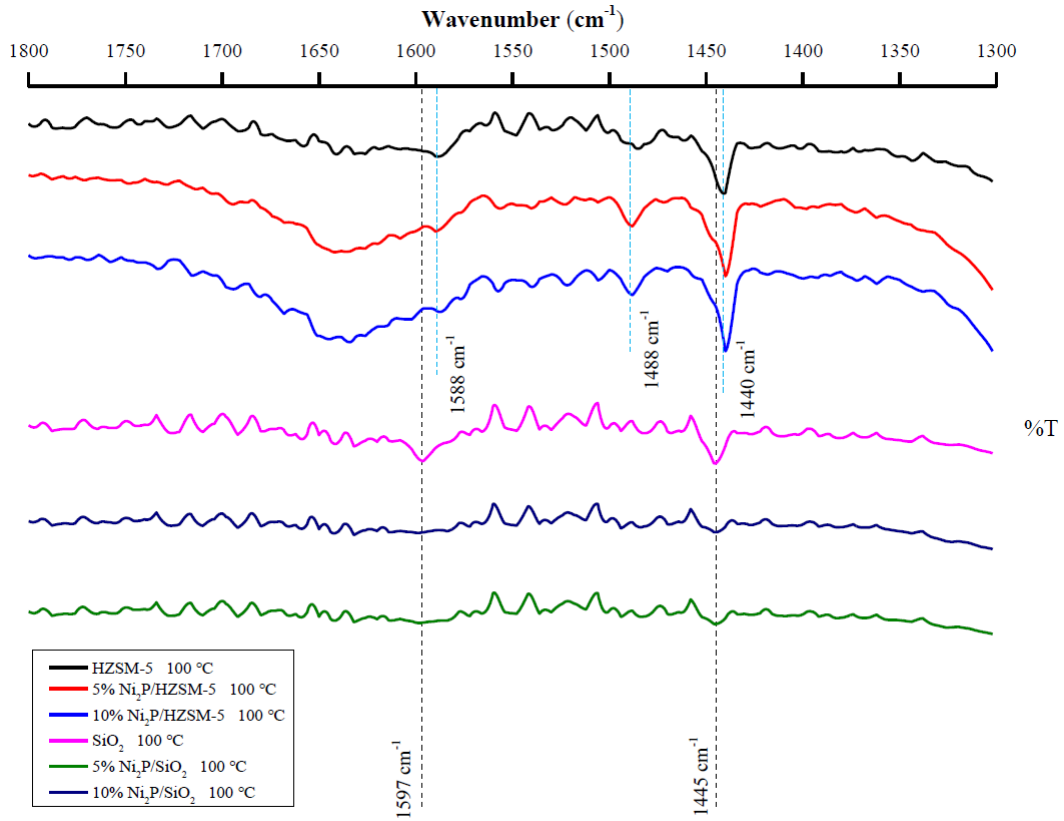

Figure 2.4 IR spectra of catalysts and supports desorbed at 100 °C after pyridine adsorption

Figure 2.5 shows the IR spectra of 5% Ni_2P/HZSM-5 without and with pyridine adsorption at different pyridine desorption temperatures. IR spectra of other catalysts can be found in *Appendix B* (*Figure A.2* to *Figure A.5*). It can be seen that no bands of acidity were detected in the sample without pyridine adsorption, and the intensity of the bands was reduced with an increase of the desorption temperature from 100 to 400 ºC. The bands observed represent normally three types of acid sites: type I (100-200 ºC), weak acid sites; type II (200-350 ºC), medium-strong acid sites; type III (350-550 ºC), strong acid sites.

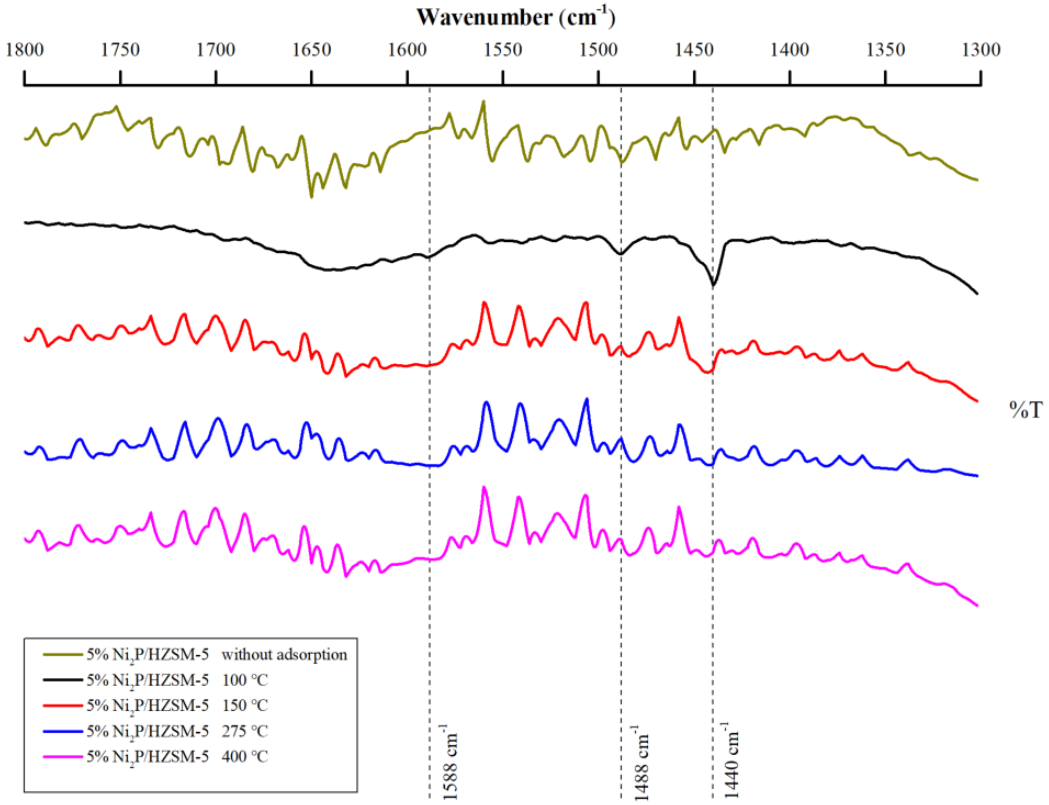

Figure 2.5 IR spectra of 5% Ni_2P/HZSM-5 catalyst at different pyridine desorption temperature

2.3.4 H_2-TPR characterization using differential scanning calorimetry (DSC)

The H_2-TPR of the catalysts precursors (not reduced) was performed using a differential scanning calorimetry (DSC) instrument with a reduction temperature range from 30 to 600 ºC, which can be applied to study the formation process of the Ni_2P active phase. As shown in *Figure 2.6*, a sharp exothermic peak and a broad peak were observed only for 10% Ni_2P/SiO_2 catalyst at 130 ºC and 150-250 ºC, respectively. The former can be explained by the unstable size of nickel oxyphosphate species ($Ni_xP_yO_z$) due to the high

initial content of Ni and P and weak interaction with the SiO_2 support. This size might further rise to a bigger and stable state with an increasing temperature in the H_2-TPR (DSC) process.

In contrast, the size of $Ni_xP_yO_z$ species for 5% and 10% Ni_2P/HZSM-5 catalysts were completely stable during the calcining stage when preparing the catalysts' precursors since the higher acidity of HZSM-5 compared to SiO_2 probably facilitated the formation of $Ni_xP_yO_z$ species. In the case of 5% Ni_2P/SiO_2, this was because the lower Ni and P initial content in comparison with 10% Ni_2P/SiO_2 helped the rapid formation of a stable size of $Ni_xP_yO_z$ species. Thus, for the initial Ni and P content of 10% Ni_2P/SiO_2 catalysts, a lot of dissociative phosphorus phases existed on its surface due to the presence of the unstable $Ni_xP_yO_z$ species. And the broad peak at 150-250 ºC was thereby attributed to the volatilization of dissociative phosphorus. This was confirmed by the results of ICP-OES (***Table 2.1***) (low P contents in prepared catalysts compared to its initial content). For the ICP-OES analysis, the phosphorus content of Ni_2P/SiO_2 catalysts, especially for 10% Ni_2P/SiO_2, was significantly lower than in other catalysts.

In addition, small peaks were found between 250 ºC - 325 ºC for 5% Ni_2P/HZSM-5 and 5% Ni_2P/SiO_2, indicating that some intermediates were formed during this stage. The further transformation of intermediates to Ni_2P via the reduction of Ni_xO_y and phosphorus species was associated with the presence of a broad peak at an onset temperature around 400 ºC. Similarly, Oyama et al. also reported almost the same reduction peak of NiO species in the H_2-TPR result of Ni_2P/ASA precursor,[120] and Zhang et al. report a higher onset reduction temperature around 500 ºC of oxidized nickel species and phosphorus species (such as PO_4^{3-}, $P_2O_7^{4-}$, and $(PO_3^-)_n$) to form Ni_2P phase.[146]

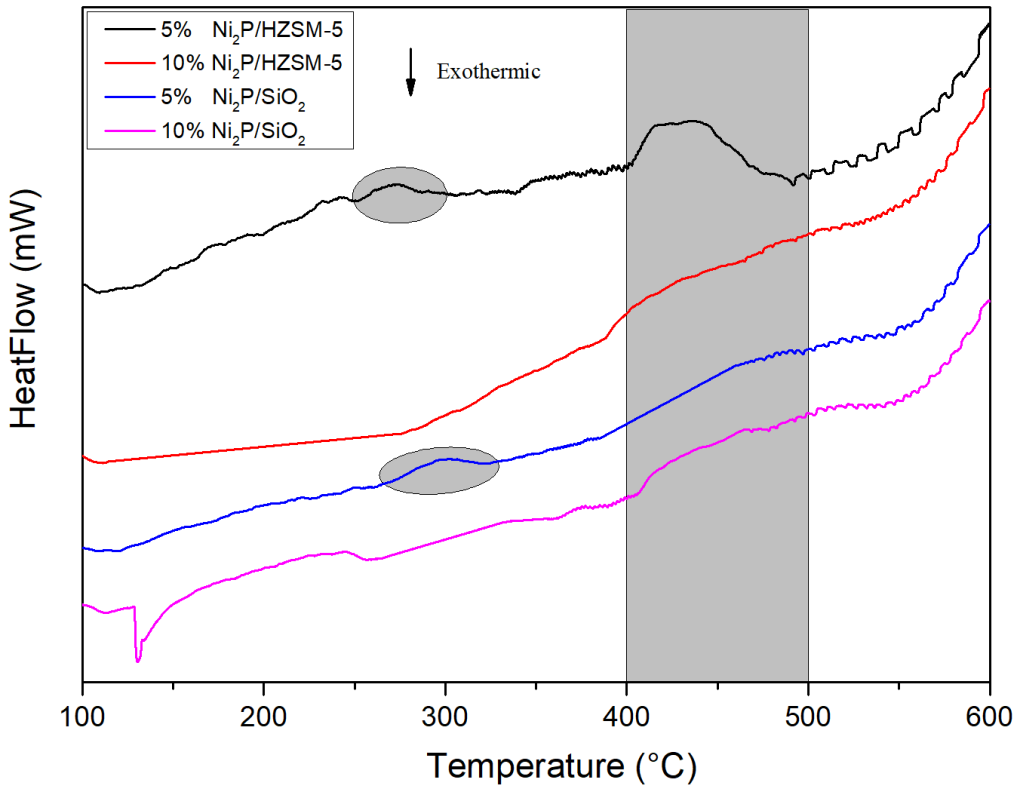

Figure 2.6 H_2-TPR (DSC) profiles of catalysts precursors

2.4 Conclusion

A thorough analysis of the catalysts (5% and 10% Ni_2P/HZSM-5, 5% and 10% Ni_2P/SiO_2) and supports (HZSM-5 and SiO_2) used in this study was presented in this chapter. A decreasing trend of the surface area of catalysts was observed with the increasing amount of nickel phosphide, leading simultaneously to pore filling. XRD characterization showed the presence of crystallized Ni_2P phase on the fresh catalysts' surfaces, respectively. In addition, the results from the pyridine FT-IR profiles provided evidence that the acid sites of HZSM-5, in particular Brønsted type, were partially displaced by the Ni_2P active phase. Also, the high-temperature reduction (H_2-TPR) of the catalysts' precursors followed by passivation during the preparation process of catalysts promotes the formation of acid sites. H_2-TPR (DSC) analysis demonstrated that high acidity of supports and low initial content of Ni and P helped to form a stable size of $Ni_xP_yO_z$ species.

Chapter 3

Catalytic upgrading of bio-oil: hydro-deoxygenation study of acetone as a molecule model of ketones

3.1 Introduction

This study is dedicated to providing detailed data on the HDO of acetone as a molecule model of the bio-oil ketones family over HZSM-5 and Ni_2P catalysts supported on HZSM-5 and silica. Acetone is a common component in pyrolysis bio-oil of biomass, for example, beech wood.[13] Of course, not all ketones will react in the same way as acetone, but it is believed that the majority of ketone molecules react similarly due to their functional group RR′CO. Firstly, the activity and stability of the nickel phosphide catalysts prepared were evaluated for the HDO of acetone. Then, various parameters were examined, such as the nature of the catalysts, the amount of supported phase, contact time (based on the weight of catalysts and feed rate of acetone), temperature, total pressure, and partial pressure of H_2. An in-depth characterization of the liquid and gas products of acetone HDO was performed. Probable HDO pathways for acetone conversion were proposed in my study,[147] which provide significant guidance for the selective preparation of liquid fuels and high-value chemicals from bio-oil.

3.2 Materials and methods

3.2.1 Materials

Acetone (AR, 99.8%) was bought from VWR Chemicals. Dimethyl sulfoxide (DMSO) (GC analysis grade) was supplied by Fisher Scientific. HZSM-5 (Φ=3 mm, L=30 mm, Si/Al ratio 38) was provided by ACS Material LLC. Nonane (AR, 99%) was obtained from Prolabo. Four Catalysts prepared in ***Section 2.2.2***, ***Chapter 2*** were used in this part.

3.3 Catalytic activity tests

3.3.1 Activity test in set-up

The global scheme of the set-up can be seen in ***Figure 3.1***. The HDO reaction of acetone was performed in a continuous fixed-bed reactor of 10 mm inner diameter and 300 mm length. For each run, the flow rate of the liquid feed from a high pressure pump was set to 0.05 mL/min. A catalyst bed of 1 cm height was placed in the middle of the reactor. The volume of the catalyst bed was then calculated based on the reactor's diameter. For example, a weight of 0.43 g of 5% Ni_2P/HZSM-5 is required for each run. Internal and external mass transfer limitations were neglected in a vapor atmosphere of acetone.

The catalyst was reduced in situ in the reactor after eliminating air in the following conditions: a 4:1 ratio of H_2:N_2, pressure of 0.1 MPa, total gas flow rate of 50 mL/min and 450 °C for 30 min. The acetone was vaporized in a preheater at a temperature of 100 °C. The total pressure was increased to the desired value (0.5 MPa) once the catalysts reduction process was complete. During the whole process, the pressure was controlled by a pressure regulator. After a predetermined reaction time of 90 min, the reactor was cooled to room temperature and the pressure dropped to atmospheric pressure. The gas products were collected in a sampling bag for subsequent off-line analysis. The liquid products were gathered in a 100 mL stainless steel condenser (-2 °C) during each run (90 min) for subsequent off-line analysis. The level of experimental error was 2%, which was calculated by experiments repeated three times.

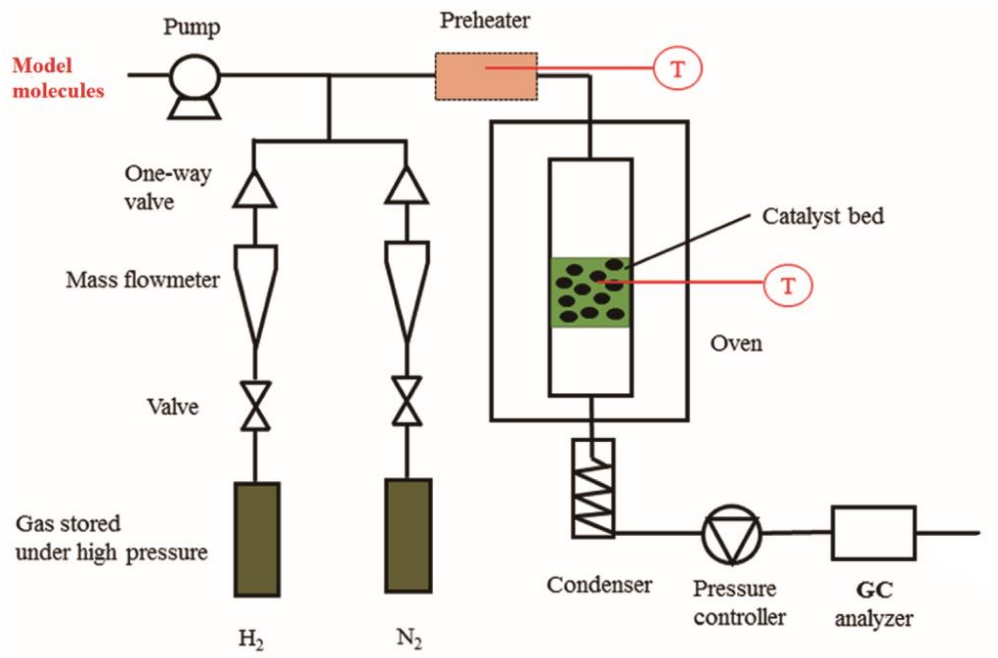

Figure 3.1 Scheme of continuous fixed-bed reactor

3.3.2 Products analysis

3.3.2.1 Liquid products

The analysis of the liquid products was carried out using two different gas chromatography apparatus: a gas chromatography-mass spectrometer (GC-MS) (Clarus 580/SQ8S) system for identification, and another one equipped with the same medium polarity VF-1701-ms column (60 m × 0.25 mm × 0.25 μm film thickness) and a flame ionization detector (GC-FID) to quantify the amounts of compounds in the liquid products. The FID response factors were calculated using the Effective Carbon Number (ECN) method.[148] This method was used to determine the relative response factors corrected by the molecular weight of the compounds relative to n-nonane, which served as the internal standard.

The oven temperature was programmed thus: held at 40 °C for 10 min, and was then increased to 70 °C at 5 °C/min and held for 5 min. It was subsequently ramped up to 100 °C at 6 °C/min and held for 5min, and finally to 250 °C at 10 °C/min and maintained for 7.5 min. A volume of 1 μL of the sample was injected into the column using a split ratio of 30:1 for each analysis. The proportions of the main components in the liquid products were defined as the peak area of the identified component divided by the total area of all identifiable peaks, including the peak for the dimethyl sulfoxide (DMSO) solvent. This analytical method can be used to quantify and identify the vast

majority of chemicals in the liquid products, and can circumvent the effect of the DMSO peak area.

3.3.2.2 Gaseous products

The non-condensable products of acetone HDO were gathered in a 7 L sampling bag and were then analyzed off-line using a Clarus 580 GC instrument from Perkin Elmer. This chromatograph is equipped with two detectors, a thermal conductivity (TCD) (for H_2 and N_2) and a flame ionization detector (FID) (for carbonated components: CH_4, C_2H_2, C_2H_4, C_2H_6, C_3H_4, C_3H_6, and C_3H_8). Helium was used as the carrier gas. The GC instrument was also comprised of a ShinCarbon ST 100 120 column, a methanizer and a hydrogen generator. The CO and CO_2 were detected with the help of the methanizer. The water content of the liquid products was determined using Karl Fischer titration (Metrohm 870 TitrinoPlus) and further verified by the method used for the analysis of the liquid product (that is the total mass of liquid subtracted from all the organic components detected).

The feed conversion X (%) is defined as:

$$X(\%) = \frac{n_{acetone^{inlet}} - n_{acetone^{outlet}}}{n_{acetone^{inlet}}} \times 100\% \quad (3.1)$$

where $n_{acetone^{inlet}}$ is the amount of acetone injected (g), and $n_{acetone^{outlet}}$ is the amount of acetone in the liquid products (g).

The selectivity Sel_i (%) of the chemical product was defined as follows:

$$Sel_i\ (\%) = \frac{Carbon\ number_i \times n_i}{Carbon\ number_{acetone} \times n_{acetone^{converted}}} \times 100\% \quad (3.2)$$

where $Carbon\ number_i$ is the number of carbon atom in the molecular formula of product *i* , e.g. C_3H_8O, $n_i = 3$; n_i: the amount of product *i* (mol); and $n_{acetone^{converted}}$ is the amount of acetone converted (mol).

The degree of deoxygenation DOD (%) was calculated according to the following equation:

$$DOD\ (\%) = 1 - \frac{Mass\ of\ O\ in\ liquid\ products}{Mass\ of\ O\ in\ acetone_{inlet}} \times 100\% \quad (3.3)$$

where $Mass\ of\ O\ in\ liquid\ products$ is the total weight of O in the liquid products (except for water), g; $Mass\ of\ O\ in\ Acetone_{inlet}$ is the total weight of O in acetone injected, g.

The water content $W\ (\%)$ was determined using the following formula：

$$W\ (\%)\ = \frac{Mass\ of\ H_2O\ in\ the\ liquid\ products}{Mass\ of\ liquid\ prodcts} \times 100\% \tag{3.4}$$

The contact time $CT\ (s)$ was found from the following equation:

$$CT\ (s)\ = \frac{V_{space}}{Q_{H_2} + Q_{N_2} + Q_{acetone}} \tag{3.5}$$

where V_{space} is the volume among the catalysts particles; Q_{H_2} is the flow rate of H_2 at normal pressure and room temperature (mL/s); Q_{N_2} is the flow rate of N_2 at normal pressure and room temperature (mL/s); and $Q_{acetone}$ is the flow rate of gaseous acetone at normal pressure and room temperature (mL/s).

3.4 Results and discussion

3.4.1 Activity of different catalysts

Figure 3.2A shows the values for the conversion rate and degree of deoxygenation (DOD) obtained using HZSM-5, 5% Ni_2P/HZSM-5, and 10% Ni_2P/HZSM-5, and the former achieved 87% to 92%. These values were significantly higher than those obtained using catalysts 5% Ni_2P/SiO_2 and 10% Ni_2P/SiO_2. These results showed clearly that the HZSM-5 and its Ni-based supported catalysts were more effective in catalyzing the HDO reaction than Ni-based SiO_2 supported catalysts. The 5% Ni_2P/HZSM-5 catalyst showed the highest conversion rate (92%) and DOD (81%). The low conversion rate of 14% and DOD of 12% were obtained using the 5% Ni_2P/SiO_2 catalyst.

The acetone molecules can be converted to intermediate alcohols through the hydrogenation (HYD) reaction. The C-O groups of intermediate alcohols can be adsorbed on the acid sites of HZSM-5. The activity of HZSM-5 was improved by the Ni_2P active phase, which was indicated by the increase of the acetone conversion with 5% Ni_2P/HZSM-5 and 10% Ni_2P/HZSM-5. Ni_2P active phase can provide the atomic hydrogen required for the HDO reaction, and this role is played by transition metal sites of Ni. The fact that the 5% Ni_2P/HZSM-5 catalyst was more active for DOD than the

10% Ni_2P/HZSM-5 can be attributed to a better dispersion of Ni-P particles. The amount of 5 wt% promotes the formation of smaller particle sizes, which is in agreement with other studies.[99,149] Besides, the surface area of 5% Ni_2P/HZSM-5 is also higher as indicated in ***Table 2.2*** (***Section 2.3.1***, ***Chapter 2***), and the high surface can contribute to improving the reaction efficiency.

The effect of the different catalysts on the distribution of acetone HDO liquid products was also compared in ***Figure 3.2B***. The detailed chemical composition of the liquid products can be seen in ***Appendix B*** (***Table B.1***). As can be seen in ***Figure 3.2B***, the main products were alcohols (ethanol) and aromatic hydrocarbons using the HZSM-5 catalyst with the highest ratio of 17.8% and 64% respectively. No aldehydes were observed with HZSM-5. Notably, the Ni and P modified catalysts 5% Ni_2P/HZSM-5 and 10% Ni_2P/HZSM-5 modified significantly on the distribution of acetone HDO products. Aldehydes percentages of 27.1% and 24.5% and aromatic hydrocarbons percentages of 59.8% and 42.4% were achieved, respectively. The 5% Ni_2P/SiO_2 and 10% Ni_2P/SiO_2 catalysts had a very low selectivity in aromatic hydrocarbons and a low conversion of feed acetone. This illustrated that HZSM-5 is a better support compared to SiO_2.

In addition, the production of acetic acid (5.66%) was observed for the high ratio of active phase of the 10% Ni_2P/HZSM-5 catalyst. This suggested that this acetic acid formation since acetaldehyde (AA) may react with water. Interestingly, in other studies, HZSM-5(100) was considered as the most favorable catalyst for acetic acid ketonization to acetone,[150] and Ga/HZSM-5 was reported as an efficient catalyst in acetic acid ketonization to acetone.[151] Thus, it can be deduced that the high amount of Ni_2P may favor the reverse reaction of ketonization of acetic acid to form acetone and to decrease the conversion rate.

To conclude from ***Figure 3.2A*** and ***B***, the HZSM-5 supported catalysts exhibited better catalytic activity than SiO_2 supported catalysts. For this reason, the 5% Ni_2P/HZSM-5 catalyst was selected for further study, involving various parameters.

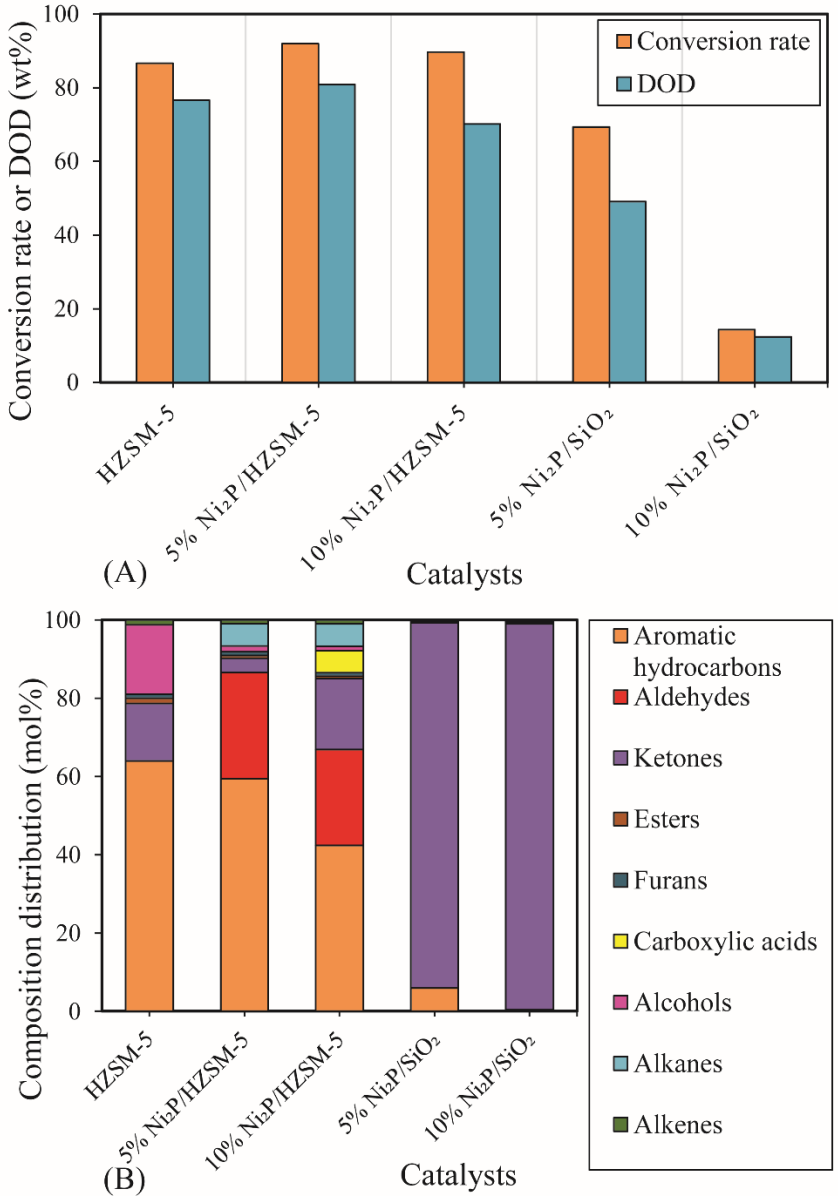

Figure 3.2 Effects of different catalysts on acetone HDO (400 ºC, 0.5 MPa, 0.05 mL/min acetone, 40 mL/min H_2, 10 mL/min N_2, reaction time: 90 min): (A) Conversion rate and DOD, (B) Chemical composition in liquid phase (acetone included in ketones)

3.4.2 Effect of contact time

3.4.2.1 Effect of catalyst mass

From many previous studies, it is clear that the thickness of the catalyst bed always has a great influence on the HDO reaction when varying the contact time. ***Table 3.1*** shows the distribution of hydrocarbons products with different contact times. It can be seen that the target products in the acetone HDO liquid are mainly aromatic hydrocarbons. The increase of contact time is associated with an improvement in the conversion rate.

In particular, although the conversion rate was just slightly enhanced from 70% to 75% when the contact time extended to 0.52 s from 0.27 s, the formation of aromatic hydrocarbons was significantly accelerated. This suggested that the contact time increase greatly promoted the HDO reaction including aldol condensation, isomerization, HYD, and deoxygenation reactions. The formation of alkanes and alkenes is potentially due to the further decarbonylation and deep HYD of methyl isobutyl ketone (MIK). Alotaibi et al. reported that a quantitative yield of 2-methyl pentane was obtained from the HYD of MIK with Pt (0.5 wt%)/CsPW or Ru (5 wt%)/CsPW catalysts.[152]

Table 3.1 also shows the four major components in the upgraded liquid of acetone HDO, which are all aromatic hydrocarbons. The results indicated that the percentages of benzene, toluene, and xylene (BTX) increased clearly with the increase of the contact time from 0.27 to 0.52 s. The formation of aromatics may be due to the deep aldol condensation, isomerization with further deoxygenation, and hydrogenation of acetone under hydrogen pressure. The percentage of toluene and xylene reached 8.45% and 14.11%, respectively. These results proved therefore that the distribution of products was influenced by the contact time.

Table 3.1 Distribution of main hydrocarbons in liquid products with different contact time

CT (s) [a]	Conversion rate (wt%)	Alkanes (mol%)	Alkenes (mol%)	four major components of aromatic hydrocarbons (mol%)			
				Benzene	Toluene	Xylene (p- & o-)	Mesitylene
0.27	70	1.01	0.34	0.56	2.08	2.36	1.04
0.52	75	2.69	-	1.39	8.45	14.11	1.24
1.05	99	0.86	0.34	1.29	8.15	9.04	0.48

[a] fixed conditions: 0.22 g, 0.43g and 0.86 g 5% Ni_2P/HZSM-5, 350 °C, 0.5 MPa, 0.05 mL/min acetone, 40 mL/min H_2, 10 mL/min N_2

3.4.2.2 Effect of feed rate

In order to evaluate the effect of the contact time on acetone HDO in other ways, a series of experiments at 450 °C were conducted at different feed rates of acetone in the range between 0.025 and 0.1 mL/min corresponding to the contact time from 0.59 s to 0.42 s. *Figure 3.3* depicts the major aromatic hydrocarbons (benzene, toluene, and

xylene) present in the products. It can be seen that a conversion rate of 94% to 100% can be achieved in these conditions. This suggested that the lowest contact time with a feed rate of 0.1 mL/min was also highly-efficient for the acetone HDO at 450 °C. The results demonstrated that the selectivity of benzene, toluene, and xylene increased with the decrease of the contact time from 0.59 s to 0.54 s, and then decreased when the contact time was reduced to 0.42 s. It can be deduced that the formation of BTX from acetone required multiple reaction steps and several acetone molecules to form aromatic hydrocarbons and that the feed rate influenced the contact time of the acetone molecules on active sites of the catalyst.

On the other hand, the excessive feed rates of 0.075 and 0.1 mL/min were performed at a low contact time, which suppressed the further reaction of intermediates to form BTX. The BTX was found to form with the highest selectivity in the case of 0.54 s corresponding to the medium feed rate of 0.05 mL/min. The selectivity of benzene, toluene, and xylene achieved 5.11%, 20.23%, and 23.62%, respectively.

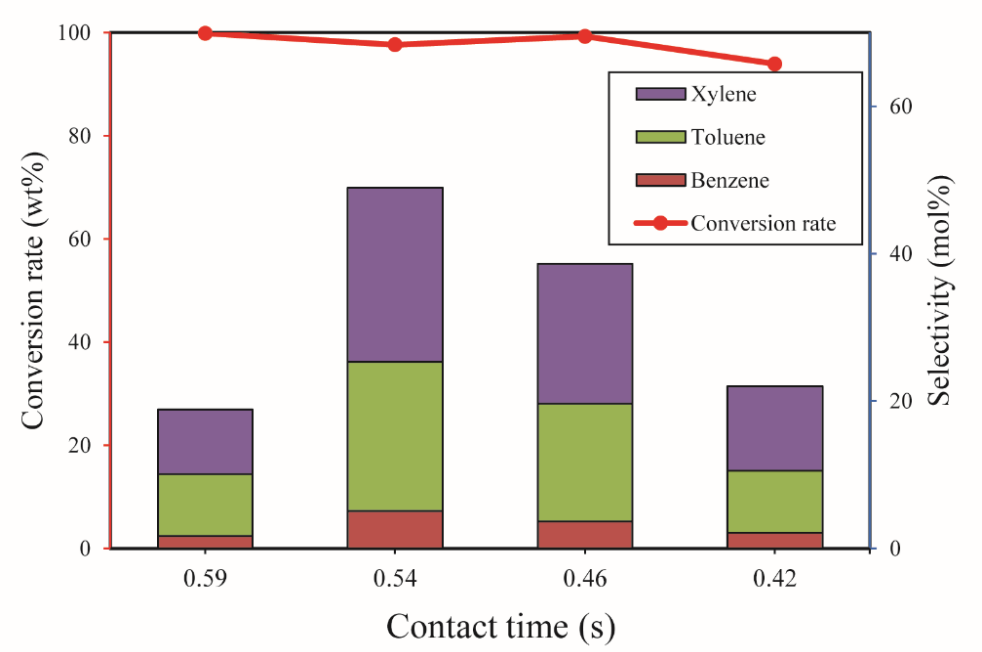

Figure 3.3 Effect of the feed rate of acetone on acetone HDO (0.43 g 5% Ni_2P/HZSM-5, 450 °C, 0.5 MPa, 40 mL/min H_2, 10 mL/min N_2, reaction time: 90 min)

3.4.3 Effect of temperature

In order to evaluate the effect of the reaction temperature, experiments were carried out with different temperatures of 200 °C, 250 °C, 300 °C, 350 °C, 400 °C, and 450 °C.

The influence of the temperature on the values of the conversion rate, DOD, and water content in the upgraded liquid is demonstrated in ***Figure 3.4A***. The results exhibit an increasing trend in the acetone conversion rate from around 28% to 98% when the temperature increased from 200 to 450 °C. The value of DOD increased from 11.6% to 83.5% with the increase of temperature. These results suggested that the temperature had a great effect on the conversion rate and DOD of acetone HDO but also on the product distribution.

Figure 3.4B shows curves for the main products' selectivity as a function of temperature over the 5% Ni_2P/HZSM-5 catalyst at 0.5 MPa. The selectivity of AA and BTX can reach 8.1% and 49.0% at 450 °C, respectively. The formation of BTX increases rapidly with the increase of temperature from 300 to 450 °C; however, the selectivity of BTX is very low when the temperature is lower than 300 °C.

Figure 3.4B also illustrates that a lot of MIK was formed when the temperature was below 300 °C, and the selectivity of MIK can reach around 29% in the temperature range of 200-250 °C. The linear MIK was probably obtained mainly due to the acetone through an aldol condensation reaction. Similar results were observed by Kong et al. during Kraft lignin catalytic hydrodeoxygenation over some nickel-based zeolite catalysts in a batch reactor system,[153] and by Zhang et al. during acetone HDO with NiMo carbide supported on SiO_2 in a fixed bed continuous reactor.[154] These results illustrated that there are few little limitations on the hydrogenation step from acetone to MIK, but a strong thermodynamic equilibrium limitation of the further condensation of MIK and acetone to aromatic hydrocarbons. This behavior was confirmed by other workers.[155,156]

The maximum water content of 39.5% was obtained at 300 °C. This can be attributed to a notable decrease in the selectivity of MIK (***Figure 3.4B***) with the increase in temperature, which was accompanied by the main dehydration to form water. Above 300 °C, the water content was decreased, probably because of the acceleration of C-C bond cleavage to form more AA. The further hydrogenolysis of AA can produce CO. The production of CO and CO_2 is therefore secondary.

The emission of various gases during the acetone HDO reaction provides a pivotal information about the main catalytic reactions. ***Figure 3.4C*** shows the selectivity of the gas products for acetone HDO as a function of temperature. The main gases obtained in this study were CO, CH_4, CO_2, C_2H_4, C_2H_6, C_3H_6 and C_3H_8. It was observed that the

temperature had a significant effect on the gas products of acetone HDO. Below 300 °C, it can be seen that the main gas obtained was C_3H_8 followed by C_3H_6, and a small amount of CO was observed. This fact reveals that hydrogenation was favored by low temperature. ***Figure 3.4C*** also suggests that the selectivity of C_3H_8 decreased with the increase in temperature below 350 °C, but, that tendency of the selectivity of C_3H_8 was completely opposite above 350 °C. Considerable CO was released because of the cracking of either carbonyl (RR′CO) or carboxyl (RCO_2H) functional groups.[157] The main gas products were CO_2, C_2H_6, C_3H_6, and C_3H_8 at high temperatures. CO_2 can be produced through water-gas shift reaction using in-situ produced CO and water vapors.[158] The cracking of the C-C bond of acetone can form AA (***Figure 3.4B***). Therefore, C_2H_6 can be formed through the deoxygenation of AA followed by HYD. The direct deoxygenation and HYD of acetone can lead to C_3H_6 and C_3H_8.

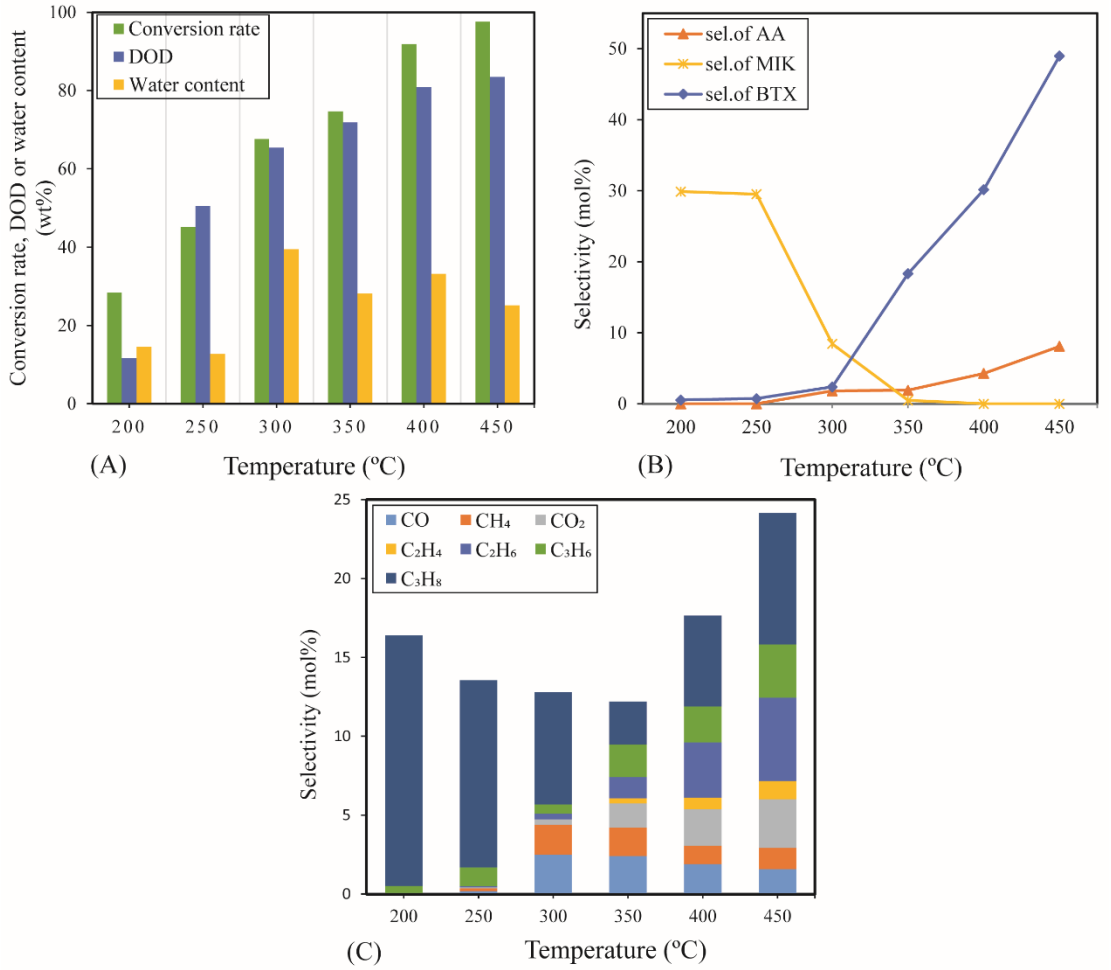

Figure 3.4 The influence of acetone HDO at different temperature (0.43 g 5% Ni_2P/HZSM-5, 0.5 MPa, 0.05 mL/min acetone, 40 mL/min H_2, 10 mL/min N_2, reaction time: 90 min): (A) Conversion rate, DOD and water content, (B) Selectivity of major liquid products, (C) Selectivity of gas products

3.4.4 Effect of reaction total pressure

To assess the effects of the reaction pressure, experiments were performed at 0.1, 0.5, 1, and 2 MPa. ***Figure 3.5*** shows the curves of the acetone conversion rate and the main product selectivities as a function of total pressure over the 5% Ni_2P/HZSM-5 catalyst at 450 °C. The results indicated an increasing trend of the acetone conversion rate from around 92% to 100% with an increase in pressure from 0.1 to 1 MPa, and full conversion was reached above 1 MPa. Below 0.5 MPa, the selectivity of AA showed a slight increase, and then a small decrease was observed when the pressure rose to 2 MPa. Meanwhile, the selectivity of ethanol first decreased and then increased. It is suggested that the AA can be converted to ethanol via hydrogenation of C=O bonds with the increase of pressure. A similar result was also found in other works.[154]

The selectivity of BTX showed almost the same value of 49% with the pressure of 0.5 MPa and 1 MPa. However, an increase in pressure had almost no effect on the DOD suggesting that the increase of pressure scarcely affected the deoxygenation reaction of acetone. On the other hand, the formation of BTX increased rapidly with the increase in pressure from 0.1 to 0.5 MPa. From 0.5 to 1 MPa, the selectivity of BTX underwent few changes. The slight decrease of the selectivity of BTX can be linked to the much greater formation of other aromatic hydrocarbons, such as mesitylene and ethylbenzene.

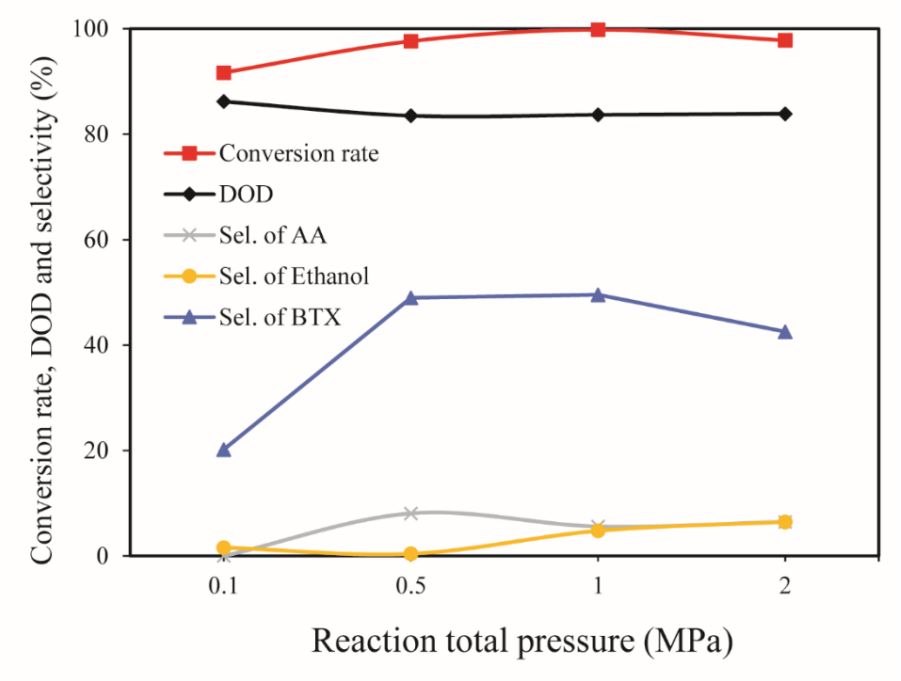

Figure 3.5 Effect of total pressure on acetone HDO (0.43 g 5% Ni_2P/HZSM-5, 450 ºC, 0.05 mL/min acetone, 50 mL/min H_2+N_2, H_2:N_2 = 4:1, reaction time: 90 min)

3.4.5 Effect of H_2/N_2 ratio

Figure 3.6 shows the curves for the acetone conversion rate and product formation (selectivity) as a function of the H_2/N_2 ratio over the 5% Ni_2P/HZSM-5 catalyst at a pressure of 0.5 MPa. The results showed a slight decreasing trend of acetone conversion from approximately 92% to 84% and a significant decrease in DOD with a decrease in the H_2/N_2 ratio. The formation of BTX was not greatly affected when the H_2/N_2 ratio decreased from 40:10 to 30:20, but a distinct decrease was noted at an H_2/N_2 ratio of 20:30 due to the suppression of HYD. Besides, the DOD curve showed a significant decrease when the partial pressure of H_2 decreased. This evolution attests that the high H_2 concentration has a remarkable effect on the acetone HDO reaction, and mainly affects the hydrogenolysis of C-O bonds. The selectivity of AA and ethanol was stable and stayed at similar values. Compared to the result of *Figure 3.5*, it can be deduced that the H_2 partial pressure does no effect on the hydrogenation of AA to form ethanol under a low total pressure of 0.5 MPa. Noticeably, in comparison to the temperature, the pressure has less of an effect on the HDO conversion.

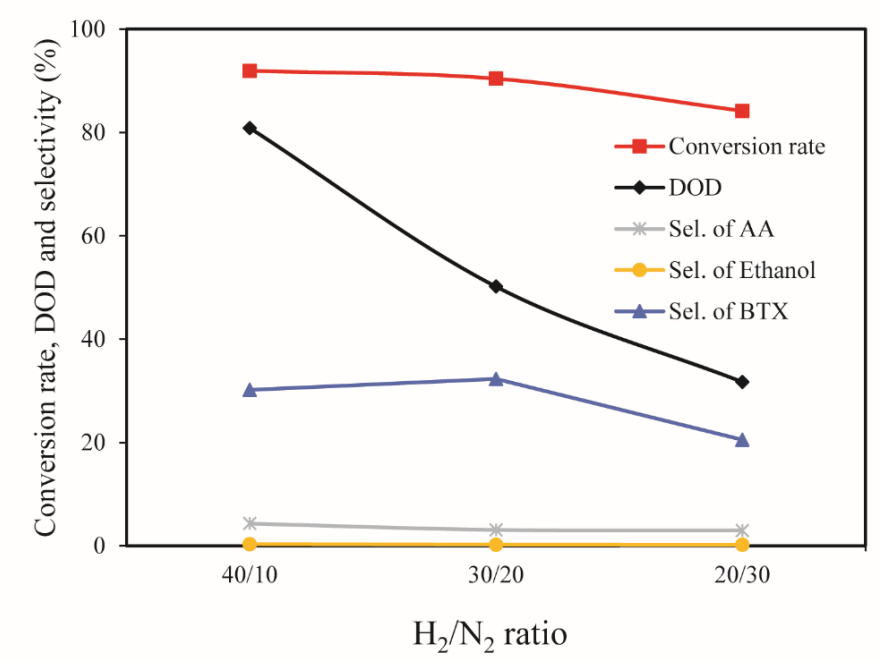

Figure 3.6 Effect of H_2/N_2 ratio on acetone HDO (0.43 g 5% Ni_2P/HZSM-5, 400 °C, 0.5 MPa, 0.05 mL/min acetone, 50 mL/min H_2+N_2, reaction time: 90 min)

3.4.6 Proposed reaction pathways of acetone HDO

Based on the products formed, a set of reaction pathways for the HDO of acetone is proposed in ***Table 3.2***. These pathways involve several basic reaction intermediates.[112,153,154,159,160] Reaction (1) corresponds to the demethylation of acetone to AA, together with the formation of CH_4. Notably, AA is a primary product of acetone HDO. From the aforementioned results, ethanol is a minor product in most cases, which suggests that reaction (2) is an HYD reaction of AA produced by reaction (1), forming ethanol as a secondary product. Reaction (3) is an acetone directly hydrogenated reaction over the metal function to IP, and that is subsequently dehydrated to C_3H_6 over the acidic function support HZSM-5 in reaction (4).[112] Acetone conceivably undergoes self-aldol condensation on acid sites of Ni_2P/HZSM-5 to rapidly convert to MIK in reaction (5). MIK is considered to be a crucial product at low temperatures. Similarly, Gamman et al.[156] reported an aldol condensation reaction pathway of acetone to form MIK over Pd/MgO/SiO_2 catalysts. Reaction (6) is the mainly hydrogenated reaction to form propane. The aromatic hydrocarbons (BTX, ethylbenzene, and mesitylene) can be formed by a further aldol condensation between MIK and acetone molecules, followed by dehydration and HYD. For example, mesitylene can be formed through that route.[156,161] In addition, other alkylbenzenes were probably produced via further

isomerization and deoxygenation reaction of intermediates (C_6-C_9 ketones). Reaction (7) illustrates a reversible reaction between acetone and acetic acid.

Table 3.2 The proposed HDO pathways of acetone

Entry	Main products	Main reaction pathways	
1	Acetaldehyde (AA)	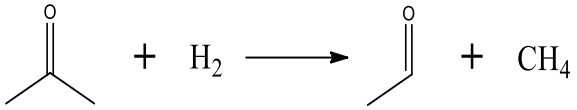	(1)
2	Ethanol	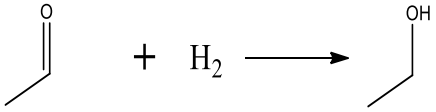	(2)
3	Isopropanol (IP)	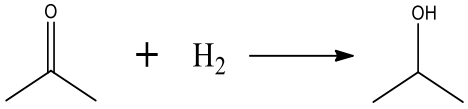	(3)
		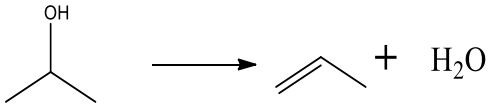	(4)
4	Methyl isobutyl ketone (MIK)	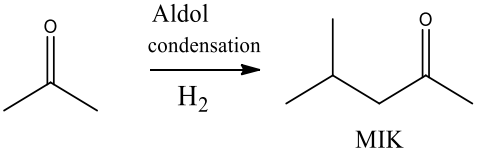	(5)
5	Propane	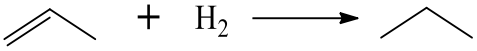	(6)
6	Acetic acid	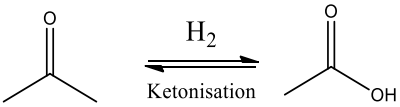	(7)

3.5 Conclusion

Commercial HZSM-5 and prepared Ni_2P/HZSM-5 and Ni_2P/SiO_2 catalysts for HDO of acetone as a molecule model of ketones of bio-oil were studied. The catalysts with zeolite exhibited higher activity than catalysts with SiO_2. The results showed that the temperature had the most significant effect on the acetone HDO. The temperature affected not only the conversion rate but also the selectivity of products (AA, BTX, MIK, and gas products). Aromatic hydrocarbons (benzene, toluene, xylene) with high octane numbers were the primary liquid products. In most cases, CO_2, C_2H_6, C_3H_6, and C_3H_8 were observed to be the dominant gas products. It was certified that the principal influencing parameters of acetone HDO were the temperature and contact time, followed by the reaction pressure and H_2 partial pressure. High selectivity of aromatic

hydrocarbons was achieved with the 5% Ni_2P/HZSM-5 catalyst. MIK and aromatic hydrocarbons were formed by a multiple-step aldol condensation reaction of acetone molecules followed by further hydrogenation.

Chapter 4

Catalytic hydro-deoxygenation of acetic acid, 4-ethylguaiacol, and furfural as model molecules of pyrolysis bio-oil

4.1 Introduction

This work is dedicated to studying the HDO of various model molecules over Ni_2P catalysts supported on HZSM-5, with the aim of making the HDO mechanism easier to understand. The comparative study of the different model molecules was carried out in the same device and under similar experimental conditions. Acetic acid, 4-ethylguaiacol, and furfural were selected as model molecules of bio-oil due to their abundance in pyrolysis oil.[13] Various parameters involving the nature of the catalysts, amount of supported phase, temperature and pressure were examined. Based on detailed analyses of gas and liquid products, pathways for the main reactions of acetic acid, 4-ethylguaiacol, and furfural HDO were thus proposed, giving further guidance for the catalytic upgrading of bio-oil.

4.2 Materials and methods

4.2.1 Materials

Acetic acid (analytical reagent grade, ≥99.7%) and isopropanol (IP) (GC analysis grade) were supplied by Fisher Scientific. Furfural (AR, 99%) and 4-ethylguaiacol (AR, ≥98%) were acquired from Aldrich. Ni_2P/HZSM-5 catalysts used in this Chapter can be found in ***Section 2.2.1***, ***Chapter 2*** .

4.2.2 Activity test in set-up

The HDO reaction of acetic acid, 4-ethylguaiacol, and furfural were performed individually in a continuous fixed-bed reactor illustrated in ***Figure 3.1***, ***Chapter 3*** . The experimental set-up and most of the operation conditions are the same as the case of acetone HDO (see ***Chapter 3*** , ***Section 3.3.1***). The differences were that the liquid reagent, acetic acid, 4-ethylguaiacol, or furfural was vaporized in a preheater at a temperature of 150 °C, 260 °C, or 200 °C, respectively. The total pressure was increased to the

desired value of 0.5 MPa or 2 MPa for acetic acid HDO and 0.5 MPa or 3 MPa for 4-ethylguaiacol or furfural HDO, and the temperature went to the designed value of 300 - 500 °C once the catalysts reduction process was completed.

4.2.3 Products analysis

The analysis of the liquid and gas products was carried out using the same instruments and methods discussed in ***Section 3.3.2*** (***Chapter 3***). The only difference was that isopropanol (IP) was selected as a solvent to better analyze the liquid products. In order to analyze the experimental results and to better understand the evolution of each model molecule, the conversion rate, selectivity, degree of deoxygenation (*DOD*) (see ***Chapter 3*** , ***Section 3.3.2.2***), and mass yield were used. The expression of mass yield is given in the following:

The yield Y_i (%) of reaction products (liquid, gas, and water) was determined using the formula：

$$Y_i\ (\%) = \frac{Mass\ of\ product_i}{Mass\ of\ feed} \times 100\% \quad (4.1)$$

where $Mass\ of\ product_i$ is the mass of product *i* in grams; e.g. mass of H_2O, *i* = H_2O; $Mass\ of\ feed$ is the total mass of the model molecule and H_2 consumed in grams.

4.3 Results and discussion

Based on the detailed liquid products and gaseous analysis of the HDO reaction model compounds of the bio-oil, the results are reported and discussed in connection with the effect of three main parameters, the catalyst, temperature, and pressure.

4.4 HDO of acetic acid

First of all, HDO of acetic acid using both the 5% and 10% Ni_2P/HZSM-5 catalysts was carried out. The specific results were presented in ***Appendix C*** (***Table C.1*** and ***Figure C.1***). In summary, both of the two catalysts exhibited excellent catalytic activity for HDO reaction, and a similar behavior of them was observed. Then, the 5% Ni_2P/HZSM-5 catalyst was thus selected for further study.

4.4.1 Effect of temperature and pressure

4.4.1.1 Conversion rate, DOD, and yield

The values of the conversion rate, DOD, and yield (liquid, gas, and H_2O) of acetic acid HDO reaction as a function of temperature and pressure are summarized in ***Table 4.1***. The results exhibited a significantly higher conversion rate (97%) and DOD (95.7%) at 450 °C than at 350 °C, suggesting that temperature had a conspicuous effect on the catalytic activity of Ni_2P/HZSM-5. The maximum yield of 50.19% for gas products was obtained at 450 °C accompanied by the minimum yield of liquid products (28.16%, H_2O free). This evolution can be attributed to a notable increase in the thermal decomposition of C-C hydrogenolysis for acetic acid followed by dehydration and hydrogenation reactions to give more gas products, especially, CO and CO_2. In a previous study, Badari et al.[162] found similar results during acetic acid HDO using a Ni/SiO_2 catalyst, namely, that this catalyst favored the C-C bond hydrogenolysis to form lighter gaseous products.

As concerns the water content, it first increased, and then decreased when the temperature increased from 350 °C to 450 °C. This suggested that dehydration was the main reaction of acetic acid HDO at 400 °C, but more decarboxylation was favored to form CO_2 at 450 °C, which is confirmed in the following section (***Figure 4.1B)***. At 350 °C, a higher yield of gas products (45.16%) and lower content of H_2O (13.52%) was obtained under 2.0 MPa, indicating a marginal improvement of the conversion rate, DOD, and gas generation, but a reduction of direct dehydration by increasing the pressure.

Table 4.1 Effect of temperature and pressure on acetic acid HDO

Item	Conditions [a]			
	0.5 MPa	0.5 MPa	0.5 MPa	2.0 MPa
	350 °C	400 °C	450 °C	350 °C
Conversion rate & DOD (wt%)				
$X_{\text{Acetic acid}}$	61	80	97	69
DOD	59.2	76.5	95.7	68.1
Yield of products (wt%)				
$Y_{\text{Lip. (free water)}}$	43.06	33.09	28.16	41.32
Y_{Gas}	40.05	41.02	50.19	45.16
Y_{H_2O}	16.89	25.89	21.65	13.52

[a] fixed conditions: 0.43 g 5% Ni_2P/HZSM-5 catalyst, 0.05 mL/min of acetic acid, H_2: 40 mL/min, N_2: 10 mL/min, 90 min

4.4.1.2 Selectivity in the liquid phase

In order to better understand the main reaction pathway of acetic acid HDO, the selectivity of major products is shown in ***Figure 4.1A,*** varying the temperature and pressure. Details of the chemicals identified in the liquid phase can be seen in ***Appendix B*** (***Table B.2***). The results exhibited a significantly increasing trend in the selectivity of BTXM (benzene, toluene, xylene, and mesitylene) from around 4.76% to 18.66% when the temperature increases from 350 °C to 450 °C. In other work, Thompson et al.[163] reported that mesitylene was formed via aldol condensation between mesityl oxide (MO) and acetone during the investigation of acetone condensation over molybdenum nitride and carbide catalysts. Wigzell et al.[164] also proposed the same reaction route during the synthesis of methyl isobutyl ketone (MIK) over Pd/MgO/SiO_2. On the other hand, MO was not detected in our work, which can be explained by the fact that the reaction from MO to MIK is spontaneous (enthalpy: ΔH_{400K} (kcal/mol) = -14.5; Gibbs free energy: ΔG_{400K} (kcal/mol) = -12.1).[164,165] Here, it can thus be speculated that the formation of BTXM can be caused by a further aldol condensation between mesityl oxide (MO) and acetone, followed by dehydration, hydrogenation, and isomerization.

Acetone was identified as the main product below 400 °C due to the self-ketonization reaction of acetic acid. This reaction was also observed in the catalytic upgrading of carboxylic acids by Huo et al.[166] and also in catalytic steam reforming of acetic acid by Zhang et al.[167] using a series of Ni/Al_2O_3 and Ni-Ba/Al_2O_3 catalysts. The linear MIK was probably obtained at 350 °C passing through the acetone by an aldol condensation

reaction.[168] These results indicate that the high temperature promotes the condensation reaction to form dimers and trimers.[30,33][166,169] Above 400 °C, the selectivity of acetone decreased sharply from 11.21% to 1.32%, which can be attributed to the conversion of acetone to aromatic hydrocarbons. In addition, acetaldehyde was observed at low temperatures (350 °C and 400 °C) owing to the direct dehydration of acetic acid.

4.4.1.3 Selectivity in the gas phase

Figure 4.1B shows the selectivity for gas products over the 5% Ni_2P/HZSM-5 catalyst at different temperatures and pressures. Gases obtained were CO, CH_4, CO_2, C_2H_4, C_2H_6, C_3H_6, and C_3H_8. At 350 °C, similar values were observed under the two different pressures, and the highest selectivity for CO (44.22%) and CH_4 (32.54%) were obtained under 2.0 MPa. The lower values of the selectivity of CO, CH_4, and C_2H_6 were attained at 400 °C and 450 °C compared to those obtained at 350 °C.

At 400 °C and 450 °C, the results also demonstrated a higher selectivity of gaseous olefins (C_2H_4 and C_3H_6) compared to 350 °C. C_2H_4 and C_3H_6 are derived from the direct deoxygenation and hydrogenation of acetaldehyde and acetone over the acid sites of the HZSM-5, respectively, and are favored by high temperature. Significant amounts of CO and CO_2 were released because of the cracking of either carbonyl (RR′CO) or carboxyl (RCO_2H) functional groups.[170] The further hydrogenation of C_2H_4 and C_3H_6 can lead to C_2H_6 and C_3H_8.

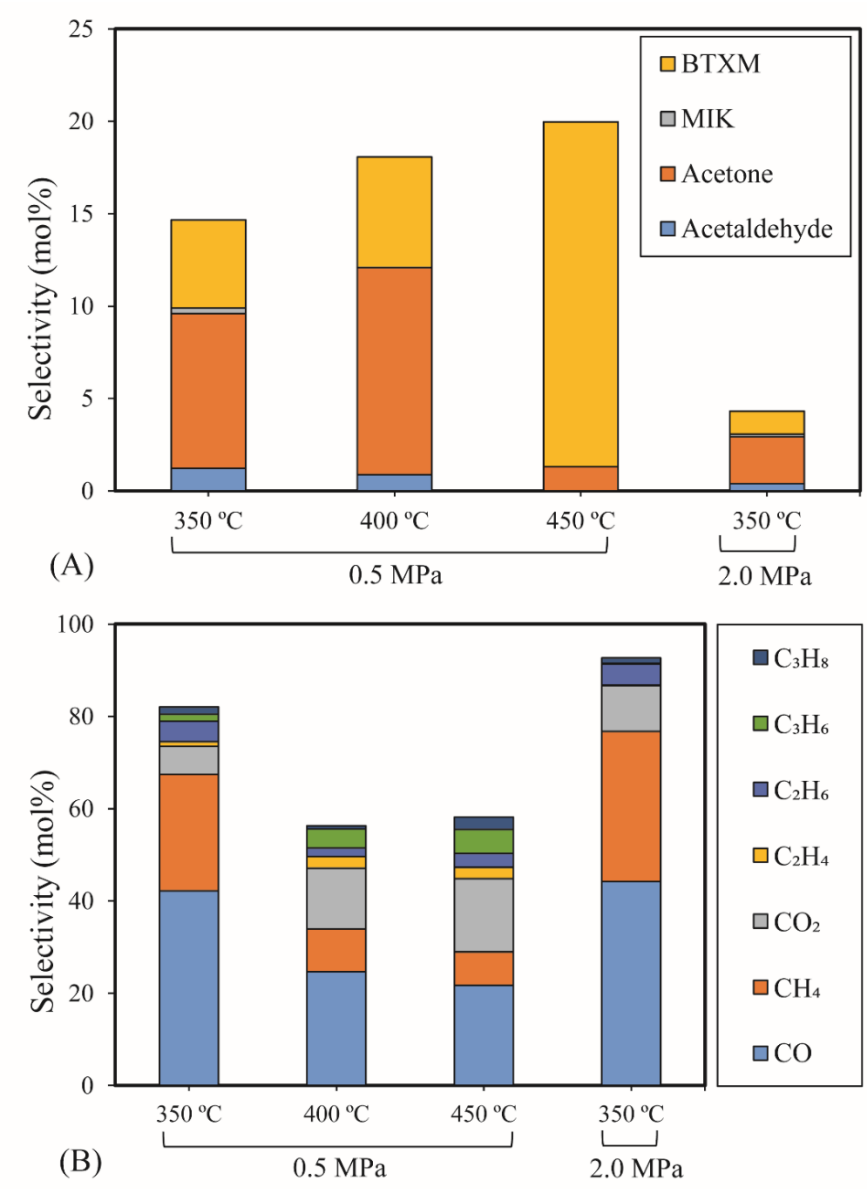

Figure 4.1 The influence of temperature and pressure on acetic acid HDO (0.43 g 5% Ni_2P/HZSM-5, 0.05 mL/min acetic acid, 40 mL/min H_2, 10 mL/min N_2, reaction time: 90 min): (A) Selectivity of major liquid products; (B) Selectivity of gas products

4.4.2 Proposed reaction pathways for acetic acid HDO

Based on the products formed, a set of reaction pathways for the HDO of acetic acid is proposed in ***Table 4.2***. These pathways involve several basic reaction intermediates.[166,168,171–173] Reaction (1) is an acetic acid direct self-ketonization and decarboxylation reaction on a coordinatively unsaturated metal site of catalyst to a ketene ($R_2C{=}C{=}O$) intermediate, and then to form acetone, CO_2 and H_2O.[174] Acetone is subsequently dehydrated to C_3H_6 over the acidic function HZSM-5 in reaction (2).[175]

Reaction (3) corresponds to the deoxygenation of acetic acid to acetaldehyde, together with the formation of H_2O. Reaction (4) is a dehydration reaction of acetaldehyde produced by the reaction (3), forming C_2H_4 and H_2O. Reaction (5) is an aldol condensation reaction of acetone molecule to produce diacetone alcohol and MO intermediates followed by dehydration and hydrogenation to form MIK.[163,168] Mesitylene can be formed by a further aldol condensation between MO and acetone molecules followed by dehydration and hydrogenation in reaction (6).[163,164] Mesitylene can be further converted to other aromatic hydrocarbons via demethylation and/or alkyl substitution, such as BTX (benzene, toluene, and xylene) and ethylbenzene. Reaction (7) is the main hydrogenated reaction to form propane.

Table 4.2 Proposed reaction pathways of HDO of acetic acid

Main products	Main reaction pathways	
Acetone	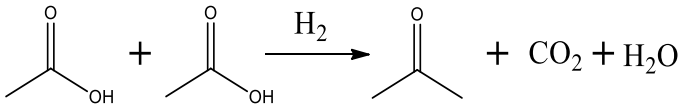	(1)
	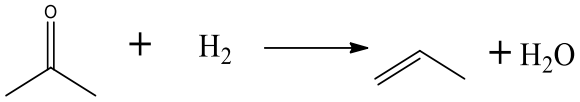	(2)
Acetaldehyde (AA)	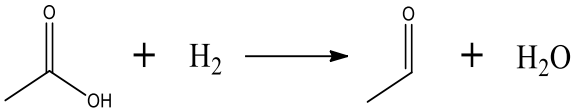	(3)
Ethylene	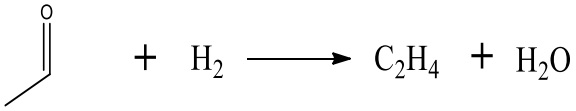	(4)
Methyl isobutyl ketone (MIK)	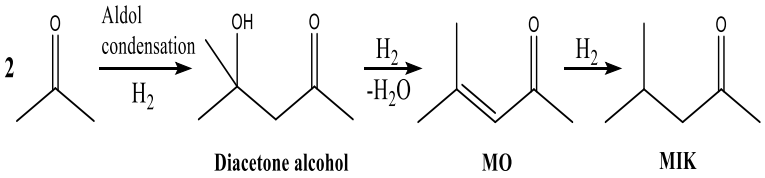	(5)
Mesitylene	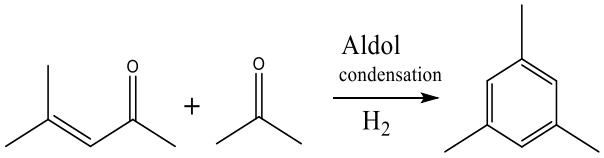	(6)
Propane	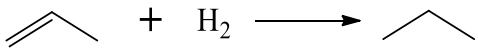	(7)

4.5 HDO of 4-ethylguaiacol

4.5.1 Effect of temperature and pressure

4.5.1.1 Conversion rate, DOD, and yield

Table 4.3 illustrates the influence of temperature and pressure on the conversion rate of 4-ethylguaiacol, DOD, and the yield of products for HDO reaction of 4-ethylguaiacol. The evolution of the conversion rate of 4-ethylguaiacol and DOD showed a small improvement when the temperature increased from 300 °C to 500 °C. At 400 °C, a significant increase of the conversion rate (84%) and DOD (50.6%) under 3.0 MPa was obtained compared to 0.5 MPa, demonstrating that the pressure had a greater effect on the conversion rate and DOD than the temperature.

It can be seen in *Table 4.3* that the yield of gas products and the amount of H_2O exhibited an increasing trend as the temperature increased. This can be attributed to an increase of the direct deethylation of 4-ethylguaiacol to form C_2H_6, C-O bond cleavage of the methoxy group for producing CH_4, and further dehydroxylation of phenols intermediates to give H_2O. The highest yield of 31.56% for gas products and of 14.19% for H_2O was accompanied by the lowest yield of liquid products (50.45%, H_2O free) at 500 °C.

In addition, a notable amount of coke (3.80%) was formed at 500 °C, although no coke formation was observed at lower temperatures (300 °C and 400 °C). It is clear that coke formation is favored by the increase of temperature, probably via the condensation of 4-ethylguaiacol during the demethoxylation reaction. In other studies, Laurent et al.[71] also reported that guaiacols lead potentially effortlessly to coke formation during the hydrotreatment of biomass pyrolysis oils. Gayubo et al.[176] found a notable coke formation from the upgrading of 2-methoxyphenol over ZSM-5 at high temperatures.

Table 4.3 Effect of temperature and pressure on 4-ethylguaiacol HDO

Item	Conditions [a]			
	3 MPa	3 MPa	3 MPa	0.5 MPa
	300 °C	400 °C	500 °C	400 °C
Conversion rate & DOD (wt%)				
$X_{4\text{-Ethylguaiacol}}$	75	84	83	44
DOD	42.8	50.6	52.8	24.4
Yield of products (wt%)				
$Y_{\text{Liq. (free water)}}$	79.25	70.55	50.45	87.24
Y_{Gas}	11.92	20.21	31.56	7.84
Y_{H_2O}	8.82	9.24	14.19	4.92
Y_{Coke}	-	-	3.80	-

[a] fixed conditons: 0.43 g 5% Ni_2P/HZSM-5 catalyst, 0.05 mL/min of 4-ethylguaiacol, H_2: 40 mL/min, N_2: 10 mL/min, 90 min

4.5.1.2 BTX selectivity

Figure 4.2A shows the selectivity values of major products of 4-ethylguaiacol HDO as a function of temperature (300 °C, 400 °C, and 500 °C) and pressure (3 MPa and 0.5 Mpa). The detail of the chemicals in the liquid products can be seen in ***Appendix B*** (***Table B.3***). The results revealed that the Ni_2P catalyzed the HDO of 4-ethylguaiacol to produce oxygen-free aromatic hydrocarbons (benzene, toluene, and xylene, etc.), mono-oxygenated aromatics (phenol, cresol (o- & p-), 2,4-dimethylphenol (DMP), etc.). At 300 °C, selectivities of 12.36% for DMP and 3.29% for 2-methoxy-4-methyl-1-(1-methylethyl)-benzene (MMMEB) were obtained under 3 MPa. DMP was the major product of 4-ethylguaiacol HDO. The results under 3 MPa showed that the selectivity of MMMEB and DMP decreased when the temperature increased from 300 °C to 500 °C. This suggested that 4-ethylguaiacol was first converted to DMP via deethylation and methoxy removal, followed by alkylation/transalkylation, and the MMMEB was formed by dehydroxylation, alkylation/transalkylation and/or isomerization of 4-ethylguaiacol. These reaction pathways can be explained by the presence of a Lewis basic benzene ring of guaiacol molecules, which should be chemisorbed on Lewis acidic Ni sites of Ni_2P phase at the outset of the reaction, and then be transformed into derivatives.[177] In particular, the outset reactions needed active H species to cleave C_{aromatic}-OCH_3 bonds since the PO-H groups on Ni_2P phase (***Chapter 2*** , ***Section 2.3.3***) allowed spillover of the H species to the chemisorbed guaiacol on the Ni sites of Ni_2P,[178] and then further transalkylation occurred on Brønsted acid sites.[179]

4.5.1.3 Cresol selectivity

In particular, the selectivity of cresol in ***Figure 4.2A*** first increased and then decreased as the temperature increased. In addition, the selectivity of phenol and BTX increased as the temperature rose. These results can be explained by the fact that the initial increase of cresol is due to the demethylation of DMP, and the following decrease to further demethylation and/or dehydroxylation to form phenol and aromatic hydrocarbons. The high temperature favored C-C and C-O bond cleavage between the aromatic ring and its branched chains. The highest selectivity of cresol (16.22%) was obtained at 400 °C and 3 MPa.

4.5.1.4 MMMEB selectivity

At 400 °C and under 0.5 MPa, it was observed in ***Figure 4.2A*** that the selectivity of MMMEB (2.93%) and DMP (14.09%) was higher than that obtained under 3 MPa, while the selectivity of cresol (8.26%), phenol (4.68%), and BTX (2.46%) decreased significantly. It is therefore clear that the high pressure favored the further reaction of MMMEB and DMP to form cresol, phenol, and BTX. Subsequently, cresol and phenol underwent dehydroxylation and/or demethylation to produce BTX. In the literature, it was also reported that BTX can be formed by dehydroxylation and/or dealkylation of phenols.[120,180,181] Other phenols identified in the liquid phase, such as 3-methyl-4-isopropylphenol and 2-ethyl-6-methylphenol, are probably produced via the isomerization of reaction intermediates. Notably, the selectivity of 2-ethyl-6-methylphenol first decreased due to a further dealkylation and then increased due to coke formation. Probably, the coke affected the pore size of the catalysts, which suppressed further dealkylation.

4.5.1.5 Gas products selectivity

Figure 4.2B shows the evolution of the selectivity of gas products for 4-ethylguaiacol HDO over the 5% Ni_2P/HZSM-5 catalyst at different temperatures and pressures. As can be seen, the selectivity of gas products increased with the increase of temperature. The main gas product was C_2H_6 at 300 °C and 400 °C, followed by C_3H_8 or CH_4. At 500 °C, CH_4 and C_2H_6 were the major products in gas phase. C_2H_6 can be produced via deethylation of 4-ethylguaiacol followed by hydrogenation. CH_4 can be formed via various reaction routes, mainly via methoxy removal from 4-ethylguaiacol followed by

further C-O bond to give some CO and, to a lesser extent, via direct demethylation of cresol intermediate.

The increase in selectivity of CH_4 and C_2H_6 revealed that the high temperature promotes C-O bond cracking of the methoxy group and multiple C-C hydrogenolysis of 4-ethylguaiacol and other intermediates. Chen et al.[182] found that methane was yielded as a main gas product in the hydrogenation of m-cresol via C-C bond cleavage on silica supported Ni catalyst. The highest selectivity of C_2H_6 (10.58%) and CH_4 (14.8%) was obtained at 500 °C. Under 3 MPa, a significant increase in the selectivity of total gas products was observed and particularly C_2H_6 and C_3H_8. This behavior proves that higher pressure improved the HDO of 4-ethylguaiacol to form gas products and especially favored C_2H_6 and C_3H_8. This last was possibly formed by an addition reaction between CH_4 and C_2H_4.

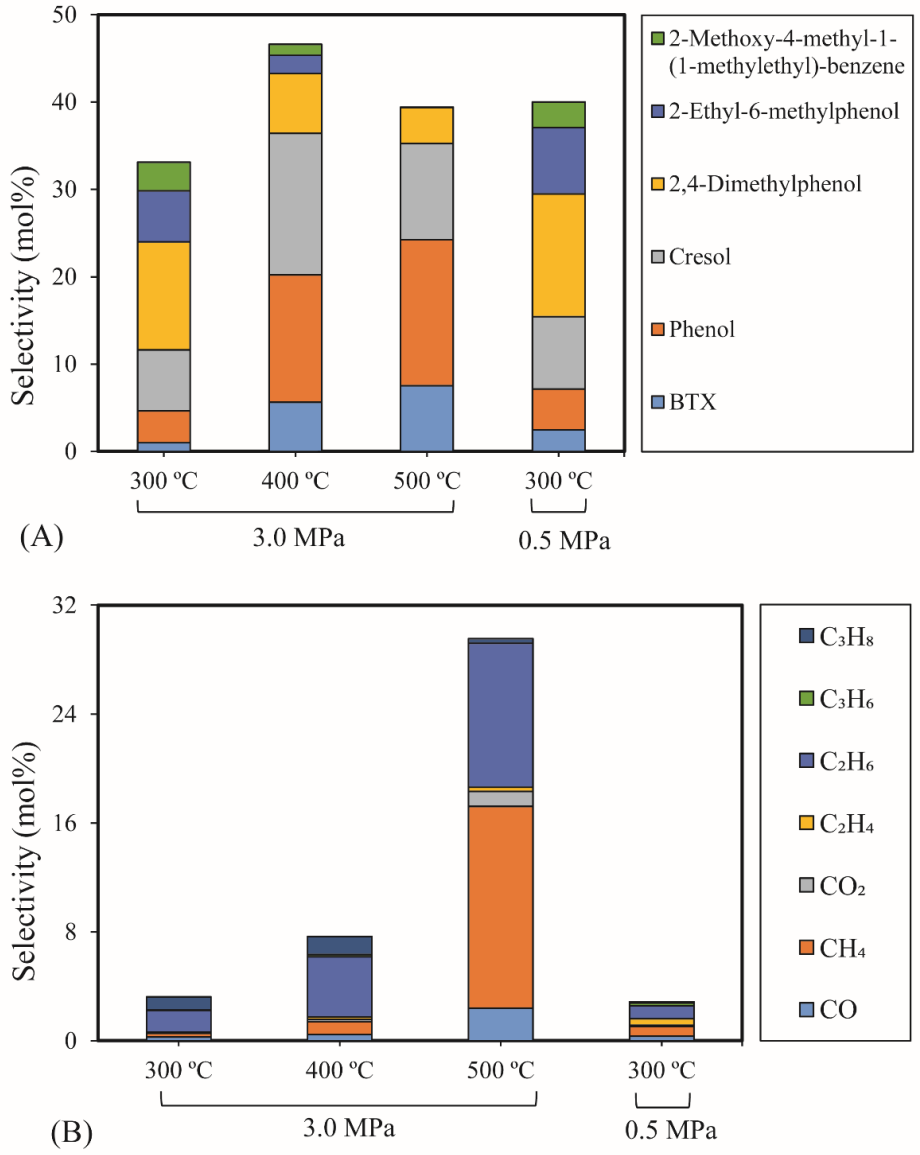

Figure 4.2 The influence of temperature and pressure on 4-ethylguaiacol HDO (0.43 g 5% Ni_2P/HZSM-5, 0.05 mL/min 4-ethylguaiacol, 40 mL/min H_2, 10 mL/min N_2, reaction time: 90 min): (A) Selectivity of major liquid products; (B) Selectivity of gas products

4.5.2 Proposed reaction pathways of 4-ethylguaiacol HDO

Based on the products formed, and the discussion in *Section 4.5.1*, a set of reaction pathways for the HDO of 4-ethylguaiacol is proposed and reported in *Table 4.4* Reaction (1) corresponds to the dealkylation of 4-ethylguaiacol to 2-methoxyphenol and demethoxylation to 4-ethylphenol on Lewis acidic Ni sites, with the formation of C_2H_4, CH_4, and H_2O. The C_2H_4 was then hydrogenated to C_2H_6. Reaction (2) is a direct demethoxylation and alkylation reaction of 4-ethylguaiacol forming DMP below

400 °C. This is a key reaction because DMP is the most primary product at 300 °C. Reaction (3) is a dehydroxygenation and alkylation reaction of 4-ethylguaiacol to form MMMEB at 300 °C and 400 °C. Instead of the alkylation reaction favored by relatively low temperatures, the dealkylation reaction was promoted by high temperatures. The DMP underwent subsequent demethylation to form cresol (p- & o-) in reaction (4). Reaction (5) is a dealkylation reaction of cresol to produce phenol and CH_4. Similarly, phenol and CH_4 were also identified as important products of guaiacol HDO.[118,180] Aromatic hydrocarbons can be formed by the further dehydroxylation reaction of alkylphenols, as shown in reactions (6) and (7). Other alkylphenols, (3-methyl-4-isopropylphenol, for example), were probably produced via the isomerization of certain intermediates.

Table 4.4 The proposed HDO pathways of 4-ethylguaiacol

Main products	Main reaction pathways	
4-Ethylphenol & 2-methoxyphenol	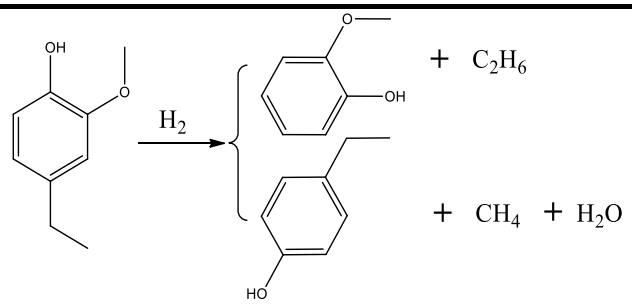	(1)
DMP	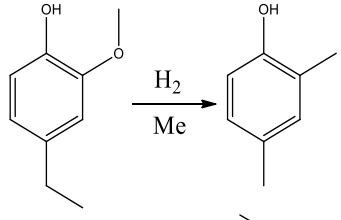	(2)
MMMEB	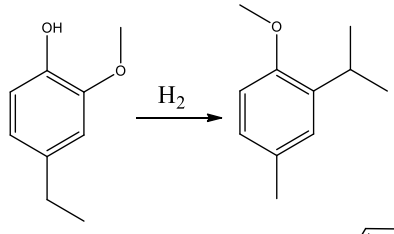	(3)
Cresol (o- & p-)	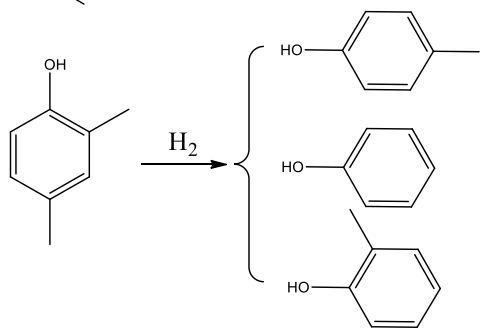	(4)

Phenol

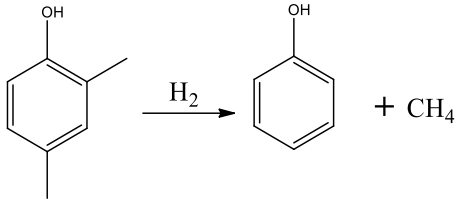

(5)

Benzene

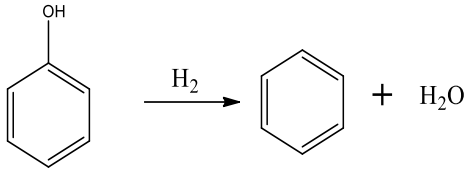

(6)

Toluene & Xylene (p- & m-)

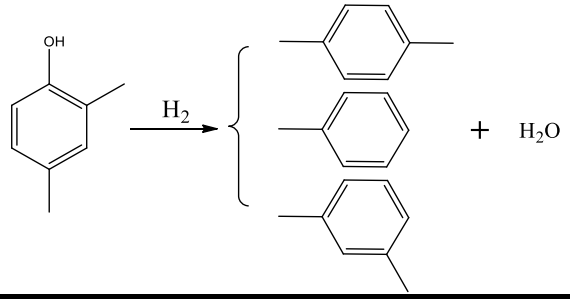

(7)

4.6 HDO of furfural

4.6.1 Effect of temperature and pressure

4.6.1.1 Conversion rate, DOD, and yield

Table 4.5 presents the effect of temperature and pressure on the conversion rate, DOD, and yield of products for furfural HDO. Results under 3 MPa pressure exhibited a significant increase in conversion rate (from 54% to 100%) and DOD (from 38.7 % to 91.5 %) when the temperature increased from 300 °C to 500 °C. The highest yields of gas products (51.23%) and H_2O (9.91%) were obtained at 500 °C and 3 MPa and were accompanied by the lowest yield of liquid products (38.86%, H_2O free). At 400 °C and 3 MPa, the results showed a slight increase of the conversion rate and a decrease of liquid products and H_2O compared to the results under 0.5 MPa. These results indicated that the high pressure promoted the C-C hydrolysis between the furan ring and its branched chains, and reduced the direct dehydration reaction to some extent.

Table 4.5 Effect of temperature and pressure on furfural HDO

Item	Conditions [a]			
	3 MPa	3 MPa	3 MPa	0.5 MPa
	300 °C	400 °C	500 °C	400 °C
Conversion rate & DOD (wt%)				
$X_{Furfural}$	54	66	100	57
DOD	38.7	50.9	91.5	34.5
Yield of products (wt%)				
$Y_{Liq.\ (free\ water)}$	74.77	63.72	38.86	65.10
Y_{Gas}	19.04	28.60	51.23	26.39
Y_{H_2O}	6.19	7.68	9.91	8.51

[a] fixed conditions: 0.43 g 5% Ni_2P/HZSM-5 catalyst, 0.05 ml/min of furfural, H_2: 40 ml/min, N_2: 10 ml/min, 90 min

4.6.1.2 Selectivity

The selectivity of major products of furfural HDO is illustrated in ***Figure 4.3A***. The detailed chemical composition of products can be found in the ***Appendix B*** (***Table B.4***). Generally, high selectivities of furan, 2-methylfuran (2-MF), butanal, BTXM and 1-methylindan were observed in these conditions.

4.6.1.3 Furan selectivity

Furan was observed as the most primary product of furfural HDO, with the selectivity of 16.96% (300 °C and 3 MPa), 22.19% (400 °C and 3 MPa) and 17.28% (400 °C and 0.5 MPa), respectively. It can be deduced that direct aldehyde removal was the main reaction of furfural HDO in these conditions, and this removal was promoted by the pressure increase. Furthermore, deoxygenation of the aldehyde group of furfural under 3 MPa was also a significant reaction, since high selectivities of 2-MF (16.83% and 9.86%) were achieved at 300 °C and 400 °C, respectively. Accordingly, these results proved that the high pressure favored the aldehyde removal and deoxygenation of furfural but less furan ring-opening on the acid sites of 5% Ni_2P/HZSM-5 catalyst. Similarly, Cai et al.[183] reported that supplied hydrogen participated in more HDO of the aldehyde group of furfural, but little further hydrogenation of the furan ring using Cu/SiO_2 catalyst. At 500 °C, a very low selectivity of furan (0.25%) was obtained demonstrating that the temperature promoted the cracking of furan.

4.6.1.4 BTXM and 1-methylindan selectivities

In ***Figure 4.3A***, a greater amount of BTXM was obtained at higher temperatures of 400 °C and 500 °C than at 300 °C. In this case, the formation of aromatic hydrocarbons can be attributed to the oligomerization of mono-olefins (C_2H_4, C_3H_6, and C_4H_8) and/or dienes followed by cyclization at high temperatures. Under 3 MPa, the selectivity of BTXM (6.29%) at 500 °C decreased slightly compared to the value of 9.63% at 400 °C, probably due to the further oligomerization reaction of BTXM and olefins to 1-methylindan with a high selectivity of 1-methylindan (21.28%). The various olefins can be produced by the ring-opening reaction of furan, 2-methylfuran, and other intermediate reactions. In the literature, Cai et al. also mentioned the role of oligomerization and cyclization of olefins to produce aromatic hydrocarbons.[183]

4.6.1.5 2-vinylfuran selectivity

A small amount of 2-vinylfuran was detected in ***Figure 4.3A***, which can be linked to the route of direct substitution reaction between furan and C_2H_4. A feasible route to produce 2-vinylfuran via furan and C_2H_4 over palladium (II) acetate catalyst was reported by Gengan.[184] Although, 2-vinylfuran was observed as a secondary product in the case of hydrotreatment of the furfural-acetone condensation reaction by Ulfa et al.[185] and the catalytic reduction of furfural-methanol by Grazia et al.,[186] a few studies reported that 2-vinylfuran was a product of furfural hydrotreatment without other co-reagents. The 2-vinylfuran can potentially be obtained from the methylenation reaction of furfural involving several consolidating approaches. The most frequently used methods for furfural conversion reaction are the Wittig[187] and Horner−Wadsworth−Emmons reactions,[188] which have the common feature of employing the co-reagent of phosphorus-substituted carbanions. One can then suggest that the active Ni_2P phase of the Ni_2P/HZSM-5 catalyst favored the olefin substitution reaction of furan via the interaction between Ni_2P and ethylene.

4.6.1.6 Other products

At low temperatures, the formation of butanal can be attributed to the ring-opening reaction and further hydrogenation of furan. The acetone was possibly produced via the ring-opening reaction of 2-MF followed by the further hydrogenolysis reaction of C-C bond together with the release of C_2H_4.

4.6.1.7 Selectivity in the gas phase

Figure 4.3B shows the analysis of various gas products during the furfural HDO reaction. The results showed a very low gas production at 300 °C due to the low conversion rate of furfural at low temperatures. The main gas product was CO with a selectivity of 17.24%. High selectivity of other gases (CH_4, CO_2, C_2H_6, C_3H_6, and C_3H_8) at 400 °C and 3 MPa was also observed. CO was mainly formed by the direct decarbonylation of furfural and aldehyde intermediates (like butanal). The CO_2 was possibly produced by the 2-MF ring-opening reaction followed by C-C bond cracking at high temperatures.

Among these gaseous products, light alkanes were formed by the hydrogenation reaction of intermediates of furfural HDO since the ring-opening reaction produced olefins. Notably, the selectivity of CH_4 (13.15%) at 500 °C is significantly higher than at 400 °C, but the selectivity of CO was lower compared to 400 °C. CH_4 can be formed mainly by the demethylation of 2-MF and probably by hydrogenation of CO and CO_2, as reported in the literature in the case of metal Ni under high pressure of H_2.[189] These results suggested that the selectivity of alkanes depends on the relative rates of the C-C bond cleavage, dehydration and hydrogenation reactions of furfural and its intermediates. Similarly, Huber et al. also stated that the selectivity of various alkanes is strongly linked to the relative rates of the C-C bond cleavage, dehydration, and hydrogenation reactions during the aqueous-phase processing of sorbitol.[189] At 400 °C, the gas products selectivity under 0.5 MPa showed a relatively narrow distribution compared to 3 MPa, and CO was the most important product, with 25.29% of selectivity. Thus, it can be deduced that the pressure had a significant effect on the distribution of gas products of furfural HDO and that the high pressure facilitated the ring-opening reactions.

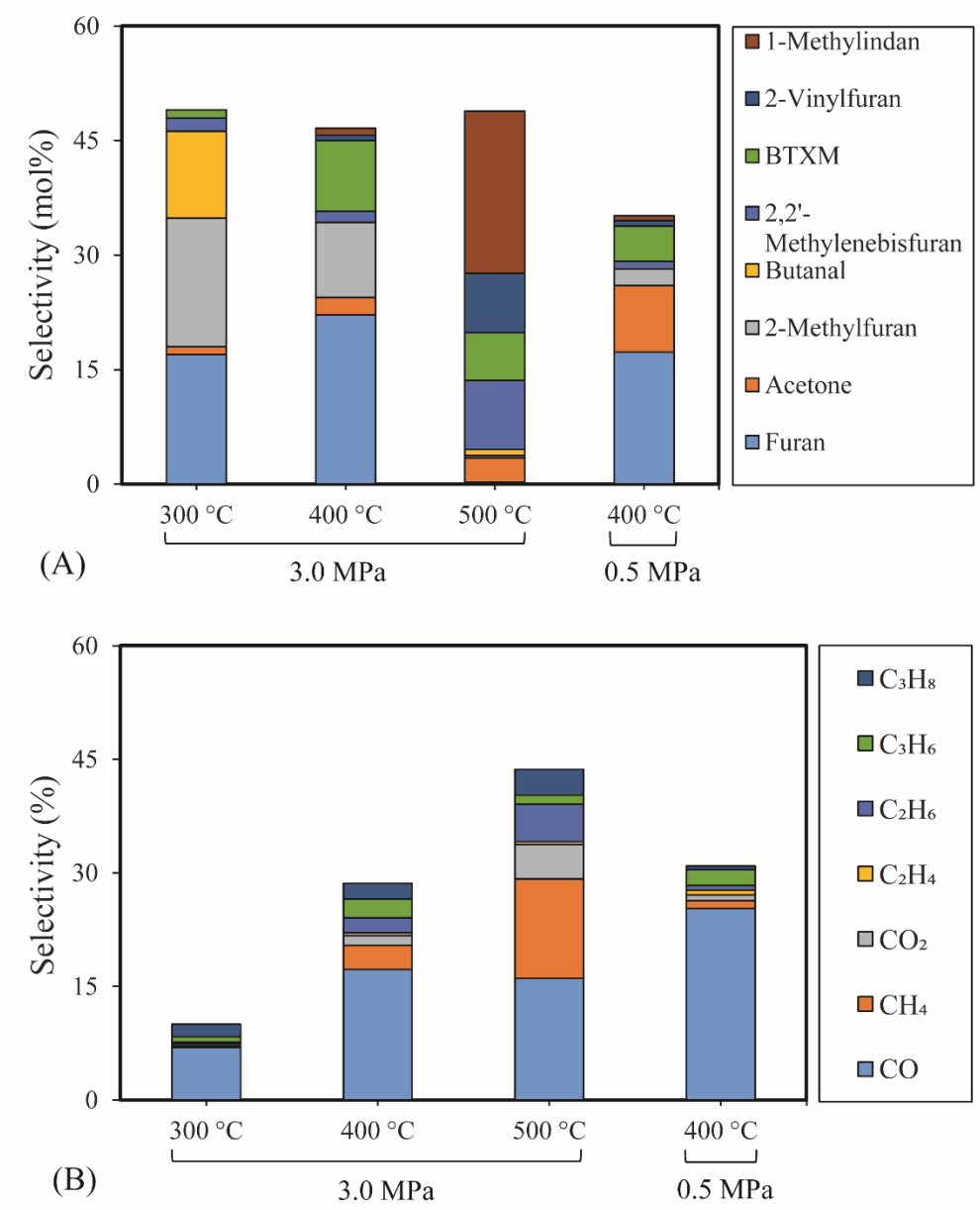

Figure 4.3 The influence of temperature and pressure on furfural HDO (0.43 g 5% Ni_2P/HZSM-5, 0.05 mL/min furfural, 40 mL/min H_2, 10 mL/min N_2, reaction time: 90 min): (A) Selectivity of major liquid products; (B) Selectivity of gas products

4.6.2 Proposed reaction pathways of furfural HDO

Table 4.6 summarizes a series of reaction pathways for the HDO of furfural according to the main products obtained. Several typical reactions[190] are involved in these reaction pathways. Reaction (1) corresponds to the hydro-dehydration of furfural to 2-MF, together with the formation of H_2O. Reaction (2) is a direct decarbonylation reaction of furfural forming furan and CO.[191] This reaction is the primary route of furan formation due to the highest selectivity of CO among other gas products (*Figure 4.3B*). Reaction

(3) can be considered a minor reaction for furan production, associated with the formation of CH_4. Acetone was produced by the ring-opening reaction of 2-methylfuran accompanying the release of C_2H_4 in reaction (4). C_3H_6 and C_3H_8 can be produced mainly from the dehydration-hydrogenation of acetone in reaction (7), and C_2H_4 can be easily converted to C_2H_6 by hydrogenation.

Furan can be converted by hydro-opening-ring and hydrogenation to form butanal in reaction (5). Subsequently, butanal can be hydrogenated then dehydrated forming C_4H_8 in reaction (6) and/or directly decarbonylated to form CO and C_3H_6. C_3H_8 is then formed by hydrogenation of C_3H_6 in reaction (7). Reaction (8) is the probable pathway allowing the formation of 2-vinylfuran from furan and C_2H_4. Reaction (9) is a condensation reaction between furfural and furan molecules to synthesize the 2,2-methylenebis-furan. Reaction (10) is a probable route of aromatic hydrocarbons via the addition reaction of olefins on Ni_2P and subsequent cyclization on HZSM-5 acidic sites. As stated in the literature, aromatic hydrocarbons can be formed by cyclization-dehydration of dienes, which comes from the oligomerization of mono-olefins (C_2H_4, C_3H_6 and C_4H_8)[183] or the Diels–Alder cycloaddition of 2,5-dimethylfuran with ethylene and subsequent dehydration to form p-xylene, followed by alkylation to other aromatics.[192,193] Thus, it can be deduced that 1-methylindan was also formed by these routes.

Table 4.6 The proposed HDO pathways of furfural

Main products	Main reaction pathways	
2-Methylfuran	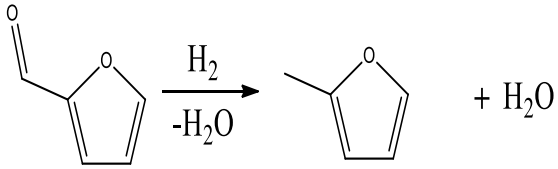	(1)
Furan & CO	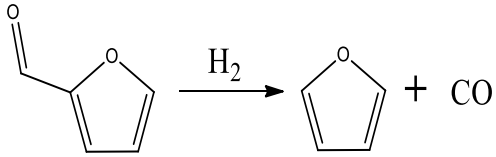	(2)
	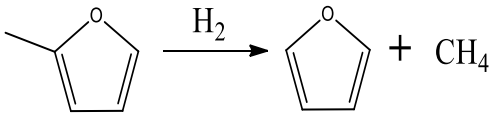	(3)
Acetone	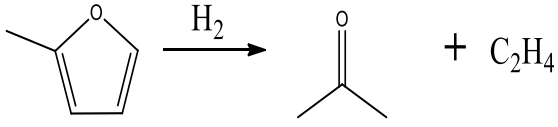	(4)

Butanal & C_4H_8

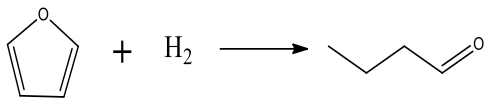

(5)

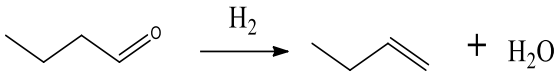

(6)

C_3H_6 & C_3H_8

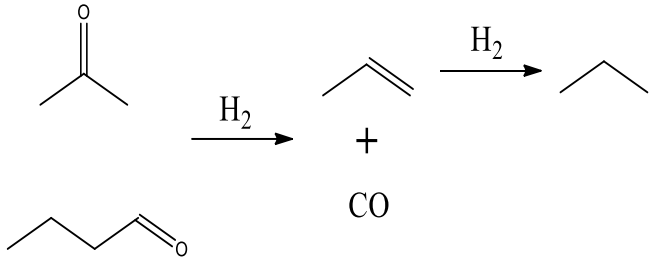

(7)

2-Vinylfuran

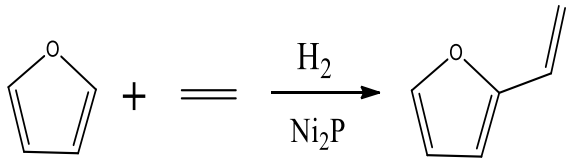

(8)

2,2-Methylenebisfuran

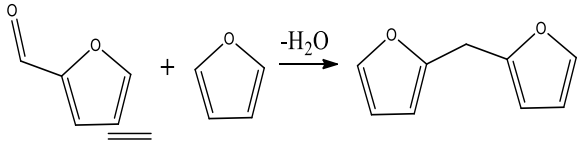

(9)

Aromatic hydrocarbons

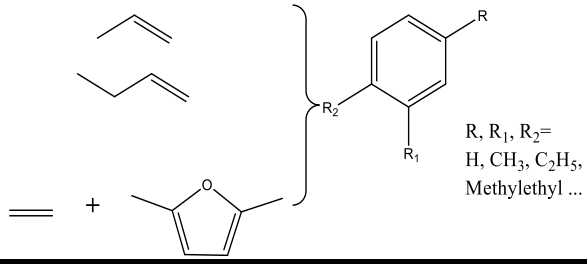

(10)

4.7 Conclusion

The HDO of acetic acid, 4-ethylguaiacol, and furfural as model molecules of bio-oil with the use of prepared Ni_2P/HZSM-5 catalysts were studied. The results showed that the reaction temperature has a pronounced effect on the conversion rate and DOD of acetic acid and furfural using 5% Ni_2P/HZSM-5 catalyst. However, the pressure had a greater effect on the conversion rate and DOD of 4-ethylguaiacol HDO than the temperature. Temperature and pressure affected not only the conversion rate but also the selectivity of products.

For acetic acid HDO, the temperature and pressure mainly affected the decarboxylation, hydrogenation, and further decarbonylation associated with the release of CO, CH_4, and

CO_2. Aromatic hydrocarbons were obtained via a further aldol condensation between methyl isobutyl ketone and acetone molecules followed by dehydration and hydrogenation.

The results of 4-ethylguaiacol HDO illustrated that 2,4-dimethylphenol, cresol, and 2-ethyl-6-methylphenol were the most important reaction intermediates. The final products, such as phenol and BTX (benzene, toluene, and xylene), can be produced from those intermediates via dealkylation, dihydroxylation, and isomerization. Notably, the coke formation had a slight effect on the conversion rate of 4-ethylguaiacol, but significantly affected the further dealkylation of the 2-ethyl-6-methylphenol intermediate.

Moreover, it was proved that the principal reaction of furfural HDO was the direct decarbonylation with furan and CO formation. Higher temperatures and pressures promoted the ring-opening reaction and C-C hydrogenlysis of furfural HDO. Aromatic hydrocarbons from furfural HDO were probably formed by the addition reaction and subsequent cyclization-dehydration of dienes, which come from the oligomerization of mono-olefins during the ring-opening and C-C bond cleavage process.

Chapter 5

Catalytic hydro-deoxygenation of model molecules mixtures and bio-oil from biomass pyrolysis

5.1 Introduction

The high complexity of oxygenated chemicals and their intertwining interactions has led to pronounced barriers in comprehending the upgrading of bio-oil. Thus, in the first part of this chapter, the HDO of two mixtures of model molecules studied in previous chapters was performed to investigate the competitive reactions and elaborate the specific reaction routes. Mixture 1 was composed of acetic acid and phenol, and Mixture 2 contained acetone, acetic acid, phenol, 4-ethylguaiacol, furfural, and water. Mixture 1 was studied because the content of acetic acid and phenol in bio-oil is very high, and the pure phenol is in a solid state at room temperature. A solvent is thus needed for its conversion. The investigation included the following parameters: the nature of the catalysts, the H_2 pressure, and the reaction temperature. Then, two reaction networks were proposed based on the detailed product analysis and discussion involving the conversion rate of single model compounds in the mixture, the degree of deoxygenation (DOD), the distribution of main chemicals in the products, etc.

The second part of this chapter was focused on the investigation of a crude bio-oil hydro-deoxygenation process co-fed with acetone. Acetone was used as the co-reagent as a result of two reseasons. One is the fact that the high viscosity of crude bio-oil restricts its use in the experimental set-up. The other is that acetone was proved in ***Chapter 3*** to be a well-performing feed to produce hydrocarbons (especially, aromatic hydrocarbons) with undetected carbonaceous formation over HZSM-5 and Ni_2P/HZSM-5 catalysts.[147] Also, various parameters are examined, such as the fraction of bio-oil, the nature of the catalysts, total pressure, H_2 pressure, and the mass ratio of acetone/bio-oil. In addition, the thermogravimetry (TG) analysis results of three spent catalysts (HZSM-5, 5% and 10% Ni_2P/HZSM-5) after bio-oil hydro-deoxygenation were also added to this chapter to highlight the formation of coke on the surface of the catalysts. Reaction pathways of bio-oil on Ni_2P/HZSM-5 catalysts are also discussed based on the composition distribution of products.

5.2 Materials and methods

5.2.1 Materials

Crude bio-oils were lab-made by intermediate pyrolysis of beech wood using a continuous drop tube reactor (DTR). Beech wood used to prepare the bio-oil samples in this part was provided by ETS Lignex Company and its average fractional size was 400 μm. The special preparation process of crude bio-oil is shown in the section below. All the other chemicals needed in this work were listed in ***Section 3.2.1***, ***Chapter 3*** and ***Section 4.2.1***, ***Chapter 4*** .

5.2.1.1 Preparation of crude bio-oil

The preparation process of the crude bio-oil from beech wood pyrolysis in a continuous DTR was simplified described in this section. The scheme of the DTR was presented in ***Figure 5.1***. Here, a three-stage condenser was connected with the DTR to recover the three fractions of bio-oil at three different temperatures. As for the specific operation conditions, a mass rate of 1.28 g/min for beech wood and a flow rate of 500 mL/min for N_2 were used for the experimental runs, corresponding to a residence time of 9.77 s. The bio-oil's fractions condensed in the first, second, and third condenser were called high-temperature fraction bio-oil (HT-FB, 110 °C), medium-temperature fraction bio-oil (MT-FB, 20 °C), and low-temperature fraction bio-oil (LT-FB, -11 °C), respectively. Furthermore, a total fraction of bio-oil (called crude bio-oil) could be recovered when only one condenser at a condensing temperature of -11 °C was used to replace the above three condensers.

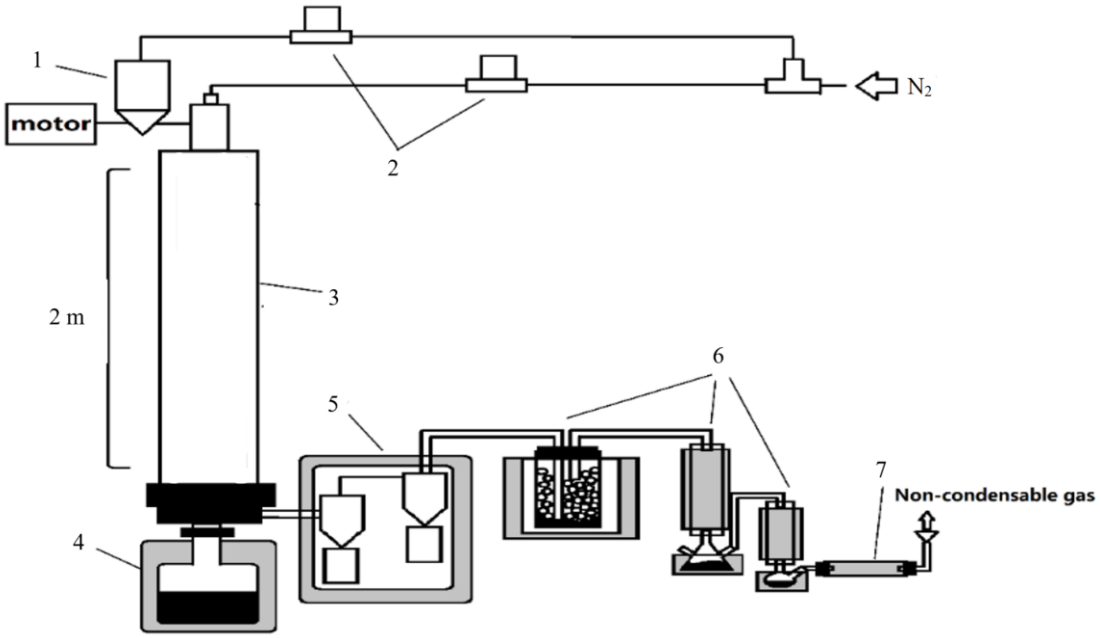

Figure 5.1 Scheme of the continuous drop tube reactor (DTR): 1, srew-bed biomass conveyor; 2, flow controller; 3, electrical resistance; 4, char collector; 5, cyclones; 6, condensers; 7, silica wool filter

The chemicals of the bio-oil identified by GC-MS was shown in ***Appendix B*** (***Figure B.1***). The composition of the crude bio-oil and its three fractions obtained in these conditions was presented in ***Figure 5.2***. In ***Figure 5.2***, carboxylic acids, sugars, and phenols were found as the top three chemical families of crude bio-oil by weight. Among the three fractions of bio-oil (LT-FB, MT-FB, and HT-FB), the MT-FB is most closely to the crude bio-oil. Also, MT-FB is lighter than crude bio-oil and contains less heavy molecules (for example, sugars and guaiacols). In this chapter, the MT-FB and crude bio-oil from beech wood pyrolysis were thus chosen as the feed for the further investigation of the bio-oil hydrotreatment.

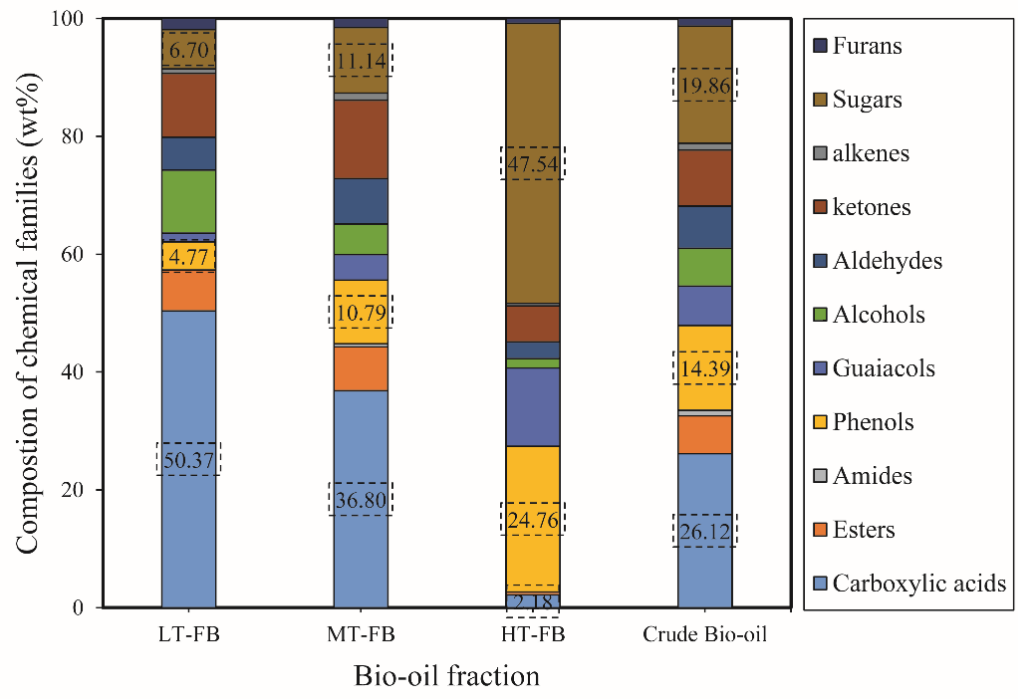

Figure 5.2 Composition of chemical families in bio-oil and its fractions

5.2.2 Activity test in set-up

The HDO activity test of mixtures was similar to the HDO process in ***Section 4.2.2, Chapter 4*** . Some differences included that the HDO reaction was performed on two mixtures (by mol%), respectively: Mixture 1 (acetic acid and phenol) and Mixture 2 (acetic acid, phenol, acetone, furfural, 4-ethylguaiacol, and H_2O). Acetic acid and phenol were selected to be mixed in Mixture 1 mainly because of their high contents and the high difficulty of phenol HDO. Mixture 2 with various model compounds was aimed at closer simulating the crude bio-oil. The content of each model compound in the Mixtures was based on the composition of the pyrolysis oil in our previous work (carboxylic acids (47%), phenols (13%), ketones (7%), aldehydes (2%), guaiacols (1%) and H_2O (15%)).[194] Besides, the liquid reagent, Mixture 1 and Mixture 2 were vaporized in a preheater at a temperature of 210 °C and 270 °C, respectively. The total pressure was increased to the desired value (3 MPa) for all cases, and the temperature rose to the designed value (300-450 °C) once the catalysts reduction process was complete.

As for the bio-oil hydro-deoxygenation, the operation conditions are similar to the case of the test set-up for mixture HDO. The first difference was that the preheater was designed to keep vertical due to the high viscosity of bio-oil, and a 0.5 cm high quartz

wool bed was used in the middle of the preheater to ensure complete vaporization of the feed. The scheme of the reactor was presented in ***Figure 5.3***. The second difference was that the liquid reagents, MT-FB and a mass ratio of 10/1 of acetone/bio-oil, were vaporized in a preheater at a temperature of 270 or 400 °C, respectively. The ratio 10/1 was used as an initial ratio to reduce the viscosity of bio-oil and the probable coke formation as low as possible. The total pressure was increased to the desired value (1 MPa, 3 MPa, and 6 MPa), and the temperature was raised to the designed value of 400 °C once the catalysts reduction process was completed.

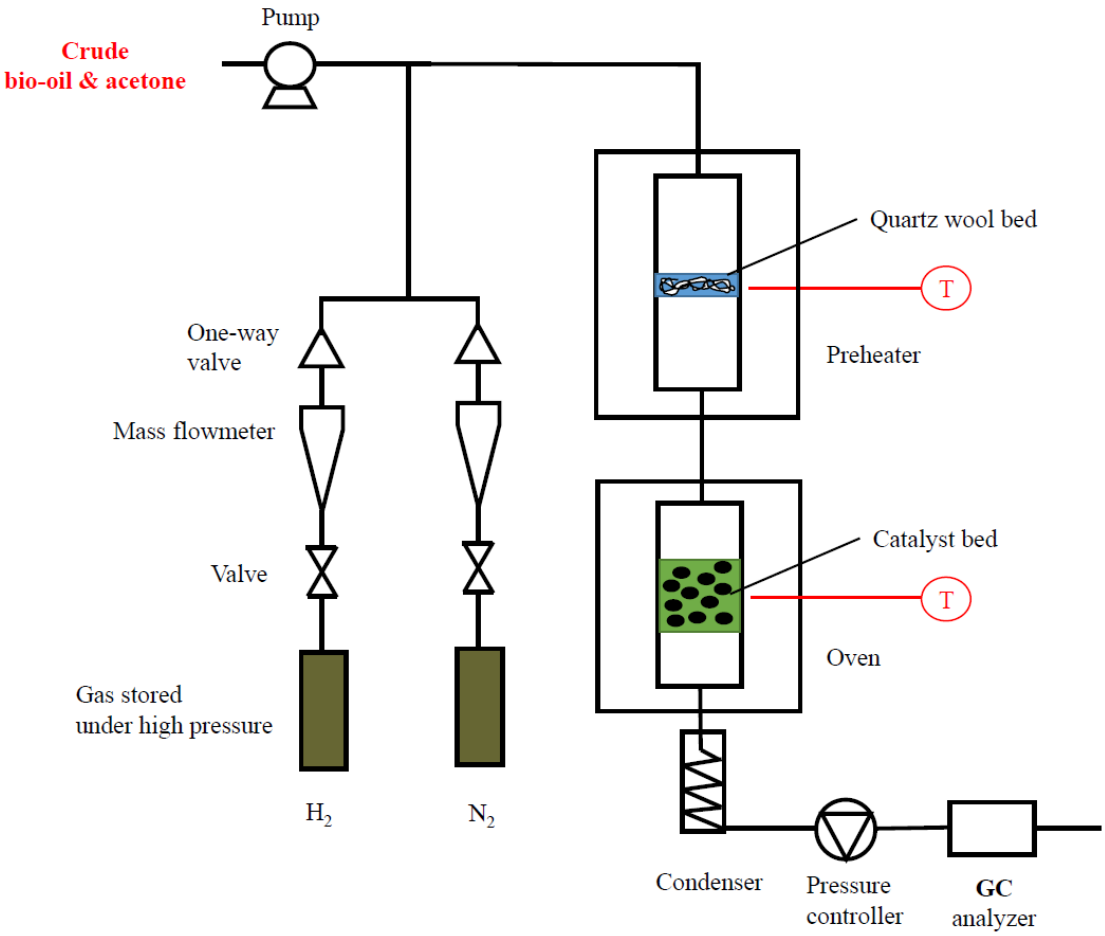

Figure 5.3 Scheme of continuous set-up for bio-oil hydro-deoxygenation

5.2.3 Products analysis

The specific characterization of the liquid and non-condensable products was similar to the description in ***Section 4.2.3***, ***Chapter 4*** . Besides, in order to analyze the experimental results and to better understand the evolution of each model molecule and their interaction, the conversion rate, degree of deoxygenation (*DOD*), yield (see ***Chapter 4*** ,

Section 4.2.3), and product distribution were used. The expression of the product distribution is given in the following:

The distribution was expressed via the molar fractions (%) of the product chemicals and defined as:

$$D\ (\%) = \frac{n_i}{N_{total}} \times 100\% \quad (5.1)$$

where n_i is the amount of product i, mol; N_{total} is the amount of total products, mol.

5.3 HDO of mixed model compounds

5.3.1 HDO of blends of phenol and acetic acid

5.3.1.1 Effect of catalysts

To compare the catalytic behavior of Mixture 1 (78.33 % of acetic acid and 21.67% of phenol) HDO, experiments with/without catalysts were carried out, and the results are shown in *Table 5.1*. Clearly, the utilization of catalysts promotes the transformation of Mixture 1, acetic acid and phenol simultaneously. Ni_2P/HZSM-5 catalysts ensure intensely the HDO reaction with conversion rates above 70% of acetic acid, 25% of phenol, and 61% of DOD compared to HZSM-5, which is probably attributable to the widespread presence of the Ni_2P active phase. In a preceding study, Berenguer et al.[110] reported that the mesoporous property of acid zeolite supports enhanced the enhancive tendency of Ni_2P dispersion, which can strengthen the HZSM-5 activity. In addition, the conversion rate of acetic acid (77%) and yield of H_2O (19.51%) over 5% Ni_2P/HZSM-5 catalyst were higher than that reached in the case of 10% Ni_2P/HZSM-5, contrary to the conversion rate of phenol. This revealed that the conversion of acetic acid occurred more easily over 5% Ni_2P/HZSM-5 as a result of the smaller pore diameter than 10% Ni_2P/HZSM-5 (see *Section 2.3.1*, *Table 2.2*). The smaller pore diameter hinders molecules of phenol from entering the active sites inside the pores, but favors the behavior of smaller molecules (acetic acid and H_2, etc.) to yield more water and gas products.

Table 5.1 Effect of catalysts on HDO of Mixture 1

Item	Conditions [a]			
	No catalysts	HZSM-5	5% Ni_2P/ HZSM-5	10% Ni_2P/ HZSM-5
Conversion rate & DOD (wt%)				
$X_{acetic\ acid}$	19	35	77	70
X_{phenol}	4	7	25	32
DOD	13.39	19.96	60.9	62.3
Yield of products (wt%)				
$Y_{Liq.\ (free\ water)}$	83.46	72.64	43.42	49.43
Y_{Gas}	12.91	17.58	37.07	40.05
Y_{H_2O}	3.63	9.77	19.51	10.53

[a] fixed conditions: (0.52 g HZSM-5, 0.43 g 5% Ni_2P/HZSM-5, 0.48 g 10% Ni_2P/HZSM-5, 400 °C, 3 MPa, 0.05 ml/min of Mixture 1, H_2: 40 ml/min, N_2: 10 ml/min, 90 min)

Liquid products

As shown in ***Figure 5.4A***, the main composition of the liquid products was ketones, aromatic hydrocarbons, and phenols in most cases. The detailed composition can be seen in ***Appendix B*** (***Table B.5***). Specifically, ketones (acetone) were formed by the self-ketonization of acetic acid, in agreement with other works by Jahangiri et al.[195] and Zhang et al..[167] Aromatic hydrocarbons can be produced by two probable routes, aldol condensation of ketones, resembling at a previous study,[163] and direct dehydroxylation of phenol to benzene followed by an alkyl substitution reaction. Alkyl-substituted phenols are likely to arise from the direct alkyl substitution of phenol molecules. Without a catalyst, the HDO of Mixture 1 does not produce aromatic hydrocarbons. The highest fractions of Alkyl-substituted phenols (60.0%), aromatic hydrocarbons (30.0%), and ketones (48.7%) were achieved in Mixture 1 HDO over HZSM-5, 5% Ni_2P/HZSM-5, and 10% Ni_2P/HZSM-5 catalysts, respectively. This suggested that the content of the Ni_2P active phase significantly affected the distribution of the products.

Gas products

Figure 5.4B presents the composition of gas products in Mixture 1 HDO. CO, CH_4, and CO_2 were obtained as the primary non-condensable products, followed by C_2H_6 and C_3H_8. Without catalysts, the fraction of CH_4 (39.6%) and CO_2 (32.7%) showed a close to 1:1 ratio, illustrating that decarboxylation of acetic acid was the main reaction type

in this case. HZSM-5 showed a very high fraction of CO_2 (76.7%), but a low fraction of CH_4 (6.3%), which can be explained by the high fraction of alkyl-substituted phenols (mainly methyl radical substitution), as shown in ***Figure 5.4A***. A high fraction of CO (45.1%), but a low fraction of CO_2 (8.4%) was observed over 5% Ni_2P/HZSM-5, implying that low Ni_2P phase content strengthened the further hydrogenation of CO_2 to CO. In addition, 10% Ni_2P/HZSM-5 gave the highest fraction of C_2H_6 (10.9%) and CH_4 (47.6%), suggesting that high Ni_2P phase content favored direct deep deoxygenation to produce C_2H_6 and hydrogenolysis to form CH_4, but suppressed the alkyl-substituted reaction of phenol. This can also be proved by the lower percentage of alkyl-substituted phenols (28.5%) on 10% Ni_2P/HZSM-5 in ***Figure 5.4A***.

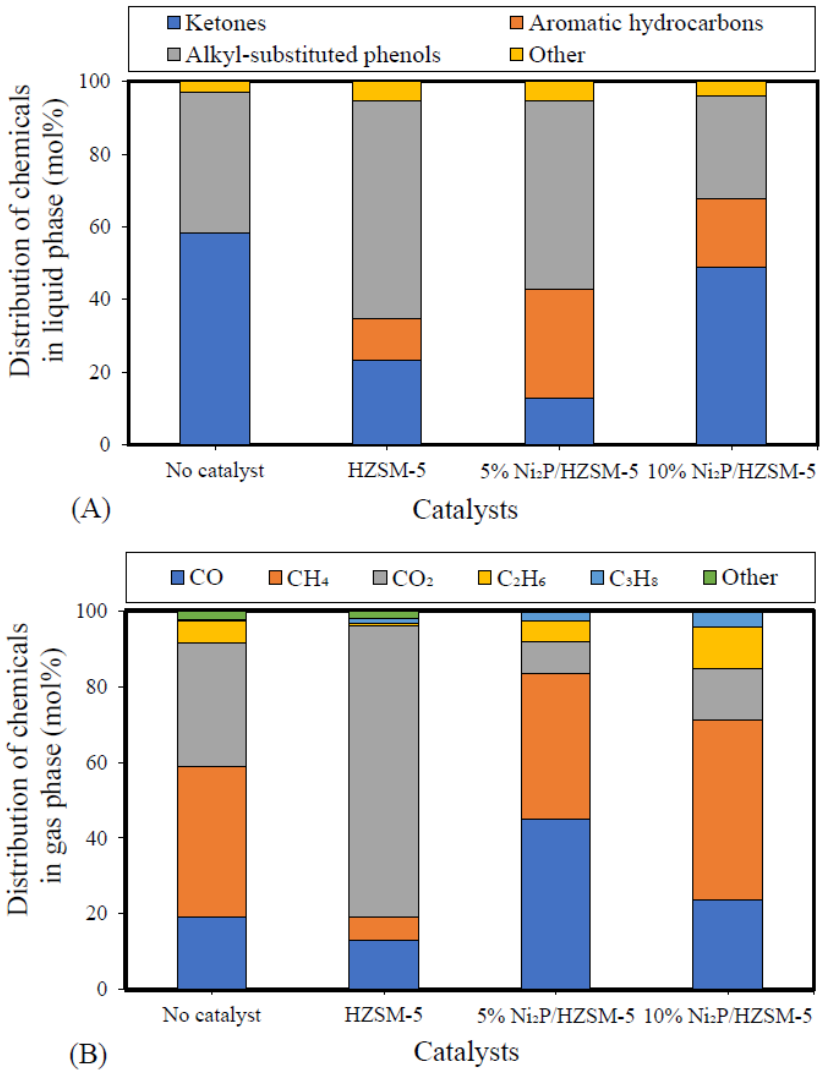

Figure 5.4 Effects of catalysts on Mixture 1 HDO (400 ºC, 3 MPa, 0.05 mL/min Mixture 1, 40 mL/min H_2, 10 mL/min N_2, reaction time: 90 min): (A) Content of chemical composition in the liquid phase (free acetic acid and phenol); (B) Content of chemicals in the gas phase

5.3.1.2 Effect of hydrogen concentration

Conversion rate, DOD, and Yield

Methanol, ethanol, formic acid, and acetic acid, etc. as inexpensive solvents are usually adopted as in-situ hydrogen donor reactants,[125] and may enable the reduction of the use of ex-situ H_2 resource and thus be of benefit to the HDO of model molecules in pyrolysis oil. Wan et al.[126] stated that acetic acid is an efficient hydrogen donor co-reactant to promote the HDO of p-cresol. In contrast, the competition between acetic acid and p-cresol noticeably limited the acetic acid conversion. To investigate the effect of H_2 concentration on the HDO of Mixture 1, experiments were performed based on various H_2/N_2 ratios. The results are presented in ***Table 5.2***. In general, the conversion rate of acetic acid and DOD showed a rising tendency from 55% to 77% and 41.3 % to 60.9% with the increase of H_2 concentration, respectively. However, the conversion rate of phenol kept a constant value at around 25% (even at 0/50 of H_2/N_2) and displayed almost no ex-situ H_2 dependence, implying that the amount of acetic acid in Mixture 1 can supply abundant in-situ hydrogen for phenol HDO in these conditions.

Liquid products

As shown in ***Table 5.2***, the yield of liquid products (free water) decreased from 76.6% to 43.4% with an increase of the ex-situ H_2 concentration and was accompanied by an increased yield of gas products and H_2O. This suggested that the increase of H_2 partial pressure favored the deoxygenation of acetic acid to form more gas products and water. In the liquid phase, the top three components were acetone, 2,4-dimethylphenol, and benzene. In detail, the distribution of acetone above 78% in cases of the H_2/N_2 ratio of 0/50 and 20/30 revealed that the low H_2 concentration favored the self-ketonization of acetic acid to give acetone, and suppressed further transformation of acetone. The amount of acetone was reduced significantly from 78% to 21.8% when H_2/N_2 ratio rose to 40/10, while a high percentage of 2,4-dimethylphenol (30.8%) and benzene (20.7%) was obtained. This suggested that the high H_2 concentration suppressed the acetic acid self-ketonization reaction and facilitated the methyl substitution and dehydroxylation reaction of phenol.

Gas products

For the composition of the gas phase in *Table 5.2*, CO, CH_4, and CO_2 were the major products. CO_2 can be produced via two routes: self-ketonization[195] and decarboxylation of acetic acid. CH_4 was formed by direct decarboxylation of acetic acid and CO_2 hydrogenation. CO came from the further hydrogenation of CO_2. The low amount of CH_4 (3.4%) and high amount of CO_2 (72.7%) at the point (H_2/N_2, 0/50) indicated that self-ketonization is dominant for the reaction without H_2. The production of CO and CH_4 increased significantly from 21.8% to 45.06% and 3.4% to 38.23% with the increase of the H_2 concentration, respectively, illustrating that the decarboxylation of acetic acid was supported by the high H_2 concentration. Subsequently, further hydrogenation of CO_2 led to a pronounced reduction of its percentage from 72.7% to 8.4%.

Table 5.2 Effect of H_2/N_2 ratio on HDO of Mixture 1

Item	Conditions [a]		
	H_2/N_2 ratio (vol.)		
	0/50	20/30	40/10
Conversion rate & DOD (wt%)			
$X_{\text{Acetic acid}}$	55	65	77
X_{Phenol}	25	26	25
DOD	41.3	58.3	60.9
Yield of products (wt%)			
$Y_{\text{Liq. (free water)}}$	76.61	62.82	43.42
Y_{Gas}	12.14	19.71	37.07
Y_{H_2O}	11.25	17.47	19.51
Distribution of products (mol%)			
Liquid phase (free water)			
Acetone	84.43	78.44	21.77
2,4-Dimethylphenol	5.23	9.30	30.82
Benzene	1.34	2.23	20.69
Gas phase			
CO	21.78	22.96	45.06
CH_4	3.40	23.61	38.25
CO_2	72.73	44.22	8.38

[a] fixed conditions: (400 °C, 0.43 g 5% Ni_2P/HZSM-5, 3 MPa, 0.05 ml/min of Mixture 1, 90 min)

5.3.1.3 Effect of temperature

To better discern the interaction in the HDO of Mixture1, experiments with varying temperatures were conducted. *Table 5.3* displays the results of the conversion rates and yields. As the reaction temperature increased from 350 °C to 450 °C, the conversion rate of acetic acid and DOD increased intensely from 44% to 93% and 29.9% to 72.5%, contrary to the value of phenol conversion, which decreased from 45% to10%. This indicated that high temperature favored the acetic acid conversion but diminished the conversion of phenol over 5% Ni_2P/HZSM-5. The explanation is likely preferential adsorption of acetic acid on the catalyst active sites compared to phenol adsorption. The inhibition of phenol HDO at high temperatures is probably a result of this competitive adsorption. The increase of DOD was due to the increasing deoxygenation of acetic acid. The reduced yield of liquid phase (H_2O free) from 62.02% to 40.21% was accompanied by an increase of gas products and H_2O, which can be attributed to increased conversion of acetic acid.

Table 5.3 Effect of temperature on HDO of Mixture 1

Item	Conditions [a]		
	350 °C	400 °C	450 °C
Conversion rate & DOD (wt%)			
$X_{\text{Acetic acid}}$	44	77	93
X_{Phenol}	45	25	10
DOD	29.9	60.9	72.5
Yield of products (wt%)			
$Y_{\text{Liq. (free water)}}$	62.02	43.42	40.21
Y_{Gas}	22.22	37.07	38.60
Y_{H_2O}	15.76	19.51	21.18

[a] fixed conditions: 0.43 g 5% Ni_2P/HZSM-5 catalyst, 3 MPa, 0.05 ml/min of Mixture 1, H_2: 40 ml/min, N_2: 10 ml/min, 90 min

Liquid products

Table 5.4 presents the principal liquid product distribution of Mixture 1 HDO in the temperature range of 350-450 °C. The compounds in the liquid phase were classified into three main categories: ketones (acetone), alkyl-substituted phenols (2,4-dimethylphenol, cresol, etc.), and aromatic hydrocarbons (benzene, toluene, xylene, etc.). As in the foregoing discussion in *Section 5.3.1.2*, acetone was formed via acetic acid self-ketonization, together with CO_2 emission. 2,4-dimethylphenol can be

produced by methyl radical substitution of phenol, and the methyl radical resulted from acetic acid decarboxylation and CO_2 hydrogenation. Aromatic hydrocarbons were synthesized by the condensation reaction of small intermediates (acetone and olefins etc.) and the following isomerization,[163,183] dehydroxylation of phenol,[196] and alkyl substitution of benzene.[197] In particular, among these aromatic hydrocarbons, benzene was mainly from the direct dehydroxylation of phenol. The acetone concentration first decreased from 26.03% to 13.49% and then increased to 20.16% when the temperature increased from 350 °C to 450 °C. The initial decrease of the acetone was due to the deoxygenation reaction of acetone to form $-CH(CH_3)_2$ and H_2O from 350 to 400 °C. Subsequently, $-CH(CH_3)_2$ reacted with benzene by an alkyl substitution reaction to synthesize 1-methylethylbenzene. At 450 °C, the strong competitive adsorption between acetic acid and phenol on 5% Ni_2P/HZSM-5 active sites limited the formation of 1-methylethylbenzene as a result of the inhibiting formation of benzene from phenol. The highest distribution of 1-methylethylbenzene (4.54%) was obtained at 400 °C. Thus, the decreasing production of 1-methylethylbenzene led to the practical increase of the acetone distribution.

Alkyl-substituted phenolsFor alkyl-substituted phenols in ***Table 5.4***, 3,4,5-trimethylphenol and 3-5-diethylphenol showed a low percentage (＜5%), and a slight decrease of their distribution was observed due to the decreasing phenol conversion with the increase of temperature. One probable explanation of the low distributions is that 3,4,5-trimethylphenol and 3-5-diethylphenol have a larger molecular structure than other alkyl-substituted phenols, and the steric hindrance disadvantaged their formation. The production of 4-ethylphenol, 2,4-dimethylphenol, and 3-ethyl-5-methylphenol first increased and then decreased when the temperature increased from 350 °C to 450 °C. The first increase can be attributed to the strengthening of substitution reaction between phenol and alkyl radicals. Alkyl radicals, $-CH_3$, $-CH_2CH_3$, and $-CH(CH_3)_2$, were formed via various pathways including decarboxylation, direct deoxygenation, and self-ketonization of acetic acid. $-CH_3$ and $-CH_2CH_3$ were the overwhelming alkyl radicals compared to the amount of $-CH(CH_3)_2$ in these conditions, resulting in a dominant distribution of methyl and/or ethyl-substituted chemicals. The second decreasing distribution of the three alkyl-substituted phenols was attributed to the low phenol conversion and rapid increase of dealkylation reaction at 450 °C. In addition, the cresol distribution increased significantly from 7.81% to 19.52% with the increase of temperature. The increasing distribution benefited from two reaction routes: the alkyl substitution of phenol and the dealkylation of other alkyl-substituted phenols. Although

the high temperature suppressed the alkyl substitution reaction and facilitated the dealkylation reaction, it can be deduced that the decreasing rate of alkyl substitution is slower than the increasing rate of dealkylation.

Aromatic hydrocarbons

For aromatic hydrocarbons in ***Table 5.4***, a high percentage of benzene (18.39%) and ethylbenzene (7.41%) was obtained at 350 °C. Afterward, their distribution underwent obvious decreases with the increasing temperature as a result of the descending phenol conversion. In addition, the distribution of toluene and xylene showed a noticeably increasing tendency, which can be attributed to the transformation of other alkyl-substituted phenols and aldol condensation of acetone intermediate followed by isomerization.

Table 5.4 Distribution of main chemicals in liquid products of Mixture 1 HDO at different temperatures

Item	Chemicals	Chemical structure	350 °C	400 °C	450 °C	Tendency
Ketones	acetone		26.03	13.49	20.16	
Alkylphenols	3,4,5-trimethylphenol	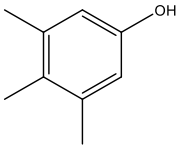	4.81	4.38	3.58	
	3-5-diethylphenol	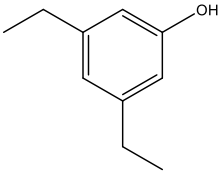	3.99	3.27	2.76	
	4-ethylphenol	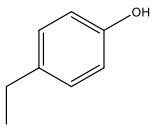	9.23	10.75	6.52	
	2,4-dimethylphenol	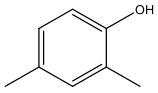	14.70	19.10	9.74	
	3-ethyl-5-methylphenol	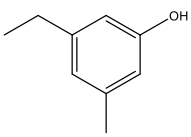	3.62	5.51	5.12	

Aromatic hydrocarbons	Cresol	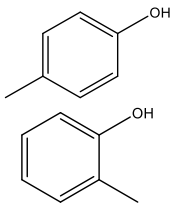	7.81	11.86	19.52	↗
	Benzene		18.39	12.83	7.68	↘
	Ethylbenzene	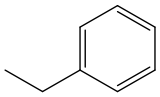	7.41	4.68	1.92	↘
	1-methylethyl benzene	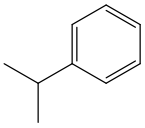	0.79	4.54	2.85	↗↘
	Toluene	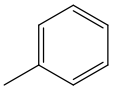	1.32	3.97	9.95	↗
	Xylene	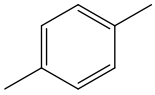	1.91	5.61	10.21	↗

Gas products

As can be seen in ***Figure 5.5***, the main products are CO and CH_4 at 350 °C and 400 °C with molar fractions above 45.1% and 38.3%, respectively. This indicated that the low temperature favored the dehydration and demethylation of acetic acid to form CH_4 and CO. The distribution of CO decreased significantly when the temperature increased from 400 °C to 450 °C, contrary to the value of CO_2. This illustrated that the high temperature promoted significantly the decarboxylation of acetic acid and the water-gas shift reaction of CO and H_2O to produce more CO_2. A reduced amount of 21.44% for CO was obtained. In addition, a small distribution of C_2H_6 and C_3H_8 was also observed. C_2H_6 was formed by direct deoxygenation of acetic acid, and C_3H_8 came from the dehydration and hydrogenation of acetone. According to the above-mentioned discussion, the detailed interaction pathway of Mixture 1 HDO is proposed in ***Figure 5.6***.

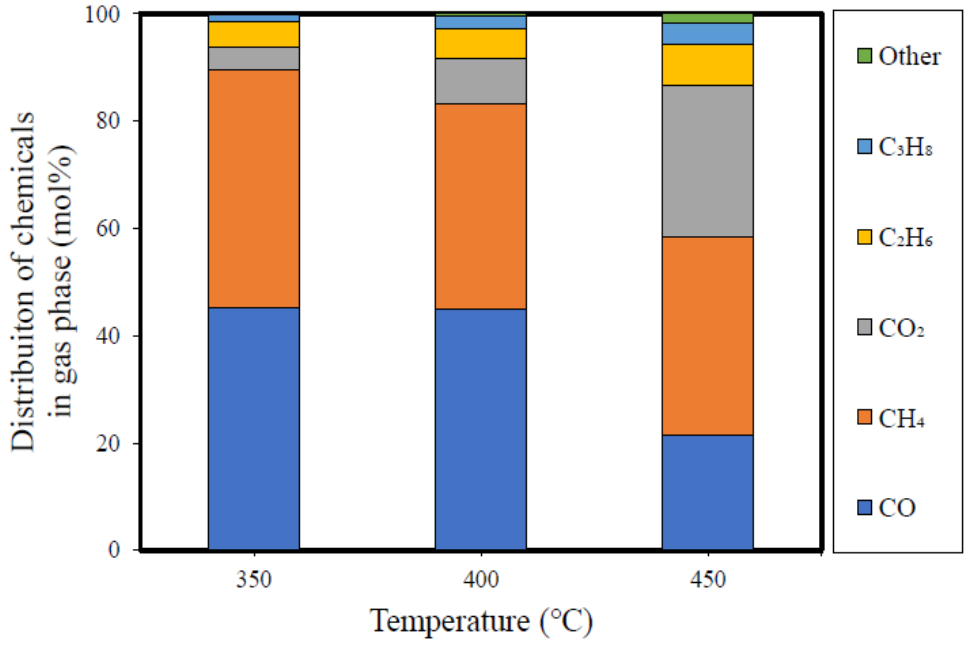

Figure 5.5 Effects of temperature on distribution of gas phase products from Mixture 1 HDO (0.43 g 5% Ni_2P/HZSM-5, 0.05 mL/min Mixture 1, 40 mL/min H_2, 10 mL/min N_2, reaction time: 90 min)

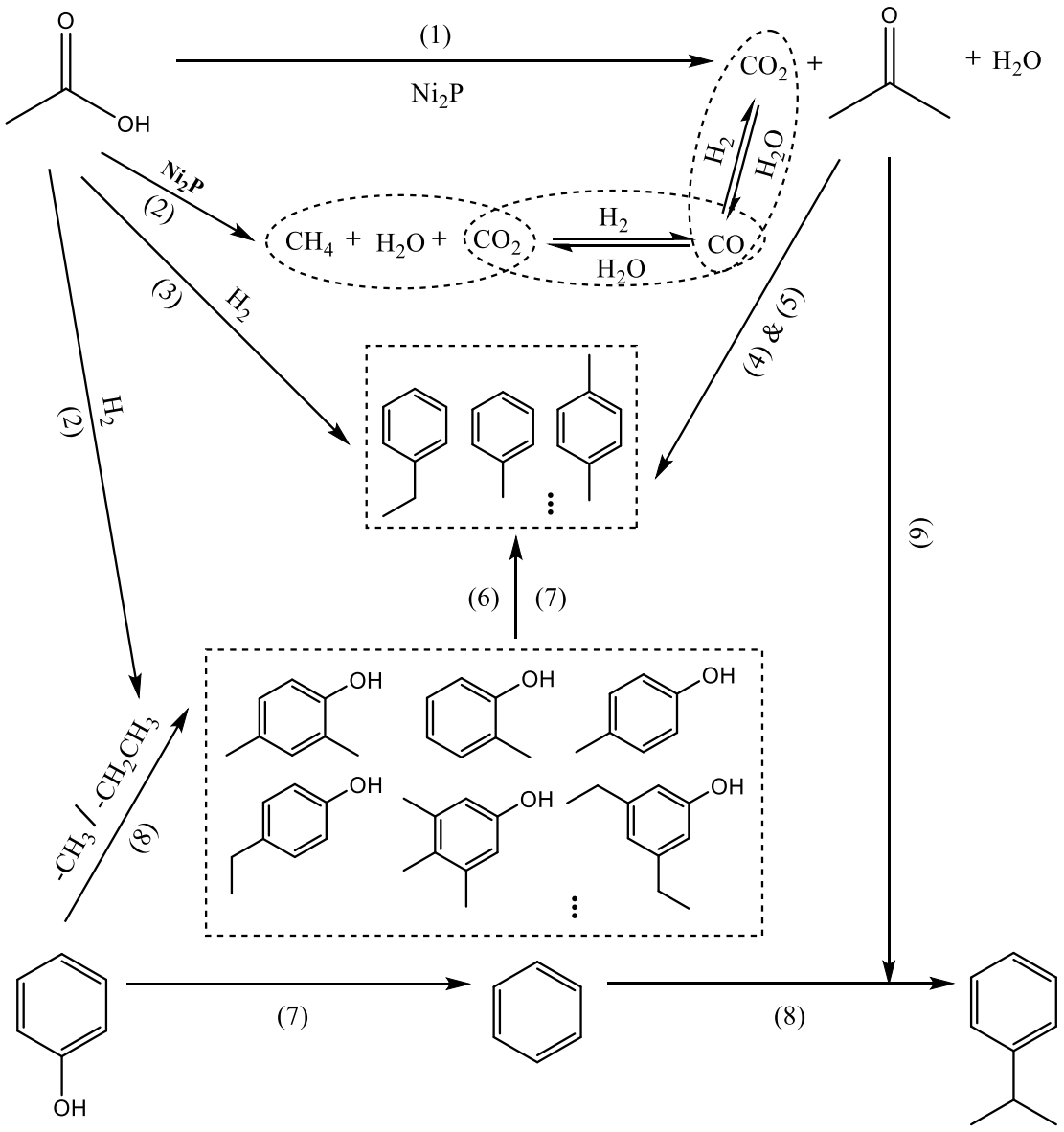

Figure 5.6 Proposed interaction network of Mixture 1 HDO on Ni_2P/HZSM-5 catalysts: (1) Self-condensation; (2) Decarboxylation; (3) Condensation; (4) Adol condensation; (5) Isomerization; (6) Dealkylation; (7) Dehydroxylation; (8) Alkylation substitution; (9) Deoxygenation

5.3.2 HDO of blends of acetone, acetic acid, 4-ethylguaiacol, phenol, furfural, and water

To further ascertain the HDO cross-reactivity in pyrolysis oil and better simulate the bio-oil, a series of HDO experiments of Mixture 2 (containing acetone (8.24%), acetic acid (55.29%), 4-ethylguaiacol (1.18%), phenol (15.29%), furfural (2.35%), and water (17.65%)) were conducted with different catalysts and at different temperatures.

5.3.2.1 Effect of catalysts

Table 5.5 shows the effect of the catalysts on the reactants' conversion rate, DOD, and yield of products in Mixture 2 HDO. The acetone production rate was -285% using the HZSM-5 catalyst. The increasing amount of acetone compared to its initial amount indicated that additional acetone was produced probably due to the pronounced acetic acid self-ketonization. Contrary to HZSM-5, Ni_2P/HZSM-5 catalysts gave a conversion rate of acetone above 81%, which revealed that the presence of the Ni_2P active phase suppressed the self-ketonization of acetic acid to some extent and favored the acetone conversion. The 5% Ni_2P/HZSM-5 catalyst showed a higher conversion rate of acetic acid (93%), phenol (13%), and DOD (74.9%), but a lower conversion rate of 4-ethlyguaiacol (41%) than the 10% Ni_2P/HZSM-5 catalyst. This can be explained by the fact that the higher surface area and smaller pore diameter of 5% Ni_2P/HZSM-5 than 10% Ni_2P/HZSM-5 (see ***Section 2.3.1***, ***Table 2.2***) favored the conversion of relatively smaller molecules. The increased amount of phenol over 10% Ni_2P/HZSM-5 was assigned to the increased 4-ethylguaiacol conversion by deethylation and methoxyl group removal. In a previous study, Ledesma et al. also reported the formation of phenol via methoxyl group and ethyl removal.[198] In this case, the highest conversion rate of 59% for 4-ethylguaiacol was obtained. Exceptionally, furfural reached a very high conversion rate in all cases and even a complete conversion, which probably benefited from the moderate size of its molecular structure. Furans in the liquid phase came mainly from furfural HDO. The three catalysts showed similar yields of products in Mixture 2 HDO and Mixture 1 HDO in ***Table 5.1***. Here, a yield of the liquid phase of 43.35% was obtained and accompanied by the value of 23.8% H_2O and 32.85% gas phase.

Table 5.5 Effect of catalysts on HDO of Mixture 2

Item	Conditions [a]		
	HZSM-5	5% Ni_2P/HZSM-5	10% Ni_2P/HZSM-5
Conversion rate & DOD (wt%)			
$X_{Acetone}$	(-) 285	81	87
$X_{Acetic\ acid}$	79	93	48
$X_{Furfural}$	100	100	97
X_{Phenol}	3	13	(-) 16
$X_{4\text{-}Ethylguaiacol}$	52	41	59
DOD	60.6	74.9	44.2
Yield of products (wt%)			
$Y_{Liq.\ (free\ water)}$	52.99	43.35	47.90
Y_{Gas}	29.11	32.85	36.07
Y_{H_2O}	17.91	23.80	16.03

[a] fixed conditions: (0.52 g HZSM-5, 0.43 g 5% Ni_2P/HZSM-5, 0.48 g 10% Ni_2P/HZSM-5, 450 °C, 3 MPa, 0.05 ml/min of Mixture 2, H_2: 40 ml/min, N_2: 10 ml/min, 90 min); "(-)", production rate (an increased amount of a certain chemical in the upgraded liquid phase compared to its initial amount)

Liquid products

As shown in ***Figure 5.7A***, the main composition of liquid products was aldehydes (acetaldehyde), aromatic hydrocarbons (BTX, etc.), alkyl-substituted phenols (cresol and DMP, etc.) followed by a small quantity of furans (2-methylfuran (2-MF) and furan, < 5%), and alcohols (α,β-dimethylbenzeneethanol, < 2%). Specially, acetaldehyde was formed by the dehydration of acetic acid with the highest percentage of 35.7% over the HZSM-5 catalyst. The formation of aromatic hydrocarbons and alkyl-substituted phenols achieved the highest values of 32.9% and 34.1% over 10% Ni_2P/HZSM-5, respectively, due to the increment of 4-ethylguaiacol conversion and the following alkyl substitution reaction. The small amount of α,β-dimethylbenzeneethanol was probably attributable to the substitution reaction between methyl ethyl ketone and benzene in these conditions. Methyl ethyl ketone can be synthesized by aldol condensation of acetaldehyde and formaldehyde intermediate. The latter was produced during the decomposition of acetic acid, furfural, and 4-ethylguaiacol.

Gas products

Figure 5.7B presents the composition of gas products in Mixture 2 HDO. CO, CH_4, CO_2, C_2H_6, and C_3H_8 were obtained. Fractions of 25% CO, 51.1% CO_2, and 9.8% C_3H_8 were obtained using the HZSM-5 catalyst. CO and CH_4 were formed via three probable ways, involving formyl group elimination of furfural,[191] methoxyl group removal of 4-ethylguaiacol,[198] and hydrogenation of CO_2. CO_2 was produced via the decarboxylation and self-ketonization of acetic acid. C_2H_6 and C_3H_8 were released mainly via direct dehydration of acetic acid and acetone hydrogenation, respectively. The percentage of CO_2 is around 5 times that of CH_4 over the HZSM-5 catalyst. Given a ratio of CO_2/CH_4 of 1:1 for acetic acid decarboxylation, HZSM-5 thus favored the self-ketonization of acetic acid to give more CO_2. The ratio of CO_2/CH_4 (close to 1:1) over Ni_2P/HZSM-5 catalysts also confirmed the suppression of acetic acid self-ketonization in the aforementioned discussion of ***Table 5.5***. Ni_2P/HZSM-5 catalysts showed a significantly higher formation of C_2H_6 above 8% than HZSM-5, indicating preferably direct deoxygenation of acetic acid on Ni_2P active phase.

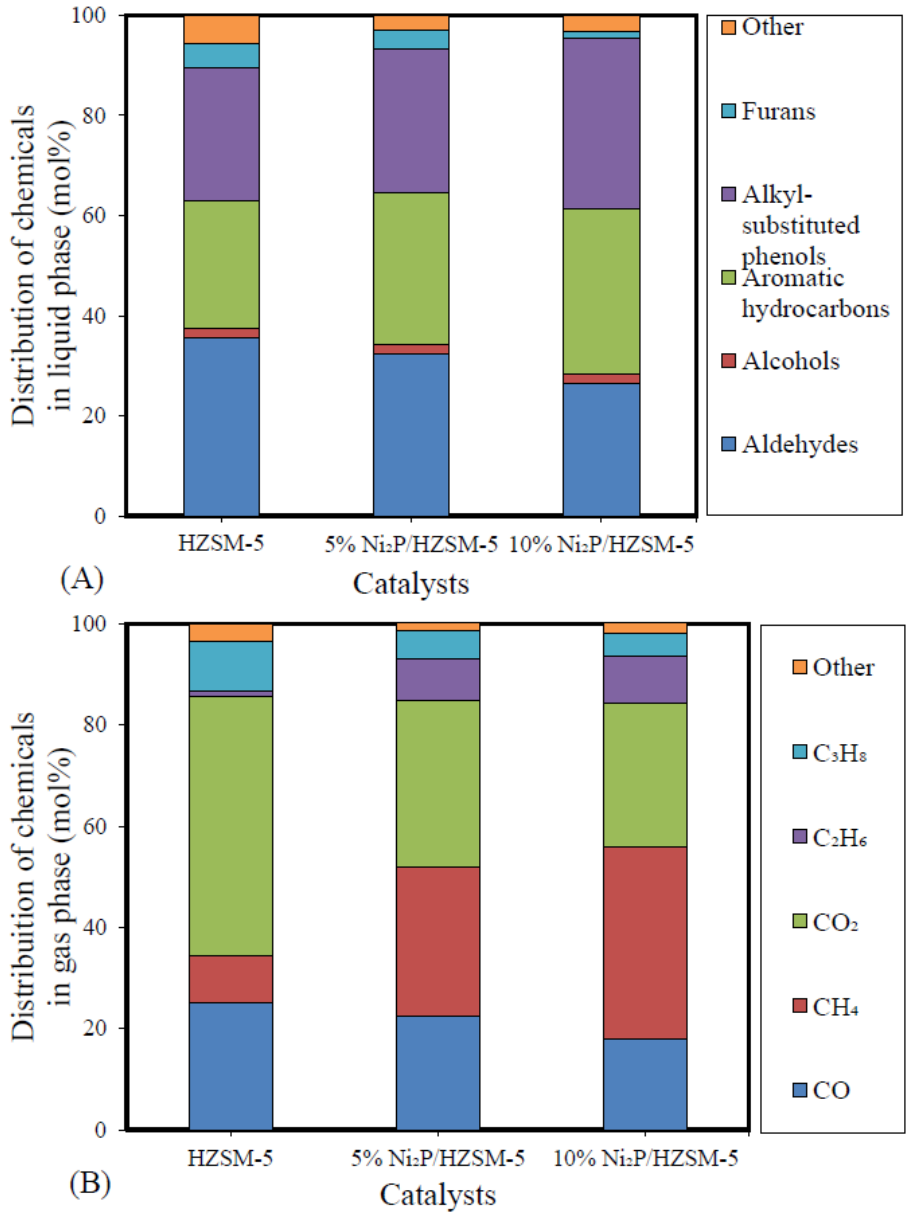

Figure 5.7 Effects of catalysts on Mixture 2 HDO (450 ºC, 3 MPa, 0.05 mL/min Mixture 2, 40 mL/min H_2, 10 mL/min N_2, reaction time: 90 min): (A) Content of chemical composition in the liquid phase; (B) Content of chemicals in the gas phase

5.3.2.2 Effect of temperature

Table 5.6 displays the effect of temperature on the conversion rate, DOD, and yields in Mixture 2 HDO using 5% Ni_2P/HZSM-5 catalyst. It can be seen that acetone, acetic acid, and 4-ethylguaiacol showed a dramatic increase of the conversion rate when the temperature increased from 350 °C to 450 °C. In contrast, phenol showed a decreasing tendency of the conversion rate from 25% to 13%. The results indicated that the high temperature significantly improved the reactivity of acetone, acetic acid, and 4-

ethylguaiacol. The decreasing conversion rate of phenol may be for two reasons. One is the competition reaction among these molecules, as observed with the result in Mixture 1 HDO in ***Section 5.3.1.3***. The other is that the 4-ethylguaiacol may convert to phenol by deethylation and methoxyl group removal. No effect of temperature on furfural was observed with a complete conversion even at the low temperature of 350 °C. The yield of liquid phase (H_2O free) decreased from 65.78% to 43.35% as a result of the increment of gas products and H_2O with the increasing temperature. This suggested that the high temperature favored the cracking reaction and the dehydration to give more gases and H_2O.

Table 5.6 Effect of temperature on HDO of Mixture 2

Item	Conditions [a]		
	350 °C	400 °C	450 °C
Conversion rate & DOD (wt%)			
$X_{Acetone}$	39	52	81
$X_{Acetic\ acid}$	46	63	93
$X_{Furfural}$	100	100	100
X_{Phenol}	25	16	13
$X_{4\text{-}Ethylguaiacol}$	27	37	41
DOD	36.2	49.9	74.9
Yield of products (wt%)			
$Y_{Liq.\ (free\ water)}$	65.78	56.64	43.35
Y_{Gas}	23.84	29.23	32.85
Y_{H_2O}	10.39	14.13	23.80

[a] fixed conditions: 0.43 g 5% Ni_2P/HZSM-5 catalyst, 3 MPa, 0.05 ml/min of Mixture 2, H_2: 40 ml/min, N_2: 10 ml/min, 90 min

Liquid products

Figure 5.8A presents the distribution of the main products in the liquid phase of Mixture 2 HDO. Esters (methyl formate, ethyl acetate, and isopropyl acetate) were only observed at the low temperature of 350 °C. Similarly, a great number of esters were found in the hydrogenation study of model bio-oil using Raney Ni catalysts by Zhang et al.[199] and also hydrogenation of furfural and acetic acid using bifunctional Pd catalysts by Yu et al.[200]. Minor compositions, such as methanol, ethanol, formaldehyde, methyl ethyl ketone, benzene, furan, etc., can be found in ***Appendix B*** (***Table B.6***). Methyl formate, ethyl acetate, and isopropyl acetate were produced by esterification of

methanol/formic acid, ethanol/acetic acid, and isopropanol/acetic acid, respectively. Although no formic acid was detected, the presence of methyl formate indicated the formation of formic acid intermediate, which was probably produced by acetic acid decarboxylation. Acetic acid was dehydrated to give ethanol. Methanol and formaldehyde can be produced via methoxyl group breakage of 4-ethylguaiacol[201] and hydrogenation/dehydration of formic acid. Isopropanol, as a rapidly converting intermediate, was formed by the hydrogenation of acetone and could not be detected. The results indicated the esterification was favored at low temperatures.

Aromatic hydrocarbons in ***Figure 5.8A***, including toluene, xylene, 1-ethyl-3-methylbenzene, and 1-methylethyl benzene, showed a similar increasing tendency of distribution when the temperature increased from 350 °C to 450 °C. It can be deduced that the increasing temperature promoted the condensation of small molecules, dehydroxylation of alkyl-substituted phenols, alkyl substitution reaction of benzene, and isomerization to form aromatic hydrocarbons. As reported in the literature, xylene can also be produced by the Diels–Alder cycloaddition of 2,5-dimethylfuran with ethylene and subsequent dehydration.[192,193] As discussed in ***Section 5.3.2.1***, α,β-dimethylbenzeneethanol can be synthesized by the substitution reaction between methyl ethyl ketone and benzene followed by hydrogenation. 2,4-dimethylphenol was mainly formed via the alkyl-substitution between methyl radical group and phenol, and reduced distribution of 2,4-dimethylphenol from 4.4% to 3.6% was linked to its demethylation and dehydroxylation when the temperature increased from 400 to 450 °C. Cresol showed a significant increase of the distribution from around 3.0% to 7.3% when the temperature rose to 450 °C. The increasing distribution of cresol at 450 °C was mainly due to the dealkylation of other alkyl-substituted phenols, for example, demethylation of 2,4-dimethylphenol. Cresol was thus formed mainly by methyl substitution of phenol at low temperatures (350 °C and 400 °C).

Gas products

Figure 5.8B displays the distribution of products at different temperatures in the gas phase of Mixture 2 HDO. The percentage of CO_2 increased significantly from 9.3% to 32.9%, indicating that the high temperature promoted the decarboxylation and self-ketonization of acetic acid, contrary to a decreasing tendency for CH_4 and CO. At 350 °C, the highest production of CO and CH_4 was obtained with the same value of 38.7%. The decreasing fraction of CH_4 was attributed to the condensation between CH_4

and other olefins or dienes to form more toluene and xylene etc. The decrease of CO can be attributed to the water-gas shift to form CO_2.[202] In addition, the formation of C_2H_6 increased by 41.3% from 350 to 400 °C, but by only 2.5% from 400 to 450 °C, consistent with the conversion rate of 4-ethylguaiacol in ***Table 5.6***. This suggested that C_2H_6 was formed mainly by the deethylation of 4-ethylguaiacol and was affected significantly by temperature. In contrast, the distribution of C_3H_8 decreased by 29.6% from 350 to 400 °C, but increased by 8% from 400 to 450 °C. This indicated that a low temperature favored the hydrogenation of acetone to C_3H_8, but a moderate temperature favored the further reaction of C_3H_6 to aromatic hydrocarbons, for example, 1-methylethylbenzene. The slight increase of C_3H_8 above 400 °C may be due to the sharp increase of acetone conversion from 52.2 to 80.6% as shown in ***Table 5.6***. Accordingly, the main interaction pathways of Mixture 2 HDO are proposed in ***Figure 5.9***.

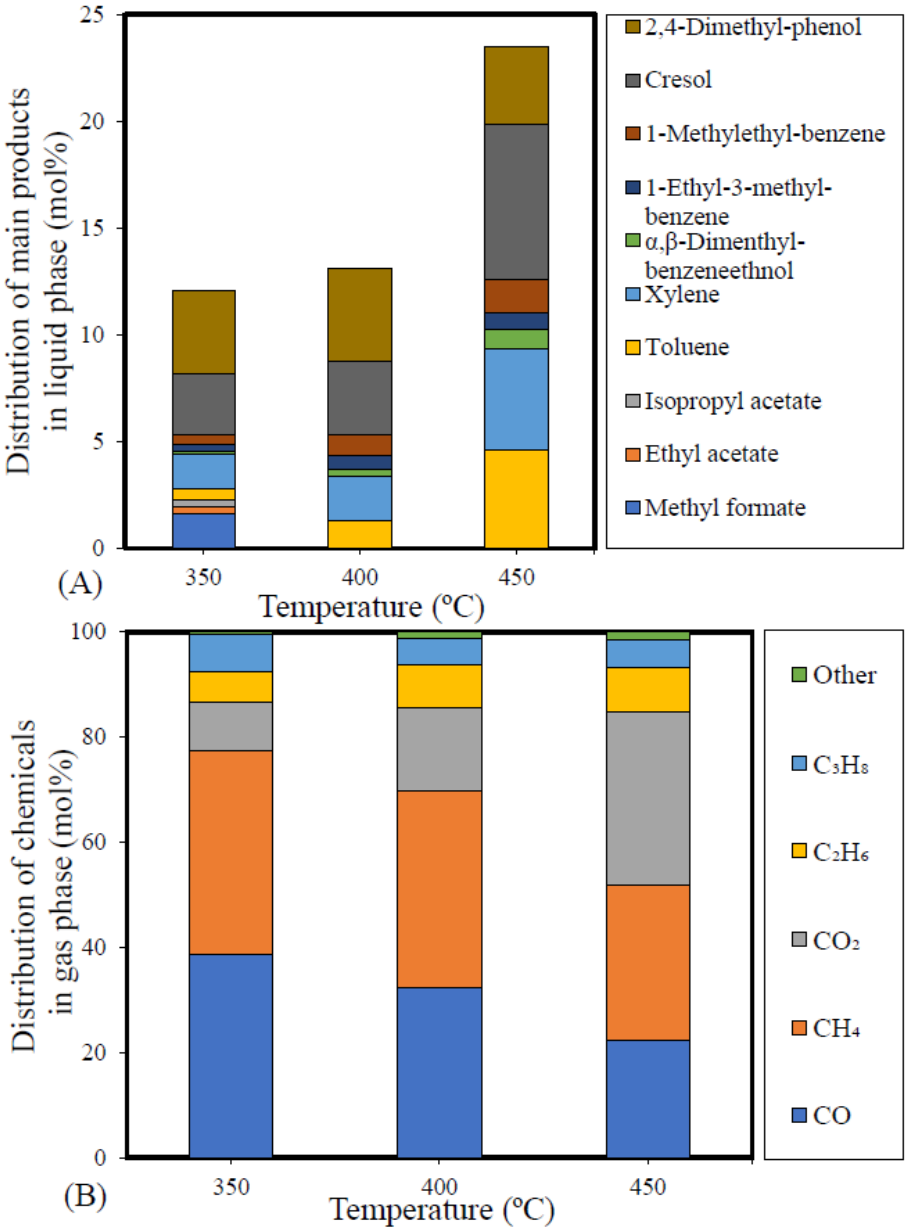

Figure 5.8 Effects of temperature on distribution of liquid and gas phase in Mixture 2 HDO (0.43 g 5% Ni_2P/HZSM-5, 0.05 mL/min Mixture 1, 40 mL/min H_2, 10 mL/min N_2, reaction time: 90 min): (A) Content of chemical composition in the liquid phase (free water); (B) Content of chemicals in the gas phase

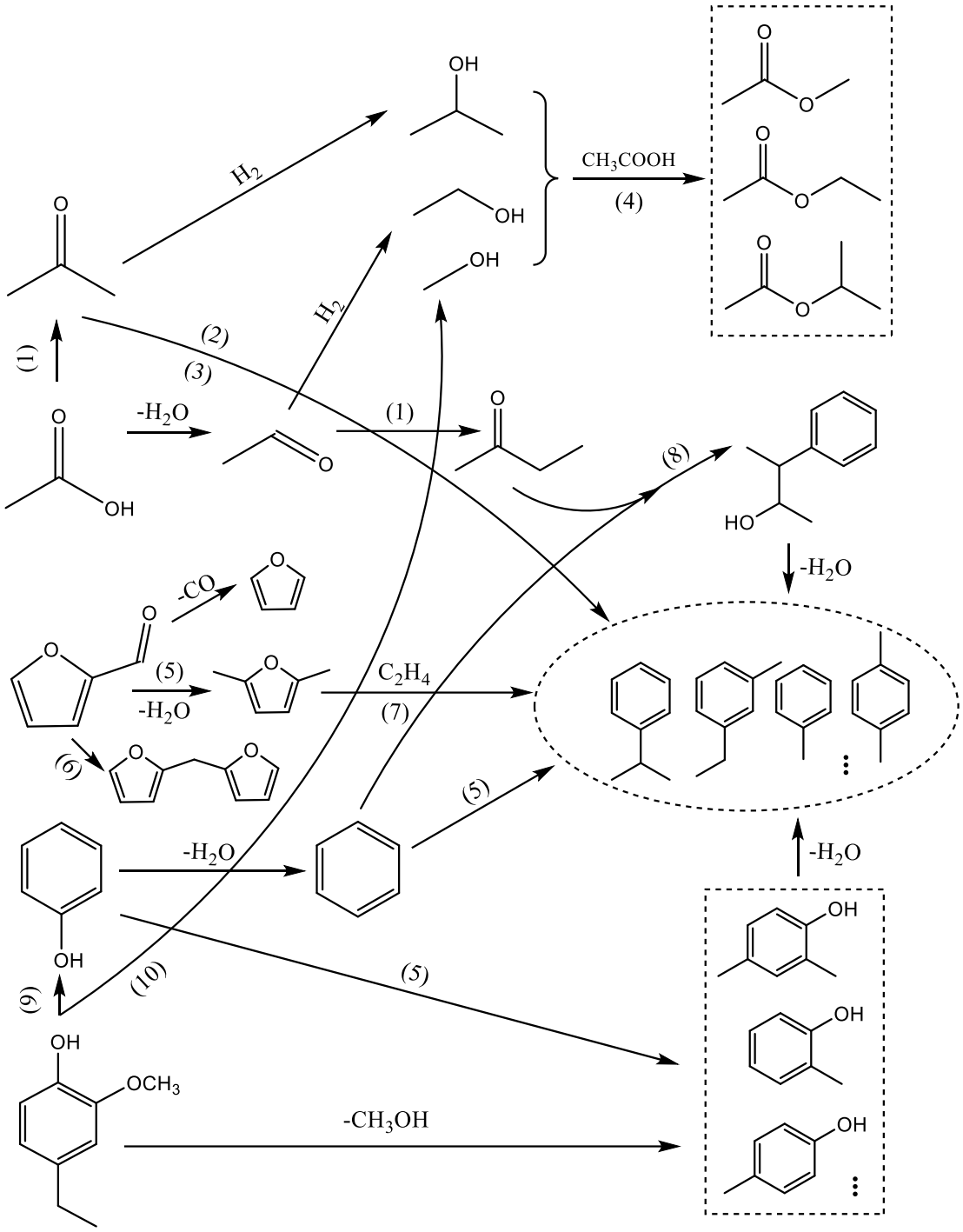

Figure 5.9 Proposed interaction network of Mixture 2 HDO: (1) Self-ketonization; (2) Adol condensation; (3) Isomerization; (4) Esterification; (5) Alkyl substitution; (6) Condensation; (7) Cycloaddition; (8) Substitution; (9) Dealkylation; (10) Methoxyl group removal

5.4 HDO of bio-oil

Based on the aforementioned discussion of the mixture HDO, the basic competition reactions and complex reaction routes among typical model molecules of bio-oil were concluded. This could help to understand the main reactions in the real bio-oil HDO. To evaluate and confirm this, HDO of medium-temperature fraction bio-oil (MT-FB) and crude bio-oil, as mentioned in ***Sections 5.2.1*** and ***5.2.2***, would be performed in the following sections. MT-FB was examined because it had a close content but less heavy molecules amount compared to the crude bio-oil. Besides, considering the high viscosity of crude bio-oil, acetone was used as a co-feed (diluent) to reduce the viscosity of bio-oil. On the other hand, acetone is also a good feed to produce aromatic hydrocarbons, prevent coke formation, and could improve the properties of upgraded bio-oil during the HDO process.

5.4.1 Upgrading of MT-FB of crude bio-oil

Table 5.7 presents the main comparative properties of MT-FB and upgraded MT-FB bio-oil. A DOD value of 90.0%, a conversion rate of acetic acid of 80%, and a high water content of 79.03% were observed by catalytic hydrotreatment, indicating that 5% Ni_2P/HZSM-5 catalyzed efficiently the light fraction bio-oil. However, the MT-FB is likely not suited for producing high-qualify biofuels due to a low yield of liquid products (13.70%) and a significant coke formation (8.99%). Notably, no phenols, guaiacols, sugars, or amides were detected after hydrotreatment due to the formation of major aromatic hydrocarbon (C_6-C_{12}, 28.87%), minor alkanes (C_5-C_7, 8.13%), and coke.

Table 5.7 Comparison of MT-FB and upgraded MT-FB

Item	DOD (wt%)	$X_{acetic\ acid}$ (wt%)	$Y_{liquid\ products\ (free\ water)}$ (wt%)	Y_{coke} (wt%)	Water content (wt%)	$D_{Aromatic\ hydrocarbons}$ (C_6-C_{12}) (wt%)	D_{Alkane} (C_5-C_7) (wt%)	$D_{Phenols/Guaiacols/Sugars/Amides}$ (wt%)
MT-FB	-	-	-	-	36.38	-	-	5.02/1.45/ 2.10/0.07
Upgraded MT-FB [a]	90.0	80	13.70	8.99	79.03	28.87	8.13	-/-/-/-

[a] fixed conditions: 0.43 g 5% Ni_2P/HZSM-5 catalyst, 400 °C (oven), 270 °C (preheater), 0.05 mL/min of MT-FB, 3 MPa, H_2: 40 mL/min, N_2: 10 mL/min, 90 min

5.4.2 Upgrading of crude bio-oil

HDO of total fraction bio-oil HDO was first carried out using HZSM-5, 5% Ni_2P/HZSM-5, and 10% Ni_2P/HZSM-5 catalysts, but the products were not analyzed since the serious coke formation blocked the reactor after 60 min reaction. The coke formation on the surface of the three spent catalysts was discussed based on the thermogravimetry analysis (TGA) in the following ***Section 5.4.2.4***.

Generally, one experiment procedure of the bio-oil HDO test with Ni-based catalysts included three stages (***Figure 5.10***): stage I, to reduce the catalysts; stage II, to increase the total pressure under N_2 to a desired value; stage III, to inject the bio-oil with the desired ratio of H_2/N_2. In this study, the optimal ratio of H_2/N_2 is 40/10 (mL/min) based on the discussion in ***Section 3.4.4***, ***Chapter 3*** .

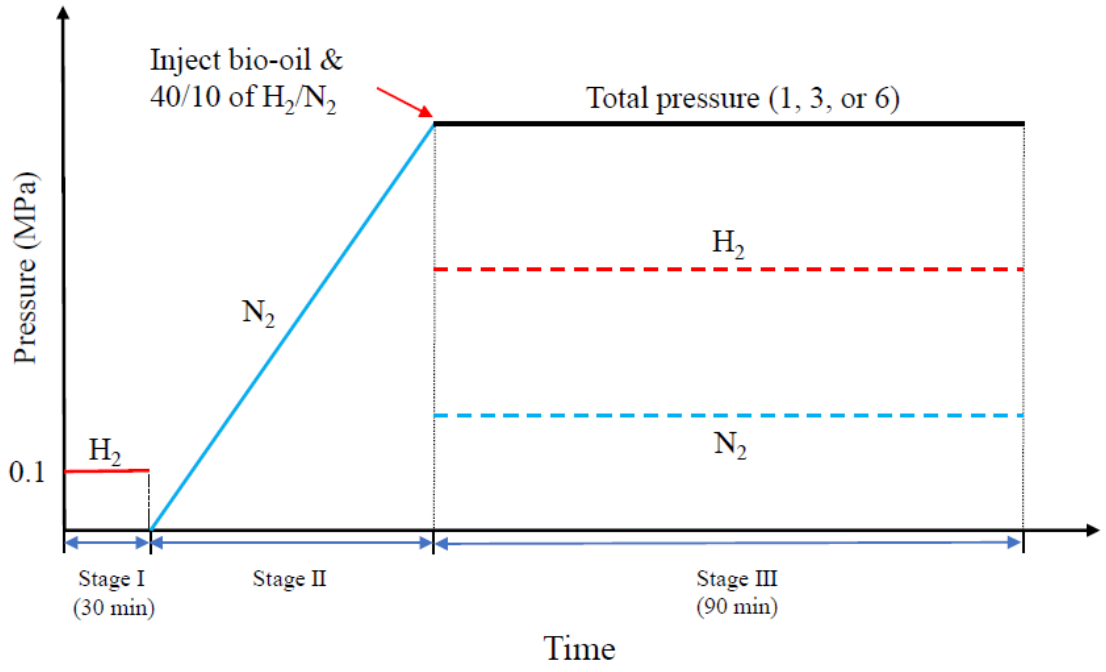

Figure 5.10 Schematic diagram of crude bio-oil HDO process

5.4.2.1 Effect of total pressure

To investigate the effect of the total pressure on the bio-oil hydro-deoxygenation using 5% Ni_2P/HZSM-5, a set of experiments at different total pressures from 1 MPa to 6 MPa was performed at 400 °C. ***Figure 5.11*** shows that a high conversion rate of acetone around 95%, of acetic acid (complete conversion) and a value of DOD around 85.0% are obtained at all the pressures, demonstrating almost no influence on the conversion

of acetone and acetic acid, nor on bio-oil deoxygenation. However, the results depicted that the yields of liquid and gas products were enhanced respectively from 41.69% to 54.46% and 20.26% to 25.53% with an increase of the pressure from 1 MPa to 6 MPa. Contrary to the yield of water, which dropped from 38.05% to 20.10%. The composition of the liquid phase was similar under different total pressure, more details of the composition of the liquid and gas products were thus shown in ***Appendix C*** (***Table C.2***). Accordingly, the total pressure had almost no effect on the conversion rate of crude bio-oil but improved the yield of useful liquid and gas products.

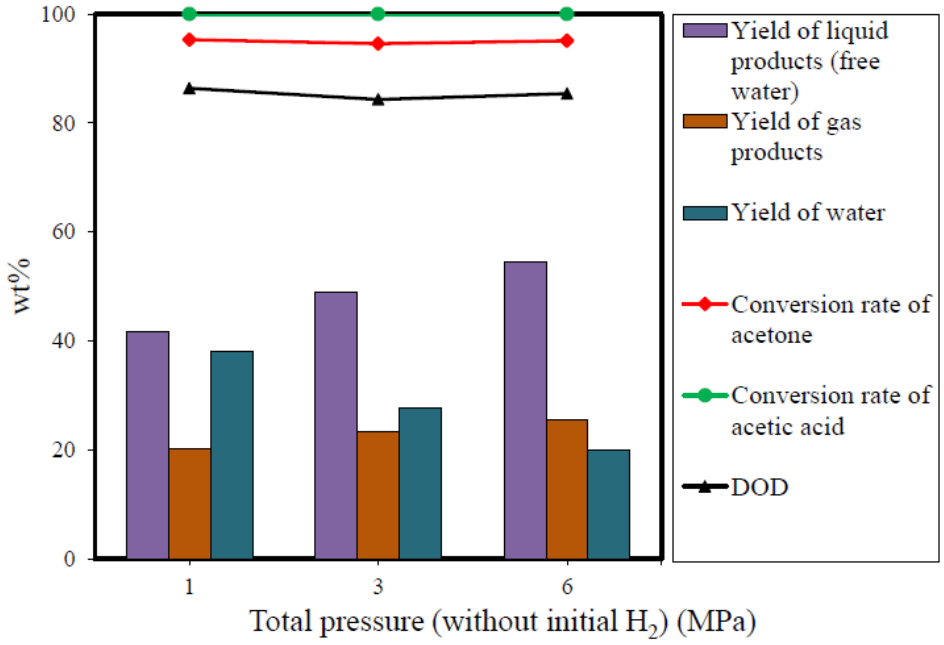

Figure 5.11 Effect of total pressure on crude bio-oil hydrotreatment (0.43 g 5% Ni_2P/HZSM-5, 400 °C (oven), 400 °C (preheater), 0.05 mL/min of feed (acetone/bio-oil = 10/1), H_2 initial pressure = 0, 40 mL/min H_2, 10 mL/min N_2, reaction time: 90 min)

5.4.2.2 Effect of bio-oil concentration in the feed

Conversion rate and DOD

Based on the above discussion, the subsequent experiments were performed under fixed conditions: 0.43 g Ni_2P/HZSM-5, total pressure 6 MPa. To examine the effect of the ratio of acetone/bio-oil, a series of experiments with varying concentrations of co-feed acetone were investigated. ***Figure 5.12*** presents the conversion/production rate of acetone and acetic acid, DOD, and yields of products. It can be seen that the conversion

rate of acetone and DOD decrease respectively from 95% to 84% and 85.4% to 76.8 % with the increase of the bio-oil concentration in the feed. Acetic acid can be converted completely at the points of 10/1 and 5/1 of acetone/bio-oil, yet its production rate falls sharply to - 9% at 1/1 of acetone/bio-oil, which is probably for three reasons. One is a competitive reaction between acetic acid molecules and other high activity molecules (like phenols) observed in our previous results (see ***Section 5.3.1.3***). A restrained reaction between acetic acid and phenol molecules was also reported in in-situ hydrogenation of bio-oil model compounds by Zhang et al. over a Ni/CMK-3 catalyst.[203] Furthermore, it may also be the case that a high conversion rate of acetic acid was reached on HDO of single acetic acid using Ni_2P/HZSM-5 catalysts (see ***Chapter 4*** , ***Section 4.4.1*** and ***Appendix C***, ***Table C.1***). On the other hand, the presence of a considerable quantity of water and coke at 1/1 of acetone/bio-oil led to much more deactivation of catalysts. Also, an increasing transformation of other chemicals (like acetic esters) favored a certain amount of acetic acid formation due to the high water content.

Yield

A slightly descending trend for the yields of both the liquid and gas products was observed when the ratio of acetone/bio-oil went to 5/1 from 10/1, but this descending trend became steeper from the point 5/1 to 1/1, contrary to the trend of water yield from 20.01% to 30.96%. The increased water yield was mainly attributed to the increasing water content of the feed with the increasing ratio of crude bio-oil (40.33% of water content in crude bio-oil). A serious coke formation of 7.69% was only found at the point of 1/1 of acetone/bio-oil. These results indicated that the use of concentrated acetone in the feed enhanced both the yield of liquid and gas products and probably prevented coke formation by reducing the potential deactivation of catalysts to some extent since no coke was observed in acetone HDO in ***Chapter 3*** . This was able to happen because the strong interaction between easily carbonizing components (i.e. guaiacol,[71] sugars,[204] etc.) of bio-oil, and acetone molecules with a smaller size could reduce the condensation reaction of these components on both the internal and external acid sites of catalysts. On the other hand, this promoted the direct dealkylation reaction of large molecules on surface acid sites of catalysts to produce gases.

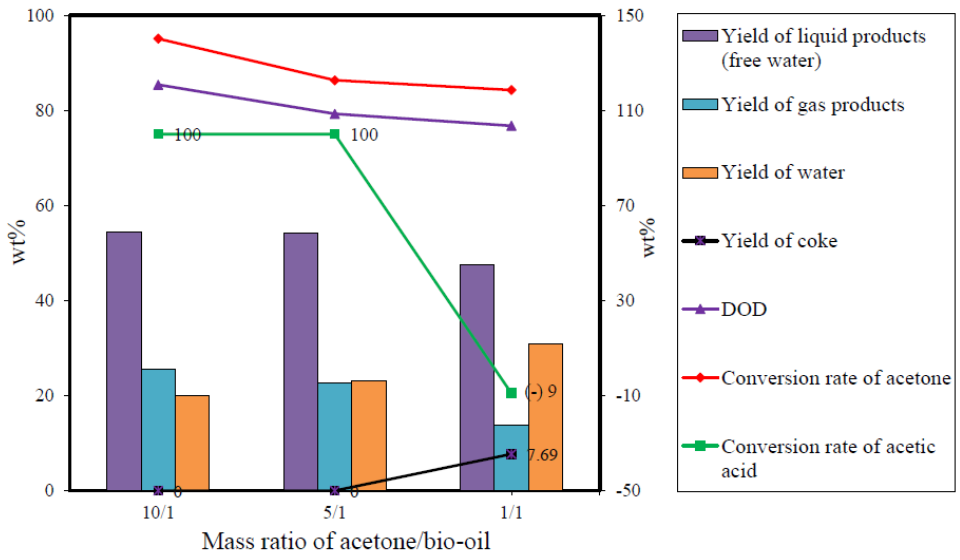

Figure 5.12 Effect of bio-oil concentration on crude bio-oil hydrotreatment (0.43 g 5% Ni_2P/HZSM-5, 400 °C (oven), 400 °C (preheater) 0.05 mL/min of feed, total pressure 6 MPa (H_2 initial pressure = 0), 40 mL/min H_2, 10 mL/min N_2, reaction time: 90 min); "(-)", production rate (an increaed amount of a certain chemical in the upgraded liquid phase compared to its initial amount)

Liquid products

Figure 5.13 depicts the composition of liquid and gas products in crude bio-oil hydro-deoxygenation with different weight ratios of acetone and bio-oil. As shown in *Figure 5.13A*, the composition of alkanes above 6% and aromatic hydrocarbons around 74% at the ratio points of acetone/bio-oil (10/1 and 5/1) was perceptibly higher than the value in the case of 1/1. The high concentration of carboxylic acids was mainly due to their low conversion rate at the point of 1/1. Furthermore, the composition of hydrocarbons (alkenes (C_4-C_6), alkanes (C_4-C_6), and aromatic hydrocarbons (C_6-C_{18})) showed close values of around 82% at the points of 10/1 and 5/1, but then significantly descended to 73.66% as the use of acetone in the feed decreased to 1/1. The greater composition of hydrocarbons might be linked to the lasting activity of catalysts attributed to the relatively slow deactivation of catalysts in the presence of concentrated acetone. This lead to the aldol condensation of acetone and subsequent isomerization to form various aromatic hydrocarbons, the route of which was observed by Thompson et al.[163] and in our previous study.[147] The high activity of catalysts also favored sufficient hydrolysis of weight molecules to form short-chain alkenes which subsequently underwent addition, cyclization, and subsequent isomerization reactions to synthesize aromatic hydrocarbons. A similar reaction pathway via cyclization and aromatization of C_2-C_6

olefins was reported in an early work by Bakhshi et al. using zeolite catalysts (i.e. HZSM-5, H-mordenite, and H-Y).[205]

Gas products

For gas products, CH_4, CO_2, and C_3H_8 were the major components detected in all cases, followed by C_2H_6, C_2H_4, and C_2H_2, as shown in ***Figure 5.13B***. Among these gases, C_2H_4, C_2H_6, and C_3H_8 kept an almost constant distribution (4%, 11%, and 33%, respectively) when the ratio of acetone/bio-oil increased from 10/1 to 5/1, and then decreased to some extent, suggesting that a high-efficiency dehydration reaction of acetic acid and acetone, and/or dealkylation of the phenolic compounds in bio-oil occurred under these conditions. CH_4 showed a significant reducing distribution when the acetone/bio-oil enhanced to 5/1, indicating suppression of demethylation during this process. In particular, an increment of the acetic acid distribution was observed with the improvement of the acetone/bio-oil rate. Considering the increasing yield of gas products in ***Figure 5.11*** and the global trend of CH_4, C_2H_4, C_2H_6, and CO_2, it can be deduced here that a low bio-oil concentration favored the direct hydrogenation of acetic acid to produce C_2H_4 and C_2H_6, but a high concentration affected acetic acid to form CO_2 via decarboxylation. Only a few C_2H_2 amounts were detected, probably revealing a high sufficiency of hydrogenation at all acetone/bio-oil ratios.

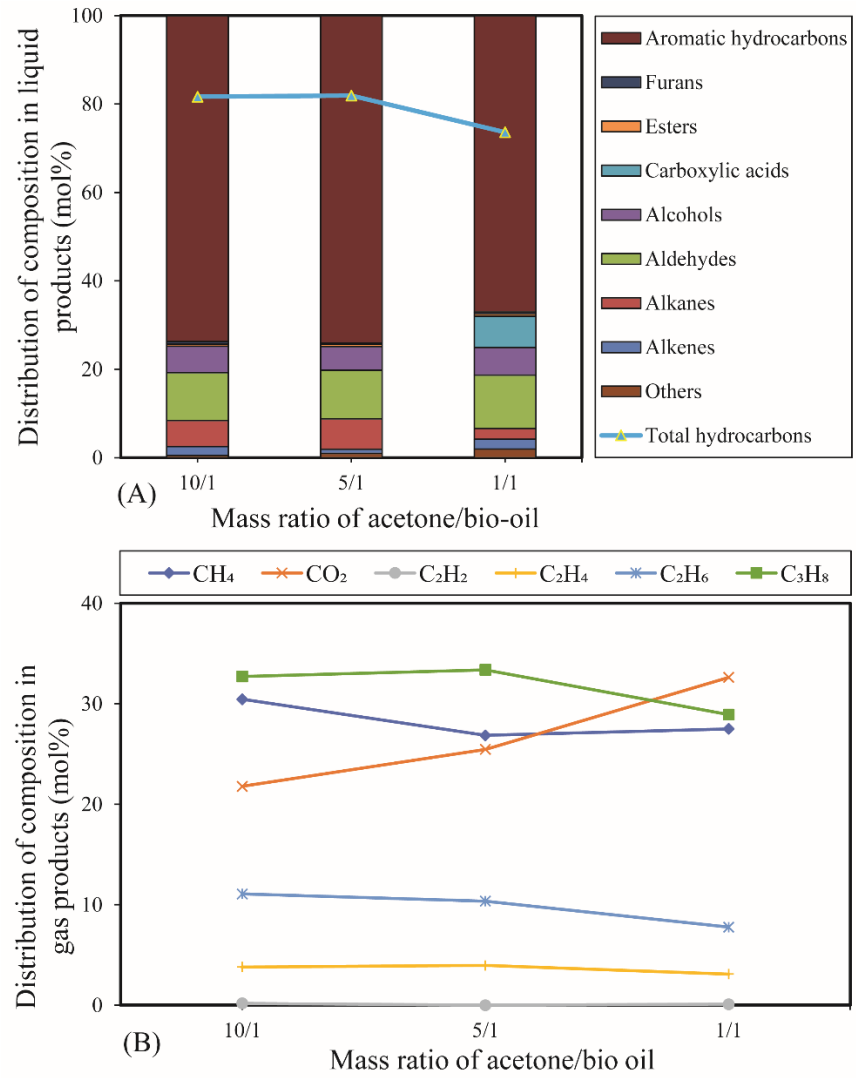

Figure 5.13 Effect of bio-oil concentration on crude bio-oil hydrotreatment (0.43 g 5% Ni_2P/HZSM-5, 400 °C (oven), 400 °C (preheater) 0.05 mL/min of feed, total pressure 6 MPa (H_2 initial pressure = 0), 40 mL/min H_2, 10 mL/min N_2, reaction time: 90 min): (A), Composition in liquid products (without considering acetone); (B), Composition in gas products.

5.4.2.3 Proposed pathways of bio-oil hydrotreatment

Figure 5.14 shows the main hydrotreatment pathways of bio-oil over Ni_2P/HZSM-5 catalysts based on the aforementioned results and discussion. These proposed pathways were focused on the hydrotreatment of the major chemical families (> 5 mol%) in bio-oil. Several basic reactions such as decarboxylation, hydrodeoxygenation, isomerization, and transalkylation were observed during the hydrotreatment process. In more detail, carboxylic acids underwent decarboxylation and hydrodeoxygenation to form C_1-C_2 gases and also acetaldehyde. Esters could be converted to aldehydes, and C_4-C_6 hydrocarbons (alkanes and alkenes) via esterlysis due to the abundant amount of

water formation, following direct decarboxylation and/or dehydration as well. These light hydrocarbons were considered to come from the hydrodeoxygenation of alcohols, aldehydes, and some of the ketones. Other ketones could transfer to higher ketones by aldol condensation and subsequent aromatic hydrocarbons by cyclization on the acid sites of the HZSM-5 support. Sugars were generally catalyzed to synthesize aromatic hydrocarbons (C_{13}-C_{18}) and even produce coke through direct dehydration followed by cyclization/isomerization. However, phenols were converted to monocyclic aromatic hydrocarbons (mainly, C_6-C_9) via dehydration and transalkylation due to the presence of alkyl radical group, which were ascribed to the effect of Ni.

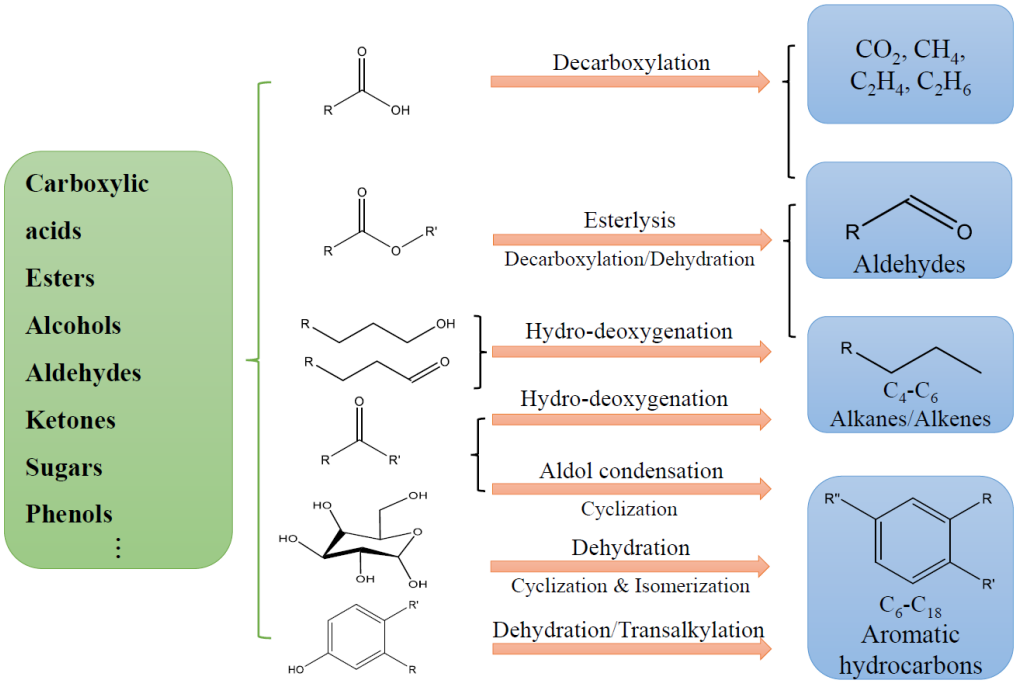

Figure 5.14 Main reaction pathways of bio-oil hydrotreatment over Ni_2P/HZSM-5 catalysts

To be concluded from the above discussion in this Chapter and proposed reaction pathways in ***Figure 5.6, Figure 5.9***, and ***Figure 5.14***, similar competition reactions and several basic reaction types existed in both the HDO process of model molecules mixtures and bio-oil. They involved the competitive reactions between acetic acid and other oxygenated chemicals and also the decarboxylation, dehydration, aldol condensation, transalkylation/alkyl-substitution, cyclization, isomerization, etc. Thus, it can be said that the simulation of bio-oil HDO using the mixture of model molecules is efficient.

5.4.2.4 Thermogravimetry analysis (TGA) of spent catalysts

To evaluate the formation of coke on the spent catalyst, the characterization of the spent catalysts was first carried out under the N_2 atmosphere (50 mL/min). ***Figure 5.15*** depicts the TGA (under N_2) profiles of the HZSM-5, 5% Ni_2P/HZSM-5, and 10% Ni_2P/HZSM-5 spent catalysts after HDO of crude bio-oils at 400 ºC. It can be seen from ***Figure 5.15A*** that the overall mass losses for the spent HZSM-5, 5% Ni_2P/HZSM-5, and 10% Ni_2P/HZSM-5 catalysts are about 10%, 8%, and 6.5%, respectively. The results indicated that the active phase of Ni_2P affected the mass loss of the spent catalysts, and a lower mass loss was observed with the increasing content of the Ni_2P phase. This is attributed to the fact that Ni_2P covered the active sites of HZSM-5, thus preventing coke formation. In the literature, Zhang et al.[206] reported that different types of coke species (soft coke, hard coke, and graphite) were formed on spent catalysts during the catalytic fast pyrolysis of biomass derivates.

Figure 5.15B shows the derivative of weight (DTG) curves of the HZSM-5, 5% Ni_2P/HZSM-5, and 10% Ni_2P/HZSM-5 spent catalysts. The spent 5% and 10% Ni_2P/HZSM-5 samples exhibited the same trend as the DTG curves, and peaks at about 370 ºC appeared due to the formation of soft coke, while a broad peak existed at 550 ºC was due to the presence of the hard coke. For the HZSM-5 sample shown in ***Figure 5.15B***, the peaks appeared, needing higher temperatures of 450 ºC and 620 ºC when compared to Ni_2P/HZSM-5 samples (370 ºC and 550 ºC). This illustrated that the coke formed on the HZSM-5 catalyst is difficult to move away because of more graphitic-like carbon in comparison with Ni_2P/HZSM-5 catalysts. Thus, it can be deduced that the Ni_2P phase plays an important role in preventing the formation of graphite carbon.

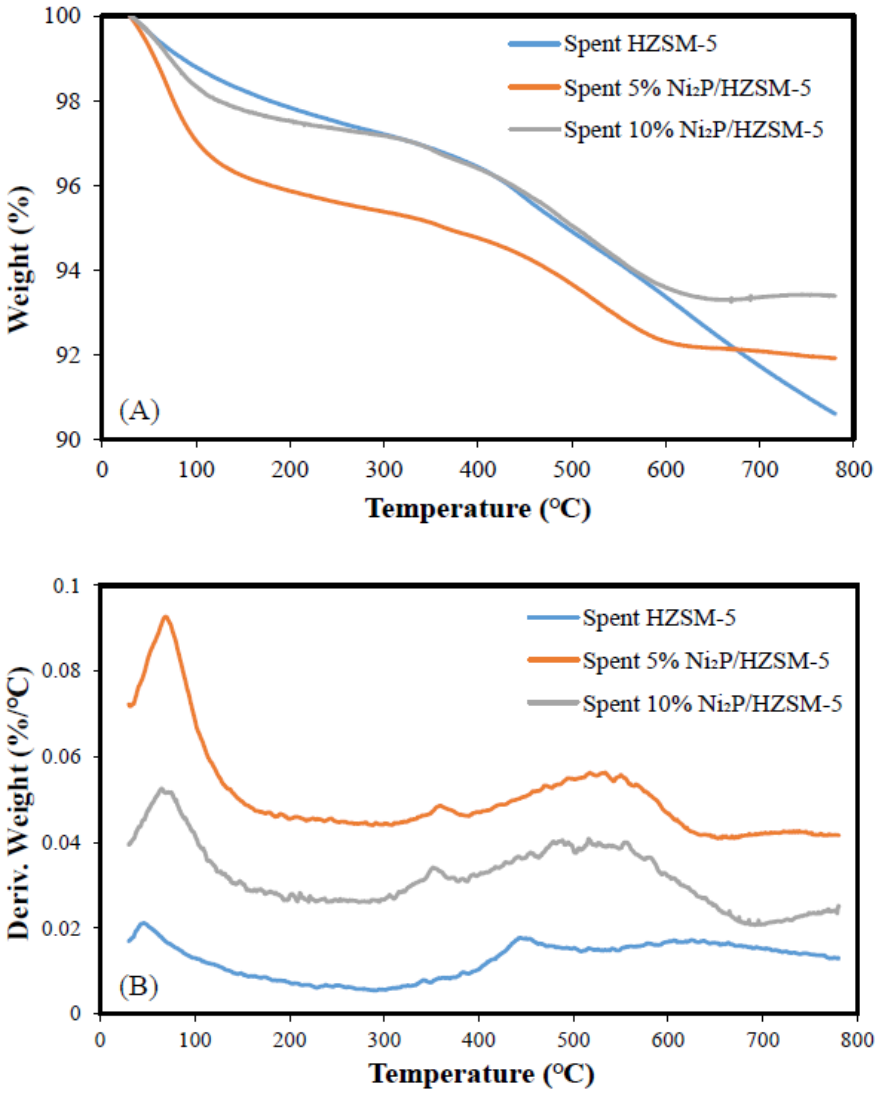

Figure 5.15 Thermogravimetry (TG) analysis results under N_2 of spent catalysts in pyrolysis oil HDO at 400 °C: (A) Weight loss, (B) Derivative of weight (DTG)

In addition, the spent catalysts were second characterized by the TG technique under air (50 mL/min) to further investigate the coke formation on the surface of the catalysts. ***Figure 5.16*** shows the TGA (under air) profiles of the HZSM-5, 5% Ni_2P/HZSM-5, and 10% Ni_2P/HZSM-5 spent catalysts after HDO of crude bio-oil at 400 °C. ***Figure 5.16A***, a total weight loss of around 10% for the spent HZSM-5 and of around 7% for spent Ni_2P/HZSM-5 catalysts, was observed. In particular, from the curves range above about 300 °C, the mass loss was due to the oxidation of coke. Thus, it can be seen that the mass loss of coke on spent HZSM-5, 5% Ni_2P/HZSM-5, and 10% Ni_2P/HZSM-5 catalysts was about 9%, 4%, and 5%, respectively. The lower weight loss of the Ni_2P/HZSM-5 catalysts compared to the value of the HZSM-5 catalyst also indicated

that the Ni_2P active phase actually reduced the formation of coke on the HZSM-5 surface during the bio-oil hydro-deoxygenation.

Figure 5.16B shows the DTG curves of the HZSM-5, 5% Ni_2P/HZSM-5, and 10% Ni_2P/HZSM-5 spent catalysts. The DTG curves show four stages: stage I, the loss of water (0-150 ºC); stage II, the release of physical adsorbents (150-300 ºC); stage III, the removal of soft coke (300-450 ºC); stage IV, the removal of hard coke and/or graphite (450-650 ºC). Similar observations are in good agreement with the results reported by Zhang et al..[206] In ***Figure 5.16B***, the peak between 300 and 375 ºC was attributed to the loss of soft coke on the surface of catalysts, and the peak at about 470 and 500 ºC was probably assigned the oxidation of hard coke and graphite, respectively. Notably, no obvious peaks at 470 ºC were observed in the above ***Figure 5.15B*** due to the much hard removal of coke under N_2, which could be also proved the oxidation of hard coke from another aspect. Then, the totally broad peak from around 300-650 ºC on the HZSM-5 catalyst was due to the release of all the soft, hard coke, and graphite by their oxidation.

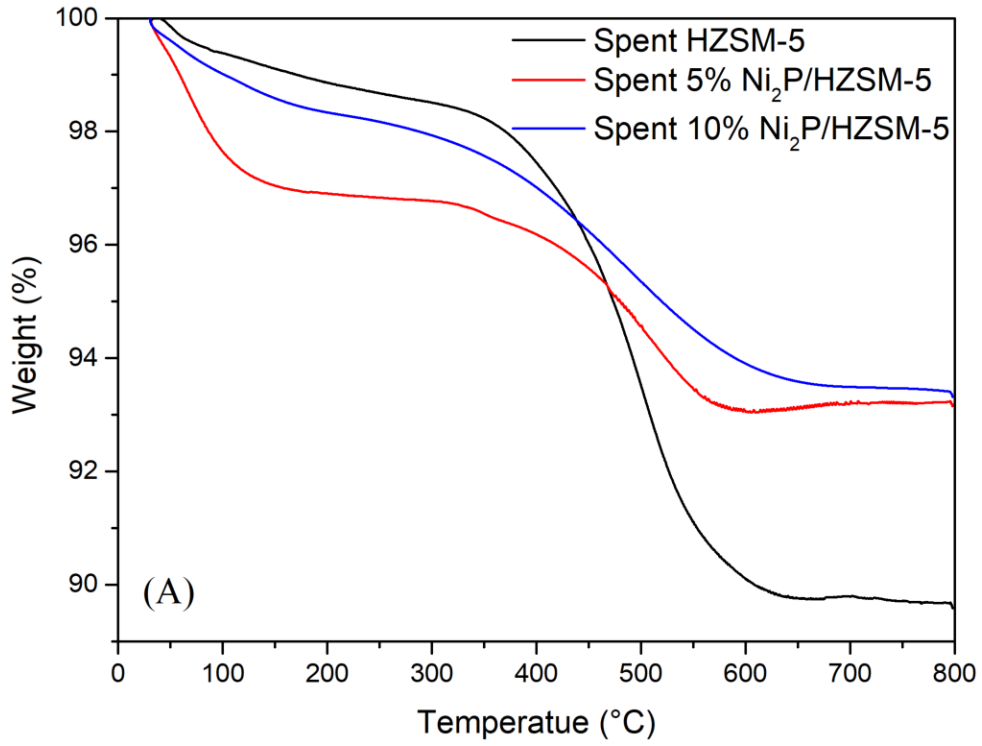

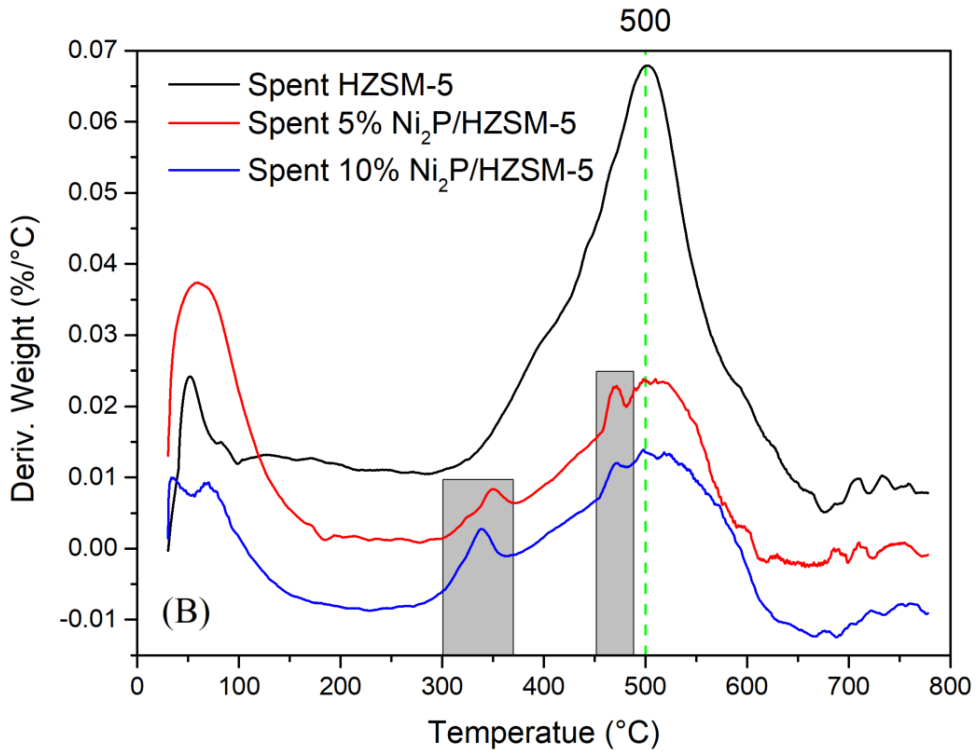

Figure 5.16 Thermogravimetry (TG) analysis results under air atmosphere of spent catalysts in pyrolysis oil HDO at 400 °C: (A) Weight loss, (B) Derivative of weight (DTG)

5.5 Conclusion

The blank HZSM-5 and prepared Ni_2P/HZSM-5 catalysts for HDO of two mixtures (involving acetone, acetic acid, phenol, 4-ethylguaiacol, furfural, and water) as model bio-oil were studied. Catalysts with Ni_2P active phases exhibited higher activity than the blank HZSM-5. The results showed that the temperature had a significant effect on the competition between acetic acid and phenol probably based on the differential absorption properties. The partial pressure of H_2 showed almost no influence on phenol conversion with the presence of acetic acid. In all cases, alkyl-substituted phenols (cresol, 2,4-dimethylphenol, etc.) and aromatic hydrocarbons (benzene, toluene, xylene, etc.) were the primary liquid products. CO, CH_4, and CO_2 were observed to be the dominant gas products. In the Mixture 2 HDO, low temperatures facilitated the formation of esters by esterification. It was certified that the primary influencing parameters of model bio-oil HDO were the nature of catalyst and temperature followed by the H_2 partial pressure. The proposed reaction networks revealed that alkyl

substitution and esterification were the main reactions, followed by condensation, isomerization, and hydrogenation.

For the bio-oil HDO, it was found that MT-FB was not a suitable feed to obtain a high yield of biofuel. In the crude bio-oil HDO, high total pressure led to a relatively high yield of the liquid products. A high ratio of acetone to bio-oil in the feed enhanced not only the yield of liquid and gas products but also the hydrocarbons production in the liquid phase and suppressed the formation of coke. A percentage of hydrocarbons of 81.92% was obtained for the upgraded bio-oil. Besides, a proposed reaction pathway revealed that decarboxylation, hydrodeoxygenation, isomerization, and transalkylation were the main reactions during the hydrotreatment process using Ni_2P/HZSM-5. The simulation of bio-oil using the mixture of model molecules was proved to be an efficient method for giving guidance to the comprehension of the bio-oil HDO. Finally, The thermogravimetry (TG) analysis results of the spent catalysts indicated that the active phase of Ni_2P reduced the formation of coke on the HZSM-5 surface during the bio-oil hydro-deoxygenation since the Ni_2P phase partially covered the active sites of HZSM-5.

General conclusion and perspectives

1 Conclusion

The main aim of the present study was to provide a detailed characterization of the catalytic upgrading of platform chemicals and pyrolysis oil from biomass sources to give high-valued chemicals and/or biofuels and comprehension of the primary reaction pathways during the hydrotreatment process with a fixed-bed continuous reactor.

Firstly, four home-made nickel phosphide catalysts (namely, 5% and 10% Ni_2P/HZSM-5, 5% and 10% Ni_2P/SiO_2) were prepared using the incipient wetness impregnation method before model molecules upgrading. Then, a commercial HZSM-5 catalyst and these four catalysts were characterized by various methods. It was found that the Ni_2P active phase was successfully formed on the catalysts based on the following results:

- The BET surface area of the catalysts decreased as a result of a partial pore filling with the enhancement of Ni_2P content.
- Significant feature peaks of crystallized Ni_2P phase, especially for 5% Ni_2P catalyst, were observed. This was further confirmed by the detected reduction peak of oxidized nickel and phosphorus species from H_2-TPR (DSC) profiles of the catalysts precursors.
- A part of the acid sites of HZSM-5 were replaced by the Ni_2P active phase due to the reduced acidity.

Secondly, the catalytic upgrading of ketones using acetone as a model compound was studied to optimize the reaction parameters, including the nature of the catalysts, contact time, temperature, and pressure. The results showed the following:

- Ni_2P/HZSM-5 catalysts exhibited higher activity than Ni_2P/SiO_2 catalysts.
- The principal influencing parameter of acetone HDO was temperature, affecting both the acetone conversion rate and the selectivity of the main products (acetaldehyde, aromatic hydrocarbons, and gas products).
- High selectivities of 64% and 59.8% for aromatic hydrocarbons were achieved separately with HZSM-5 and 5% Ni_2P/HZSM-5 catalyst.
- A multiple steps aldol condensation of acetone led to the formation of MIK and subsequent aromatic hydrocarbons.

Thirdly, the catalytic hydrodeoxygenation of three other model compounds: acetic acid, 4-ethylguaiacol, and furfural, was examined based with varying the temperature and pressure using the HZSM-5 and Ni_2P/HZSM-5 catalysts. The results indicated the following:

- The decarboxylation, hydrogenation, and further decarbonylation during acetic acid HDO were markedly affected by the temperature and pressure, leading to the release of CO, CH_4, and CO_2.
- Cresol, 2,4-dimethylphenol, and 2-ethyl-6-methylphenol as the most important reaction intermediates of 4-ethylguaiacol HDO could be converted to phenol and BTX via dealkylation, dihydroxylation, and isomerization. Besides, the further dealkylation of 2-ethyl-6-methylphenol intermediate was reduced by the formation of coke.
- The principal reaction of furfural HDO was the decarbonylation, producing furan and CO. And the addition and subsequent cyclization-dehydration of dienes were probably responsible for the synthesis of aromatic hydrocarbons.

Finally, the competitive and cross-reactions of the HDO of two blends of bio-oils model molecules (involving acetone, acetic acid, phenol, 4-ethylguaiacol, furfural, and water) was investigated using the prepared Ni_2P/HZSM-5 catalysts. Besides, the bio-oil hydro-deoxygenation was explored based on the optimization of the total pressure, and H_2 pressure, and the solvent ratio. From the results, it was concluded that:

- The temperature affected significantly the competition between acetic acid and phenol reaction due to their different adsorption properties.
- Alkyl substitution reaction and esterification were the main reactions of the blends HDO, followed by condensation, isomerization, and hydrogenation.
- High total pressures give a relatively high yield of liquid products. And, a high ratio of acetone to bio-oil in the feed enhanced not only the yield of liquid and gas products but also the hydrocarbons distribution of the liquid phase and suppressed the formation of coke.
- The active phase of Ni_2P actually reduced the formation of coke on HZSM-5 surface during the bio-oil hydro-deoxygenation. A distribution including 81.92% of hydrocarbons for hydrotreated bio-oils was obtained.
- Decarboxylation, hydrodeoxygenation, isomerization, and transalkylation were the main reactions taking place on Ni_2P/HZSM-5.

- The simulation of bio-oil using single model molecules and their mixtures was proved to be an efficient method for giving guidance to comprehension of the bio-oil HDO.

2 Perspectives

Although the previous sub-part has provided an overall conclusion of the present work and its principle results, some recommendations for future investigations can be proposed as follows:

1) Developing the kinetic modeling of bio-oils upgrading, including both model molecules and real bio-oils to further confirm the proposed reaction pathways.

As shown in this work, catalytic upgrading of several platform compounds, their mixture, and crude bio-oil was carried out in a continuous system. And a relatively high yield of high-value chemicals and upgraded bio-oils was reached via various probable reaction routes. However, it would be useful to develop the specific kinetic modeling of these reactions, to give a more accurate comprehension of the reaction pathways and help to further improve the selectivity of useful chemicals as well as the yield of upgraded bio-oils with a high hydrocarbons content.

2) Using other types of solvent (such as alcohols and alkanes) with crude bio-oils in the feed to compare the quality of upgraded bio-oils.

As mentioned in ***Chapter 3*** and ***Chapter 5*** (***Section 5.4***), acetone proved to be a suitable platform molecule and solvent for crude bio-oil upgrading due to its good chemical, physical, and hydrotreating properties. However, it would still be interesting to compare its efficiency with the performance of other common solvents and to finally find the best way to produce commercializable bio-oil based on economic, environmental, and other considerations.

3) Optimizing and deeply characterizing the fresh and spent catalysts to improve their performance and their resistance to the formation of coke.

The reaction pathways in this work currently proposed were based on the content of chemicals in the liquid and gas products. Thus, to deeply explore the reaction mechanism, it is useful to further optimize the fresh catalysts involving the content of

Ni_2P phase and the initial ratio of Ni/P. On the other hand, it is also interesting to deeply characterize the fresh catalysts and spent catalysts by using more techniques. It would also be interesting to develop a catalyst allowing to have a narrower distribution of products.

4) Performing the subsequent utilization of oxygenated gas products (CO and CO_2) to produce biofuels and simultaneously reduce the emission of greenhouse gas.

Bio-oil is known to have a high content of carboxylic acid, leading to the formation of a great amount of oxygenated gas (mainly CO_2) during its hydro-deoxygenation via decarboxylation and hydrocracking. However, the direct release of CO_2 (especially on an industrial scale) will increase global climate warming due to the greenhouse effect and will not meet the requirements of the Paris Climate Agreement. Thus, it is necessary to reutilize the CO_2 produced during the hydro-deoxygenation of bio-oil via a subsequent catalytic system (***Figure 6.1***).

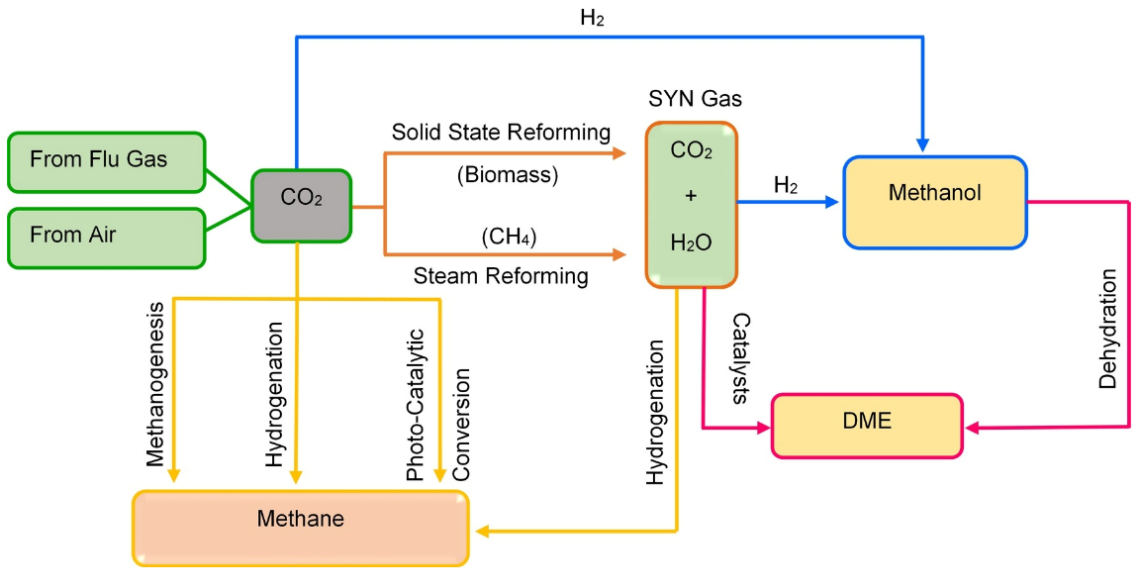

Figure 6.1 Entire CO_2 capture and utilization schematic pathways

Bibliography

(1) Ambursa, M. M.; Juan, J. C.; Yahaya, Y.; Taufiq-Yap, Y. H.; Lin, Y.-C.; Lee, H. V. A Review on Catalytic Hydrodeoxygenation of Lignin to Transportation Fuels by Using Nickel-Based Catalysts. *Renewable and Sustainable Energy Reviews* **2021**, *138*, 110667. https://doi.org/10.1016/j.rser.2020.110667.

(2) Höök, M.; Tang, X. Depletion of Fossil Fuels and Anthropogenic Climate Change—A Review. *Energy Policy* **2013**, *52*, 797–809. https://doi.org/10.1016/j.enpol.2012.10.046.

(3) Akhtar, A.; Krepl, V.; Ivanova, T. A Combined Overview of Combustion, Pyrolysis, and Gasification of Biomass. *Energy Fuels* **2018**, *32* (7), 7294–7318. https://doi.org/10.1021/acs.energyfuels.8b01678.

(4) Popp, J.; Kovács, S.; Oláh, J.; Divéki, Z.; Balázs, E. Bioeconomy: Biomass and Biomass-Based Energy Supply and Demand. *New Biotechnology* **2021**, *60*, 76–84. https://doi.org/10.1016/j.nbt.2020.10.004.

(5) Rover, M.; Smith, R.; Brown, R. C. Enabling Biomass Combustion and Co-Firing through the Use of Lignocol. *Fuel* **2018**, *211*, 312–317. https://doi.org/10.1016/j.fuel.2017.09.076.

(6) Hossain, M. A.; Jewaratnam, J.; Ganesan, P. Prospect of Hydrogen Production from Oil Palm Biomass by Thermochemical Process – A Review. *International Journal of Hydrogen Energy* **2016**, *41* (38), 16637–16655. https://doi.org/10.1016/j.ijhydene.2016.07.104.

(7) Chen, W.-H.; Lin, B.-J.; Huang, M.-Y.; Chang, J.-S. Thermochemical Conversion of Microalgal Biomass into Biofuels: A Review. *Bioresource Technology* **2015**, *184*, 314–327. https://doi.org/10.1016/j.biortech.2014.11.050.

(8) dos Santos, A. C.; Ximenes, E.; Kim, Y.; Ladisch, M. R. Lignin–Enzyme Interactions in the Hydrolysis of Lignocellulosic Biomass. *Trends in Biotechnology* **2019**, *37* (5), 518–531. https://doi.org/10.1016/j.tibtech.2018.10.010.

(9) Wang, Y.; He, T.; Liu, K.; Wu, J.; Fang, Y. From Biomass to Advanced Bio-Fuel by Catalytic Pyrolysis/Hydro-Processing: Hydrodeoxygenation of Bio-Oil Derived from Biomass Catalytic Pyrolysis. *Bioresource Technology* **2012**, *108*, 280–284. https://doi.org/10.1016/j.biortech.2011.12.132.

(10) Guedes, R. E.; Luna, A. S.; Torres, A. R. Operating Parameters for Bio-Oil Production in Biomass Pyrolysis: A Review. *Journal of Analytical and Applied Pyrolysis* **2018**, *129*, 134–149. https://doi.org/10.1016/j.jaap.2017.11.019.

(11) Berenguer, A.; Bennett, J. A.; Hunns, J.; Moreno, I.; Coronado, J. M.; Lee, A. F.; Pizarro, P.; Wilson, K.; Serrano, D. P. Catalytic Hydrodeoxygenation of M-Cresol over Ni2P/Hierarchical ZSM-5. *Catalysis Today* **2018**, *304*, 72–79. https://doi.org/10.1016/j.cattod.2017.08.032.

(12) Mortensen, P. M.; Grunwaldt, J.-D.; Jensen, P. A.; Knudsen, K. G.; Jensen, A. D. A Review of Catalytic Upgrading of Bio-Oil to Engine Fuels. *Applied*

Catalysis A: General **2011**, *407* (1), 1–19. https://doi.org/10.1016/j.apcata.2011.08.046.

(13) Mohabeer, C.; Abdelouahed, L.; Marcotte, S.; Taouk, B. Comparative Analysis of Pyrolytic Liquid Products of Beech Wood, Flax Shives and Woody Biomass Components. *Journal of Analytical and Applied Pyrolysis* **2017**, *127*, 269–277. https://doi.org/10.1016/j.jaap.2017.07.025.

(14) Baloch, H. A.; Nizamuddin, S.; Siddiqui, M. T. H.; Riaz, S.; Jatoi, A. S.; Dumbre, D. K.; Mubarak, N. M.; Srinivasan, M. P.; Griffin, G. J. Recent Advances in Production and Upgrading of Bio-Oil from Biomass: A Critical Overview. *Journal of Environmental Chemical Engineering* **2018**, *6* (4), 5101–5118. https://doi.org/10.1016/j.jece.2018.07.050.

(15) Lian, X.; Xue, Y.; Zhao, Z.; Xu, G.; Han, S.; Yu, H. Progress on Upgrading Methods of Bio-Oil: A Review. *International Journal of Energy Research* **2017**, *41* (13), 1798–1816. https://doi.org/10.1002/er.3726.

(16) Jiang, X.; Ellis, N. Upgrading Bio-Oil through Emulsification with Biodiesel: Thermal Stability. *Energy Fuels* **2010**, *24* (4), 2699–2706. https://doi.org/10.1021/ef901517k.

(17) Liang, J.; Qian, Y.; Yuan, X.; Leng, L.; Zeng, G.; Jiang, L.; Shao, J.; Luo, Y.; Ding, X.; Yang, Z.; Li, X. Span80/Tween80 Stabilized Bio-Oil-in-Diesel Microemulsion: Formation and Combustion. *Renewable Energy* **2018**, *126*, 774–782. https://doi.org/10.1016/j.renene.2018.04.010.

(18) Elliott, D. C.; Hart, T. R.; Neuenschwander, G. G.; Rotness, L. J.; Zacher, A. H. Catalytic Hydroprocessing of Biomass Fast Pyrolysis Bio-Oil to Produce Hydrocarbon Products. *Environmental Progress & Sustainable Energy* **2009**, *28* (3), 441–449. https://doi.org/10.1002/ep.10384.

(19) Xu, Y.; Wang, Q.; Hu, X.; Li, C.; Zhu, X. Characterization of the Lubricity of Bio-Oil/Diesel Fuel Blends by High Frequency Reciprocating Test Rig. *Energy* **2010**, *35* (1), 283–287. https://doi.org/10.1016/j.energy.2009.09.020.

(20) Leng, L.; Yuan, X.; Chen, X.; Huang, H.; Wang, H.; Li, H.; Zhu, R.; Li, S.; Zeng, G. Characterization of Liquefaction Bio-Oil from Sewage Sludge and Its Solubilization in Diesel Microemulsion. *Energy* **2015**, *82*, 218–228. https://doi.org/10.1016/j.energy.2015.01.032.

(21) Xiu, S.; Shahbazi, A. Bio-Oil Production and Upgrading Research: A Review. *Renewable and Sustainable Energy Reviews* **2012**, *16* (7), 4406–4414. https://doi.org/10.1016/j.rser.2012.04.028.

(22) Wang, J.-J.; Chang, J.; Fan, J. Upgrading of Bio-Oil by Catalytic Esterification and Determination of Acid Number for Evaluating Esterification Degree. *Energy Fuels* **2010**, *24* (5), 3251–3255. https://doi.org/10.1021/ef1000634.

(23) Lu, Y.; Zong, Z. M.; Liu, F. J.; Wang, S. Z.; Qing, Y.; Yue, X. M.; Sun, B.; Wei, X. Y. Componential Analysis of Esterified Bio-Oil Prepared from Pyrolysis of Rice Stalk. *Advanced Materials Research* **2011**, *236–238*, 130–133. https://doi.org/10.4028/www.scientific.net/AMR.236-238.130.

(24) Zhou, L.; Zong, Z.-M.; Tang, S.-R.; Zong, Y.; Xie, R.-L.; Ding, M.-J.; Zhao, W.; Zhu, X.-F.; Xia, Z.-L.; Wu, L.; Wei, X.-Y. FTIR and Mass Spectral Analyses of

an Upgraded Bio-Oil. *null* **2009**, *32* (4), 370–375. https://doi.org/10.1080/15567030802467340.

(25) WANG, J.; CHANG, J.; FAN, J. Catalytic Esterification of Bio-Oil by Ion Exchange Resins. *Journal of Fuel Chemistry and Technology* **2010**, *38* (5), 560–564. https://doi.org/10.1016/S1872-5813(10)60045-X.

(26) Trane, R.; Dahl, S.; Skjøth-Rasmussen, M. S.; Jensen, A. D. Catalytic Steam Reforming of Bio-Oil. *International Journal of Hydrogen Energy* **2012**, *37* (8), 6447–6472. https://doi.org/10.1016/j.ijhydene.2012.01.023.

(27) Wang, W.; Wang, Y.; Liu, Y. Production of Hydrogen by Ethanol Steam Reforming over Nickel–Metal Oxide Catalysts Prepared via Urea–Nitrate Combustion Method. *International Journal of Energy Research* **2011**, *35* (6), 501–506. https://doi.org/10.1002/er.1705.

(28) Medrano, J. A.; Oliva, M.; Ruiz, J.; García, L.; Arauzo, J. Hydrogen from Aqueous Fraction of Biomass Pyrolysis Liquids by Catalytic Steam Reforming in Fluidized Bed. *Energy* **2011**, *36* (4), 2215–2224. https://doi.org/10.1016/j.energy.2010.03.059.

(29) Remón, J.; Medrano, J. A.; Bimbela, F.; García, L.; Arauzo, J. Ni/Al–Mg–O Solids Modified with Co or Cu for the Catalytic Steam Reforming of Bio-Oil. *Applied Catalysis B: Environmental* **2013**, *132–133*, 433–444. https://doi.org/10.1016/j.apcatb.2012.12.015.

(30) Wang, D.; Czernik, S.; Montané, D.; Mann, M.; Chornet, E. Biomass to Hydrogen via Fast Pyrolysis and Catalytic Steam Reforming of the Pyrolysis Oil or Its Fractions. *Ind. Eng. Chem. Res.* **1997**, *36* (5), 1507–1518. https://doi.org/10.1021/ie960396g.

(31) Trane-Restrup, R.; Resasco, D. E.; Jensen, A. D. Steam Reforming of Light Oxygenates. *Catal. Sci. Technol.* **2013**, *3* (12), 3292–3302. https://doi.org/10.1039/C3CY00635B.

(32) Trane-Restrup, R.; Jensen, A. D. Steam Reforming of Cyclic Model Compounds of Bio-Oil over Ni-Based Catalysts: Product Distribution and Carbon Formation. *Applied Catalysis B: Environmental* **2015**, *165*, 117–127. https://doi.org/10.1016/j.apcatb.2014.09.026.

(33) Zhang, J.; Luo, Z.; Dang, Q.; Wang, J.; Chen, W. Upgrading of Bio-Oil over Bifunctional Catalysts in Supercritical Monoalcohols. *Energy Fuels* **2012**, *26* (5), 2990–2995. https://doi.org/10.1021/ef201934a.

(34) Tang, Z.; Zhang, Y.; Guo, Q. Catalytic Hydrocracking of Pyrolytic Lignin to Liquid Fuel in Supercritical Ethanol. *Ind. Eng. Chem. Res.* **2010**, *49* (5), 2040–2046. https://doi.org/10.1021/ie9015842.

(35) Peng, J.; Chen, P.; Lou, H.; Zheng, X. Catalytic Upgrading of Bio-Oil by HZSM-5 in Sub- and Super-Critical Ethanol. *Bioresource Technology* **2009**, *100* (13), 3415–3418. https://doi.org/10.1016/j.biortech.2009.02.007.

(36) Li, W.; Pan, C.; Zhang, Q.; Liu, Z.; Peng, J.; Chen, P.; Lou, H.; Zheng, X. Upgrading of Low-Boiling Fraction of Bio-Oil in Supercritical Methanol and Reaction Network. *Bioresource Technology* **2011**, *102* (7), 4884–4889. https://doi.org/10.1016/j.biortech.2011.01.053.

(37) Li, W.; Pan, C.; Sheng, L.; Liu, Z.; Chen, P.; Lou, H.; Zheng, X. Upgrading of High-Boiling Fraction of Bio-Oil in Supercritical Methanol. *Bioresource Technology* **2011**, *102* (19), 9223–9228. https://doi.org/10.1016/j.biortech.2011.07.071.

(38) CUI, H.; MA, C.; LI, Z.; YI, W. Effect of the Reactive Compounds in Bio-Oils on Esterification of the Contained Carboxylic Acids in Supercritical Methanol. *Journal of Fuel Chemistry and Technology* **2011**, *39* (5), 347–354. https://doi.org/10.1016/S1872-5813(11)60025-X.

(39) Duan, P.; Savage, P. E. Catalytic Hydrotreatment of Crude Algal Bio-Oil in Supercritical Water. *Applied Catalysis B: Environmental* **2011**, *104* (1), 136–143. https://doi.org/10.1016/j.apcatb.2011.02.020.

(40) CUI, H.; WANG, J.; WEI, shu-qin; ZHUO, S.; LI, Z.; WANG, L.; YI, W. Upgrading Bio-Oil by Esterification under Supercritical CO2 Conditions. *Journal of Fuel Chemistry and Technology* **2010**, *38* (6), 673–678. https://doi.org/10.1016/S1872-5813(11)60003-0.

(41) Dang, Q.; Luo, Z.; Zhang, J.; Wang, J.; Chen, W.; Yang, Y. Experimental Study on Bio-Oil Upgrading over Pt/SO42-/ZrO2/SBA-15 Catalyst in Supercritical Ethanol. *Fuel* **2013**, *103*, 683–692. https://doi.org/10.1016/j.fuel.2012.06.082.

(42) Lee, J.-H.; Lee, I.-G.; Park, J.-Y.; Lee, K.-Y. Efficient Upgrading of Pyrolysis Bio-Oil over Ni-Based Catalysts in Supercritical Ethanol. *Fuel* **2019**, *241*, 207–217. https://doi.org/10.1016/j.fuel.2018.12.025.

(43) Adjaye, J. D.; Bakhshi, N. N. Catalytic Conversion of a Biomass-Derived Oil to Fuels and Chemicals I: Model Compound Studies and Reaction Pathways. *Biomass and Bioenergy* **1995**, *8* (3), 131–149. https://doi.org/10.1016/0961-9534(95)00018-3.

(44) Guo, X.; Zheng, Y.; Zhang, B.; Chen, J. Analysis of Coke Precursor on Catalyst and Study on Regeneration of Catalyst in Upgrading of Bio-Oil. *Biomass and Bioenergy* **2009**, *33* (10), 1469–1473. https://doi.org/10.1016/j.biombioe.2009.07.002.

(45) Wang, S.; Guo, Z.; Cai, Q.; Guo, L. Catalytic Conversion of Carboxylic Acids in Bio-Oil for Liquid Hydrocarbons Production. *Biomass and Bioenergy* **2012**, *45*, 138–143. https://doi.org/10.1016/j.biombioe.2012.05.023.

(46) Huber, G. W.; Corma, A. Synergies between Bio- and Oil Refineries for the Production of Fuels from Biomass. *Angewandte Chemie International Edition* **2007**, *46* (38), 7184–7201. https://doi.org/10.1002/anie.200604504.

(47) Corma, A.; Huber, G. W.; Sauvanaud, L.; O'Connor, P. Processing Biomass-Derived Oxygenates in the Oil Refinery: Catalytic Cracking (FCC) Reaction Pathways and Role of Catalyst. *Journal of Catalysis* **2007**, *247* (2), 307–327. https://doi.org/10.1016/j.jcat.2007.01.023.

(48) Twaiq, F. A.; Zabidi, N. A. M.; Mohamed, A. R.; Bhatia, S. Catalytic Conversion of Palm Oil over Mesoporous Aluminosilicate MCM-41 for the Production of Liquid Hydrocarbon Fuels. *Fuel Processing Technology* **2003**, *84* (1), 105–120. https://doi.org/10.1016/S0378-3820(03)00048-1.

(49) Adam, J.; Antonakou, E.; Lappas, A.; Stöcker, M.; Nilsen, M. H.; Bouzga, A.; Hustad, J. E.; Øye, G. In Situ Catalytic Upgrading of Biomass Derived Fast Pyrolysis Vapours in a Fixed Bed Reactor Using Mesoporous Materials. *Microporous and Mesoporous Materials* **2006**, *96* (1), 93–101. https://doi.org/10.1016/j.micromeso.2006.06.021.

(50) Zhang, Q.; Chang, J.; Wang, T.; Xu, Y. Review of Biomass Pyrolysis Oil Properties and Upgrading Research. *Energy Conversion and Management* **2007**, *48* (1), 87–92. https://doi.org/10.1016/j.enconman.2006.05.010.

(51) Wang, Y.; Fang, Y.; He, T.; Hu, H.; Wu, J. Hydrodeoxygenation of Dibenzofuran over Noble Metal Supported on Mesoporous Zeolite. *Catalysis Communications* **2011**, *12* (13), 1201–1205. https://doi.org/10.1016/j.catcom.2011.04.010.

(52) de Miguel Mercader, F.; Groeneveld, M. J.; Kersten, S. R. A.; Way, N. W. J.; Schaverien, C. J.; Hogendoorn, J. A. Production of Advanced Biofuels: Co-Processing of Upgraded Pyrolysis Oil in Standard Refinery Units. *Applied Catalysis B: Environmental* **2010**, *96* (1), 57–66. https://doi.org/10.1016/j.apcatb.2010.01.033.

(53) Hong, D.-Y.; Miller, S. J.; Agrawal, P. K.; Jones, C. W. Hydrodeoxygenation and Coupling of Aqueous Phenolics over Bifunctional Zeolite-Supported Metal Catalysts. *Chem. Commun.* **2010**, *46* (7), 1038–1040. https://doi.org/10.1039/B918209H.

(54) Cheng, S.; Wei, L.; Julson, J.; Rabnawaz, M. Upgrading Pyrolysis Bio-Oil through Hydrodeoxygenation (HDO) Using Non-Sulfided Fe-Co/SiO2 Catalyst. *Energy Conversion and Management* **2017**, *150*, 331–342. https://doi.org/10.1016/j.enconman.2017.08.024.

(55) Zhang, S.; Yan, Y.; Li, T.; Ren, Z. Upgrading of Liquid Fuel from the Pyrolysis of Biomass. *Bioresource Technology* **2005**, *96* (5), 545–550. https://doi.org/10.1016/j.biortech.2004.06.015.

(56) Jahromi, H.; Agblevor, F. A. Upgrading of Pinyon-Juniper Catalytic Pyrolysis Oil via Hydrodeoxygenation. *Energy* **2017**, *141*, 2186–2195. https://doi.org/10.1016/j.energy.2017.11.149.

(57) Zhang, Q.; Wang, T.; Xu, Y.; Zhang, Q.; Ma, L. Production of Liquid Alkanes by Controlling Reactivity of Sorbitol Hydrogenation with a Ni/HZSM-5 Catalyst in Water. *Energy Conversion and Management* **2014**, *77*, 262–268. https://doi.org/10.1016/j.enconman.2013.09.032.

(58) Popov, A.; Kondratieva, E.; Mariey, L.; Goupil, J. M.; El Fallah, J.; Gilson, J.-P.; Travert, A.; Maugé, F. Bio-Oil Hydrodeoxygenation: Adsorption of Phenolic Compounds on Sulfided (Co)Mo Catalysts. *Journal of Catalysis* **2013**, *297*, 176–186. https://doi.org/10.1016/j.jcat.2012.10.005.

(59) Nimmanwudipong, T.; Runnebaum, R. C.; Block, D. E.; Gates, B. C. Catalytic Reactions of Guaiacol: Reaction Network and Evidence of Oxygen Removal in Reactions with Hydrogen. *Catalysis Letters* **2011**, *141* (6), 779–783. https://doi.org/10.1007/s10562-011-0576-4.

(60) Han, Y.; Gholizadeh, M.; Tran, C.-C.; Kaliaguine, S.; Li, C.-Z.; Olarte, M.; Garcia-Perez, M. Hydrotreatment of Pyrolysis Bio-Oil: A Review. *Fuel Processing Technology* **2019**, *195*, 106140. https://doi.org/10.1016/j.fuproc.2019.106140.

(61) Elkasabi, Y.; Mullen, C. A.; Pighinelli, A. L. M. T.; Boateng, A. A. Hydrodeoxygenation of Fast-Pyrolysis Bio-Oils from Various Feedstocks Using Carbon-Supported Catalysts. *Fuel Processing Technology* **2014**, *123*, 11–18. https://doi.org/10.1016/j.fuproc.2014.01.039.

(62) Guo, C.; Rao, K. T. V.; Yuan, Z.; He, S. (Quan); Rohani, S.; Xu, C. (Charles). Hydrodeoxygenation of Fast Pyrolysis Oil with Novel Activated Carbon-Supported NiP and CoP Catalysts. *Chemical Engineering Science* **2018**, *178*, 248–259. https://doi.org/10.1016/j.ces.2017.12.048.

(63) Elliott, D. C.; Hart, T. R.; Neuenschwander, G. G.; Rotness, L. J.; Olarte, M. V.; Zacher, A. H.; Solantausta, Y. Catalytic Hydroprocessing of Fast Pyrolysis Bio-Oil from Pine Sawdust. *Energy Fuels* **2012**, *26* (6), 3891–3896. https://doi.org/10.1021/ef3004587.

(64) Elliott, D. C.; Neuenschwander, G. G.; Hart, T. R. Hydroprocessing Bio-Oil and Products Separation for Coke Production. *ACS Sustainable Chem. Eng.* **2013**, *1* (4), 389–392. https://doi.org/10.1021/sc300103y.

(65) Routray, K.; Barnett, K. J.; Huber, G. W. Hydrodeoxygenation of Pyrolysis Oils. *Energy Technology* **2017**, *5* (1), 80–93. https://doi.org/10.1002/ente.201600084.

(66) Gholizadeh, M.; Gunawan, R.; Hu, X.; Hasan, M. M.; Kersten, S.; Westerhof, R.; Chaitwat, W.; Li, C.-Z. Different Reaction Behaviours of the Light and Heavy Components of Bio-Oil during the Hydrotreatment in a Continuous Pack-Bed Reactor. *Fuel Processing Technology* **2016**, *146*, 76–84. https://doi.org/10.1016/j.fuproc.2016.01.026.

(67) Elliott, D. C.; Neuenschwander, G. G. Liquid Fuels by Low-Severity Hydrotreating of Biocrude. In *Developments in Thermochemical Biomass Conversion: Volume 1 / Volume 2*; Bridgwater, A. V., Boocock, D. G. B., Eds.; Springer Netherlands: Dordrecht, 1997; pp 611–621. https://doi.org/10.1007/978-94-009-1559-6_48.

(68) Baldauf, W.; Balfanz, U.; Rupp, M. Upgrading of Flash Pyrolysis Oil and Utilization in Refineries. *Biomass and Bioenergy* **1994**, *7* (1), 237–244. https://doi.org/10.1016/0961-9534(94)00065-2.

(69) Chaiwat, W.; Gunawan, R.; Gholizadeh, M.; Li, X.; Lievens, C.; Hu, X.; Wang, Y.; Mourant, D.; Rossiter, A.; Bromly, J.; Li, C.-Z. Upgrading of Bio-Oil into Advanced Biofuels and Chemicals. Part II. Importance of Holdup of Heavy Species during the Hydrotreatment of Bio-Oil in a Continuous Packed-Bed Catalytic Reactor. *Fuel* **2013**, *112*, 302–310. https://doi.org/10.1016/j.fuel.2013.05.004.

(70) Yang, Y.; Gilbert, A.; Xu, C. (Charles). Hydrodeoxygenation of Bio-Crude in Supercritical Hexane with Sulfided CoMo and CoMoP Catalysts Supported on MgO: A Model Compound Study Using Phenol. *Applied Catalysis A: General* **2009**, *360* (2), 242–249. https://doi.org/10.1016/j.apcata.2009.03.027.

(71) Laurent, E.; Centeno, A.; Delmon, B. Coke Formation during the Hydrotreating of Biomass Pyrolysis Oils: Influence of Guaiacol Type Compounds. In *Studies in Surface Science and Catalysis*; Delmon, B., Froment, G. F., Eds.; Elsevier, 1994; Vol. 88, pp 573–578. https://doi.org/10.1016/S0167-2991(08)62790-1.

(72) Bui, V. N.; Laurenti, D.; Delichère, P.; Geantet, C. Hydrodeoxygenation of Guaiacol: Part II: Support Effect for CoMoS Catalysts on HDO Activity and Selectivity. *Applied Catalysis B: Environmental* **2011**, *101* (3), 246–255. https://doi.org/10.1016/j.apcatb.2010.10.031.

(73) Centeno, A.; Laurent, E.; Delmon, B. Influence of the Support of CoMo Sulfide Catalysts and of the Addition of Potassium and Platinum on the Catalytic Performances for the Hydrodeoxygenation of Carbonyl, Carboxyl, and Guaiacol-Type Molecules. *Journal of Catalysis* **1995**, *154* (2), 288–298. https://doi.org/10.1006/jcat.1995.1170.

(74) Gao, D.; Schweitzer, C.; Hwang, H. T.; Varma, A. Conversion of Guaiacol on Noble Metal Catalysts: Reaction Performance and Deactivation Studies. *Ind. Eng. Chem. Res.* **2014**, *53* (49), 18658–18667. https://doi.org/10.1021/ie500495z.

(75) Zhao, C.; Song, W.; Lercher, J. A. Aqueous Phase Hydroalkylation and Hydrodeoxygenation of Phenol by Dual Functional Catalysts Comprised of Pd/C and H/La-BEA. *ACS Catal.* **2012**, *2* (12), 2714–2723. https://doi.org/10.1021/cs300418a.

(76) Newman, C.; Zhou, X.; Goundie, B.; Ghampson, I. T.; Pollock, R. A.; Ross, Z.; Wheeler, M. C.; Meulenberg, R. W.; Austin, R. N.; Frederick, B. G. Effects of Support Identity and Metal Dispersion in Supported Ruthenium Hydrodeoxygenation Catalysts. *Applied Catalysis A: General* **2014**, *477*, 64–74. https://doi.org/10.1016/j.apcata.2014.02.030.

(77) Li, Y.; Zhang, C.; Liu, Y.; Hou, X.; Zhang, R.; Tang, X. Coke Deposition on Ni/HZSM-5 in Bio-Oil Hydrodeoxygenation Processing. *Energy Fuels* **2015**, *29* (3), 1722–1728. https://doi.org/10.1021/ef5024669.

(78) Chen, W.; Luo, Z.; Yu, C.; Li, G.; Yang, Y.; Zhang, H. Upgrading of Bio-Oil in Supercritical Ethanol: Catalysts Screening, Solvent Recovery and Catalyst Stability Study. *The Journal of Supercritical Fluids* **2014**, *95*, 387–393. https://doi.org/10.1016/j.supflu.2014.09.041.

(79) Lee, H.; Kim, Y.-M.; Lee, I.-G.; Jeon, J.-K.; Jung, S.-C.; Chung, J. D.; Choi, W. G.; Park, Y.-K. Recent Advances in the Catalytic Hydrodeoxygenation of Bio-Oil. *Korean Journal of Chemical Engineering* **2016**, *33* (12), 3299–3315. https://doi.org/10.1007/s11814-016-0214-3.

(80) Stankovikj, F.; Tran, C.-C.; Kaliaguine, S.; Olarte, M. V.; Garcia-Perez, M. Evolution of Functional Groups during Pyrolysis Oil Upgrading. *Energy Fuels* **2017**, *31* (8), 8300–8316. https://doi.org/10.1021/acs.energyfuels.7b01251.

(81) Bergem, H.; Xu, R.; Brown, R. C.; Huber, G. W. Low Temperature Aqueous Phase Hydrogenation of the Light Oxygenate Fraction of Bio-Oil over Supported Ruthenium Catalysts. *Green Chem.* **2017**, *19* (14), 3252–3262. https://doi.org/10.1039/C7GC00367F.

(82) Jin, S.; Xiao, Z.; Li, C.; Chen, X.; Wang, L.; Xing, J.; Li, W.; Liang, C. Catalytic Hydrodeoxygenation of Anisole as Lignin Model Compound over Supported Nickel Catalysts. *Catalysis Today* **2014**, *234*, 125–132. https://doi.org/10.1016/j.cattod.2014.02.014.

(83) Yang, Y.; Ochoa-Hernández, C.; de la Peña O'Shea, V. A.; Pizarro, P.; Coronado, J. M.; Serrano, D. P. Effect of Metal–Support Interaction on the Selective Hydrodeoxygenation of Anisole to Aromatics over Ni-Based Catalysts. *Applied Catalysis B: Environmental* **2014**, *145*, 91–100. https://doi.org/10.1016/j.apcatb.2013.03.038.

(84) Zhao, C.; Kasakov, S.; He, J.; Lercher, J. A. Comparison of Kinetics, Activity and Stability of Ni/HZSM-5 and Ni/Al2O3-HZSM-5 for Phenol Hydrodeoxygenation. *Journal of Catalysis* **2012**, *296*, 12–23. https://doi.org/10.1016/j.jcat.2012.08.017.

(85) Ruddy, D. A.; Schaidle, J. A.; Ferrell III, J. R.; Wang, J.; Moens, L.; Hensley, J. E. Recent Advances in Heterogeneous Catalysts for Bio-Oil Upgrading via "Ex Situ Catalytic Fast Pyrolysis": Catalyst Development through the Study of Model Compounds. *Green Chem.* **2014**, *16* (2), 454–490. https://doi.org/10.1039/C3GC41354C.

(86) Robinson, A. M.; Hensley, J. E.; Medlin, J. W. Bifunctional Catalysts for Upgrading of Biomass-Derived Oxygenates: A Review. *ACS Catal.* **2016**, *6* (8), 5026–5043. https://doi.org/10.1021/acscatal.6b00923.

(87) Chen, J. G. Carbide and Nitride Overlayers on Early Transition Metal Surfaces: Preparation, Characterization, and Reactivities. *Chem. Rev.* **1996**, *96* (4), 1477–1498. https://doi.org/10.1021/cr950232u.

(88) Whiffen, V. M. L.; Smith, K. J. Hydrodeoxygenation of 4-Methylphenol over Unsupported MoP, MoS2, and MoOx Catalysts. *Energy Fuels* **2010**, *24* (9), 4728–4737. https://doi.org/10.1021/ef901270h.

(89) Chen, J.; Shi, H.; Li, L.; Li, K. Deoxygenation of Methyl Laurate as a Model Compound to Hydrocarbons on Transition Metal Phosphide Catalysts. *Applied Catalysis B: Environmental* **2014**, *144*, 870–884. https://doi.org/10.1016/j.apcatb.2013.08.026.

(90) Zhao, H. Y.; Li, D.; Bui, P.; Oyama, S. T. Hydrodeoxygenation of Guaiacol as Model Compound for Pyrolysis Oil on Transition Metal Phosphide Hydroprocessing Catalysts. *Applied Catalysis A: General* **2011**, *391* (1), 305–310. https://doi.org/10.1016/j.apcata.2010.07.039.

(91) Badawi, M.; Paul, J.-F.; Cristol, S.; Payen, E. Guaiacol Derivatives and Inhibiting Species Adsorption over MoS2 and CoMoS Catalysts under HDO Conditions: A DFT Study. *Catalysis Communications* **2011**, *12* (10), 901–905. https://doi.org/10.1016/j.catcom.2011.02.010.

(92) Li, K.; Wang, R.; Chen, J. Hydrodeoxygenation of Anisole over Silica-Supported Ni2P, MoP, and NiMoP Catalysts. *Energy Fuels* **2011**, *25* (3), 854–863. https://doi.org/10.1021/ef101258j.

(93) Odebunmi, E. O.; Ollis, D. F. Catalytic Hydrodeoxygenation: III. Interactions between Catalytic Hydrodeoxygenation of m-Cresol and Hydrodenitrogenation

of Indole. *Journal of Catalysis* **1983**, *80* (1), 76–89. https://doi.org/10.1016/0021-9517(83)90231-2.

(94) Jahromi, H.; Agblevor, F. A. Hydrodeoxygenation of Aqueous-Phase Catalytic Pyrolysis Oil to Liquid Hydrocarbons Using Multifunctional Nickel Catalyst. *Ind. Eng. Chem. Res.* **2018**, *57* (39), 13257–13268. https://doi.org/10.1021/acs.iecr.8b02807.

(95) Zhao, H. Y.; Li, D.; Bui, P.; Oyama, S. T. Hydrodeoxygenation of Guaiacol as Model Compound for Pyrolysis Oil on Transition Metal Phosphide Hydroprocessing Catalysts. *Applied Catalysis A: General* **2011**, *391* (1), 305–310. https://doi.org/10.1016/j.apcata.2010.07.039.

(96) Ted Oyama, S.; Onkawa, T.; Takagaki, A.; Kikuchi, R.; Hosokai, S.; Suzuki, Y.; Bando, K. K. Production of Phenol and Cresol from Guaiacol on Nickel Phosphide Catalysts Supported on Acidic Supports. *Topics in Catalysis* **2015**, *58* (4), 201–210. https://doi.org/10.1007/s11244-015-0361-5.

(97) Patil, M. L.; Lali, A. M.; Dalai, A. K. Catalytic Hydrodeoxygenation of Bio-Oil Model Compound for Production of Fuel Grade Oil. *Asia-Pacific Journal of Chemical Engineering* **2019**, *14* (4), e2317. https://doi.org/10.1002/apj.2317.

(98) Mortensen, P. M.; Grunwaldt, J.-D.; Jensen, P. A.; Jensen, A. D. Influence on Nickel Particle Size on the Hydrodeoxygenation of Phenol over Ni/SiO2. *Catalysis Today* **2016**, *259*, 277–284. https://doi.org/10.1016/j.cattod.2015.08.022.

(99) Berenguer, A.; Bennett, J. A.; Hunns, J.; Moreno, I.; Coronado, J. M.; Lee, A. F.; Pizarro, P.; Wilson, K.; Serrano, D. P. Catalytic Hydrodeoxygenation of M-Cresol over Ni2P/Hierarchical ZSM-5. *Catalysis Today* **2018**, *304*, 72–79. https://doi.org/10.1016/j.cattod.2017.08.032.

(100) Gonçalves, V. O. O.; de Souza, P. M.; Cabioc'h, T.; da Silva, V. T.; Noronha, F. B.; Richard, F. Hydrodeoxygenation of M-Cresol over Nickel and Nickel Phosphide Based Catalysts. Influence of the Nature of the Active Phase and the Support. *Applied Catalysis B: Environmental* **2017**, *219*, 619–628. https://doi.org/10.1016/j.apcatb.2017.07.042.

(101) Parikh, J.; Srivastava, S.; Jadeja, G. C. Selective Hydrogenation of Furfural to Tetrahydrofurfuryl Alcohol Using Supported Nickel–Cobalt Catalysts. *Ind. Eng. Chem. Res.* **2019**, *58* (35), 16138–16152. https://doi.org/10.1021/acs.iecr.9b01443.

(102) Li, Y.; Fu, J.; Chen, B. Highly Selective Hydrodeoxygenation of Anisole, Phenol and Guaiacol to Benzene over Nickel Phosphide. *RSC Adv.* **2017**, *7* (25), 15272–15277. https://doi.org/10.1039/C7RA00989E.

(103) Tu, C.; Chen, J.; Li, W.; Wang, H.; Deng, K.; Vinokurov, V. A.; Huang, W. Hydrodeoxygenation of Bio-Derived Anisole to Cyclohexane over Bi-Functional IM-5 Zeolite Supported Ni Catalysts. *Sustainable Energy Fuels* **2019**, *3* (12), 3462–3472. https://doi.org/10.1039/C9SE00554D.

(104) Zhang, J.; Matsubara, K.; Yun, G.-N.; Zheng, H.; Takagaki, A.; Kikuchi, R.; Oyama, S. T. Comparison of Phosphide Catalysts Prepared by Temperature-Programmed Reduction and Liquid-Phase Methods in the Hydrodeoxygenation

of 2-Methylfuran. *Applied Catalysis A: General* **2017**, *548*, 39–46. https://doi.org/10.1016/j.apcata.2017.06.009.

(105) Joshi, N.; Lawal, A. Hydrodeoxygenation of Acetic Acid in a Microreactor. *Chemical Engineering Science* **2012**, *84*, 761–771. https://doi.org/10.1016/j.ces.2012.09.018.

(106) Le, T. A.; Ly, H. V.; Kim, J.; Kim, S.-S.; Choi, J. H.; Woo, H.-C.; Othman, M. R. Hydrodeoxygenation of 2-Furyl Methyl Ketone as a Model Compound in Bio-Oil from Pyrolysis of Saccharina Japonica Alga in Fixed-Bed Reactor. *Chemical Engineering Journal* **2014**, *250*, 157–163. https://doi.org/10.1016/j.cej.2014.04.003.

(107) Berenguer, A.; Sankaranarayanan, T. M.; Gómez, G.; Moreno, I.; Coronado, J. M.; Pizarro, P.; Serrano, D. P. Evaluation of Transition Metal Phosphides Supported on Ordered Mesoporous Materials as Catalysts for Phenol Hydrodeoxygenation. *Green Chem.* **2016**, *18* (7), 1938–1951. https://doi.org/10.1039/C5GC02188J.

(108) Gutiérrez-Rubio, S.; Moreno, I.; Serrano, D. P.; Coronado, J. M. Hydrotreating of Guaiacol and Acetic Acid Blends over Ni2P/ZSM-5 Catalysts: Elucidating Molecular Interactions during Bio-Oil Upgrading. *ACS Omega* **2019**, *4* (25), 21516–21528. https://doi.org/10.1021/acsomega.9b03221.

(109) Shi, H.; Chen, J.; Yang, Y.; Tian, S. Catalytic Deoxygenation of Methyl Laurate as a Model Compound to Hydrocarbons on Nickel Phosphide Catalysts: Remarkable Support Effect. *Fuel Processing Technology* **2014**, *118*, 161–170. https://doi.org/10.1016/j.fuproc.2013.08.010.

(110) Berenguer, A.; Gutiérrez-Rubio, S.; Linares, M.; Ochoa-Hernández, C.; Moreno, I.; García-Fierro, J. L.; Coronado, J. M.; Serrano, D. P.; Pizarro, P. On the Feasibility of Using Hierarchical ZSM-5 and Beta Zeolites as Supports of Metal Phosphides for Catalytic Hydrodeoxygenation of Phenol. *Energy Technology* **2019**, *7* (6), 1900214. https://doi.org/10.1002/ente.201900214.

(111) Li, Z.; Jiang, E.; Xu, X.; Sun, Y.; Tu, R. Hydrodeoxygenation of Phenols, Acids, and Ketones as Model Bio-Oil for Hydrocarbon Fuel over Ni-Based Catalysts Modified by Al, La and Ga. *Renewable Energy* **2020**, *146*, 1991–2007. https://doi.org/10.1016/j.renene.2019.08.012.

(112) Witsuthammakul, A.; Sooknoi, T. Selective Hydrodeoxygenation of Bio-Oil Derived Products: Ketones to Olefins. *Catal. Sci. Technol.* **2015**, *5* (7), 3639–3648. https://doi.org/10.1039/C5CY00367A.

(113) Joshi, N.; Lawal, A. Hydrodeoxygenation of Acetic Acid in a Microreactor. *Chemical Engineering Science* **2012**, *84*, 761–771. https://doi.org/10.1016/j.ces.2012.09.018.

(114) Chen, B. S.; Falconer, J. L. Hydrogenation of Organic Oxygenates on Ni/Al2O3 and Ni/SiO2 Catalysts. *Journal of Catalysis* **1994**, *147* (1), 72–81. https://doi.org/10.1006/jcat.1994.1115.

(115) Peng, B.; Zhao, C.; Kasakov, S.; Foraita, S.; Lercher, J. A. Manipulating Catalytic Pathways: Deoxygenation of Palmitic Acid on Multifunctional

Catalysts. *Chemistry – A European Journal* **2013**, *19* (15), 4732–4741. https://doi.org/10.1002/chem.201203110.

(116) Berenguer, A.; Bennett, J. A.; Hunns, J.; Moreno, I.; Coronado, J. M.; Lee, A. F.; Pizarro, P.; Wilson, K.; Serrano, D. P. Catalytic Hydrodeoxygenation of M-Cresol over Ni2P/Hierarchical ZSM-5. *Catalysis Today* **2018**, *304*, 72–79. https://doi.org/10.1016/j.cattod.2017.08.032.

(117) Tu, C.; Chen, J.; Li, W.; Wang, H.; Deng, K.; Vinokurov, V. A.; Huang, W. Hydrodeoxygenation of Bio-Derived Anisole to Cyclohexane over Bi-Functional IM-5 Zeolite Supported Ni Catalysts. *Sustainable Energy Fuels* **2019**, *3* (12), 3462–3472. https://doi.org/10.1039/C9SE00554D.

(118) Broglia, F.; Rimoldi, L.; Meroni, D.; De Vecchi, S.; Morbidelli, M.; Ardizzone, S. Guaiacol Hydrodeoxygenation as a Model for Lignin Upgrading. Role of the Support Surface Features on Ni-Based Alumina-Silica Catalysts. *Fuel* **2019**, *243*, 501–508. https://doi.org/10.1016/j.fuel.2019.01.157.

(119) Zhang, P.; Sun, Y.; Lu, M.; Zhu, J.; Li, M.; Shan, Y.; Shen, J.; Song, C. High-Loading Nickel Phosphide Catalysts Supported on SiO2–TiO2 for Hydrodeoxygenation of Guaiacol. *Energy Fuels* **2019**, *33* (8), 7696–7704. https://doi.org/10.1021/acs.energyfuels.9b01538.

(120) Ted Oyama, S.; Onkawa, T.; Takagaki, A.; Kikuchi, R.; Hosokai, S.; Suzuki, Y.; Bando, K. K. Production of Phenol and Cresol from Guaiacol on Nickel Phosphide Catalysts Supported on Acidic Supports. *Topics in Catalysis* **2015**, *58* (4), 201–210. https://doi.org/10.1007/s11244-015-0361-5.

(121) Xinghua, Z.; Tiejun, W.; Longlong, M.; Chuangzhi, W. Aqueous-Phase Catalytic Process for Production of Pentane from Furfural over Nickel-Based Catalysts. *Fuel* **2010**, *89* (10), 2697–2702. https://doi.org/10.1016/j.fuel.2010.05.043.

(122) Zhao, C.; Lercher, J. A. Upgrading Pyrolysis Oil over Ni/HZSM-5 by Cascade Reactions. *Angewandte Chemie International Edition* **2012**, *51* (24), 5935–5940. https://doi.org/10.1002/anie.201108306.

(123) Wang, Z.; Fu, Z.; Lin, W.; Li, S.; Song, W. In-Situ Hydrodeoxygenation of Furfural to Furans over Supported Ni Catalysts in Aqueous Solution. *Korean Journal of Chemical Engineering* **2019**, *36* (8), 1235–1242. https://doi.org/10.1007/s11814-019-0305-z.

(124) Chen, W.; Luo, Z.; Yu, C.; Li, G.; Yang, Y.; Zhang, J.; Lu, K. Catalytic Transformations of Acids, Aldehydes, and Phenols in Bio-Oil to Alcohols and Esters. *Fuel* **2014**, *135*, 55–62. https://doi.org/10.1016/j.fuel.2014.06.003.

(125) Zeng, Y.; Wang, Z.; Lin, W.; Song, W. In Situ Hydrodeoxygenation of Phenol with Liquid Hydrogen Donor over Three Supported Noble-Metal Catalysts. *Chemical Engineering Journal* **2017**, *320*, 55–62. https://doi.org/10.1016/j.cej.2017.03.028.

(126) Wan, H.; Chaudhari, R. V.; Subramaniam, B. Aqueous Phase Hydrogenation of Acetic Acid and Its Promotional Effect on P-Cresol Hydrodeoxygenation. *Energy Fuels* **2013**, *27* (1), 487–493. https://doi.org/10.1021/ef301400c.

(127) Funkenbusch, L. T.; Mullins, M. E.; Salam, M. A.; Creaser, D.; Olsson, L. Catalytic Hydrotreatment of Pyrolysis Oil Phenolic Compounds over Pt/Al2O3 and Pd/C. *Fuel* **2019**, *243*, 441–448. https://doi.org/10.1016/j.fuel.2019.01.139.

(128) Yu, W.; Tang, Y.; Mo, L.; Chen, P.; Lou, H.; Zheng, X. One-Step Hydrogenation–Esterification of Furfural and Acetic Acid over Bifunctional Pd Catalysts for Bio-Oil Upgrading. *Bioresource Technology* **2011**, *102* (17), 8241–8246. https://doi.org/10.1016/j.biortech.2011.06.015.

(129) Fisk, C. A.; Morgan, T.; Ji, Y.; Crocker, M.; Crofcheck, C.; Lewis, S. A. Bio-Oil Upgrading over Platinum Catalysts Using in Situ Generated Hydrogen. *Applied Catalysis A: General* **2009**, *358* (2), 150–156. https://doi.org/10.1016/j.apcata.2009.02.006.

(130) Gayubo, A. G.; Aguayo, A. T.; Atutxa, A.; Valle, B.; Bilbao, J. Undesired Components in the Transformation of Biomass Pyrolysis Oil into Hydrocarbons on an HZSM-5 Zeolite Catalyst. *Journal of Chemical Technology & Biotechnology* **2005**, *80* (11), 1244–1251. https://doi.org/10.1002/jctb.1316.

(131) Reddy Kannapu, H. P.; Mullen, C. A.; Elkasabi, Y.; Boateng, A. A. Catalytic Transfer Hydrogenation for Stabilization of Bio-Oil Oxygenates: Reduction of p-Cresol and Furfural over Bimetallic Ni–Cu Catalysts Using Isopropanol. *Fuel Processing Technology* **2015**, *137*, 220–228. https://doi.org/10.1016/j.fuproc.2015.04.023.

(132) Sankaranarayanan, T. M.; Kreider, M.; Berenguer, A.; Gutiérrez-Rubio, S.; Moreno, I.; Pizarro, P.; Coronado, J. M.; Serrano, D. P. Cross-Reactivity of Guaiacol and Propionic Acid Blends during Hydrodeoxygenation over Ni-Supported Catalysts. *Fuel* **2018**, *214*, 187–195. https://doi.org/10.1016/j.fuel.2017.10.059.

(133) Gutiérrez-Rubio, S.; Moreno, I.; Serrano, D. P.; Coronado, J. M. Hydrotreating of Guaiacol and Acetic Acid Blends over Ni2P/ZSM-5 Catalysts: Elucidating Molecular Interactions during Bio-Oil Upgrading. *ACS Omega* **2019**, *4* (25), 21516–21528. https://doi.org/10.1021/acsomega.9b03221.

(134) Liu, X.; Li, Z.; Zhang, B.; Hu, M. Improvement of Hydrodeoxygenation Stability of Nickel Phosphide Based Catalysts by Silica Modification as Structural Promoter. *Fuel* **2017**, *204*, 144–151. https://doi.org/10.1016/j.fuel.2017.05.054.

(135) Zarchin, R.; Rabaev, M.; Vidruk-Nehemya, R.; Landau, M. V.; Herskowitz, M. Hydroprocessing of Soybean Oil on Nickel-Phosphide Supported Catalysts. *Fuel* **2015**, *139*, 684–691. https://doi.org/10.1016/j.fuel.2014.09.053.

(136) Liu, S.; Zhu, Q.; Guan, Q.; He, L.; Li, W. Bio-Aviation Fuel Production from Hydroprocessing Castor Oil Promoted by the Nickel-Based Bifunctional Catalysts. *Bioresource Technology* **2015**, *183*, 93–100. https://doi.org/10.1016/j.biortech.2015.02.056.

(137) Pham, L. K. H.; Dinh Ngo, S.; Tran, T. T. V.; Kongparakul, S.; Reubroycharoen, P.; Chaiya, C.; Vo, D.-V. N.; Guan, G.; Samart, C. Integrated Catalytic Hydrodeoxygenation of Napier Grass Pyrolysis Vapor Using a Ni2P/C Catalyst.

Journal of Analytical and Applied Pyrolysis **2019**, *140*, 170–178. https://doi.org/10.1016/j.jaap.2019.03.012.

(138) Shafaghat, H.; Kim, J. M.; Lee, I.-G.; Jae, J.; Jung, S.-C.; Park, Y.-K. Catalytic Hydrodeoxygenation of Crude Bio-Oil in Supercritical Methanol Using Supported Nickel Catalysts. *Renewable Energy* **2019**, *144*, 159–166. https://doi.org/10.1016/j.renene.2018.06.096.

(139) Alothman, Z. A Review: Fundamental Aspects of Silicate Mesoporous Materials. *Materials* **2012**, *5*, 2874–2902. https://doi.org/10.3390/ma5122874.

(140) Eddaoudi, M. Characterization of Porous Solids and Powders: Surface Area, Pore Size and Density By S. Lowell (Quantachrome Instruments, Boynton Beach), J. E. Shields (C. W. Post Campus of Long Island University), M. A. Thomas, and M. Thommes (Quantachrome In-Struments). Kluwer Academic Publishers: Dordrecht, The Netherlands. 2004. Xiv + 348 Pp. $159.00. ISBN 1-4020-2302-2. *J. Am. Chem. Soc.* **2005**, *127* (40), 14117–14117. https://doi.org/10.1021/ja041016i.

(141) Wang, S.; Cai, Q.; Chen, J.; Zhang, L.; Zhu, L.; Luo, Z. Co-Cracking of Bio-Oil Model Compound Mixtures and Ethanol over Different Metal Oxide-Modified HZSM-5 Catalysts. *Fuel* **2015**, *160*, 534–543. https://doi.org/10.1016/j.fuel.2015.08.011.

(142) Chen, G.; Liu, J.; Li, X.; Zhang, J.; Yin, H.; Su, Z. Investigation on Catalytic Hydrodeoxygenation of Eugenol Blend with Light Fraction in Bio-Oil over Ni-Based Catalysts. *Renewable Energy* **2020**, *157*, 456–465. https://doi.org/10.1016/j.renene.2020.05.040.

(143) Topaloğlu Yazıcı, D.; Bilgiç, C. Determining the Surface Acidic Properties of Solid Catalysts by Amine Titration Using Hammett Indicators and FTIR-Pyridine Adsorption Methods. *Surface and Interface Analysis* **2010**, *42* (6-7), 959–962. https://doi.org/10.1002/sia.3474.

(144) Lee, Y.-K.; Oyama, S. T. Bifunctional Nature of a SiO2-Supported Ni2P Catalyst for Hydrotreating: EXAFS and FTIR Studies. *Journal of Catalysis* **2006**, *239* (2), 376–389. https://doi.org/10.1016/j.jcat.2005.12.029.

(145) Mohabeer, C.; Reyes, L.; Abdelouahed, L.; Marcotte, S.; Taouk, B. Investigating Catalytic De-Oxygenation of Cellulose, Xylan and Lignin Bio-Oils Using HZSM-5 and Fe-HZSM-5. *Journal of Analytical and Applied Pyrolysis* **2019**, *137*, 118–127. https://doi.org/10.1016/j.jaap.2018.11.016.

(146) Chen, J.; Sun, L.; Wang, R.; Zhang, J. Hydrodechlorination of Chlorobenzene Over Ni2P/SiO2 Catalysts: Influence of Ni2P Loading. *Catal Lett* **2009**, *133* (3), 346. https://doi.org/10.1007/s10562-009-0191-9.

(147) Wang, J.; Jabbour, M.; Abdelouahed, L.; Mezghich, S.; Estel, L.; Thomas, K.; Taouk, B. Catalytic Upgrading of Bio-Oil: Hydrodeoxygenation Study of Acetone as Molecule Model of Ketones. *The Canadian Journal of Chemical Engineering n/a* (n/a). https://doi.org/10.1002/cjce.23909.

(148) Korányi, T. I.; Huang, X.; Coumans, A. E.; Hensen, E. J. M. Synergy in Lignin Upgrading by a Combination of Cu-Based Mixed Oxide and Ni-Phosphide

Catalysts in Supercritical Ethanol. *ACS Sustainable Chem. Eng.* **2017**, *5* (4), 3535–3543. https://doi.org/10.1021/acssuschemeng.7b00239.

(149) Li, Y.; Yang, X.; Zhu, L.; Zhang, H.; Chen, B. Hydrodeoxygenation of Phenol as a Bio-Oil Model Compound over Intimate Contact Noble Metal–Ni2P/SiO2 Catalysts. *RSC Adv.* **2015**, *5* (98), 80388–80396. https://doi.org/10.1039/C5RA11203F.

(150) Vervecken, M.; Servotte, Y.; Wydoodt, M.; Jacobs, L.; Martens, J. A.; Jacobs, P. A. Zeolite-Induced Selectivity in the Conversion of the Lower Aliphatic Carboxylic Acids. In *Chemical Reactions in Organic and Inorganic Constrained Systems*; Setton, R., Ed.; Springer Netherlands: Dordrecht, 1986; pp 95–114. https://doi.org/10.1007/978-94-009-4582-1_8.

(151) Jahangiri, H.; Osatiashtiani, A.; Ouadi, M.; Hornung, A.; Lee, F. A.; Wilson, K. Ga/HZSM-5 Catalysed Acetic Acid Ketonisation for Upgrading of Biomass Pyrolysis Vapours. *Catalysts* **2019**, *9* (10). https://doi.org/10.3390/catal9100841.

(152) Alotaibi, M. A.; Kozhevnikova, E. F.; Kozhevnikov, I. V. Efficient Hydrodeoxygenation of Biomass-Derived Ketones over Bifunctional Pt-Polyoxometalate Catalyst. *Chem. Commun.* **2012**, *48* (57), 7194–7196. https://doi.org/10.1039/C2CC33189F.

(153) Kong, L.; Liu, C.; Gao, J.; Wang, Y.; Dai, L. Efficient and Controllable Alcoholysis of Kraft Lignin Catalyzed by Porous Zeolite-Supported Nickel-Copper Catalyst. *Bioresource Technology* **2019**, *276*, 310–317. https://doi.org/10.1016/j.biortech.2019.01.015.

(154) Zhang, W.; Zhang, Y.; Zhao, L.; Wei, W. Catalytic Activities of NiMo Carbide Supported on SiO2 for the Hydrodeoxygenation of Ethyl Benzoate, Acetone, and Acetaldehyde. *Energy Fuels* **2010**, *24* (3), 2052–2059. https://doi.org/10.1021/ef901222z.

(155) Nikolopoulos, A. A.; Jang, B. W.-L.; Spivey, J. J. Acetone Condensation and Selective Hydrogenation to MIBK on Pd and Pt Hydrotalcite-Derived MgAl Mixed Oxide Catalysts. *Applied Catalysis A: General* **2005**, *296* (1), 128–136. https://doi.org/10.1016/j.apcata.2005.08.022.

(156) Gamman, J. J.; Jackson, S. D.; Wigzell, F. A. Synthesis of Methyl Isobutyl Ketone over Pd/MgO/SiO2. *Ind. Eng. Chem. Res.* **2010**, *49* (18), 8439–8443. https://doi.org/10.1021/ie100770e.

(157) Zhang, H.; Xiao, R.; Jin, B.; Xiao, G.; Chen, R. Biomass Catalytic Pyrolysis to Produce Olefins and Aromatics with a Physically Mixed Catalyst. *Bioresource Technology* **2013**, *140*, 256–262. https://doi.org/10.1016/j.biortech.2013.04.094.

(158) Kumar, R.; Strezov, V.; Lovell, E.; Kan, T.; Weldekidan, H.; He, J.; Dastjerdi, B.; Scott, J. Bio-Oil Upgrading with Catalytic Pyrolysis of Biomass Using Copper/Zeolite-Nickel/Zeolite and Copper-Nickel/Zeolite Catalysts. *Bioresource Technology* **2019**, *279*, 404–409. https://doi.org/10.1016/j.biortech.2019.01.067.

(159) Nakagawa, Y.; Liu, S.; Tamura, M.; Tomishige, K. Catalytic Total Hydrodeoxygenation of Biomass-Derived Polyfunctionalized Substrates to Alkanes. *ChemSusChem* **2015**, *8* (7), 1114–1132. https://doi.org/10.1002/cssc.201403330.

(160) Simakova, I. L.; Murzin, D. Yu. Transformation of Bio-Derived Acids into Fuel-like Alkanes via Ketonic Decarboxylation and Hydrodeoxygenation: Design of Multifunctional Catalyst, Kinetic and Mechanistic Aspects. *Journal of Energy Chemistry* **2016**, *25* (2), 208–224. https://doi.org/10.1016/j.jechem.2016.01.004.

(161) Bej, S. K.; Thompson, L. T. Acetone Condensation over Molybdenum Nitride and Carbide Catalysts. *Applied Catalysis A: General* **2004**, *264* (2), 141–150. https://doi.org/10.1016/j.apcata.2003.12.051.

(162) Badari, A. C.; Harnos, Sz.; Lónyi, F.; Onyestyák, Gy.; Štolcová, M.; Kaszonyi, A.; Valyon, J. A Study of the Selective Catalytic Hydroconversion of Biomass-Derived Pyrolysis or Fermentation Liquids Using Propylamine and Acetic Acid as Model Reactants. *Catalysis Communications* **2015**, *58*, 1–5. https://doi.org/10.1016/j.catcom.2014.07.041.

(163) Bej, S. K.; Thompson, L. T. Acetone Condensation over Molybdenum Nitride and Carbide Catalysts. *Applied Catalysis A: General* **2004**, *264* (2), 141–150. https://doi.org/10.1016/j.apcata.2003.12.051.

(164) Gamman, J. J.; Jackson, S. D.; Wigzell, F. A. Synthesis of Methyl Isobutyl Ketone over Pd/MgO/SiO2. *Ind. Eng. Chem. Res.* **2010**, *49* (18), 8439–8443. https://doi.org/10.1021/ie100770e.

(165) Nikolopoulos, A. A.; Jang, B. W.-L.; Spivey, J. J. Acetone Condensation and Selective Hydrogenation to MIBK on Pd and Pt Hydrotalcite-Derived MgAl Mixed Oxide Catalysts. *Applied Catalysis A: General* **2005**, *296* (1), 128–136. https://doi.org/10.1016/j.apcata.2005.08.022.

(166) Huo, X.; Huq, N. A.; Stunkel, J.; Cleveland, N. S.; Starace, A. K.; Settle, A. E.; York, A. M.; Nelson, R. S.; Brandner, D. G.; Fouts, L.; St. John, P. C.; Christensen, E. D.; Luecke, J.; Mack, J. H.; McEnally, C. S.; Cherry, P. A.; Pfefferle, L. D.; Strathmann, T. J.; Salvachúa, D.; Kim, S.; McCormick, R. L.; Beckham, G. T.; Vardon, D. R. Tailoring Diesel Bioblendstock from Integrated Catalytic Upgrading of Carboxylic Acids: A “Fuel Property First” Approach. *Green Chem.* **2019**, *21* (21), 5813–5827. https://doi.org/10.1039/C9GC01820D.

(167) Zhang, Z.; Wang, Y.; Sun, K.; Shao, Y.; Zhang, L.; Zhang, S.; Zhang, X.; Liu, Q.; Chen, Z.; Hu, X. Steam Reforming of Acetic Acid over Ni–Ba/Al2O3 Catalysts: Impacts of Barium Addition on Coking Behaviors and Formation of Reaction Intermediates. *Journal of Energy Chemistry* **2020**, *43*, 208–219. https://doi.org/10.1016/j.jechem.2019.08.023.

(168) Zhang, W.; Zhang, Y.; Zhao, L.; Wei, W. Catalytic Activities of NiMo Carbide Supported on SiO2 for the Hydrodeoxygenation of Ethyl Benzoate, Acetone, and Acetaldehyde. *Energy Fuels* **2010**, *24* (3), 2052–2059. https://doi.org/10.1021/ef901222z.

(169) Correction for Balakrishnan et al., Novel Pathways for Fuels and Lubricants from Biomass Optimized Using Life-Cycle Greenhouse Gas Assessment. *Proc Natl Acad Sci USA* **2015**, *112* (29), E3969. https://doi.org/10.1073/pnas.1511659112.

(170) Zhang, H.; Xiao, R.; Jin, B.; Xiao, G.; Chen, R. Biomass Catalytic Pyrolysis to Produce Olefins and Aromatics with a Physically Mixed Catalyst. *Bioresource Technology* **2013**, *140*, 256–262. https://doi.org/10.1016/j.biortech.2013.04.094.

(171) Simakova, I. L.; Murzin, D. Yu. Transformation of Bio-Derived Acids into Fuel-like Alkanes via Ketonic Decarboxylation and Hydrodeoxygenation: Design of Multifunctional Catalyst, Kinetic and Mechanistic Aspects. *Journal of Energy Chemistry* **2016**, *25* (2), 208–224. https://doi.org/10.1016/j.jechem.2016.01.004.

(172) Kong, L.; Liu, C.; Gao, J.; Wang, Y.; Dai, L. Efficient and Controllable Alcoholysis of Kraft Lignin Catalyzed by Porous Zeolite-Supported Nickel-Copper Catalyst. *Bioresource Technology* **2019**, *276*, 310–317. https://doi.org/10.1016/j.biortech.2019.01.015.

(173) Nakagawa, Y.; Liu, S.; Tamura, M.; Tomishige, K. Catalytic Total Hydrodeoxygenation of Biomass-Derived Polyfunctionalized Substrates to Alkanes. *ChemSusChem* **2015**, *8* (7), 1114–1132. https://doi.org/10.1002/cssc.201403330.

(174) Pham, T. N.; Sooknoi, T.; Crossley, S. P.; Resasco, D. E. Ketonization of Carboxylic Acids: Mechanisms, Catalysts, and Implications for Biomass Conversion. *ACS Catal.* **2013**, *3* (11), 2456–2473. https://doi.org/10.1021/cs400501h.

(175) Witsuthammakul, A.; Sooknoi, T. Selective Hydrodeoxygenation of Bio-Oil Derived Products: Acetic Acid to Propylene over Hybrid CeO2–Cu/Zeolite Catalysts. *Catal. Sci. Technol.* **2016**, *6* (6), 1737–1745. https://doi.org/10.1039/C5CY01485A.

(176) Gayubo, A. G.; Aguayo, A. T.; Atutxa, A.; Aguado, R.; Bilbao, J. Transformation of Oxygenate Components of Biomass Pyrolysis Oil on a HZSM-5 Zeolite. I. Alcohols and Phenols. *Ind. Eng. Chem. Res.* **2004**, *43* (11), 2610–2618. https://doi.org/10.1021/ie030791o.

(177) Xue, M.; Hu, S.; Chen, H.; Fu, Y.; Shen, J. Preparation of Highly Loaded and Dispersed Ni/SiO2 Catalysts. *Catalysis Communications* **2011**, *12* (5), 332–336. https://doi.org/10.1016/j.catcom.2010.10.002.

(178) Wu, S.-K.; Lai, P.-C.; Lin, Y.-C. Atmospheric Hydrodeoxygenation of Guaiacol over Nickel Phosphide Catalysts: Effect of Phosphorus Composition. *Catalysis Letters* **2014**, *144* (5), 878–889. https://doi.org/10.1007/s10562-014-1231-7.

(179) Zhu, X.; Lobban, L. L.; Mallinson, R. G.; Resasco, D. E. Bifunctional Transalkylation and Hydrodeoxygenation of Anisole over a Pt/HBeta Catalyst. *Journal of Catalysis* **2011**, *281* (1), 21–29. https://doi.org/10.1016/j.jcat.2011.03.030.

(180) Lan, X.; Hensen, E. J. M.; Weber, T. Hydrodeoxygenation of Guaiacol over Ni2P/SiO2–Reaction Mechanism and Catalyst Deactivation. *Applied Catalysis A: General* **2018**, *550*, 57–66. https://doi.org/10.1016/j.apcata.2017.10.018.

(181) Griffin, M. B.; Baddour, F. G.; Habas, S. E.; Ruddy, D. A.; Schaidle, J. A. Evaluation of Silica-Supported Metal and Metal Phosphide Nanoparticle Catalysts for the Hydrodeoxygenation of Guaiacol Under Ex Situ Catalytic Fast Pyrolysis Conditions. *Topics in Catalysis* **2016**, *59* (1), 124–137. https://doi.org/10.1007/s11244-015-0512-8.

(182) Chen, C.; Chen, G.; Yang, F.; Wang, H.; Han, J.; Ge, Q.; Zhu, X. Vapor Phase Hydrodeoxygenation and Hydrogenation of M-Cresol on Silica Supported Ni, Pd and Pt Catalysts. *Chemical Engineering Science* **2015**, *135*, 145–154. https://doi.org/10.1016/j.ces.2015.04.054.

(183) Cai, Q.; Xu, J.; Zhang, S.; Wang, S. Aromatic Hydrocarbon Production from Bio-Oil by a Dual-Stage Hydrogenation-Cocracking Process: Furfural as a Model Compound. *Ind. Eng. Chem. Res.* **2016**, *55* (41), 10839–10849. https://doi.org/10.1021/acs.iecr.6b02713.

(184) Gengan, R. M. A Study to Identify a Feasible Route for the Production of the Monomer 2-Vinylfuran from Furan by Evaluating the Effect of Variables on the Final Yield and to Recommend Suitable Conditions Applicable to the Chemical Industry. Thesis, 1992.

(185) Ulfa, S. M.; Munandar, R.; Prihartini, D. Batch and Continuous Flow Hydrodeoxygenation of Furfural and Acetone Condensation Adduct Catalyzed by Ni/ZrO2-SiO2. *AIP Conference Proceedings* **2018**, *2049* (1), 020005. https://doi.org/10.1063/1.5082410.

(186) Grazia, L.; Bonincontro, D.; Lolli, A.; Tabanelli, T.; Lucarelli, C.; Albonetti, S.; Cavani, F. Exploiting H-Transfer as a Tool for the Catalytic Reduction of Bio-Based Building Blocks: The Gas-Phase Production of 2-Methylfurfural Using a FeVO4 Catalyst. *Green Chem.* **2017**, *19* (18), 4412–4422. https://doi.org/10.1039/C7GC01749A.

(187) Arekion, J.; Delmas, M.; Gaset, A. Biomass as a Source of Monomers: I — Synthesis of 2-Vinylfuran. *Biomass* **1983**, *3* (1), 59–65. https://doi.org/10.1016/0144-4565(83)90008-2.

(188) Reichwein, J. F.; Pagenkopf, B. L. A New Horner−Wadsworth−Emmons Type Coupling Reaction between Nonstabilized β-Hydroxy Phosphonates and Aldehydes or Ketones. *J. Am. Chem. Soc.* **2003**, *125* (7), 1821–1824. https://doi.org/10.1021/ja027658s.

(189) Davda, R. R.; Shabaker, J. W.; Huber, G. W.; Cortright, R. D.; Dumesic, J. A. Aqueous-Phase Reforming of Ethylene Glycol on Silica-Supported Metal Catalysts. *Applied Catalysis B: Environmental* **2003**, *43* (1), 13–26. https://doi.org/10.1016/S0926-3373(02)00277-1.

(190) Nakagawa, Y.; Tamura, M.; Tomishige, K. Catalytic Reduction of Biomass-Derived Furanic Compounds with Hydrogen. *ACS Catal.* **2013**, *3* (12), 2655–2668. https://doi.org/10.1021/cs400616p.

(191) Jaatinen, S. K.; Karinen, R. S.; Lehtonen, J. S. Liquid Phase Furfural Hydrotreatment to 2-Methylfuran with Carbon Supported Copper, Nickel, and Iron Catalysts. *ChemistrySelect* **2017**, *2* (1), 51–60. https://doi.org/10.1002/slct.201601947.

(192) Williams, C. L.; Chang, C.-C.; Do, P.; Nikbin, N.; Caratzoulas, S.; Vlachos, D. G.; Lobo, R. F.; Fan, W.; Dauenhauer, P. J. Cycloaddition of Biomass-Derived Furans for Catalytic Production of Renewable p-Xylene. *ACS Catal.* **2012**, *2* (6), 935–939. https://doi.org/10.1021/cs300011a.

(193) Chang, C.-C.; Green, S. K.; Williams, C. L.; Dauenhauer, P. J.; Fan, W. Ultra-Selective Cycloaddition of Dimethylfuran for Renewable p-Xylene with H-BEA. *Green Chem.* **2014**, *16* (2), 585–588. https://doi.org/10.1039/C3GC40740C.

(194) Pyrolysis of Beech Wood in A Continuous Drop Tube Reactor in Comparison to A Batch Reactor. *Journal*.

(195) Jahangiri, H.; Osatiashtiani, A.; Ouadi, M.; Hornung, A.; Lee, A. F.; Wilson, K. Ga/HZSM-5 Catalysed Acetic Acid Ketonisation for Upgrading of Biomass Pyrolysis Vapours. *Catalysts* **2019**, *9* (10). https://doi.org/10.3390/catal9100841.

(196) Zhang, X.; Tang, J.; Zhang, Q.; Liu, Q.; Li, Y.; Chen, L.; Wang, C.; Ma, L. Hydrodeoxygenation of Lignin-Derived Phenolic Compounds into Aromatic Hydrocarbons under Low Hydrogen Pressure Using Molybdenum Oxide as Catalyst. *Catalysis Today* **2019**, *319*, 41–47. https://doi.org/10.1016/j.cattod.2018.03.068.

(197) Guo, S.; Wu, Y.; Jin, T.; Wang, H.; Dong, C.; Zhang, J.; Ding, M. Controllable Alkylation of Benzene with Mixed Olefins for Producing C8-C15 Aromatics in Jet Fuel. *Fuel* **2020**, *275*, 117890. https://doi.org/10.1016/j.fuel.2020.117890.

(198) Mullery, A. A.; Hoang, J. N.; Nguyen, A. T.; Luong, C. D.; Ledesma, E. B. Thermal Decomposition Pathways of 4-Ethylguaiacol under Fast Pyrolysis and Gasification Conditions. *Journal of Analytical and Applied Pyrolysis* **2017**, *123*, 83–91. https://doi.org/10.1016/j.jaap.2016.12.023.

(199) Xu, Y.; Zhang, L.; Chang, J.; Zhang, X.; Ma, L.; Wang, T.; Zhang, Q. One Step Hydrogenation–Esterification of Model Compounds and Bio-Oil to Alcohols and Esters over Raney Ni Catalysts. *Energy Conversion and Management* **2016**, *108*, 78–84. https://doi.org/10.1016/j.enconman.2015.10.062.

(200) Yu, W.; Tang, Y.; Mo, L.; Chen, P.; Lou, H.; Zheng, X. One-Step Hydrogenation–Esterification of Furfural and Acetic Acid over Bifunctional Pd Catalysts for Bio-Oil Upgrading. *Bioresource Technology* **2011**, *102* (17), 8241–8246. https://doi.org/10.1016/j.biortech.2011.06.015.

(201) Li, W.; Wang, H.; Wu, X.; Betancourt, L. E.; Tu, C.; Liao, M.; Cui, X.; Li, F.; Zheng, J.; Li, R. Ni/Hierarchical ZSM-5 Zeolites as Promising Systems for Phenolic Bio-Oil Upgrading: Guaiacol Hydrodeoxygenation. *Fuel* **2020**, *274*, 117859. https://doi.org/10.1016/j.fuel.2020.117859.

(202) Kumar, R.; Strezov, V.; Lovell, E.; Kan, T.; Weldekidan, H.; He, J.; Dastjerdi, B.; Scott, J. Bio-Oil Upgrading with Catalytic Pyrolysis of Biomass Using

Copper/Zeolite-Nickel/Zeolite and Copper-Nickel/Zeolite Catalysts. *Bioresource Technology* **2019**, *279*, 404–409. https://doi.org/10.1016/j.biortech.2019.01.067.

(203) Xu, Y.; Li, Y.; Wang, C.; Wang, C.; Ma, L.; Wang, T.; Zhang, X.; Zhang, Q. In-Situ Hydrogenation of Model Compounds and Raw Bio-Oil over Ni/CMK-3 Catalyst. *Fuel Processing Technology* **2017**, *161*, 226–231. https://doi.org/10.1016/j.fuproc.2016.08.018.

(204) Kadarwati, S.; Hu, X.; Gunawan, R.; Westerhof, R.; Gholizadeh, M.; Hasan, M. D. M.; Li, C.-Z. Coke Formation during the Hydrotreatment of Bio-Oil Using NiMo and CoMo Catalysts. *Fuel Processing Technology* **2017**, *155*, 261–268. https://doi.org/10.1016/j.fuproc.2016.08.021.

(205) Adjaye, J. D.; Bakhshi, N. N. Production of Hydrocarbons by Catalytic Upgrading of a Fast Pyrolysis Bio-Oil. Part II: Comparative Catalyst Performance and Reaction Pathways. *Fuel Processing Technology* **1995**, *45* (3), 185–202. https://doi.org/10.1016/0378-3820(95)00040-E.

(206) Zhang, H.; Shao, S.; Xiao, R.; Shen, D.; Zeng, J. Characterization of Coke Deposition in the Catalytic Fast Pyrolysis of Biomass Derivates. *Energy Fuels* **2014**, *28* (1), 52–57. https://doi.org/10.1021/ef401458y.

(207) Zhang, Z.; Tian, Y.; Zhang, L.; Hu, S.; Xiang, J.; Wang, Y.; Xu, L.; Liu, Q.; Zhang, S.; Hu, X. Impacts of Nickel Loading on Properties, Catalytic Behaviors of Ni/γ–Al2O3 Catalysts and the Reaction Intermediates Formed in Methanation of CO2. *International Journal of Hydrogen Energy* **2019**, *44* (18), 9291–9306. https://doi.org/10.1016/j.ijhydene.2019.02.129.

Appendices

Appendix A Pyridine-FTIR characterization of catalysts and supports at different temperatures

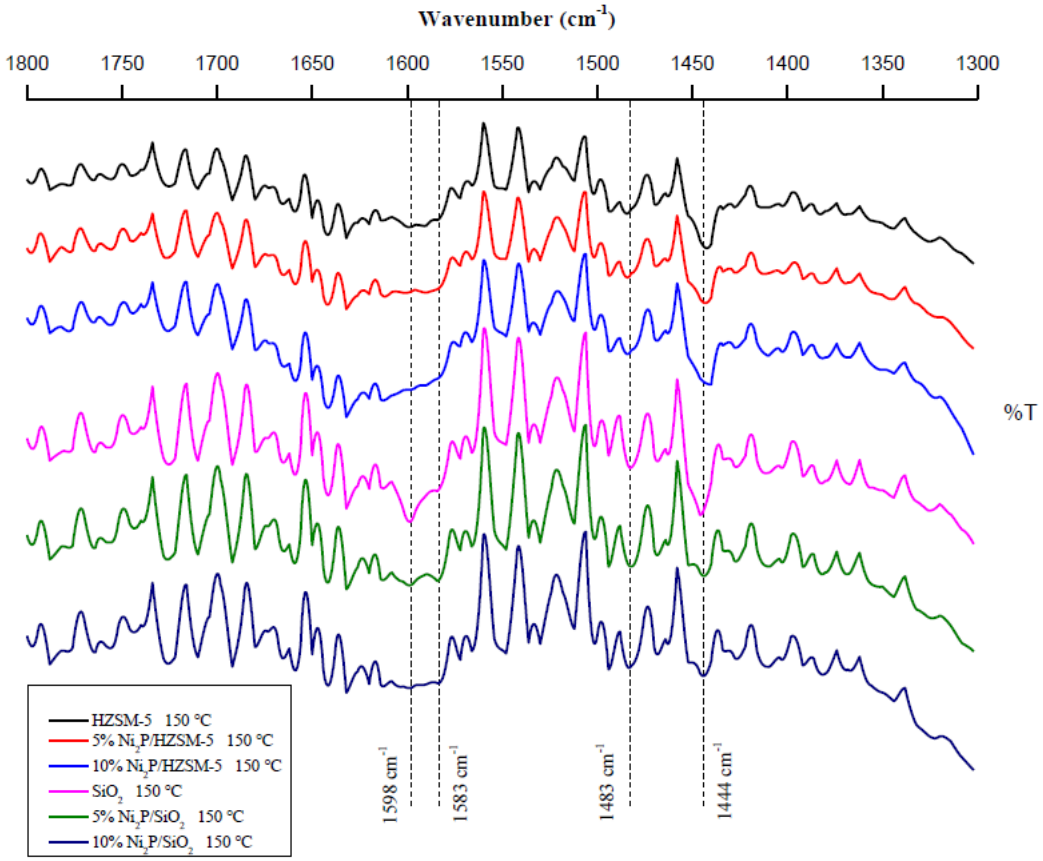

Figure A.1 IR spectra of catalysts and supports at 150 ºC

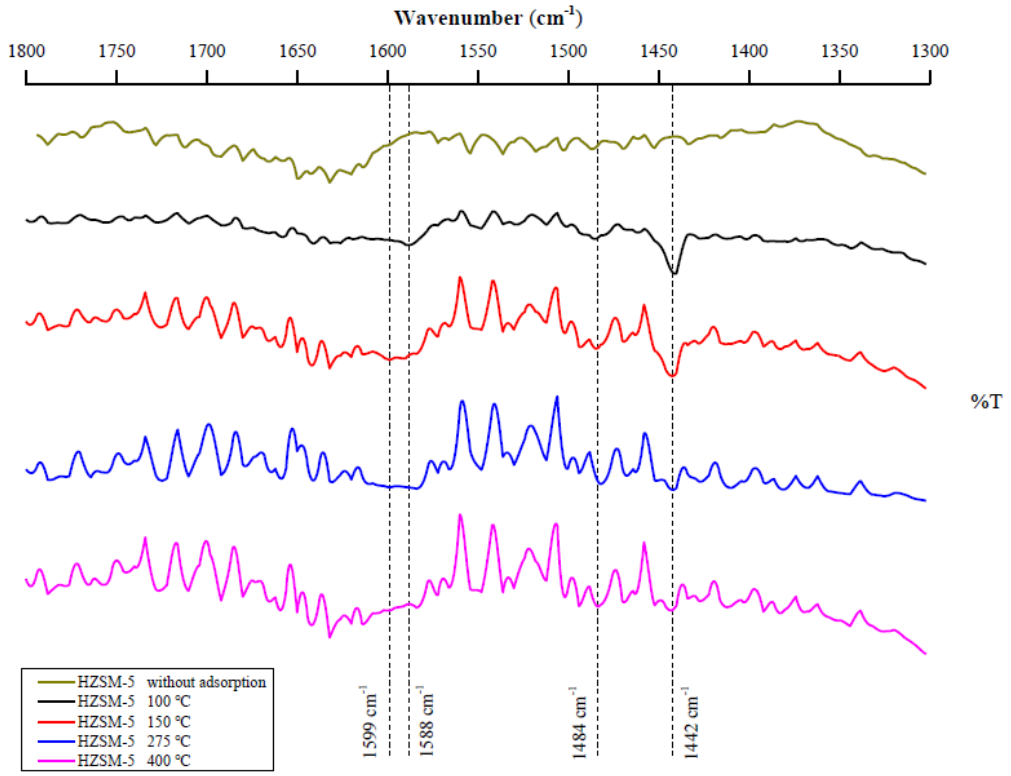

Figure A.2 IR spectra of HZSM-5 catalysts at different desorption temperature

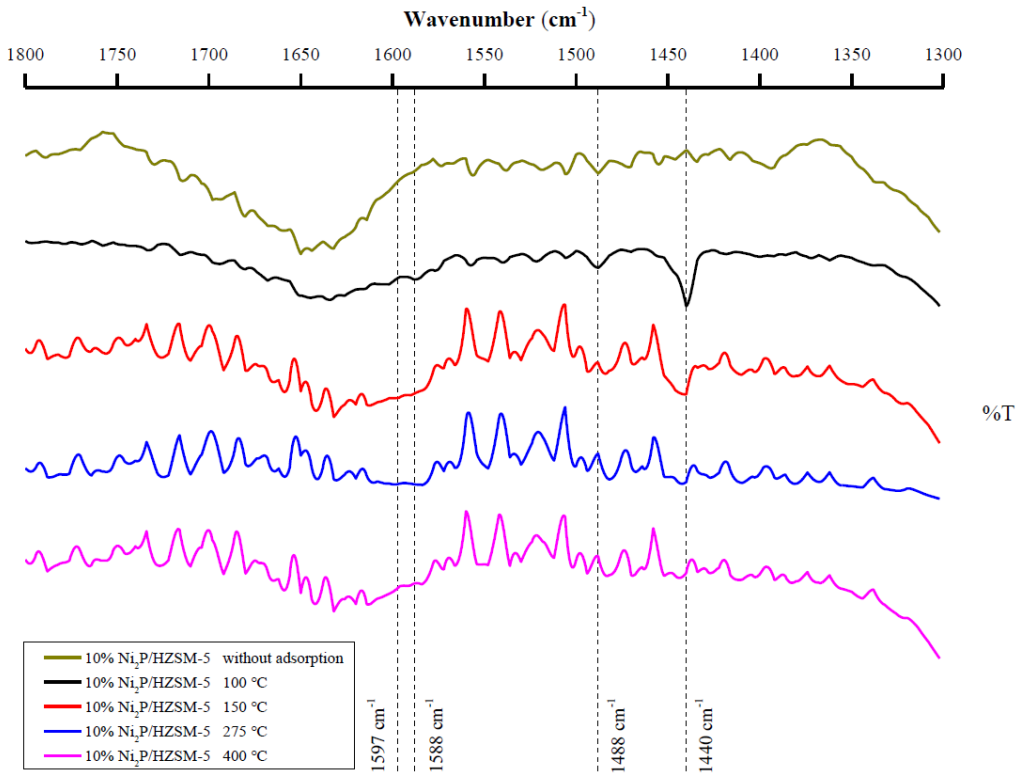

Figure A.3 IR spectra of 10% Ni_2P/HZSM-5 catalysts at different desorption temperature

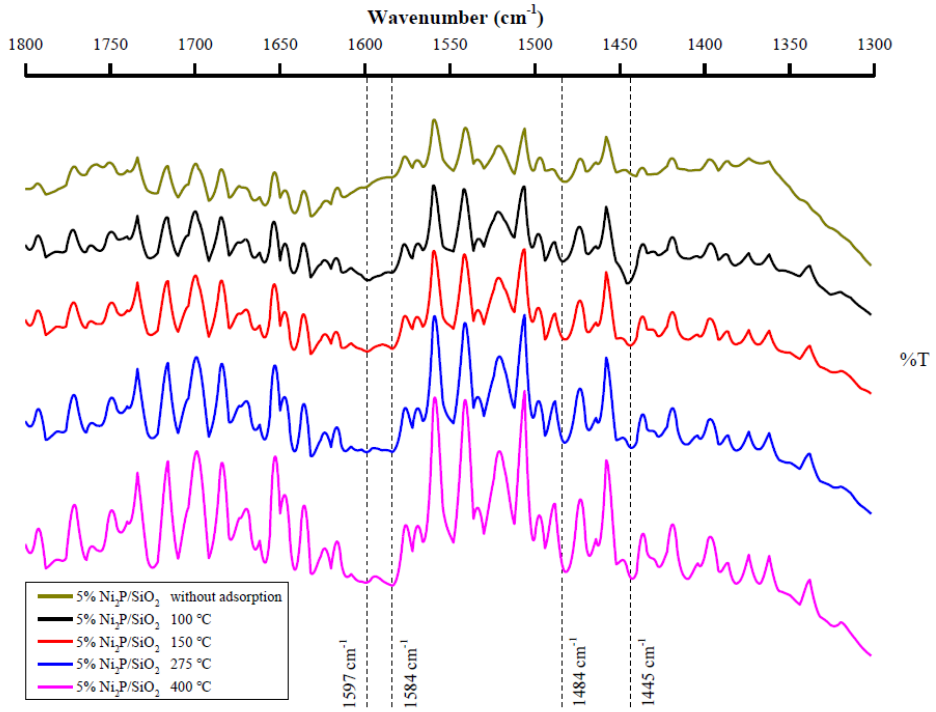

Figure A.4 IR spectra of 5% Ni_2P/SiO_2 catalysts at different desorption temperature

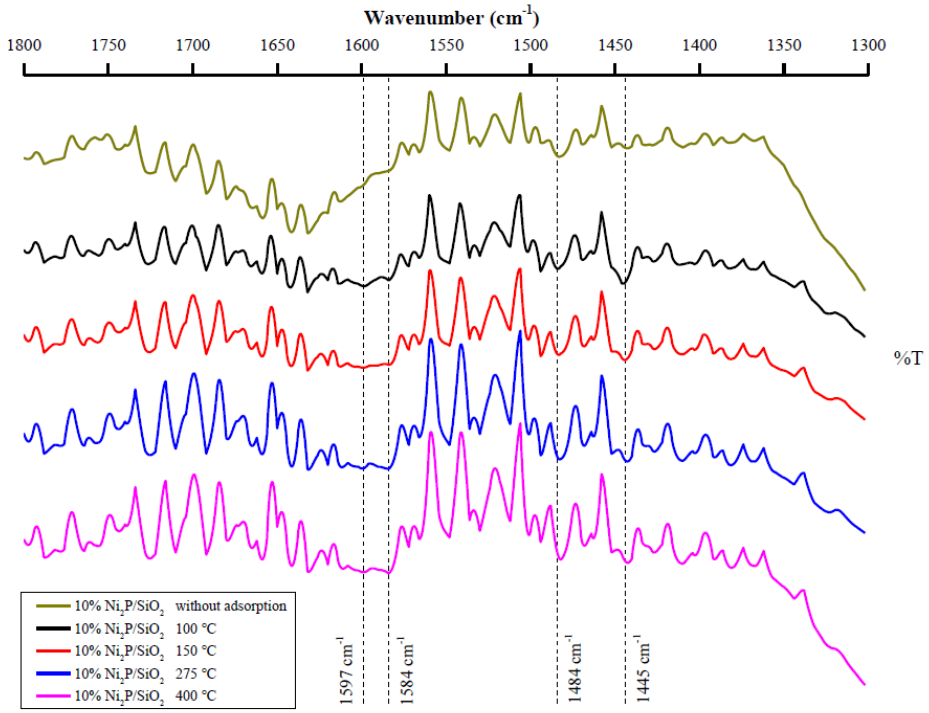

Figure A.5 IR spectra of 10% Ni_2P/SiO_2 catalysts at different desorption temperature

Appendix B Identification of main chemicals in the liquid phase

Table B.1 Main chemicals in the liquid phase of acetone HDO

Classification	Chemicals [a]	Formula	O wt%
Aldehydes	Acetaldehyde	C_2H_4O	36.4
Alcohols	Ethanol	C_2H_5OH	34.8
	Isopropanol	C_3H_8O	26.7
Furans	2-Methyfuran	C_5H_6O	19.5
Carboxylic acids	Acetic acid	CH_3COOH	53.3
Esters	(Z)-3-Hexenol acetate	$C_8H_{14}O_2$	22.5
Ketones	Acetone [b]	C_3H_6O	27.6
	Methyl isobutyl ketone	$C_6H_{12}O$	16.0
Alkanes	N-Pentane	C_5H_{12}	
	Butane	C_4H_{10}	
Alkenes	4-Methyl-1-pentene	C_6H_{12}	
Aromatic hydrocarbons	Benzene	C_6H_6	
	Toluene	C_7H_8	
	Ethylbenzene	C_8H_{10}	
	P-xylene	C_8H_{10}	
	O-xylene	C_8H_{10}	
	1-Ethyl-2-methylbenzene	C_9H_{12}	
	1-Ethyl-3-methylbenzene	C_9H_{12}	
	1-Ethyl-4-methylbenzene	C_9H_{12}	
	Mesitylene	C_9H_{12}	
	2,3-Dihydro-4-methyl-1H-indene	$C_{10}H_{12}$	
	2,2-Dimethylindene, 2,3-dihydro-	$C_{11}H_{14}$	
	p-Cymene	$C_{10}H_{14}$	

[a] only chemicals with content >1 mol% were presented in this table

[b] unreacted acetone

Table B.2 Main chemicals in the liquid phase of acetic acid HDO

Classification	Chemicals [a]	Formula	O *wt%*
Aldehydes	Acetaldehyde	C_2H_4O	36.4
Alcohols	1-Phenyl-1,2-butanediol	$C_{10}H_{14}O_2$	19.3
Carboxylic acids	Acetic acid [b]	CH_3COOH	53.3
Esters	2-Naphthalenol, 1,2-dihydro-, acetate	$C_{12}H_{12}O_2$	17.0
Ketones	Acetone	C_3H_6O	27.6
	Methyl isobutyl ketone	$C_6H_{12}O$	16.0
Aromatic hydrocarbons	Benzene	C_6H_6	
	Toluene	C_7H_8	
	Ethylbenzene	C_8H_{10}	
	P-xylene	C_8H_{10}	
	O-xylene	C_8H_{10}	
	PropylBenzene	C_9H_{12}	
	Isopropylbenzene	C_9H_{12}	
	1-Ethyl-2-methylbenzene	C_9H_{12}	
	Mesitylene	C_9H_{12}	
	1-Methylindan	$C_{10}H_{12}$	
	2,3-Dihydro-4-methyl-1H-indene	$C_{10}H_{12}$	
	2,3-dihydro-4,7-dimethyl-1H-Indene	$C_{11}H_{14}$	
	2,3-Dihydro-2,2-dimethylindene,	$C_{11}H_{14}$	
	1-ethylidene-1H-Indene	$C_{11}H_{14}$	
	1,3-Dimethyl-Naphthalene	$C_{12}H_{12}$	
	p-Cymene	$C_{10}H_{14}$	

[a]only chemicals with content >1 mol% were presented in this table

[b]unreacted acetic acid

Table B.3 Main chemicals in the liquid phase of 4-ethylguaiacol HDO

Classification	Chemicals [a]	Formula	O *wt%*
Ethers	1-Methoxy-4-(1-methylpropyl)-benzene	$C_{11}H_{16}O$	9.8
	2-Methoxy-4-methyl-1-(1-methylethyl)-benzene	$C_{11}H_{16}O$	9.8
Alcohols	α,β-Dimenthyl-benzeneethnol	$C_{10}H_{14}O$	10.7
Ketones	Acetone	C_3H_6O	27.6
Phenols	Phenol	C_6H_6O	17.0
	Cresol (p- & o-)	C_7H_8O	25.8
	3-Ethylphenol	$C_8H_{10}O$	14.8
	4-Ethylphenol	$C_8H_{10}O$	14.8
	2-Ethylphenol	$C_8H_{10}O$	14.8
	2,4-Dimethylphenol	$C_8H_{10}O$	14.8
	3,4-Dimethylphenol	$C_8H_{10}O$	14.8
	2-Ethyl-6-methylphenol	$C_9H_{12}O$	11.8
	2-Ethyl-4-methylphenol	$C_9H_{12}O$	11.8
	3-Methyl-4-isopropylphenol	$C_{10}H_{14}O$	10.7
	3-Ethyl-5-methylphenol	$C_9H_{12}O$	11.8
	3,4,5-Trimethylphenol	$C_9H_{12}O$	11.8
	3-5-Diethylphenol	$C_{10}H_{14}O$	10.7
	Thymol	$C_{10}H_{14}O$	10.7
Guaiacols	2-Methoxyphenol	$C_7H_8O_2$	25.8
	4-Ethylguaiacol [b]	$C_9H_{12}O_2$	21.1
Alkenes	2,3-Dihydro-1,1,6-trimethyl-1H-Indene	$C_{12}H_{16}$	
	9,10-Dihydro-9-(1-methylpropyl)-Anthracene	$C_{18}H_{20}$	
Aromatic hydrocarbons	Benzene	C_6H_6	
	Toluene	C_7H_8	
	P-xylene	C_8H_{10}	
	M-xylene	C_8H_{10}	
	1-Methylethyl-benzene	C_9H_{12}	
	1,9-Dimethyl-9H-Fluorene	$C_{15}H_{14}$	
	2-Ethyl-Naphthalene	$C_{12}H_{12}$	

[a]only chemicals with content >1 mol% were presented in this table

[b]unreacted 4-ethylguaiacol

Table B.4 Main chemicals in the liquid phase of furfural HDO

Classification	Chemicals [a]	Formula	O *wt*%
Aldehydes	Butanal	C_4H_8O	22.2
	Furfural [b]	$C_5H_4O_2$	33.3
Ketones	Acetone	C_3H_6O	27.6
Furans	Furan	C_4H_4O	23.5
	2-Methyfuran	C_5H_6O	19.5
	3-Methylfuran	C_5H_6O	19.5
	2,5-Dimethylfuran	C_6H_8O	16.7
	2-Vinylfuran	C_6H_6O	17.0
	2,2'-Methylenebis-furan	$C_9H_8O_2$	21.6
Aromatic hydrocarbons	Benzene	C_6H_6	
	Toluene	C_7H_8	
	Ethylbenzene	C_8H_{10}	
	P-xylene	C_8H_{10}	
	1-Methylethyl-benzene	C_9H_{12}	
	1-Ethyl-3-methylbenzene	C_9H_{12}	
	Mesitylene	C_9H_{12}	
	1-Methylindan	$C_{10}H_{12}$	

[a]only chemicals with content >1 mol% were presented in this table

[b]unreacted furfural

Table B.5 Main chemicals in the liquid phase of Mixture 1 HDO

Classification	Chemicals [a]	Formula	O *wt*%
Carboxylic acids	Acetic acid [b]	$C_2H_4O_2$	53.3
Ketones	Acetone	C_3H_6O	27.6
Phenols	Phenol [b]	C_6H_6O	17.0
	3-Ethyl-5-methylphenol	$C_9H_{12}O$	11.8
	Cresol (p- & o-)	C_7H_8O	25.8
	4-Ethylphenol	$C_9H_{12}O_2$	21.1
	2,4-Dimethylphenol	$C_8H_{10}O$	14.8
	3,4,5-trimethylphenol	$C_9H_{12}O$	11.8
	3,5-Diethylphenol	$C_{10}H_{14}O$	10.7
Aromatic hydrocarbons	Benzene	C_6H_6	
	Toluene	C_7H_8	
	Ethylbenzene	C_8H_{10}	
	Xylene (p- & o-)	C_8H_{10}	
	1-Methylethylbenzene	C_9H_{12}	

[a] only chemicals with content > 1 mol% were presented in this table

[b] unreacted raw model compounds

Table B.6 Main chemicals in the liquid phase of Mixture 2 HDO

Classification	Chemicals [a]	Formula	O *wt%*
Aldehydes	Acetaldehyde	C_2H_4O	22.2
Carboxylic acids	Acetic acid [b]	$C_2H_4O_2$	53.3
Alcohols	Methanol	CH_4O	50.0
	Ethanol	C_2H_4O	36.4
	Isopropanol	C_3H_8O	26.7
	α,β-Dimenthyl-benzeneethnol	$C_{10}H_{14}O$	10.7
Ketones	Acetone [b]	C_3H_6O	27.6
Esters	Methyl formate	$C_2H_4O_2$	53.3
	Ethyl acetate	$C_4H_8O_2$	36.4
	Isopropyl acetate	$C_5H_{10}O_2$	31.4
Phenols	Phenol [b]	C_6H_6O	17.0
	Cresol (p- & o-)	C_7H_8O	25.8
	4-Ethylphenol	$C_8H_{10}O$	14.8
	2,4-Dimethylphenol	$C_8H_{10}O$	14.8
Guaiacols	4-Ethylguaiacol [b]	$C_9H_{12}O_2$	21.1
Furans	Furan	C_4H_4O	23.5
	Furfural [b]	$C_5H_4O_2$	33.3
	2,5-Dimethylfuran	C_6H_8O	16.7
	2,2'-Methylenebis-furan	$C_9H_8O_2$	21.6
Aromatic hydrocarbons	Benzene	C_6H_6	
	Toluene	C_7H_8	
	Xylene (p- & m-)	C_8H_{10}	
	1-Ethyl-3-methylbenzene	C9H12	
	1-Methylethyl-benzene	C9H12	

[a] only chemicals with content > 1 mol% were presented in this table

[b] unreacted raw model compounds

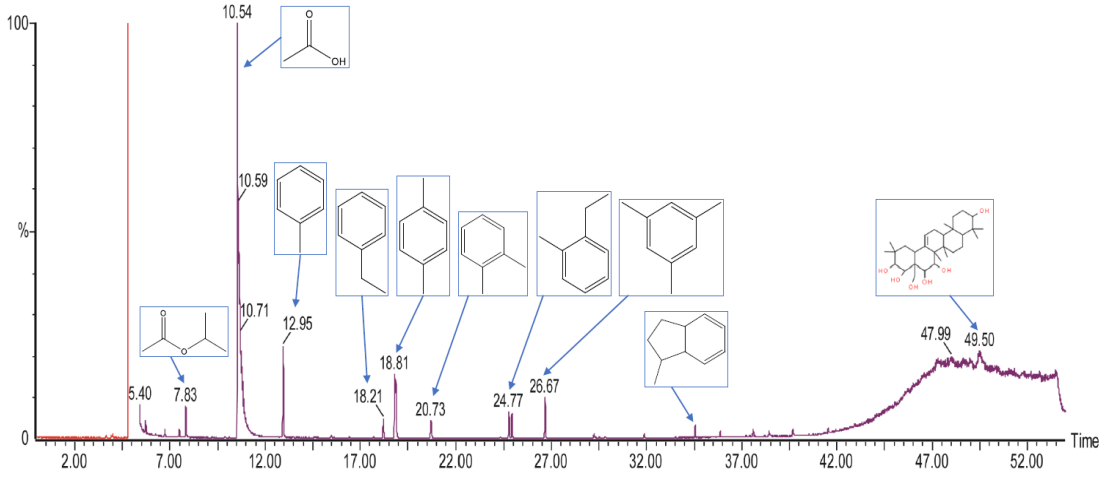

Figure B.1 Identification of chemicals of bio-oil HDO in GC-MS

Appendix C Conversion rate, yield, and distribution of component

As shown in ***Table C.1*** the conversion rate and DOD reached around 81% and 77%, respectively. Clearly, results showed that these catalysts were effective in catalyzing the HDO reaction.

Table C.1 Comparison of different catalysts in acetic acid HDO

Item	Conditions [a]	
	5% Ni_2P/HZSM-5	10% Ni_2P/HZSM-5
Conversion rate & DOD (wt%)		
$X_{acetic\ acid}$	80	81
DOD	77.0	76.1
Yield of products (wt%)		
$Y_{Liq.\ (free\ water)}$	33.09	32.87
Y_{Gas}	41.02	39.66
Y_{H_2O}	25.89	27.46

[a] fixed conditions: 0.43 g 5% Ni_2P/HZSM-5; 0.47 g 10% Ni_2P/HZSM-5; 400 °C, 0.5 MPa, 0.05 ml/min of acetic acid, H_2: 40 ml/min, N_2: 10 ml/min, 90 min

The effect of the 5% and 10% Ni_2P/HZSM-5 catalysts on the selectivity for the chemical composition in liquid products of acetic acid HDO is compared in ***Figure C.1A***. Ketones and aromatic hydrocarbons were the primary products using 5% Ni_2P/HZSM-5, with the selectivity of 11.2% and 13.8%. The 10% Ni_2P/HZSM-5 showed similar values of 12.6% for ketones and 12.9% for aromatic hydrocarbons.

Figure C.1B shows the effect of the 5% and 10% Ni_2P/HZSM-5 catalysts on the selectivity for chemicals of acetic acid HDO in gas products. It can be seen that CO, CO_2 and CH_4 were obtained as the main products of acetic acid HDO on Ni_2P/HZSM-5 catalysts with the selectivities of 24.7% for CO and of 13.1% for CO_2. The highest selectivity of CH_4 (14.3%) was obtained using 10% Ni_2P/HZSM-5. Probably, the high content of Ni_2P facilitates the decarboxylation reaction of acetic acid for more CH_4 and CO_2 formation. However, the 10% Ni_2P/HZSM-5 catalyst showed a slightly lower selectivity of CO_2 than the value from 5% Ni_2P/HZSM-5. This can be explained by the fact that some of the CO_2 and CO was further reacted with H_2 via the methanation reaction to form CH_4 and H_2O. Similarly, Zhang et al.[207] performed the methanation of CO_2 over Ni/Al_2O_3 and found that the nickel loading of 27.5% allowed the best activity for CH_4 formation at 400 °C. What's more, a higher yield of H_2O using 10%

Ni_2P/HZSM-5 than 5% Ni_2P/HZSM-5 (*Table C.1*) was noted, which also confirms that the methanation reaction of CO_2 took place.

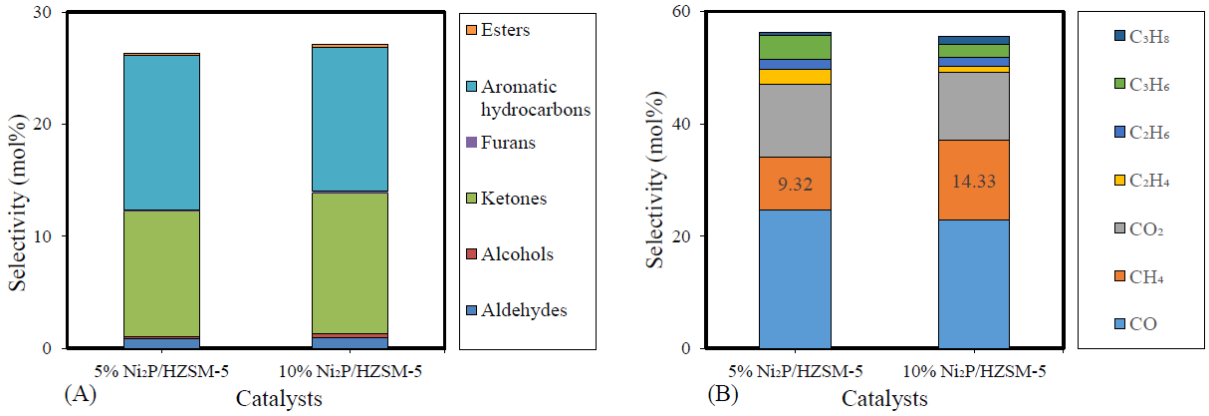

Figure C.1 Effects of catalysts on acetic acid HDO (400 °C, 0.5 MPa, 0.05 mL/min acetic acid, 40 mL/min H_2, 10 mL/min N_2, reaction time: 90 min): (a) Selectivity of chemical composition in liquid phase; (b) Selectivity of chemicals in gas phase

Table C.2 Effect of total N_2 pressure on bio-oil hydrotreatment

Item	Conditions [a]		
	1 MPa (Total pressure)	3 MPa (Total pressure)	6 MPa (Total pressure)
Composition in liquid products (%) [b]			
Alkenes	1.11	1.15	1.97
Alkanes	6.58	7.2	5.94
Aldehydes	11.81	12.72	11.15
Alcohols	6.61	4.94	6.10
Carboxylic acids	-		-
Esters	0.49	0.47	0.52
Furans	0.49	0.45	0.56
Aromatic hydrocarbons	73.27	73.06	73.76
Total hydrocarbons	80.96	81.41	81.67
Composition in gas products (%)			
CH_4	30.30	25.53	30.45
CO_2	26.77	17.91	21.79
C_2H_6	22.78	16.36	11.07
C_3H_8	15.55	37.06	32.71
Others	4.60	3.14	5.16

[a] fixed conditions: 0.43 g 5% Ni_2P/HZSM-5, 400 °C (oven 2), 400 °C (preheater) 0.05 mL/min of feed (acetone/bio-oils=10/1), initial H_2 = 0 MPa, 40 mL/min H_2, 10 mL/min N_2, reaction time: 90 min

[b] without considering acetone composition

Abbreviation

Nomination

HFRR: High-frequency reciprocating test rig

HTL: Hydrothermal liquefaction

GC/MS: Gas chromatography/mass spectroscopy

FT-IR: Fourier transform infrared spectroscopy

OSR: Oxidative steam reforming

SCFs: Supercritical fluids

TAN: Total acid number

HHV: Higher heating value

FCC: Fluid catalytic cracking

HDO: Hydro-deoxygenation

DOD: Degree of deoxygenation

LHSV: Liquid hourly space velocity

WHSV: Weight hourly space velocity

HYD: Hydrogenation

2-FMK: 2-Furyl methyl ketone

TPR: Temperature-programmed reaction

ICP-OES: Inductively coupled plasma-optical emission spectrometry

BJH: Barrett-Joyner-Halenda

TG: Thermogravimetry

TGA: Thermogravimetry analysis

XRD: X-ray Powder Diffraction

DSC: Differential scanning calorimetry

IUPAC: International union of pure and applied chemistry

DTG: Derivative of weight

FID: Flame ionization detector

TCD: Thermal conductivity

ECN: Effective Carbon Number

DMSO: Dimethyl sulfoxide

IP: Isopropanol

MIK: Methyl isobutyl ketone

AA: Acetaldehyde

BTX: Benzene, Toluene, and Xylene

MO: Mesityl oxide

DMP: 2,4-Dimethylphenol

MMMEB: 2-Methoxy-4-methyl-1-(1-methylethyl)-benzene

2-MF: 2-Methylfuran

BTXM: Benzene, toluene, xylene, and mesitylene

DTR: Drop tube reactor

HT-FB: High-temperature fraction bio-oil

MT-FB: Medium-temperature fraction bio-oil

LT-FB: Low-temperaure fraction bio-oil

Mixture 1: Mixture acetic acid and phenol

Mixture 2: Mixture acetic acid, phenol, acetone, furfural, 4-ethylguaiacol and H_2O

Symbols

X (%): conversion rate

Sel_i (%): The selectivity of product chemicals

W (%): Water content

CT (s): Contact time

(D) (%): Product distribution

V_{space}: The volume among the catalysts particles

Q_{H_2}: The flow rate of H_2 at normal pressure and room temperature

Q_{N_2}: The flow rate of N_2 at normal pressure and room tempera

Y_i (%): The yield of products (liquid phase, gas phase, water, and coke)

Subscripts and superscripts

List of Figures

List of Tables

List of publications and conferences

Publications

1), Jundong Wang, Michael Jabbour, Lokmane Abdelouahed, Soumaya Mezghich, Lionel Estel, Karine Thomas, Bechara Taouk. Catalytic upgrading of bio-oil: Hydrodeoxygenation study of acetone as molecule model of ketones. The Canadian Journal of Chemical Engineering. https://doi.org/10.1002/cjce.23909

2), Jie Xu, Nicolas Brodu, Jundong Wang, Lokmane Abdelouahed, Bechara Taouk. Chemical characteristics of bio-oil from beech wood pyrolysis separated by fractional condensation and additional water extraction. (Submitted)

3), Jundong Wang, Lokmane Abdelouahed, Michael Jabbour, Bechara Taouk. Catalytic hydrodeoxygenation of acetic acid, 4-ethylguaiacol, and furfural as model molecules of pyrolysis bio-oil using Ni_2P/HZSM-5 catalysts. (Submitted)

4), Jundong Wang, Lokmane Abdelouahed, Jie Xu, Bechara Taouk. Catalytic hydro-deoxygenation of simulated bio-oil using Ni_2PHZSM-5 catalysts: comprehension of

reactive interaction. The special issue of Chemical Engineering & Technology. (Submitted)

Conferences

1). Jundong Wang, Lokmane Abdelouahed, Jie Xu, Nicolas Brodu, Bechara Taouk. Enhanced hydrocarbons production from bio-oil hydrotreatment in acetone by nickel phosphide modified HZSM-5. The International Congress of Chemical and Process Engineering (CHISA, virtually). March 15th-18th 2021, Praha, Czech. Oral presentation

2). Jundong Wang, Lokmane Abdelouahed, Michael Jabbour, Bechara Taouk. Hydro-deoxygenation of bio-oil model compounds over nickel phosphide catalysts. la 17ème congrès de la société française de Genie des Procèdes (SFGP). October 15th-17th 2019. Nantes, France. Poster

3). Jundong Wang, Lokmane Abdelouahed, Luis Reyes, Bechara Taouk. Hydrodeoxygenation of bio-oil model compounds over the nickel phosphide catalysts. The 12th European Congress of Chemical Engineering (ECCE 12). September 15th-19th 2019. Florence, Italy. Poster

4). Jundong Wang, Nourelhouda Boukaous, Lokmane Abdelouahed, Chetna Mohabeer, Lionel Estel, Bechara Taouk. Catalytic hydro-deoxygenation of bio-oil in a fixed bed reactor and a batch reactor. The 5th International Conference on New Trends in Chemistry. April 22^{ed}-24th 2019. Athens, Greece. Poster